AD-760 582

INVESTIGATION OF THERMAL FATIGUE IN NON-TUBULAR REGENERATIVELY COOLED THRUST CHAMBERS. VOLUME I

D. Fulton

Rockwell International Corporation

Prepared for:

Air Force Rocket Propulsion Laboratory

May 1973

AFRPL-TR-73-10
VOLUME I

INVESTIGATION OF THERMAL FATIGUE IN NON-TUBULAR REGENERATIVELY COOLED THRUST CHAMBERS

FINAL REPORT
VOLUME I

D. FULTON
ADVANCED PROGRAMS

ROCKETDYNE DIVISION, ROCKWELL INTERNATIONAL
6633 Canoga Avenue, Canoga Park, California

TECHNICAL REPORT AFRPL-TR-73-10, VOLUME I

May 1973

Approved for public release, distribution unlimited.

Air Force Rocket Propulsion Laboratory
Director of Science & Technology
Air Force Systems Command
United States Air Force
Edwards, California

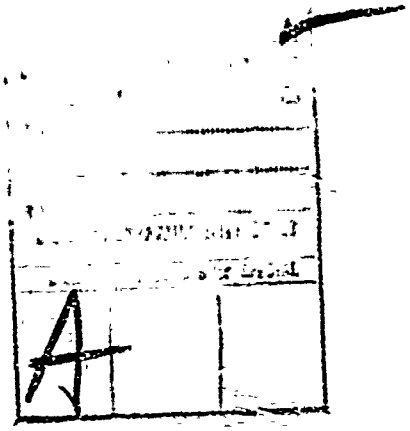

"When U. S. Government drawings, specifications, or other data are used for any purpose other than a definitely related Government procurement operation, the Government thereby incurs no responsibility nor any obligation whatsoever, and the fact that the Government may have formulated, furnished, or in any way supplied the said drawings, specifications, or other data, is not to be regarded by implication or otherwise, or in any manner licensing the holder or any person or corporation, or conveying any rights or permission to manufacture, use, or sell any patented invention that may in any way be related thereto."

Unclassified

Security Classification

DOCUMENT CONTROL DATA - R & D

Security classification of title, body of abstract and indexing annotation must be entered when the overall report is classified

1 ORIGINATING ACTIVITY (Corporate author) ROCKETDYNE DIVISION ROCKWELL INTERNATIONAL CORPORATION 6633 Canoga Avenue, Canoga Park, California 91304	2a. REPORT SECURITY CLASSIFICATION Unclassified 2b GROUP --

3 REPORT TITLE

Investigation of Thermal Fatigue in Non-Tubular Regeneratively Cooled Thrust Chambers, Volume I

4 DESCRIPTIVE NOTES (Type of report and inclusive dates)

5 AUTHOR(S) (First name, middle initial, last name)

Donald L. Fulton

6 REPORT DATE	7a. TOTAL NO. OF PAGES	7b. NO. OF REFS
May 1973	165	23

8a. CONTRACT OR GRANT NO	9a. ORIGINATOR'S REPORT NUMBER(S)
F04611-70-C-0014 b. PROJECT NO. 3058 c. Task 305810 d.	R-9093 9b. OTHER REPORT NO(S) (Any other numbers that may be assigned this report) AFRPL-TR-73-10 Volume I

10 DISTRIBUTION STATEMENT

Approval for public release; distribution unlimited

11 SUPPLEMENTARY NOTES	12. SPONSORING MILITARY ACTIVITY
	Air Force Rocket Propulsion Laboratory

13 ABSTRACT

An analytical method for predicting the thermal cycle life capability of non-tubular regeneratively cooled thrust chambers was developed. Included in the method are the effects of time-dependent creep damage and strain range-dependent fatigue damage. The method was calibrated using material mechanical properties, isothermal fatigue, and tensile creep specimen data.

Isothermal cyclic data on laboratory specimens to determine the effect of strain rate, temperature, strain range, and tensile and/or compression hold time on fatigue life of four candidate rocket engine thrust chamber materials was obtained. The experimental data and test procedure are presented. Also obtained was basic material data on the materials of interest.

Supporting thermal analyses were conducted and regeneratively cooled thrust chambers were designed for subsequent fabrication and hot-fire cycle testing to verify the life prediction.

DD FORM 1 NOV 65 1473

Unclassified

Security Classification

14 KEY WORDS	LINK A		LINK B		LINK C	
	ROLE	WT	ROLE	WT	ROLE	WT
Thermal Fatigue Prediction Analysis						
Parametric Heat Transfer Analysis						
Life of Non-Tubular Chambers						
Material Properties						
Isothermal Fatigue Data						
Chamber Designs						
Fatigue and Panel Testing						
Copper Alloys for Chambers						
Nickel for Chambers						

ja

AFRPL-TR-73-10
VOLUME I

INVESTIGATION OF THERMAL FATIGUE IN NON-TUBULAR REGENERATIVELY COOLED THRUST CHAMBERS

FINAL REPORT

VOLUME I

D. FULTON
ADVANCED PROGRAMS

ROCKETDYNE DIVISION, ROCKWELL INTERNATIONAL
6633 Canoga Avenue, Canoga Park, California

TECHNICAL REPORT AFRPL-TR-73-10, VOLUME I

May 1973

Air Force Rocket Propulsion Laboratory
Director of Science & Technology
Air Force Systems Command
United States Air Force
Edwards, California

16

FOREWORD

The information reported herein was prepared under sponsorship of the Air Force Rocket Propulsion Laboratory, Edwards, California, under Contract F04611-70-C-0014, Project 3058, Task 305810, Rocketdyne Report No. R-9093.

Acknowledgment is made to the many North American Rockwell personnel who contributed to this effort. Major contributors were:

Thermal Analysis	- R. D. Tobin J. M. Shoji
Structural and Life Analysis	- R. A. Cooper
Design	- L. H. Russell R. G. Barnsdale
Laboratory Fatigue Testing	- Dr. R. P. Jewett J. J. Vrolyk
Materials and Processes	- J. G. Somerville

The Air Force Project Engineer was Mr. C. D. Penn, AFRPL/LKCG.

This report (R-9093) has been reviewed and is approved.

Carlton D. Penn
Project Engineer
Liquid Rocket Division
Air Force Rocket Propulsion Laboratory
Edwards, California

ABSTRACT

An analytical method for predicting the thermal cycle life capability of non-tubular regeneratively cooled thrust chambers was developed. Included in the method are the effect of time dependent creep damage and strain range dependent fatigue damage. The method was calibrated using material mechanical properties, isothermal fatigue and tensile creep specimen data.

Isothermal cyclic data on laboratory specimens to determine the effect of strain rate, temperature, strain range and tensile and/or compression hold time on fatigue life of four candidate rocket engine thrust chamber materials was obtained. The experimental data and test procedure are presented. Also obtained was basic material data on the materials of interest.

Supporting thermal analyses were conducted and regeneratively cooled thrust chambers were designed for subsequent fabrication and hot fire cycle testing to verify the life prediction.

CONTENTS

ILLUSTRATIONS

TABLES

INTRODUCTION

The next generation of liquid rocket engine thrust chambers will employ non-tubular construction methods and will have a requirement for long life and multiple re-use. The practicality of producing non-tubular thrust chambers of the candidate materials has been demonstrated over a range of thrust and chamber pressure levels. However, very little effort has been expended in evaluating the long life characteristics of such chambers.

The Air Force Rocket Propulsion Laboratory (AFRPL) awarded the Rocketdyne Division, Rockwell International, a contract to analytically and experimentally explore the long life characteristics of non-tubular thrust chambers. This program was entitled "Investigation of the Thermal Fatigue Characteristics of Non-Tubular Regeneratively Cooled Thrust Chambers (F04611-70-C-0014).

The objective of this program was to (1) define design criteria for the thermal cycling capability of non-tubular regeneratively cooled thrust chambers, and (2) to demonstrate this cycling capability.

The results of the first part Phase I - Development of Design Criteria are presented herein. The Results of Phase II - Thermal Cycling Demonstration are presented in Volume II.

SUMMARY

Phase I of this program (entitled Development of Design Criteria) consisted of five discrete tasks:

Task I - Preliminary Design
Task II - Thermal Fatigue Analysis
Task III - Materials and Panel Testing
Task IV - Final Design - Regeneratively Cooled Thrust Chambers
Task V - Final Design - Calorimeter Thrust Chamber Assembly

Task I consisted of a preliminary thermal analysis effort to establish predicted operating temperatures and coolant passage geometry for use in subsequent analysis and laboratory test effort. For continuity a point design was established for the regeneratively cooled thrust chambers. Pertinent parameters of this point design were:

Propellants	O_2/H_2 and F_2/H_2
Thrust (vacuum), lb	3300
Nozzle Expansion Ratio	60:1
Chamber Pressure (maximum), psia	750
Mixture Ratio (nominal) (o/f)	
O_2/H_2	6:1
F_2/H_2	12:1
Throttle Ratio	9:1
Number of Restarts	750
Total Life, hours	5

Further, the chambers designed in Task IV and V were to interface with AFRPL designed injectors. Materials of interest for the hot gas wall of the regeneratively cooled chambers were:

Wrought Nickel
Sintered Nickel (as processed by the Rocketdyne powder metallurgy process)
Zirconium-Copper
NARloy-Z (a Rocketdyne-develor a copper alloy)

It is noted that although the Phase I effort was centered around the point design discussed previously the results were to be applicable to thrust chambers of any thrust level.

TASK I - PRELIMINARY DESIGN

The Task I effort consisted of a preliminary thermal analysis to establish typical operation conditions and chamber design criteria for use in the subsequent tasks of Phase I.

Chambers employing the materials of interest were thermally analyzed for operation with both O_2/H_2 and F_2/H_2 propellants. Initial analysis was conducted using a theoretical heat flux profile. The analysis was then modified as hot fire test data became available from the AFRPL.

TASK II - THERMAL FATIGUE ANALYSIS

In this task the thermal fatigue life of non-tubular regeneratively cooled thrust chambers was evaluated by the individual accumulation of fatigue and creep damage. A survey of candidate analytical techniques for predicting fatigue life was completed. The one selected for use, and modified to account for varying temperature experienced during the strain cycle was Manson's Universal Slopes Equation (Ref. 1 and 13). This equation is stated as:

$$\varepsilon_t = 3.5\left(\frac{F_{Tu}}{E}\right) N_f^{-.12} + \varepsilon_f^{.6}\, N_f^{-.6}$$

where

ε_t = total calculated strain range
F_{tu} = ultimate tensile strength
E = Young's modulus
ε_f = fracture ductility, $\ln \frac{100}{100-RA}$
RA = percent reduction in area

The life prediction analyses is based on the theory that failure depends on the accumulation of creep and fatigue damage (Fig. 1).

In this theory creep damage is evaluated from the stress-time-temperature cycle and fatigue damage from the strain-time measurement cycle. Isothermal fatigue test data (discussed later) on the materials of interest was used to calibrate the analysis.

TASK III - MATERIALS AND PANEL TESTING

To support the Task I and Task II analytical efforts, materials and panel test efforts were conducted to determine basic material data and isothermal fatigue data on the materials of interest. Major points with respect to the relative properties of the zirconium-copper and NARloy-Z alloys were:

(1) The NARloy-Z has significantly higher strength over the entire temperature range.

(2) The zirconium copper has somewhat higher elongation and reduction of area properties.

(3) The elevated temperature thermal conductivity of the two alloys is virtually the same.

(4) The NARloy-Z exhibits significantly better stress rupture properties.

(5) The NARloy-Z exhibited longer isothermal fatigue life for similar conditions.

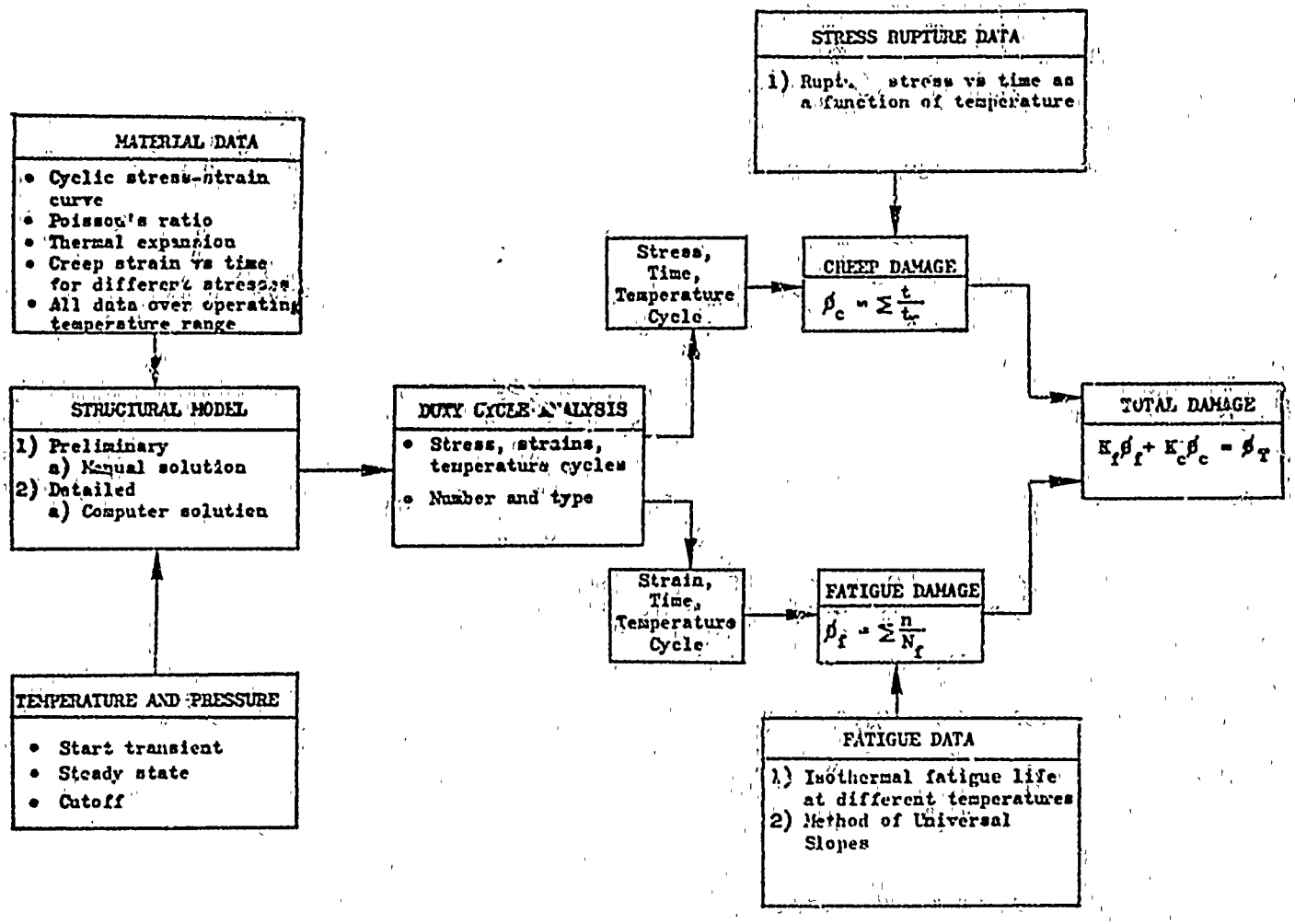

Figure 1. Life Analysis Logic

(6) Slow strain rate tests significantly effected the life of zirconium-copper but had no effect on the NARloy-Z.

(7) Isothermal fatigue testing with hold time at peak tensile strain lowered the life of both alloys.

The differential temperature fatigue tests and the panel test efforts conducted as a part of this task showed promise; however, their development was considered beyond the scope of this program.

TASK IV - FINAL DESIGN - REGENERATIVELY COOLED THRUST CHAMBERS

Non-tubular regeneratively cooled chambers employing spun and machined wrought nickel-200, zirconium-copper and NARloy-Z were designed using the thermal analysis results of Task I. Chamber closeout was annealed electroformed nickel.

Operating criteria were:

Thrust, lb	3300
Chamber Pressure, psia	750
Propellants	O_2/H_2
Mixture Ratio (o/f)	6:1

The nickel-200 chamber incorporated 72 step width channels, 0.040 inches wide in the nozzle and throat region and 0.080 wide in the combustion zone. Passage height was varied from 0.030 inch in the throat to 0.090 in the combustion zone and nozzle while the hot gas wall thickness was 0.025 throughout.

The two copper alloy chambers were identical and incorporated 40 constant width (0.080) variable depth channels (0.064 in the throat to 0.120 in combustion zone and nozzle). The hot gas wall thickness was 0.035 throughout.

As discussed previously all chambers had an annealed electroformed nickel closure and were designed to interface with the AFRPL injectors.

TASK V - CALORIMETER THRUST CHAMBER ASSEMBLY DESIGN

To aid in establishing an experimental heat flux profile for use in defining the thermal environment that the regeneratively cooled chambers were exposed to, a calorimeter thrust chamber assembly was designed. The assembly consisted of a calorimeter thrust chamber and a coaxial element injector. The calorimeter chamber incorporated 16 circumferential coolant passages machined into an OFHC-copper liner with an electroformed nickel closure. Individual water coolant manifolds were incorporated into each passage such that bulk temperature rise of the water in each passage could be used to establish a heat flux profile.

The injector was a 40 element coaxial design with a rigimesh face built to an AFRPL design.

DISCUSSION

This program was undertaken with the objective of defining design criteria for the thermal cycling capability of non-tubular regeneratively cooled thrust chambers and to demonstrate this cycling capability. The program effort was divided into two phases:

Phase I - Development of Design Criteria
Phase II - Thermal Cycling Demonstration

The results of the Phase I effort are presented herein. Results of Phase II are presented in Volume 2 of this report.

PHASE I - DEVELOPMENT OF DESIGN CRITERIA

During Phase I design criteria were developed for regeneratively cooled thrust chambers operating under the following conditions:

Propellants	O_2/H_2 and F_2/H_2
Thrust (vacuum), lb	3300
Nozzle Expansion Ratio	60:1
Chamber Pressure (maximum), psia	750
Mixture Ratio (o/f)	
O_2/H_2	6:1 Nominal, 5:1 to 7:1 Range
F_2/H_2	12:1 Nominal, 10:1 to 13:1 Range
Throttle Ratio	9:1
Coolant	H_2
Number of Restarts	750
Total Operating Life, hours	5

The initial propellant combination selected for this program was F_2/H_2; however, as the program progessed it became apparent that the most probable applications for long life regeneratively cooled thrust chambers would use the O_2/H_2 propellant combinations. This fact, combined with the fact that comparable test results (thermal environment) could be achieved with O_2/H_2 at significantly lower cost (fluorine is much more expensive than oxygen), resulted in a contract change to include the O_2/H_2 propellant combination in the analytical effort and to design the hot firing hardware for use with O_2/H_2 propellants.

Inlet Temperature (at ϵ = 60), R	70
Inlet Pressure (at ϵ = 60), psia	
Full Thrust	1200
Minimum Thrust (9:1 Throttle Point)	150
Coolant Pressure Drop (goal), psia	
Full Thrust	200
Minimum Thrust	25

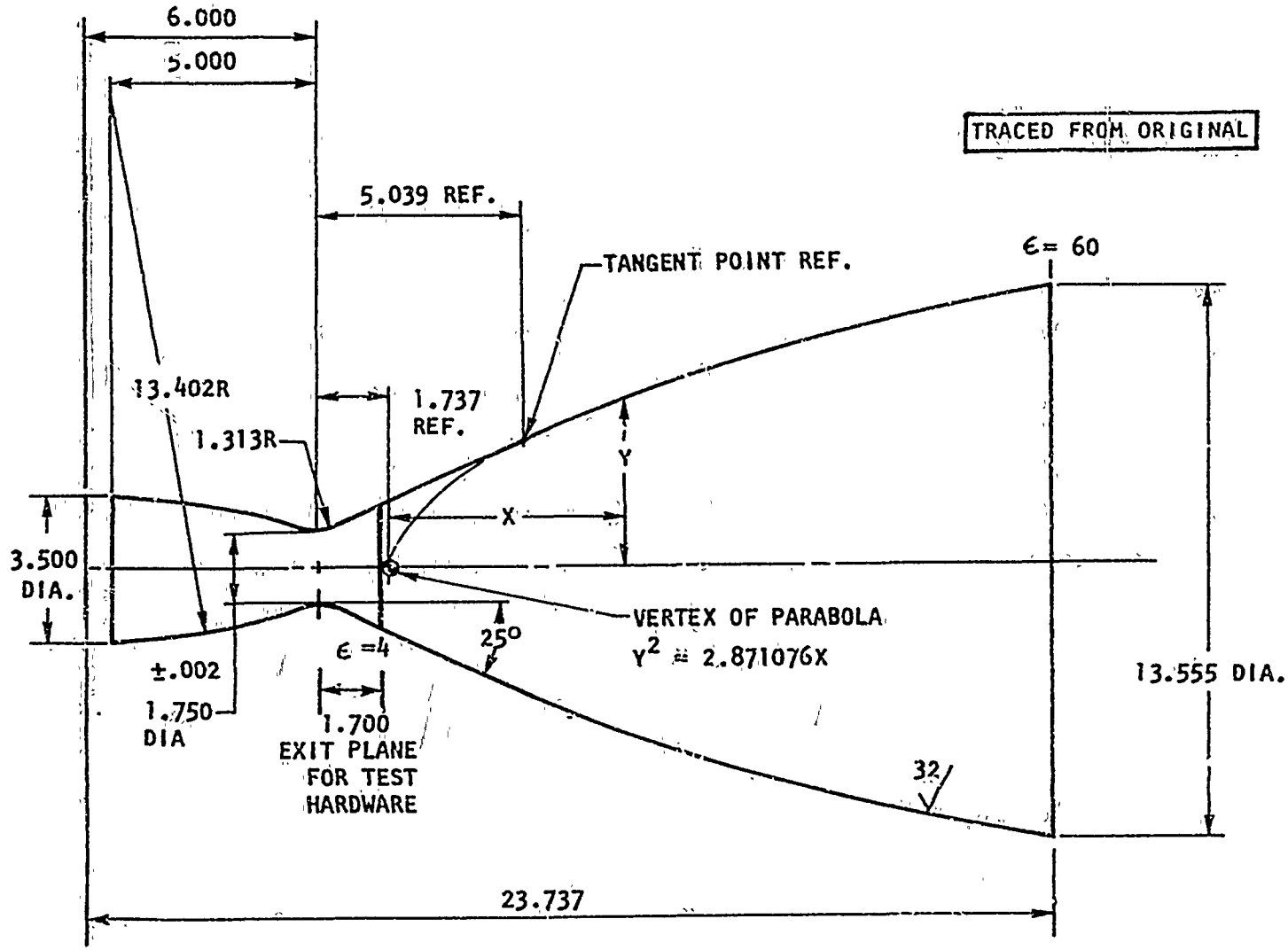

Figure 2. Rocket Engine Chamber Contour Internal Dimensions
(AFRPL Drawing No. X69B16164)

The thrust chamber internal contour was specified by AFRPL drawing No. X69B16164 (Fig. 2). The only difference between the O_2/H_2 and the F_2/H_2 was that the combustion zone of the O_2/H_2 chambers was 1 inch longer than that of the F_2/H_2 chamber. It was felt that the O_2/H_2 chamber would require a greater combustor length to assure attainment of good combustion performance. The hot firing hardware of Phase II was to use this same contour but have a truncated nozzle ($\varepsilon = 4$) to allow testing at site ambient pressures. Non-tubular fabrication methods were to be used for the thrust chambers and materials of interest were:

Wrought Nickel 200
Sintered Nickel
Zirconium Copper
NARloy-Z

In addition a calorimeter thrust chamber assembly was designed, fabricated and tested to establish the heat flux profile to be used in the design of the regeneratively cooled chambers. The calorimeter chamber had the same contour as the O_2/H_2 regeneratively cooled chambers.

The Phase I effort consisted of five discrete tasks:

Task I - Preliminary Design
Task II - Thermal Fatigue Analysis
Task III - Materials and Panel Testing
Task IV - Final Design - Regeneratively Cooled Thrust Chambers
Task V - Final Design - Calorimeter Thrust Chamber Assembly

A detailed discussion of the results of each task is presented in subsequent sections of this report.

TASK I - PRELIMINARY DESIGN

Task I involved a preliminary thermal analysis effort to establish predicted wall temperature and coolant passage geometry for use in subsequent analysis, design and laboratory test effort of Phase I. Sequentially the analysis was completed in the following order.

Initially, the Nickel 200 and the two copper alloy chambers were analyzed for operation with F_2/H_2 and O_2/H_2 propellants using a theoretical heat flux profile. As noted previously the original propellant combination was F_2/H_2; however, this was later changed to O_2/H_2 based on consideration of most probable application and reduced propellant cost during the Phase II hot fire test effort.

Initial Thermal Analysis - F_2/H_2 Propellants

The initial thermal analysis of the nickel and copper alloy chamber was completed for F_2/H_2 propellant at a mixture ratio of 12:1 using the theoretical heat flux profile shown in Fig. 3. This profile was determined using the Rocketdyne Boundary Layer Program and assumed a combustion efficiency of 99 percent.

The first case analyzed for the nickel chamber considered 60 constant width channels running from $\epsilon = 4$ to the injector face. Pertinent parameters are shown in Fig. 4. Two dimensional isothermal plots are shown in Fig. 5. Resulting wall temperatures were 1365 to 1488 F; considered too high for a long life thrust chamber. (A preliminary life analysis had indicated that maximum wall temperature should be limited to ~1400 F to achieve the 750 thermal cycle goal).

Consequently, a design refinement was initiated which considered 72 coolant channels and a step change in channel width at a plane 2 inches upstream and 1 inch downstream of the throat plane. Resulting temperatures (based on a two-dimensional analysis) plus other pertinent parameters are shown in Fig. 6 and 7 for the full thrust and throttled cases respectively.

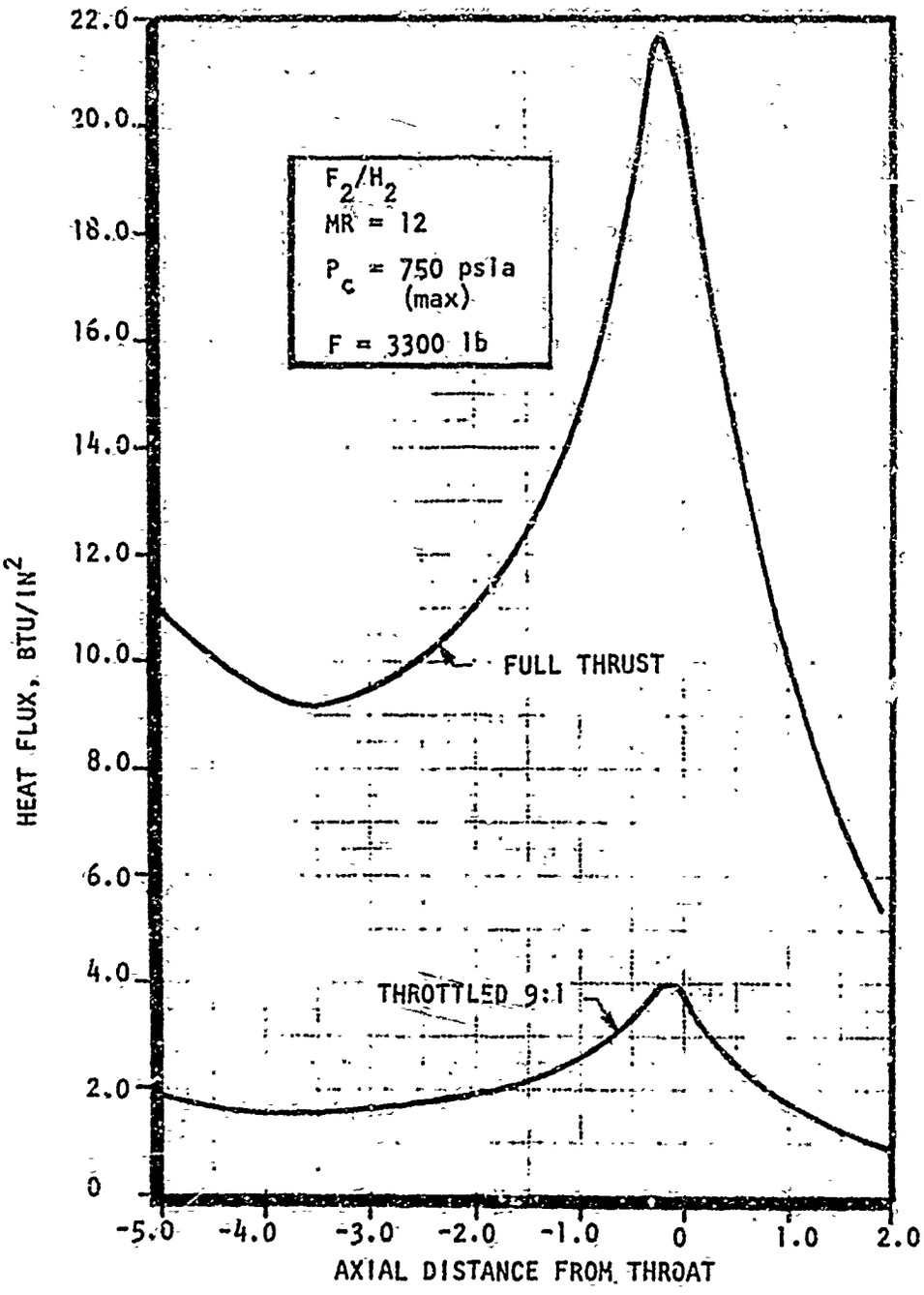

Figure 3. Theoretical Heat Flux Profile

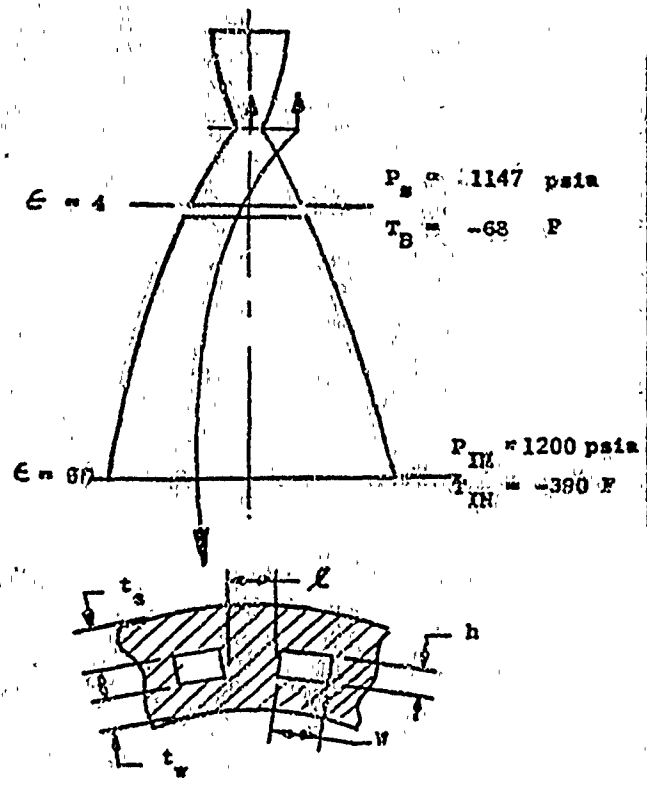

PARAMETER	LOCATION	INJECTOR FACE	THROAT PLANE	ϵ = 4
PASSAGE CRITERIA	t_w, in	.022	—	—
	t_s, in	.030	—	—
	W, in	.062	—	—
	h, in	.064	.047	.075
	ℓ, in	.124	.034	.124
WALL TEMPERATURE	T_{wg} (2-D), F	1365	1479	—
	T_{wc} (2-D), F	947	718	—
	T_{wb} (2-D), F	470	68	—
COOLANT PARAMETERS	T_B, F	283	20	-68
	P_s, psia	1035	1098	1147

COMMENTS

Nickel-200 Chamber
F_2/H_2 Propellants
MR = 12:1
P_c = 750 psia
60 Constant Width Channels

Figure 4. Channel Geometry - Nickel 200 Chamber (Full Thrust)

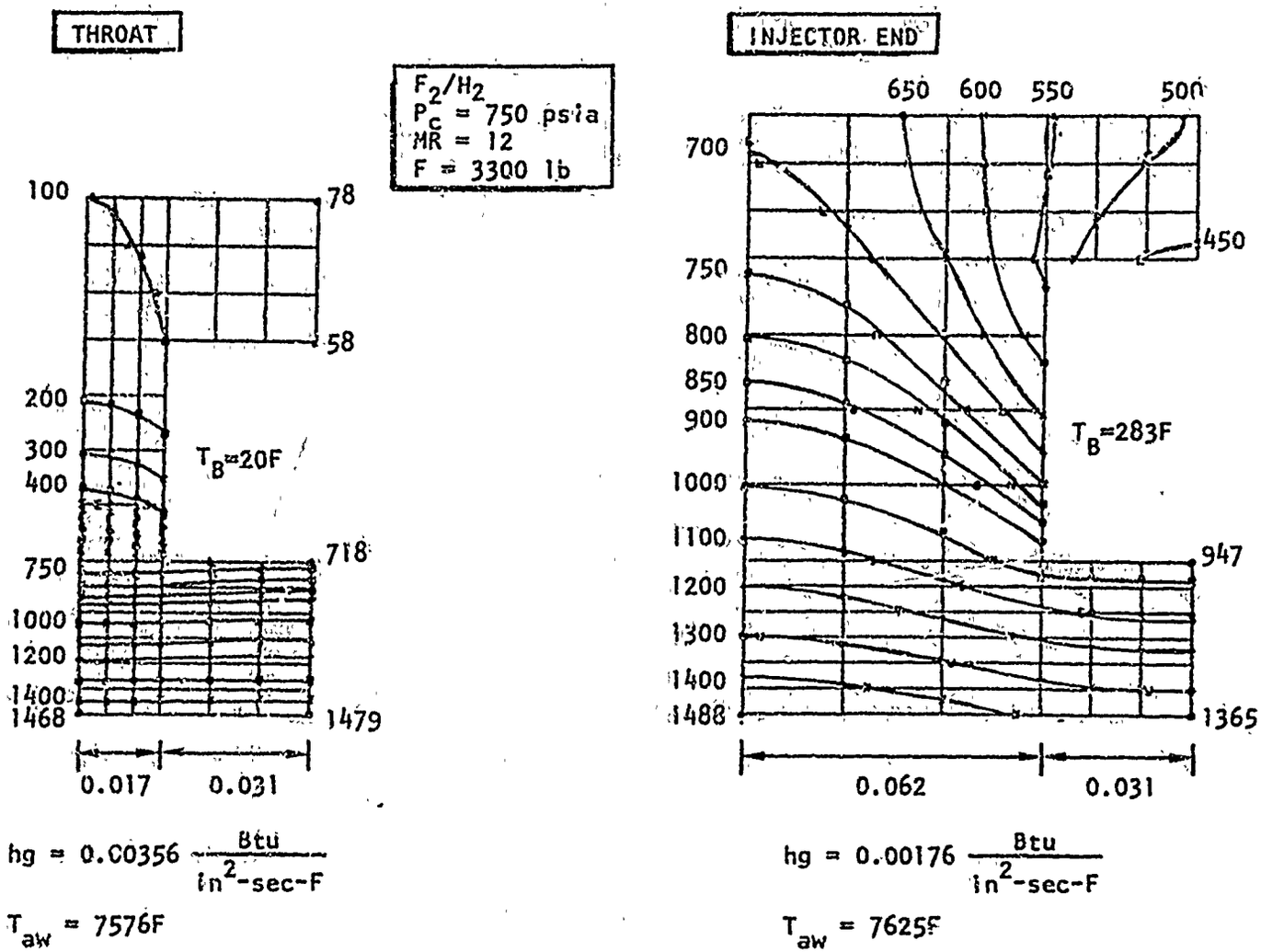

Figure 5. Temperature Distribution - Nickel 200 Chamber (60 Constant Width Channels)

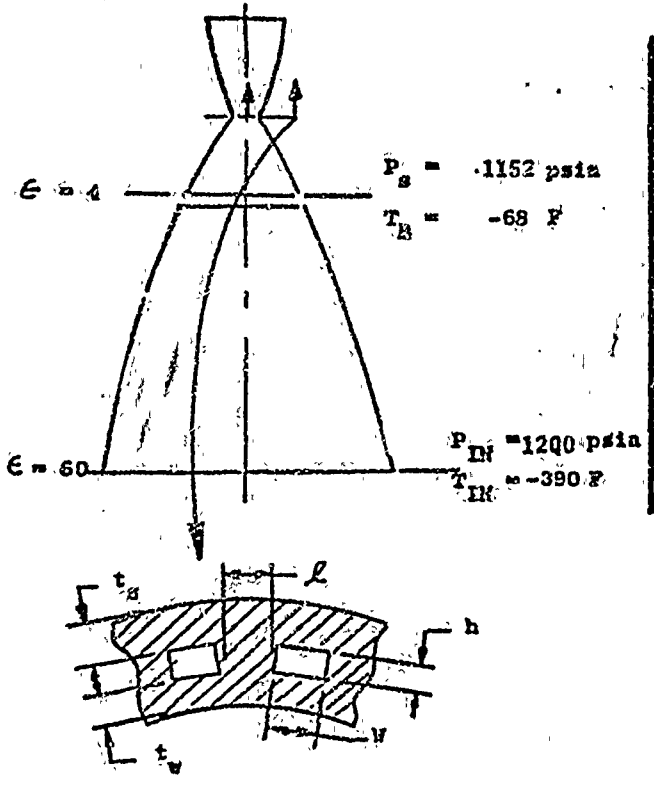

PARAMETER \ LOCATION		INJECTOR FACE	THROAT PLANE	ϵ = 4
PASSAGE CRITERIA	t_w, in	.030	.030	.030
	t_s, in	.060	.060	.060
	W, in	.080	.040	.080
	h, in	.043	.040	.060
	ℓ, in	.075	.040	.075
WALL TEMPERATURE	T_{wg}(2-D), F	1284	1295	507
	T_{wc}(2-D), F	894	477	332
	T_{wb}(2-D), F	452	85	30
COOLANT PARAMETERS	T_B, F	285	21	-68
	P_s, psia	1000	1014	1152

COMMENTS

Nickel-200 Chamber
F_2/H_2 Propellants
MR = 12:1
P_c = 750 psia
72 Channels (Step Width change @ X = -2 & +1 in.)

Figure 6. Channel Geometry for Nickel 200 Chambers (Full Thrust)

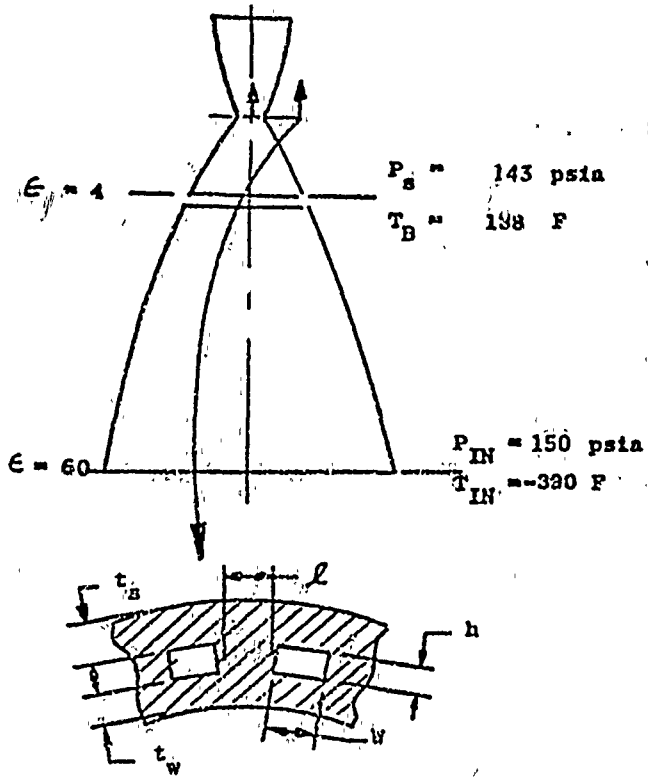

PARAMETER	LOCATION	INJECTOR FACE	THROAT PLANE	ϵ = 4
PASSAGE CRITERIA	t_w, in	.030	.030	.030
	t_B, in	.060	.060	.060
	W, in	.080	.040	.080
	h, in	.043	.040	.060
	ℓ, in	.075	.040	.075
WALL TEMPERATURE	T_{wg} (2-D), F	1137	753	510
	T_{wc} (2-D), F	1078	615	482
	T_{wb} (2-D), F	940	444	382
COOLANT PARAMETERS	T_B, F	712	290	138
	P_g, psia	113	111	143

COMMENTS

Nickel-200 Chamber
F_2/H_2 Propellants
MR = 12:1
P_c = 83 psia (throttled 9:1)
72 Channels (Step Width Change @ X = -2 & +1 in.)

Figure 7. Channel Geometry for Nickel 200 Chambers (Throttled 9:1)

In a similar manner the NARloy-Z and zirconium-copper chambers were thermally analyzed (the thermal conductivity of the two alloys is nearly the same so that the analysis is applicable to either material), to establish channel geometry and coolant requirements when operating with fluorine-hydrogen propellants at a mixture ratio of 12:1. Results are shown in Fig. 8 through 13 for two candidate designs.

In addition a parametric analysis was conducted on the nickel-200 chamber to determine sensitivity of the design variations in channel dimensions, wall thickness, etc.

The two-dimensional gas-side wall temperature may be decreased by increasing the number of channels and decreasing the channel width in the throat region. The corresponding increase in pressure drop is partially compensated by widening the channel in the nozzle and injector end and thinning the wall slightly. The effect on wall temperature of varying these land and channel dimensions is shown in Fig. 14 for the throat region of the nickel 200 chamber.

In the vicinity of this operating point the two-dimensional gas-side wall temperature changes 30 degrees per 0.010 inch change in land width and 20 degrees per 0.010 inch change in channel width. Average back wall temperature varies 10 degrees per 0.010 inch change in land width and negligibly with channel width. These are based on a constant coolant mass velocity achieved through adjusting passage height and number of passages per inch of circumference.

In general minimum wall temperature is achieved with minimum land and channel width at the expense of pressure drop.

Varying hot-wall thickness results in a much stronger change in gas-side wall temperature as seen in Fig. 15. The gradient is 240 degrees per 0.010 inch change in wall thickness at the throat.

Similar plots for the injector end are presented in Fig. 16 and 17, except that the sum of land and passage width is used as the parameter for convenience since

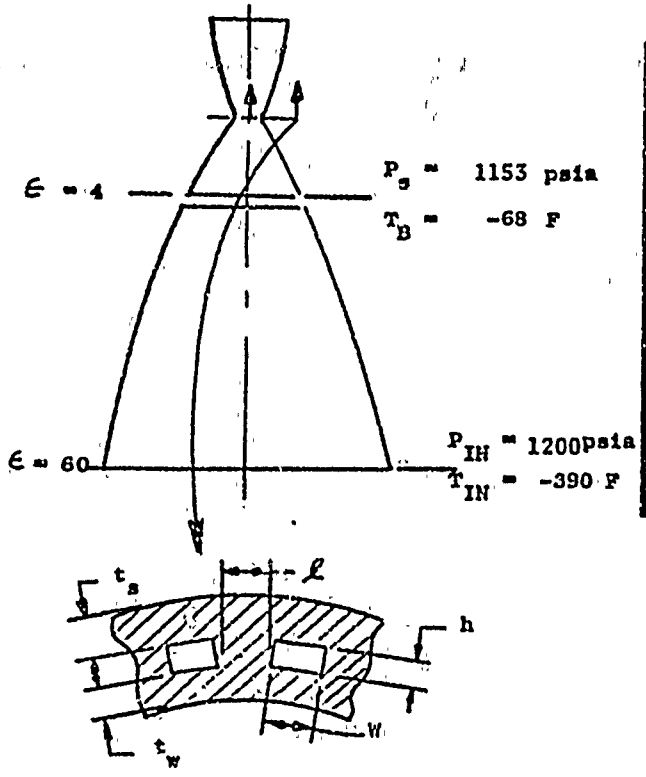

PARAMETER \ LOCATION		INJECTOR FACE	THROAT PLANE	ε = 1
PASSAGE CRITERIA	t_w, in	.032	———	———
	t_s, in	.050	———	———
	W, in	.118	.062	.118
	h, in	.032	.044	.032
	ℓ, in.	.068	.033	.068
WALL TEMPERATURE	T_{wg}(2-D), F	896	743	--
	T_{wc}(2-D), F	812	575	--
	T_{wb}(2-D), F	454	200	--
COOLANT PARAMETERS	T_B, F	302	32	-68
	P_s, psia	1038	1095	1153

COMMENTS

Copper Alloy Chamber
F_2/H_2 Propellants
P_c = 750
MR = 12:1
60 Stepped Width Channels (at X = -2.0)

Figure 8. Channel Geometry Copper Alloy Chamber

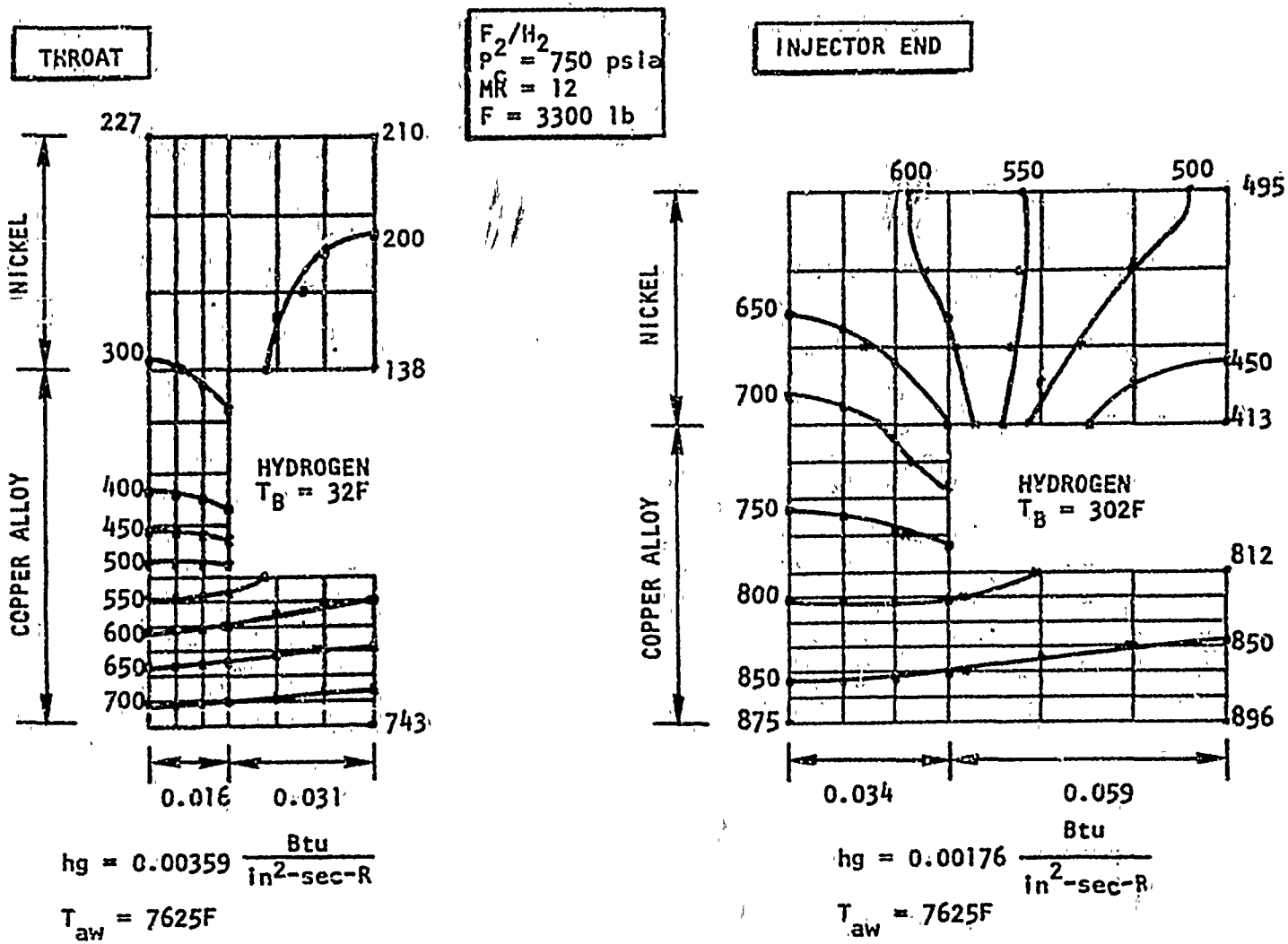

Figure 9. Temperature Distribution for Copper Alloy Chambers (Stepped Width Channels)

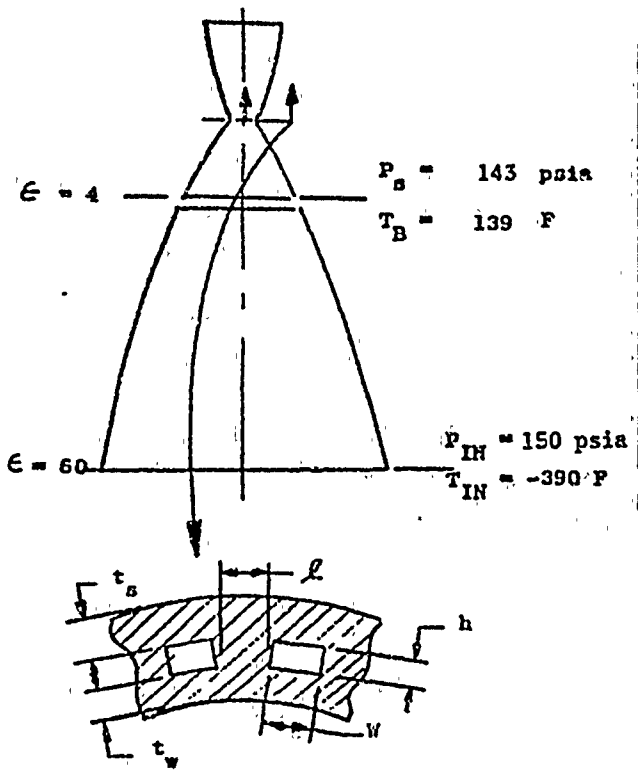

PARAMETER \ LOCATION		INJECTOR FACE	THROAT PLANE	ϵ = 4
PASSAGE CRITERIA	t_w, in	.032	"	"
	t_s, in	.050	"	"
	W, in	.118	.062	.118
	h, in	.032	.044	.032
	ℓ, in	.068	.033	.068
WALL TEMPERATURE	T_{wg}(2-D), F	1052	685	--
	T_{wc}(2-D), F	1039	659	--
	T_{wb}(2-D), F	938	560	--
COOLANT PARAMETERS	T_B, F	722	305	139
	P_s, psia	120	132	143

COMMENTS

Co[illegible]Alloy Chamber
F_2/H_2 Propellants
P_c = 83 psia (Throttled 9:1)
60 Stepped Width Channels

Figure 10. Channel Geometry - Copper Alloy Chambers (Throttled 9:1)

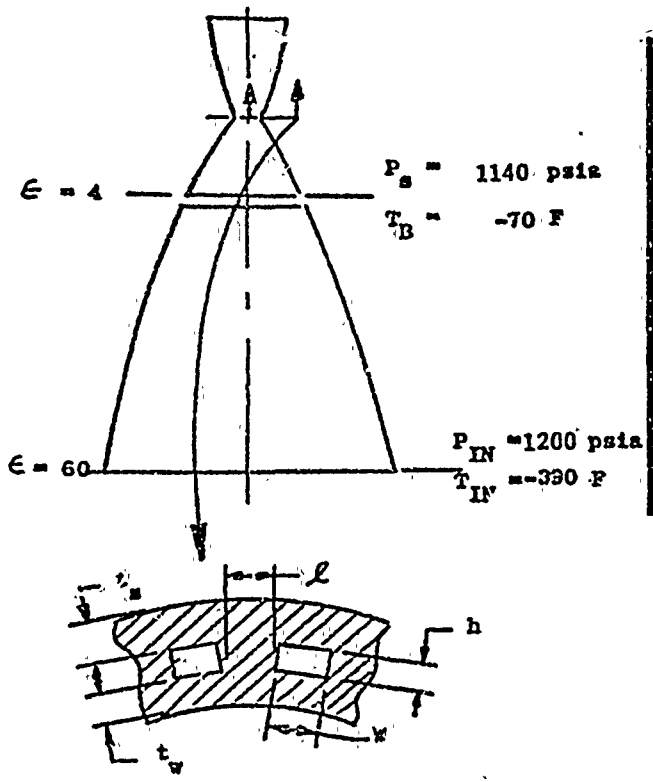

PARAMETER \ LOCATION		INJECTOR FACE	THROAT PLANE	ϵ = 4
PASSAGE CRITERIA	t_w, in	.030	.030	.030
	t_s, in	.060	.060	.060
	W, in	.055	.055	.055
	h, in	.050	.051	.065
	ℓ, in	.131	.041	.131
WALL TEMPERATURE	T_{wg} (2-D), F	844	707	202
	T_{wc} (2-D), F	761	564	165
	T_{wb} (2-D), F	589	220	72
COOLANT PARAMETERS	T_B, F	305	25	-70
	P_s, psia	1000	1083	1140

COMMENTS

Copper Alloy Chambers
F_2/H_2 Propellants
P_c = 750 psia

60 Constant Width Channels

Figure 11. Channel Geometry for Copper Alloy Chamber (Full Thrust)

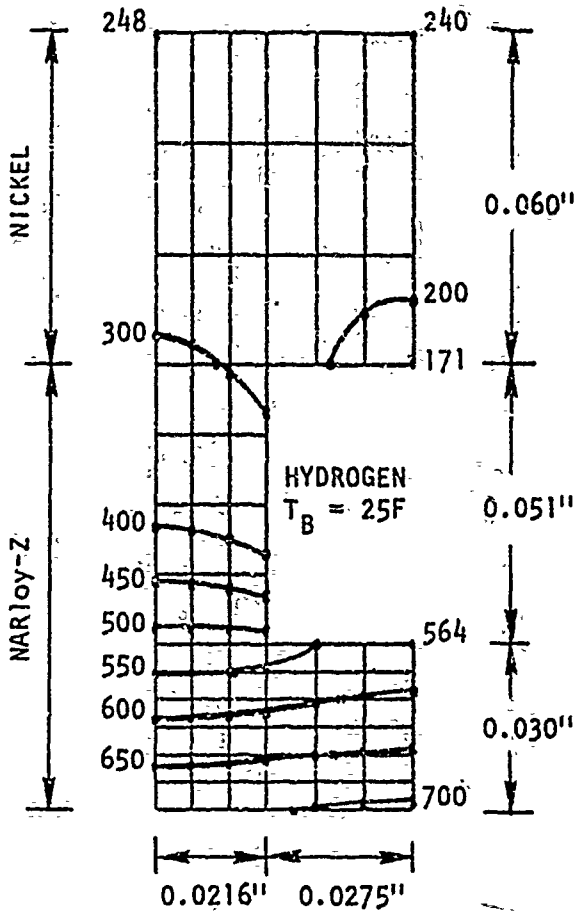

Figure 12. Temperature Distribution for Throat Section of NARloy-Z Chamber

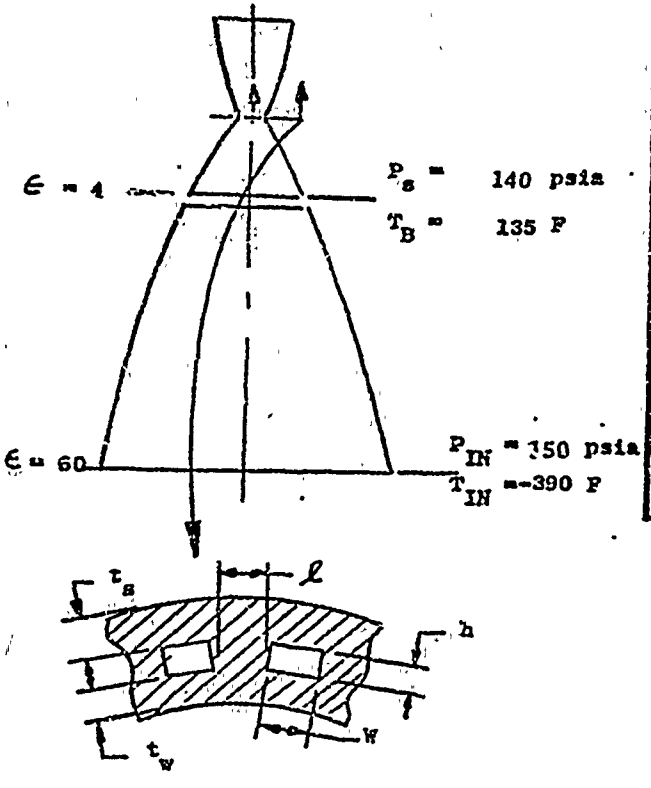

PARAMETER \ LOCATION		INJECTOR FACE	THROAT PLANE	ϵ = 4
PASSAGE CRITERIA	t_w, in	.030	.030	.030
	t_s, in	.060	.060	.060
	W, in	.055	.055	.055
	h, in	.050	.051	.065
	ℓ, in	.131	.041	.131
WALL TEMPERATURE	T_{wg}(2-D), F	1049	674	410
	T_{wc}(2-D), F	1036	651	434
	T_{wb}(2-D), F	997	570	383
COOLANT PARAMETERS	T_B, F	720	292	135
	P_s, psia	100	130	140

COMMENTS

Copper Alloy Chamber
F_2/H_2 Propellants
MR = 12:1
P_c = 83 psia (Throttled 9:1)
60 Constant Width Channels

Figure 13. Channel Geometry for Copper Alloy Chambers Throttled 9:1

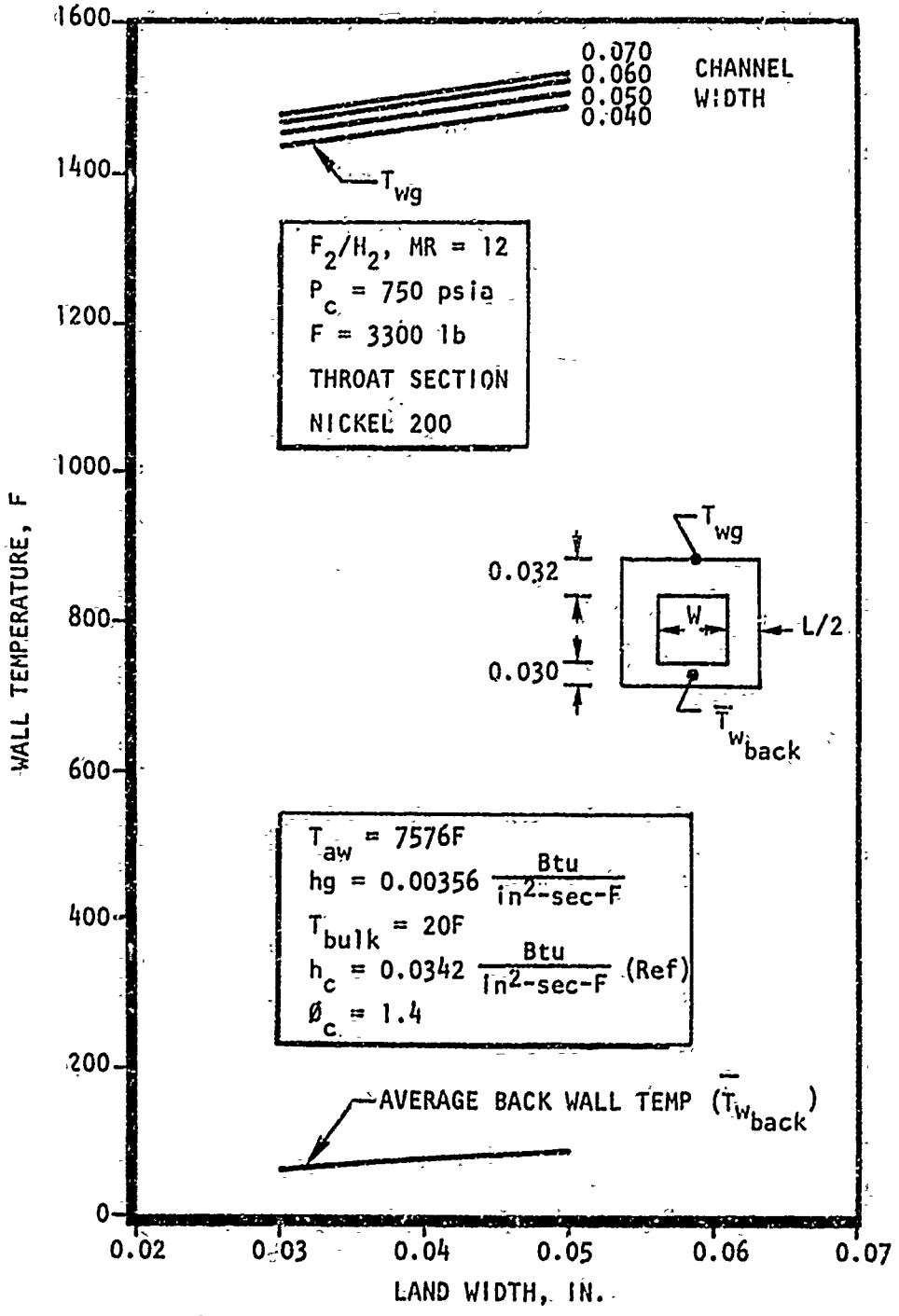

Figure 14. Effect of Channel Dimensions on Throat Wall Temperatures

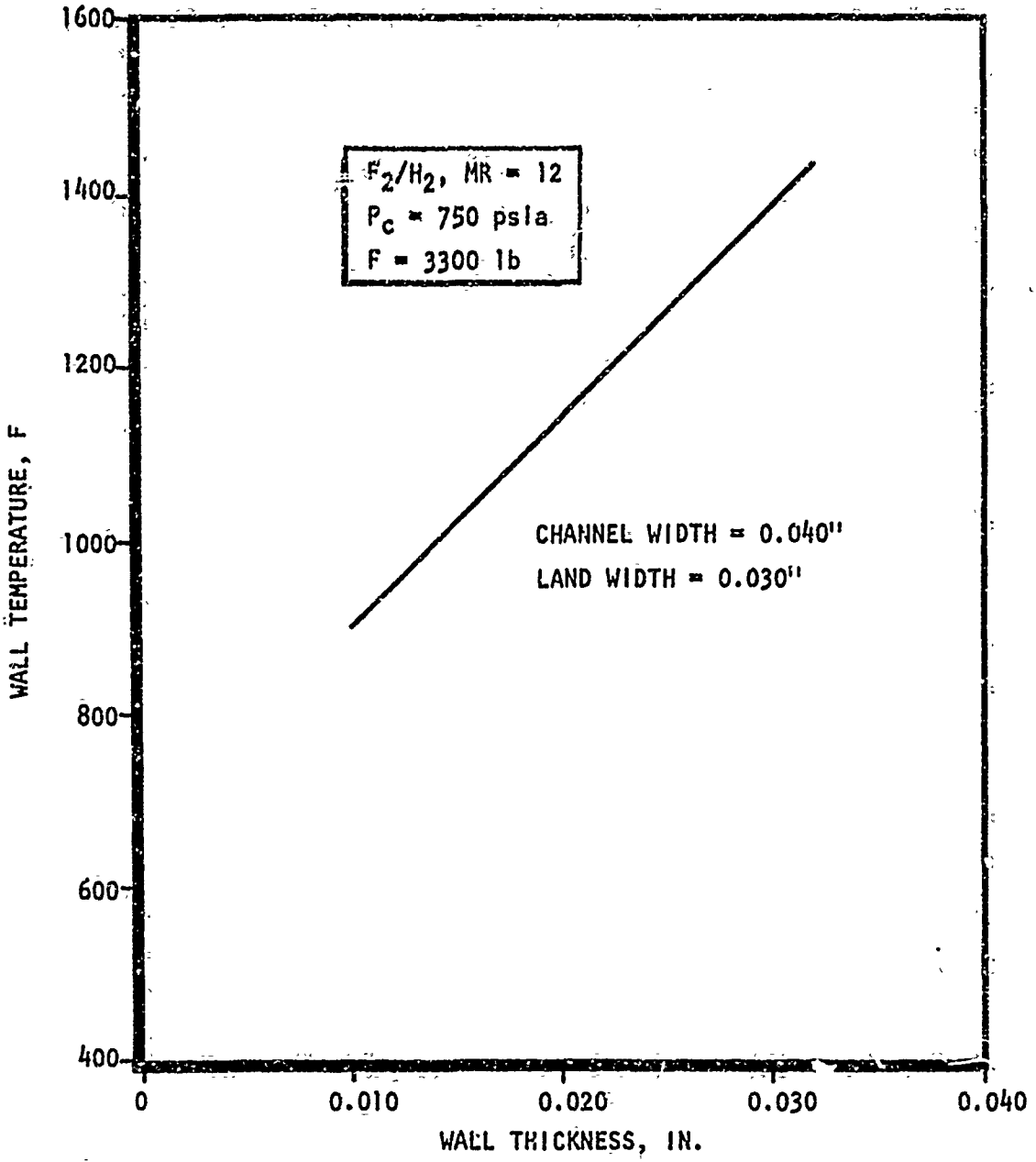

Figure 15. Effect of Hot-Wall Thickness on Maximum Wall Temperatures for All-Nickel Throat Section

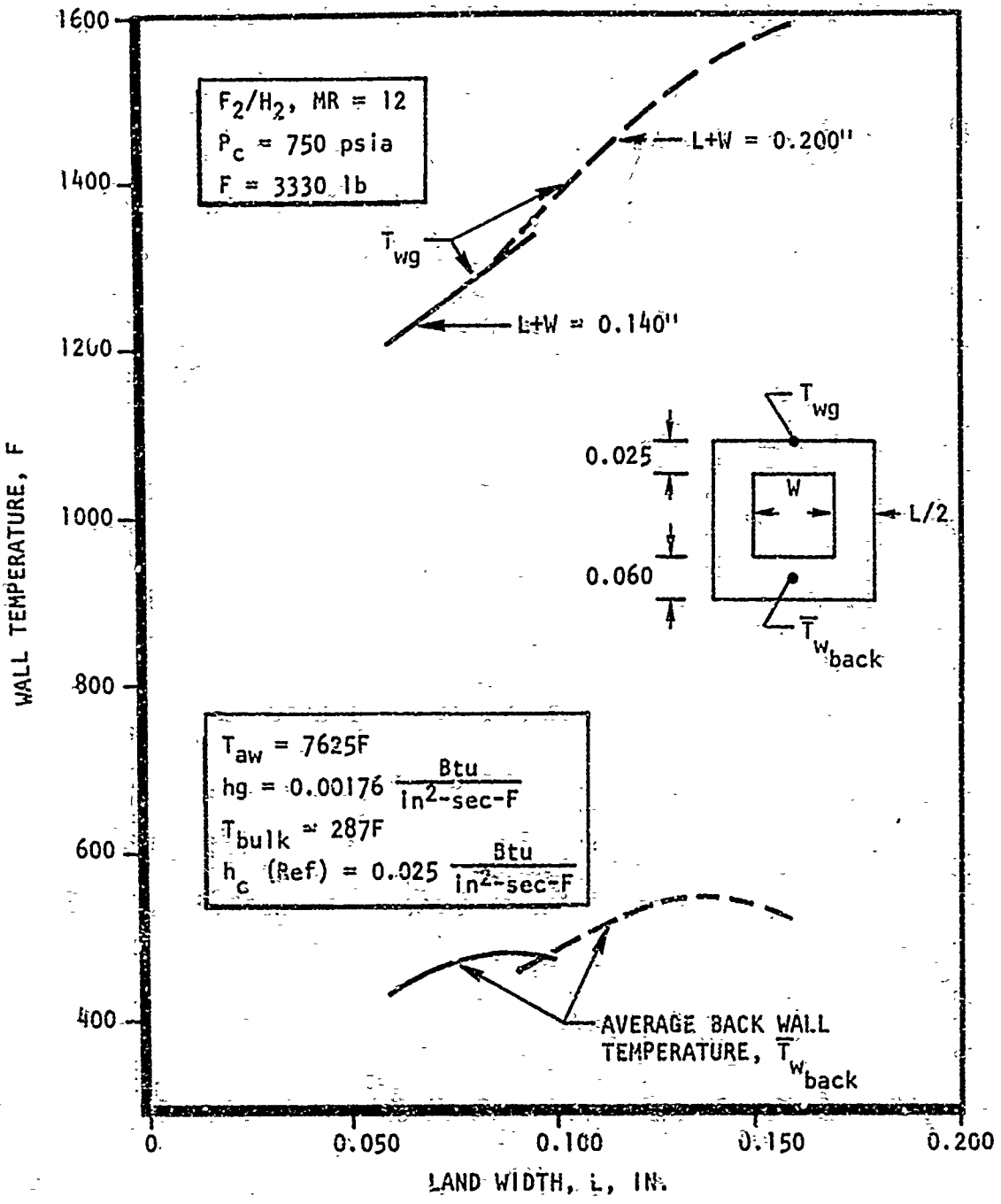

Figure 16. Effect of Channel Dimensions on Wall Temperature for All-Nickel Chamber (Injector End)

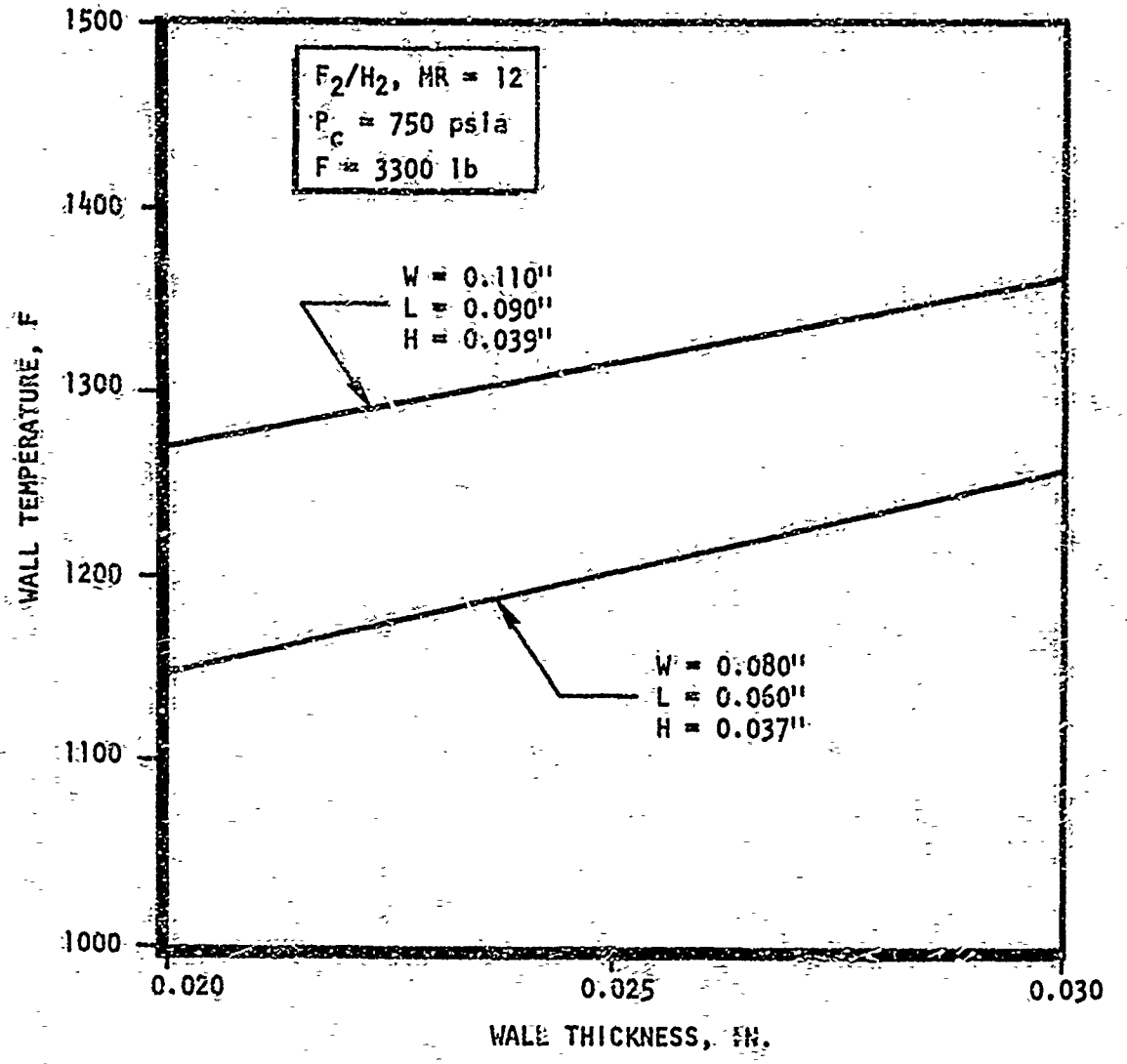

Figure 17. Effect of Hot-Wall Thickness on Maximum Wall Temperature for All-Nickel Chamber-Injector End

it is related to the throat value by the contraction ratio:

$$(L + W)_{injector} = \varepsilon_c \, (L + W)_{throat}$$

At the injector end the gas-side wall temperature varies 35 degrees per 0.010 inch change in channel width. Average back wall temperature changes 22 degrees per 0.010 inch change in land width, reaching a maximum, then declining with increasing land due to the two-dimensional heat flow to the back of the channel. Gas-side wall temperature decreases 100 degrees per 0.010 inch decrease in wall thickness at the injector end.

Revised Thermal Analysis - F_2/H_2 Propellants

As a result of experimental heat flux data obtained by the AFRPL in copper heat sink chambers the gas side film coefficient was revised (Fig. 18). This film coefficient profile was established analytically using the Rocketdyne Boundary Layer Program modified to integrate the experimental data from the AFRPL test effort. This experimental data indicated the boundary should be initiated approximately two inches above the throat.

Using this gas-side film coefficient, heat flux profiles were established for a nickel 200 chamber (T_{wg} = 1400 F) and a copper alloy (NARloy-Z or zirconium-copper) chamber (T_{wg} = 1000 F). These are shown in Fig. 19 and 20, and reflect peak heat flux values of 27.1 Btu/in.^{2}-sec for the nickel 200 design and 27.6 Btu/in.^{2}-sec for the copper alloy designs; occurring at the same point, ~0.10 inches forward of the geometric throat.

Nickel 200 Thrust Chamber. Resulting analysis on the nickel 200 chamber established a coolant circuit geometry consisting of 72 channels. These channels are 0.040 inches wide from the exit (ε = 4) to -2.75 inches forward of the throat where a step width increase to 0.080 inches is made. The passage height varies from 0.020 inch at the exit and injector ends to 0.030 inch at the throat. The passage pressure drop predicted is slightly below 300 psi with a 10 psi exit loss. Bulk temperature rise is 410 F. The predicted two dimensional gas-side wall

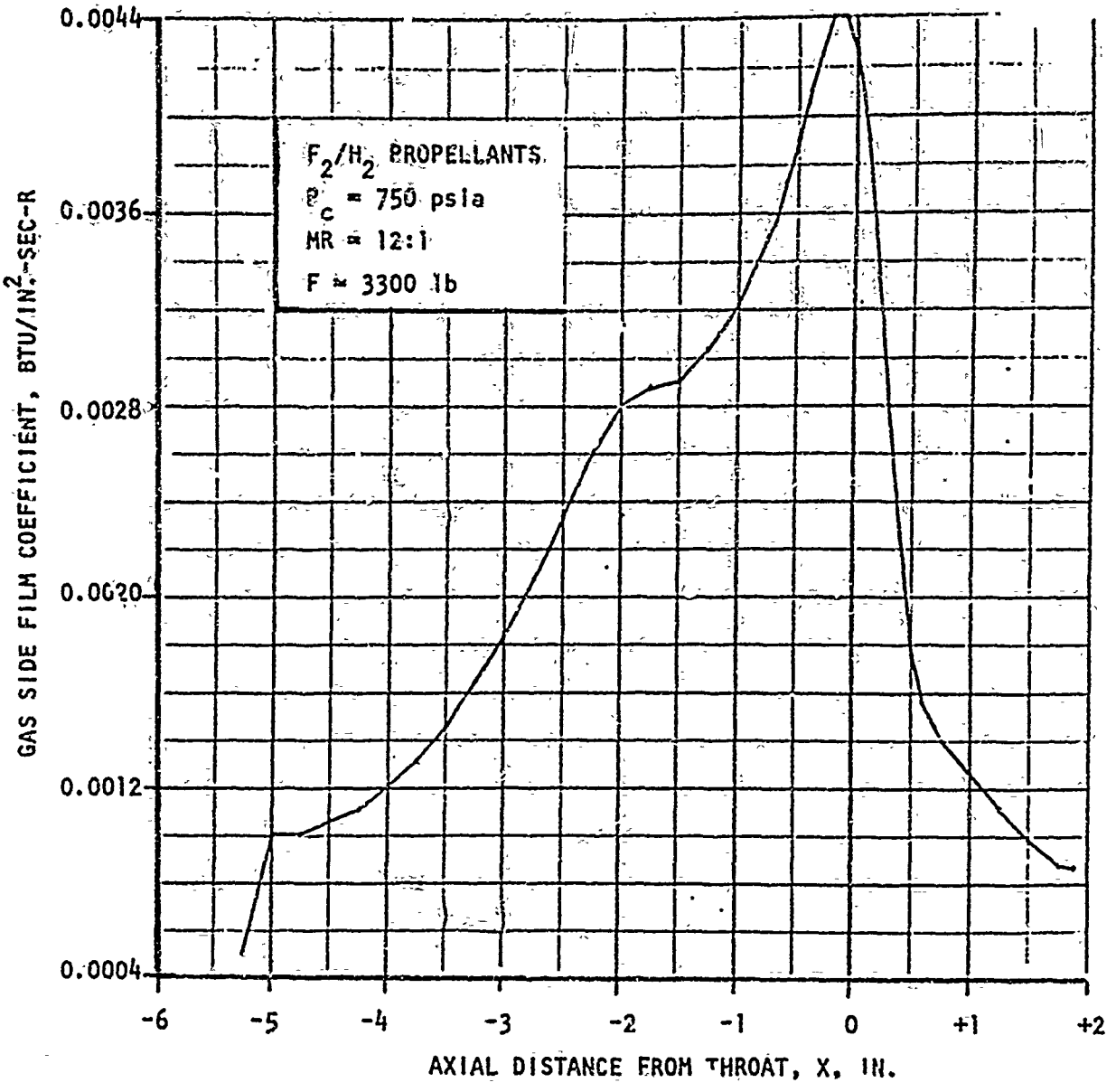

Figure 18. Gas-Side Film Coefficient Distribution

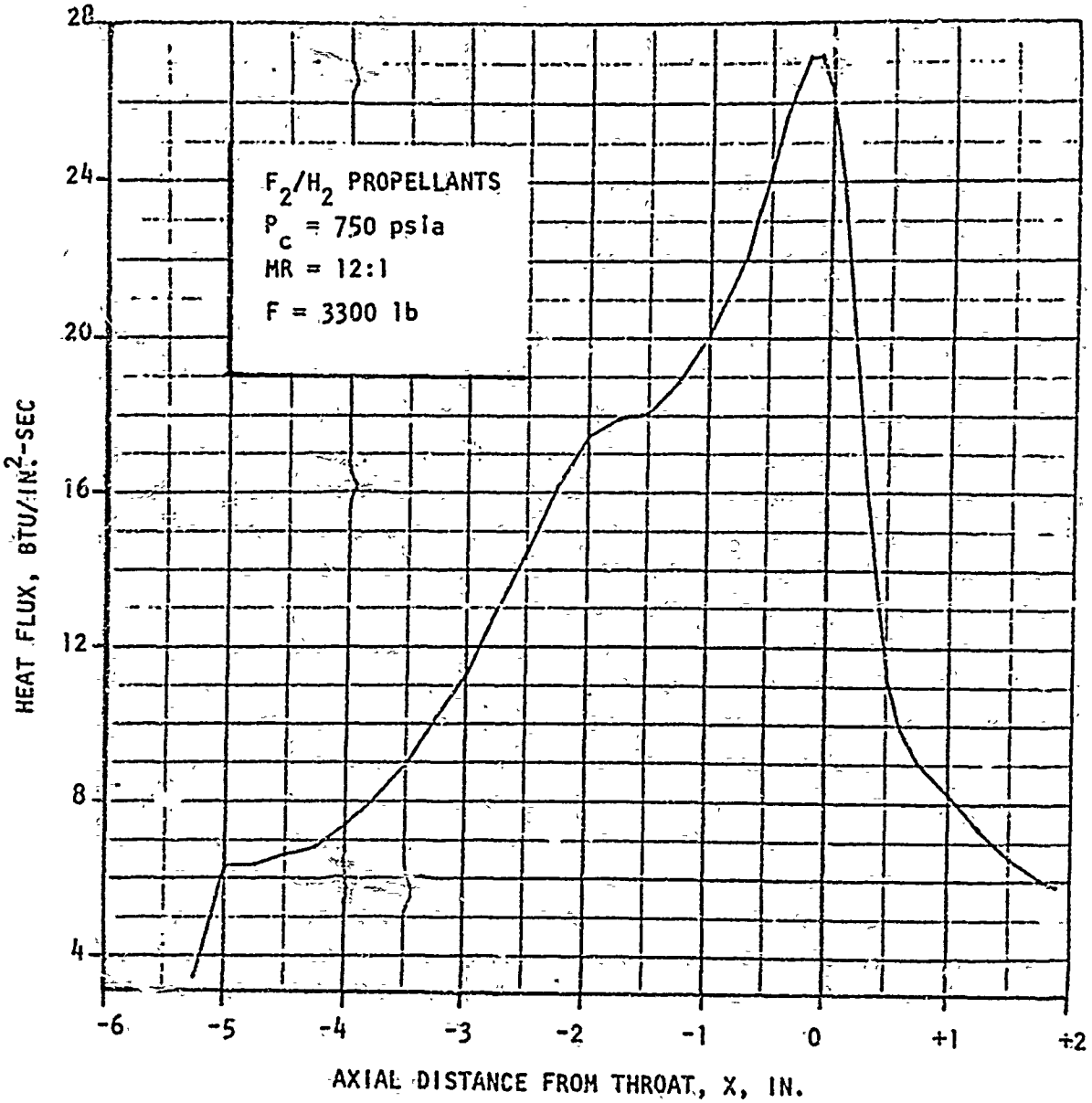

Figure 19. Heat Flux Distribution for Spun Nickel Chamber

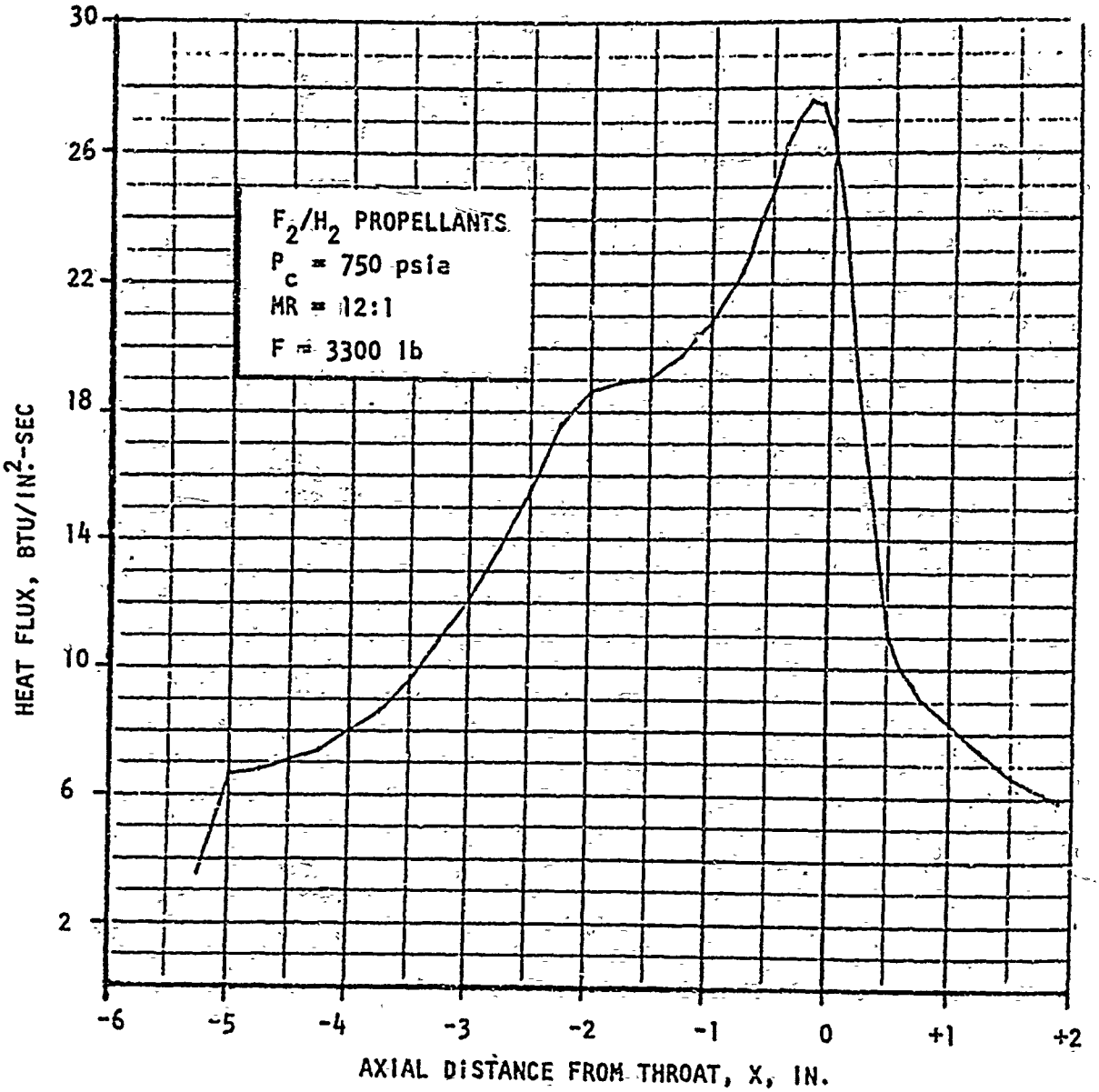

Figure 20. Heat Flux Distribution for Copper Alloy Chamber

temperatures (Fig. 21) are close to 1450 F from the throat upstream to about -2.75 inches decreasing somewhat uniformly to 1200 F at the injector and 700 F at the nozzle exit.

Chamber operating conditions are summarized in Fig. 22.

Copper Alloy Thrust Chambers. Using the heat flux profile presented previously (Fig. 20), the copper alloy chambers were also analyzed. As discussed previously, the elevated temperature thermal conductivities of the two copper alloys are virtually the same, therefore, the chambers can be identical from a thermal standpoint.

The thermal analysis showed that 60 constant-width (0.055 inches) channels were suitable for these designs. Passage height varied from 0.090 inch at the exit and injector ends to 0.046 inches in the throat and 0.030 at -2.25 inches above the throat. Pressure drop in the coolant passage was about 240 psi with a 30 psi exit loss, and bulk temperature rise of 428 F. Two-dimensional gas-side wall temperatures were about 1000 F from the throat to -2.25 inches upstream (Fig. 23). Chamber operating conditions are summarized in Fig. 24.

Initial Thermal Analysis O_2/H_2 Propellant

Copper Alloy Chamber. The NARloy-Z and zirconium-copper thrust chambers were also analyzed for operation with LO_2/H_2 propellants under the conditions specified previously and an assumed injector combustion efficiency (η_{c*}) of 99 percent. (The use of O_2/H_2 propellant insteady of F_2/H_2 provides a comparable thermal environment with reduced propellant cost). A boundary layer analysis of the combustor contour with a 6 inch length results in the gas-side film coefficient distribution shown in Fig. 25 for LO_2/H_2. The combustor for the O_2/H_2 design was 1 inch longer than that for the F_2/H_2 design to assure good combustion efficiency was achieved. The 30 percent increase in film coefficient (as compared to the F_2/H_2 data) is largely compensated by lower combustion temperature to yield an only slightly higher peak heat flux (28 Btu/in.^{2}-sec) at the sonic point (Fig. 26). Integrated heat load is about 44 percent higher with LO_2/H_2

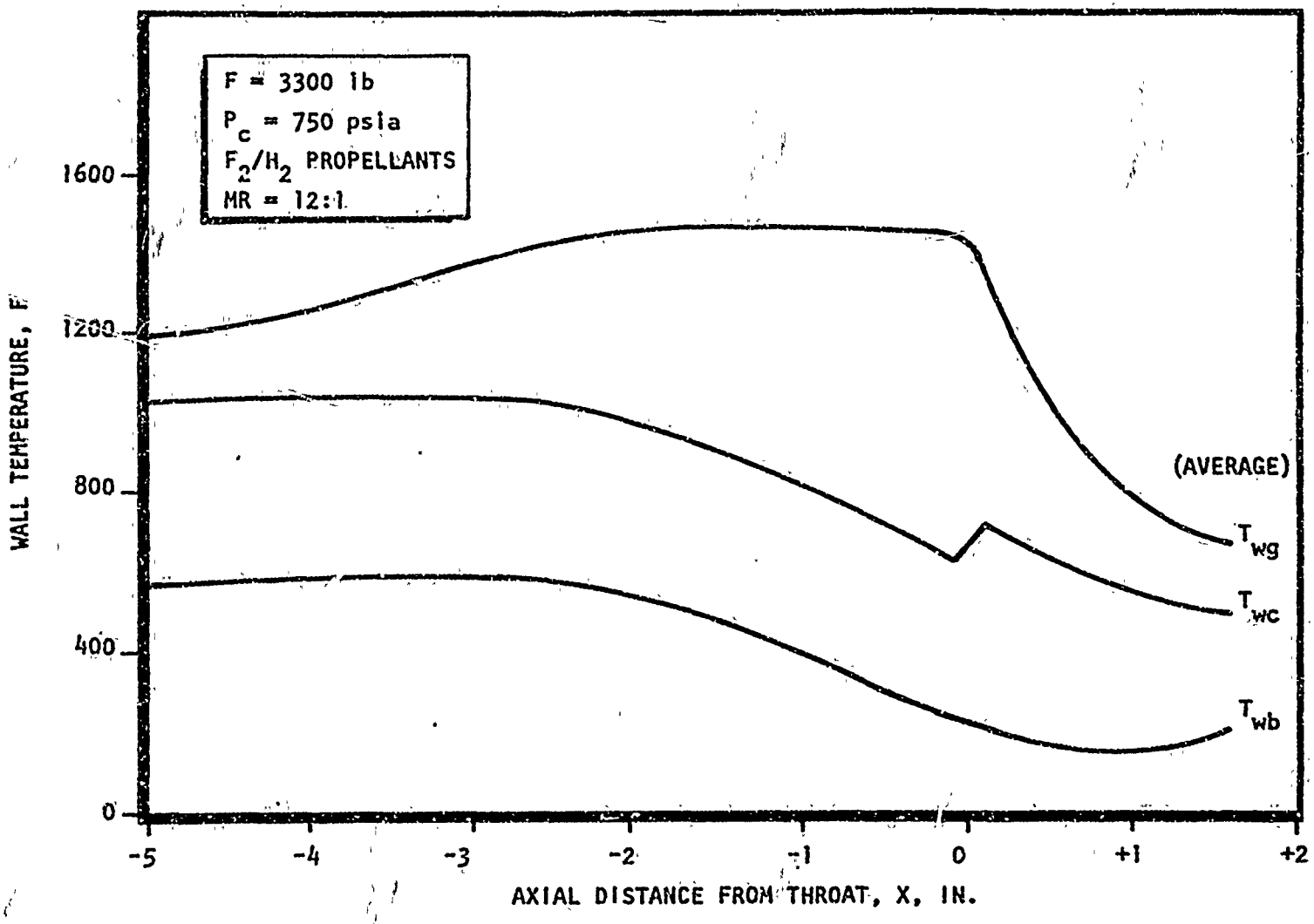

Figure 21. Thermal Fatigue Thrust Chamber Wall Temperature Distribution (2-D) Spun Nickel 200

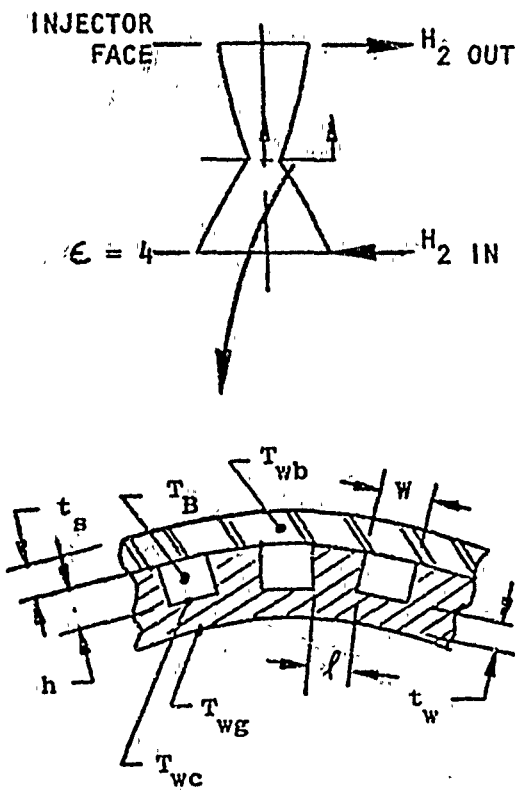

FABRICATION CONCEPT: SPUN AND MACHINED NICKEL LINERS

PARAMETER \ LOCATION*	1.875	-0.1	-1.75	-2.75	-3.0	-4.75
	NOZZLE (ϵ=4)	THROAT	CHAMBER	CHAMBER	CHAMBER	INJECTOR END
Passage Criteria						
t_w, in.	.025	.025	.025	.025	.025	.025
t_s, in.	.060	.060	.060	.060	.060	.060
W, in.	.040	.040	.040	.040	.080	.080
h, in.	.090	.0305	.0435	.0700	.050	.090
ℓ, in.	.1146	.0398	.0808	.100	.0627	.0749
N	72	72	72	72	72	72
Temperature						
T_{wg} (2-D) F	675	1452	1473	1424	1385	1190
T_{wc} (2-D) F	495	633	930	1046	1086	1020
T_{wb} (2-D) F	210	255	535	590	550	585
Coolant						
T_B, F	80	152	285	364	380	480
P_{static}, psia	1181	897	826	853	880	891

F_2/H_2 PROPELLANTS
P_c = 750 PSIA
MR = 12:1

* Inches from geometric throat

Figure 22. Final Design - Nickel 200 Thrust Chambers

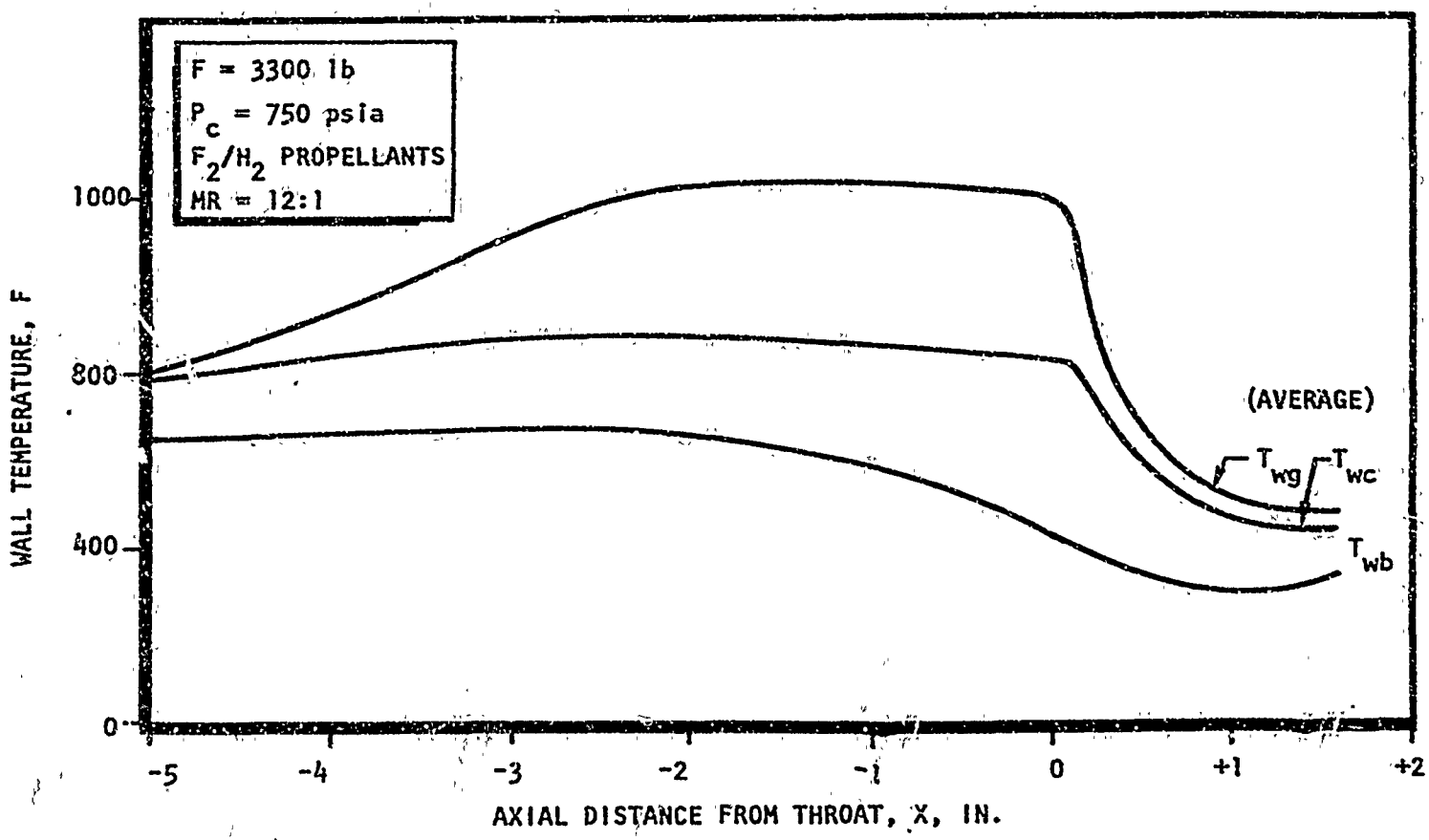

Figure 23. Thermal Fatigue Thrust Chamber Wall Temperature Distribution (2-D) Copper Alloy

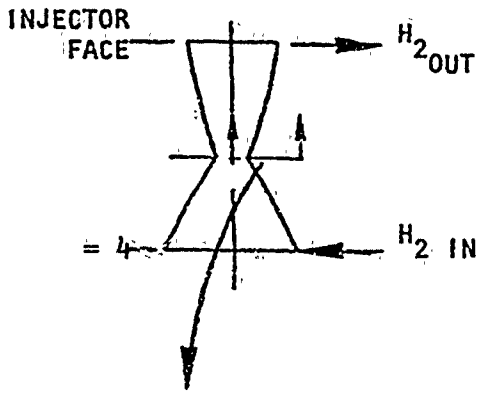

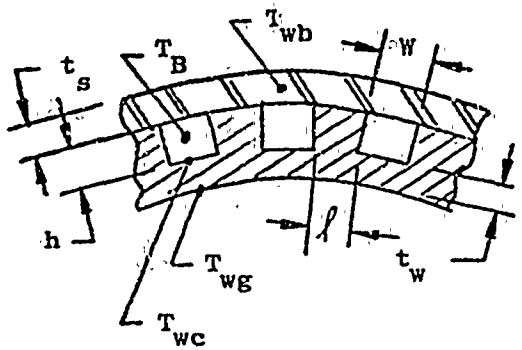

FABRICATION CONCEPT: SPUN AND MACHINED COPPER ALLOY LINER

LOCATION* / PARAMETER	1.875 EXIT	-0.1 THROAT	-1.75 CHAMBER	-2.25 CHAMBER	-3.0 CHAMBER	-5.0 INJECTOR
Passage Criteria						
t_w, in.	.030	.030	.030	.030	.030	.030
t_s, in.	.060	.060	.060	.060	.060	.060
W, in.	.055	.055	.055	.055	.055	.055
h, in.	.090	.046	.037	.030	.0598	.090
ℓ, in.	.131	.0413	.0905	.103	.117	.131
N	60	60	60	60	60	60
Temperature						
T_{wg} (2-D) F	490	1001	1007	941	994	840
T_{wc} (2-D) F	460	827	881	817	916	805
T_{wb} (2-D) F	338	440	655	645	728	690
Coolant						
T_B, F	80	155	291	332	385	498
P_{static}, psia	1186	1114	962	753	924	933

* Inches from geometric throat

F_2/H_2 PROPELLANTS
P_c = 750 PSIA
MR = 12:1

Figure 24. Final Design - Copper Alloy Thrust Chambers

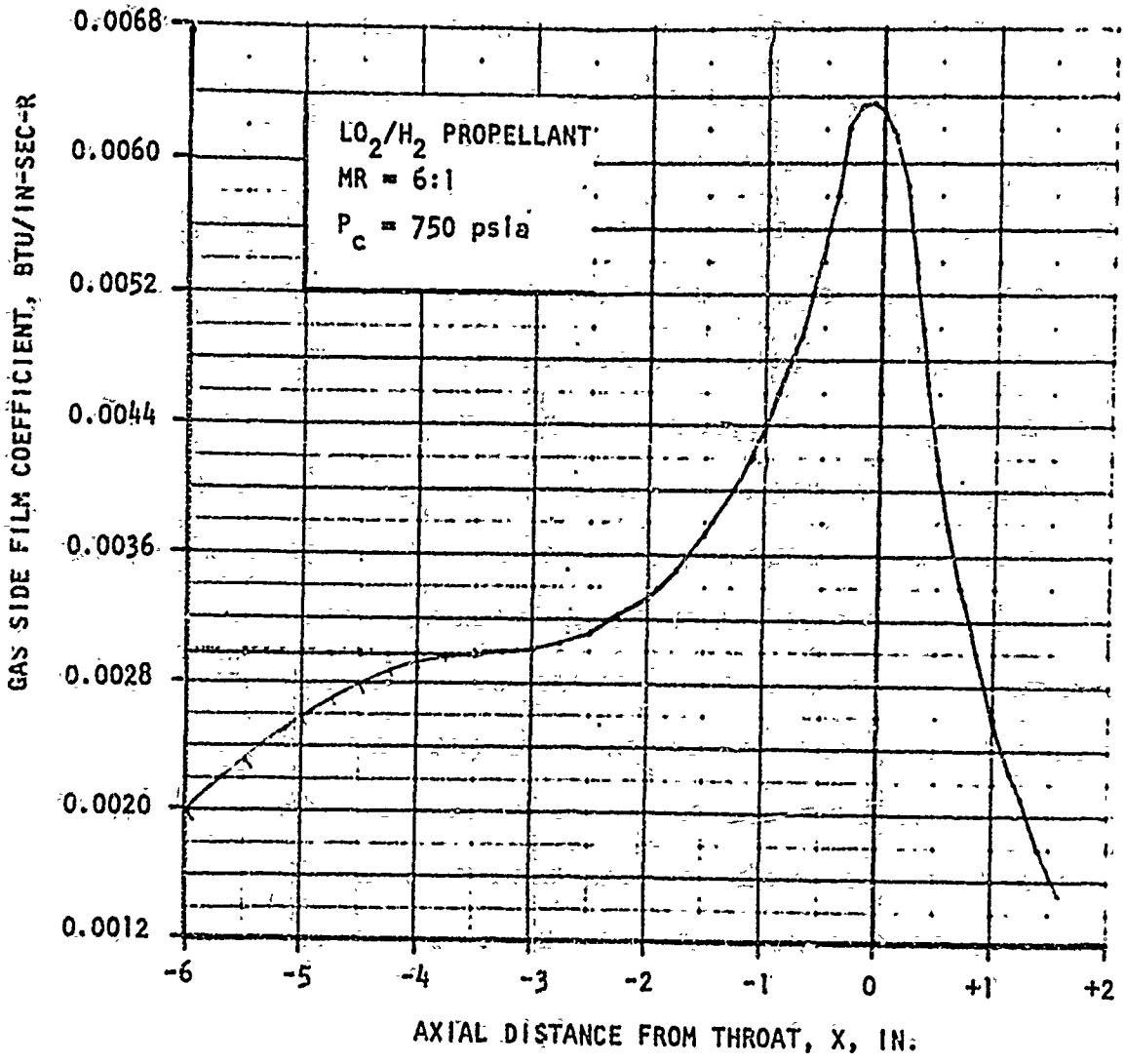

Figure 25. Gas-Side Film Coefficient

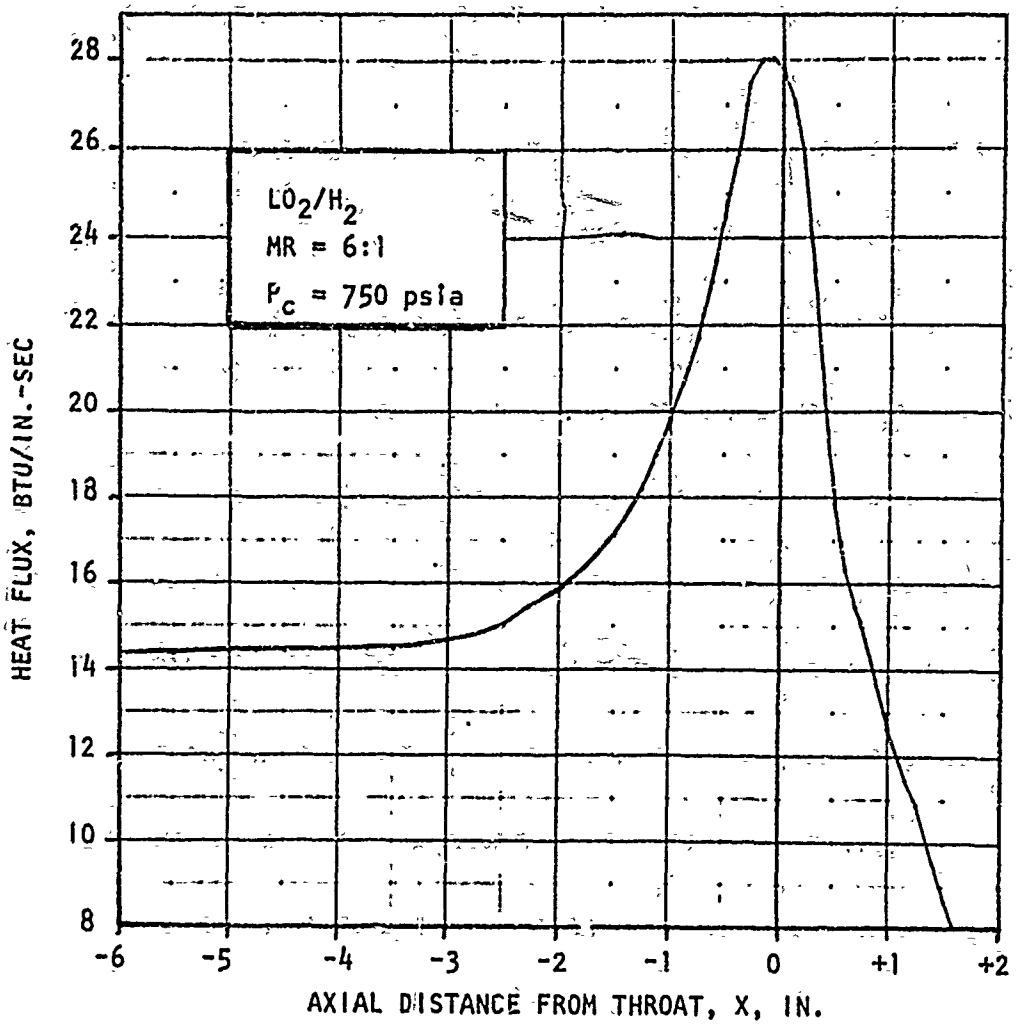

Figure 26. Heat Flux Profile

and the longer (6 inch) combustor. This heat flux profile was used to establish the coolant channel geometry for both copper alloy chambers. The design was optimized for 200 R hydrogen inlet at an area ratio of 4:1. This simulates the approximate bulk temperature at an area ratio of 4:1 of a cooled 60:1 nozzle with an inlet temperature of 65 R. The design consisted of 40 channels 0.080 inches wide with a nominal wall thickness of 0.035 inches. The coolant pressure drop was 125 psi based on an inlet pressure of 1200 psia. The coolant pressure profiles (total and static) are presented in Fig. 27.

The wall temperature profile is shown in Fig. 28. In the throat region the wall temperature is below 900 F. Near the injector the wall temperature increases to about 900 F. Also shown in Fig. 28 for comparison is a temperature profile for the same chamber but using ambient temperature hydrogen as the coolant. The coolant flowrate was increased in the case of ambient hydrogen in order to match throat wall temperatures and, hopefully, thermal strains. Consideration was given to the use of ambient temperature hydrogen as the coolant since this would preclude the need for delivery of conditioned hydrogen to the hardware and to allow for testing with coolant flow in parallel with the injector hydrogen flow. It is apparent, however, that the back wall temperatures for the ambient inlet hydrogen are almost 200 F higher than the nominal (200 R inlet temperature) design. The thermal strains are, therefore, not as severe for the ambient hydrogen case considered as compared to the nominal design conditions. Reduced flowrate for the ambient hydrogen case would increase the thermal strains but would also increase the maximum wall temperatures.

Nickel-200 Chamber. The nickel-200 chamber, which was originally analyzed for operation with fluorine hydrogen propellants was reanalyzed for use with oxygen-hydrogen propellants and ambient temperature hydrogen coolant. Coolant channel height and flowrate were adjusted such that the chamber would operate with gas-side wall temperatures similar to those with cryogenic coolant. It was recognized, however, that the back wall temperature would be much higher resulting in a lower thermal strain range than that experienced by a comparable chamber cooled with cryogenic hydrogen.

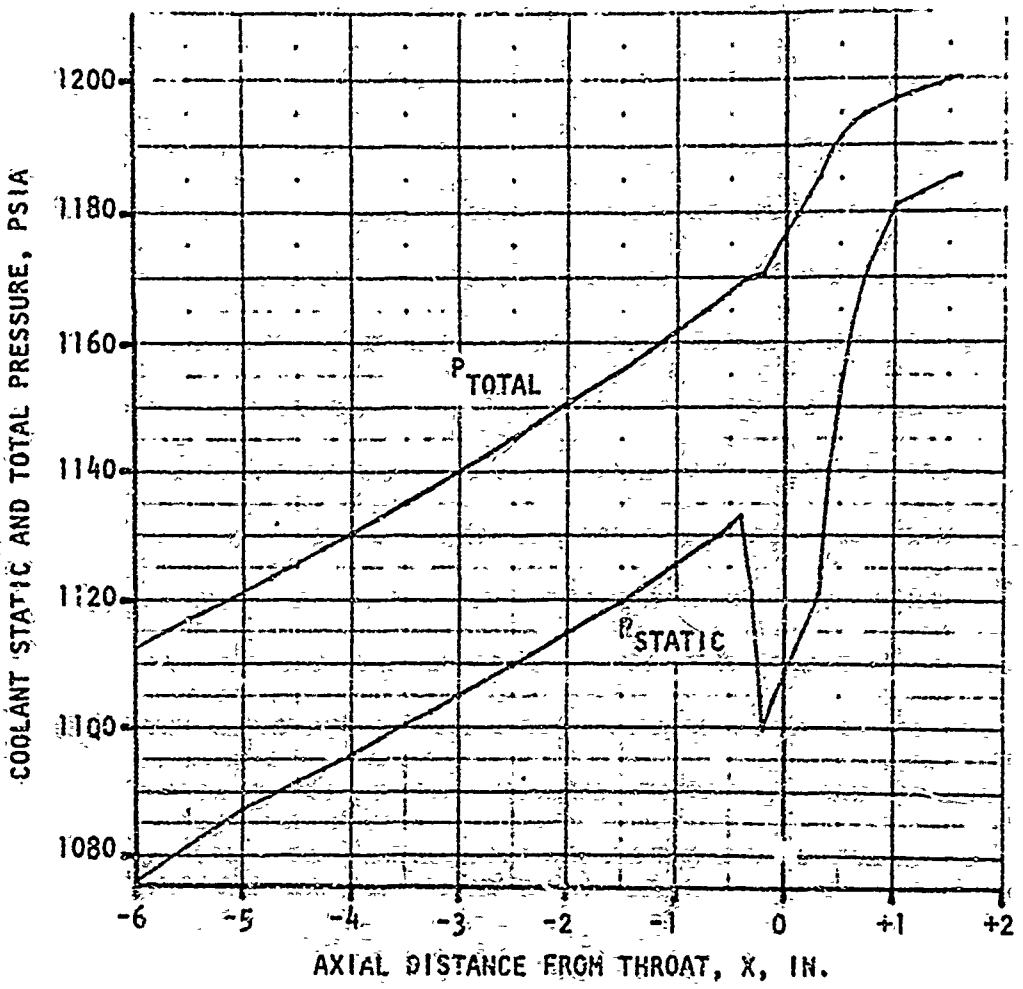

Figure 27. Coolant Pressure Profile for the NARloy-Z Thermal Fatigue Thrust Chamber

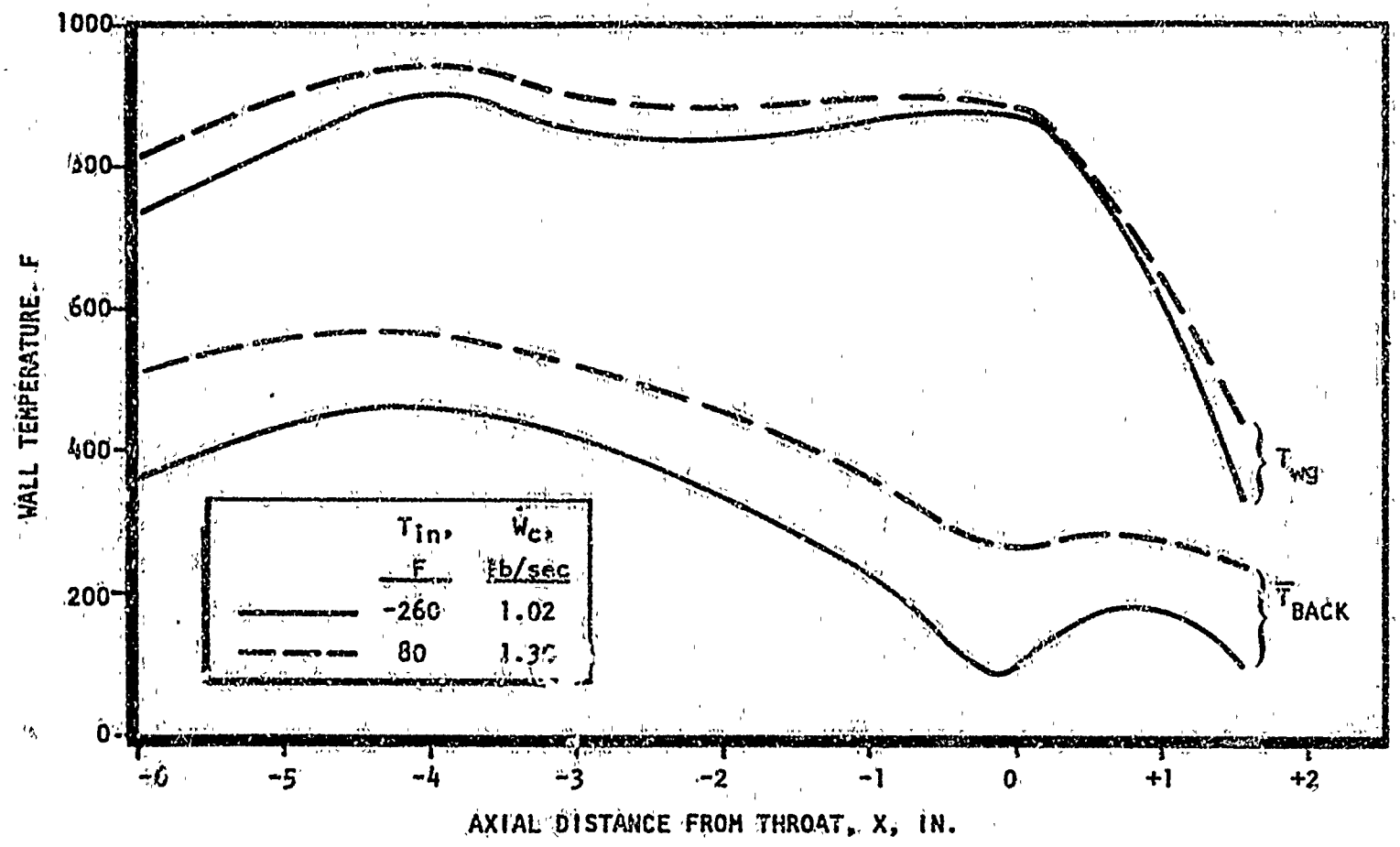

Figure 28. Wall Temperature Profiles for the NARloy-Z Thermal Fatigue Thrust Chamber

The modifications to the nickel-200 chamber design were as follows. The wall thickness was reduced to a uniform 0.025 inch. The 0.040 inch passage width extended from -2.75 inches above the throat to the exit. The passage width stepped to 0.080 inches wide at -2.75 inches and extended to the injector end. Passage height tapered from 0.090 inch at the injector to 0.0305 at the throat and back to 0.090 inch at the exit end.

Revised Thermal Analysis - O_2/H_2 Propellants

The thermal analysis of the nickel and copper alloy chamber was revised based on experimental heat flux data obtained by the AFRPL. This data was obtained from a copper water-cooled calorimeter chamber utilizing O_2/H_2 propellants at a mixture ratio of about 6:1. The nominal chamber pressure was 743 psia. The resulting heat flux profile for the calorimeter chamber is presented in Fig. 29. The original design heat flux profile is also presented for comparison purposes.

It is apparent that the experimental heat flux is considerably lower than the design value in the combustion zone region. The low heat flux values near the injector face are typical of coaxial type injectors. The high design value in this region was selected to provide considerable margin of safety in case of injector streaking.

The experimental throat heat flux is about 31 Btu/in.^{2}-sec compared to a predicted value of 28 Btu/in.^{2}-sec. These heat flux levels are based on a nominal hot-gas wall temperature of 1200 F. The slightly higher (~10 percent) throat heat flux level does not significantly effect the chamber operating limits as will be shown.

The revised heat flux profile was used in conjunction with the regenerative cooling analysis to predict the coolant bulk temperature rise and chamber wall temperature profiles. In order to accomplish the computer analysis it was necessary to convert the heat flux profile to a combustion gas convective film coefficient (h_g) profile. This was accomplished using the relation:

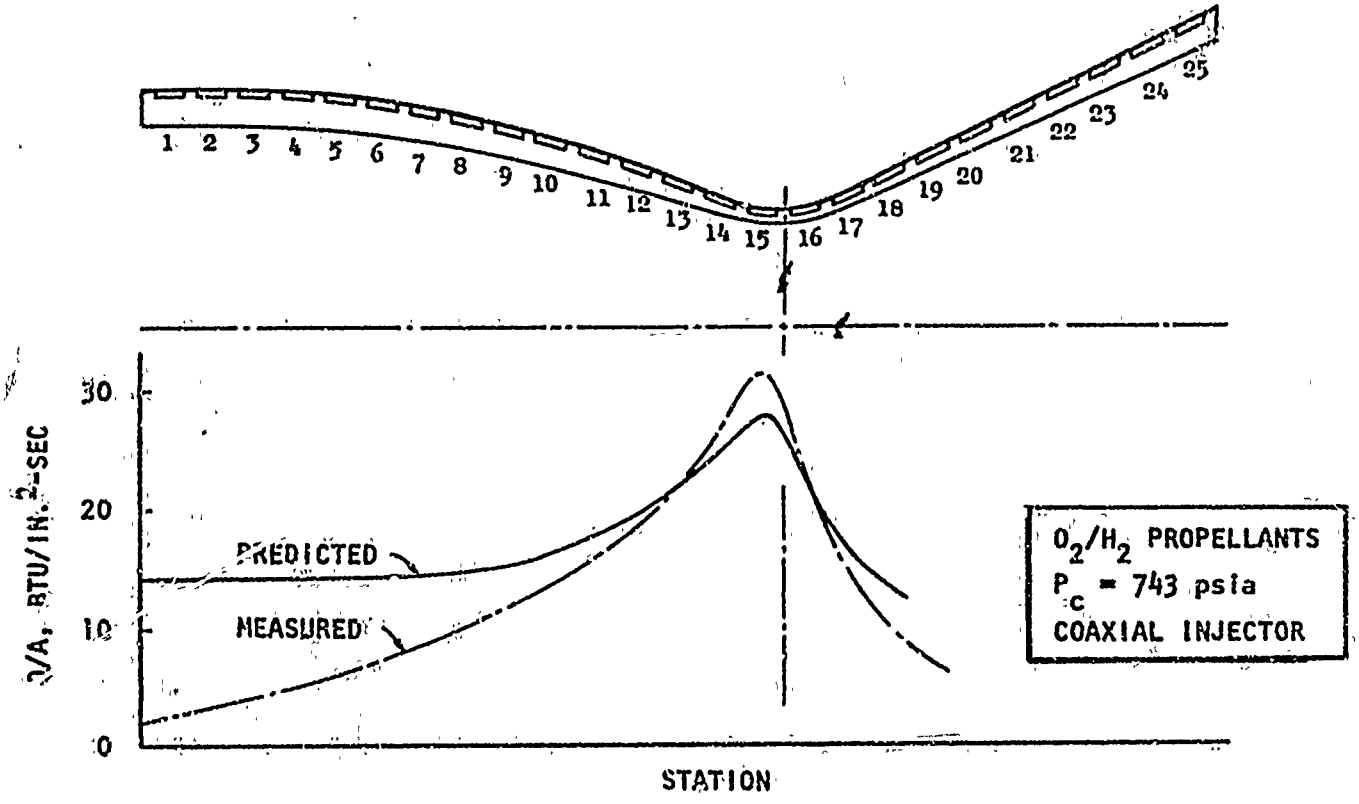

Figure 29. Calorimetric Chamber Heat Flux Profile

$$h_g = \frac{Q/A}{T_{aw} - T_{wg}}$$

It was assumed that the hot gas wall temperature (T_{wg}) of the calorimeter chamber was 1200 F for purposes of determining the film coefficient. A more detailed evaluation of the heat flux data would be required to determine actual wall temperatures and thereby increase the accuracy of the film coefficient profile. The uniform wall temperature assumption is sufficiently accurate (± 10 percent) for the preliminary thrust chamber analysis. The resulting film coefficient profile is shown in Fig. 30 and the heat flux profile is shown in Fig 31.

The nickel-200 thrust chamber was then analyzed using the experimental results discussed previously. A nominal hydrogen coolant flowrate of 0.65 lb/sec was selected to obtain a direct comparison to cooled chamber test results. The resulting coolant pressure, coolant bulk temperature and hot-gas wall temperature profiles are presented in Fig. 32, 33 and 34, respectively.

The nominal coolant bulk temperature rise is estimated to be 306 F. The maximum hot gas wall temperature is about 1480 F and occurs slightly upstream of the throat. Near the injector the wall temperature decreases to less than 700 F.

The copper-alloy thrust chambers were also analyzed at various operating conditions using the experimental combustion gas convective heat transfer results. The chamber was analyzed at nominal operating conditions (P_c = 750 psia, MR = 6, W_c = 1.07 lb/sec) with ambient and conditioned temperature hydrogen. The conditioned hydrogen inlet temperature (360 R) was selected so as to deliver ambient temperature propellant to the injector in a regenerative cooling configuration. Over-cooled operation with ambient inlet temperature hydrogen was also investigated at chamber pressures of 750, 500, and 300 psia.

These analyses were done since it was planned to conduct the initial hot firing tests of both chambers at lower chamber pressure using ambient temperature hydrogen as the coolant in a bypass mode. In this manner the environment is less severe than at the design point, reducing the risk to the hardware during initial

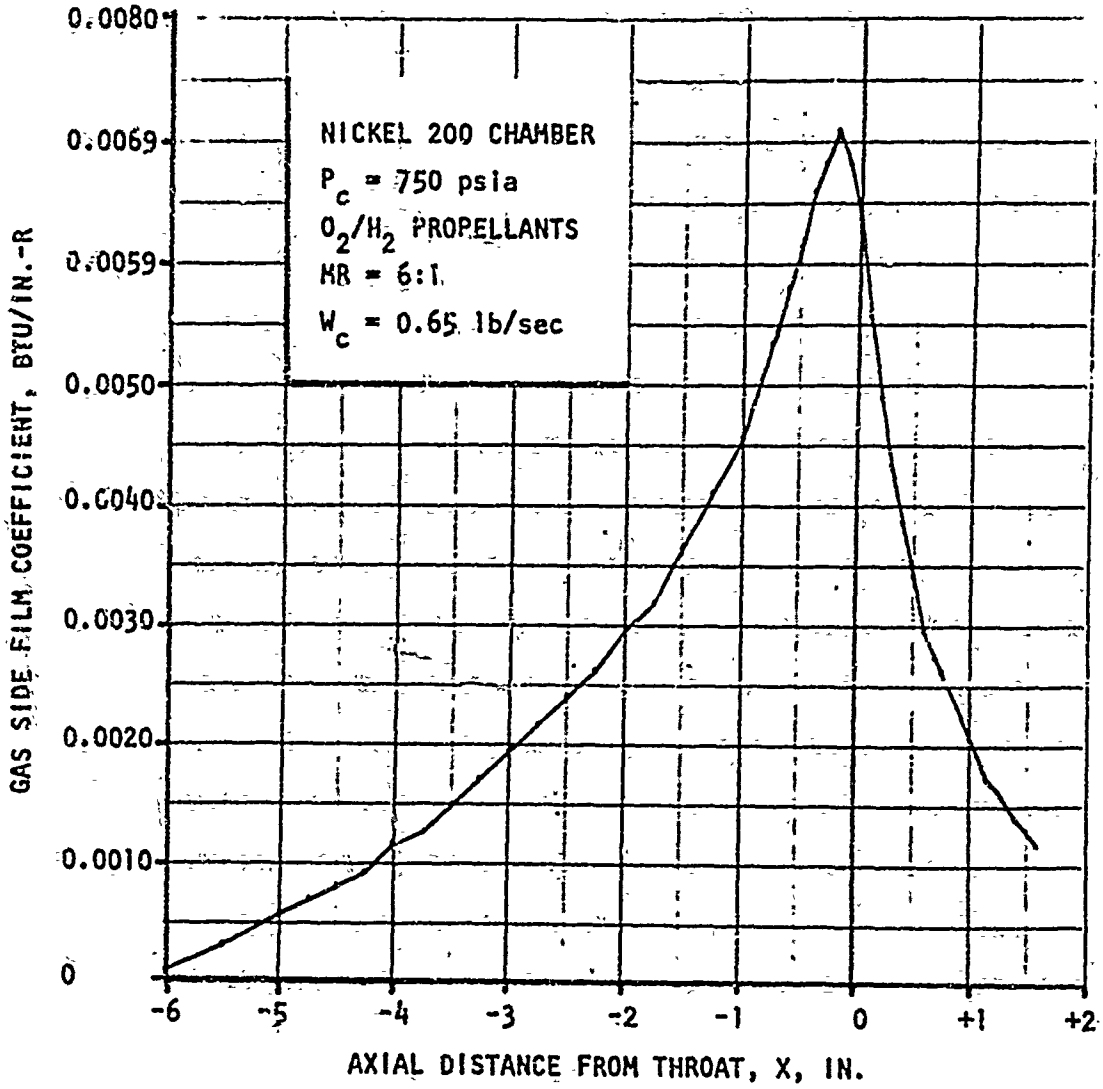

Figure 30. Experimental Combustion Gas Convective Film Coefficient Profile

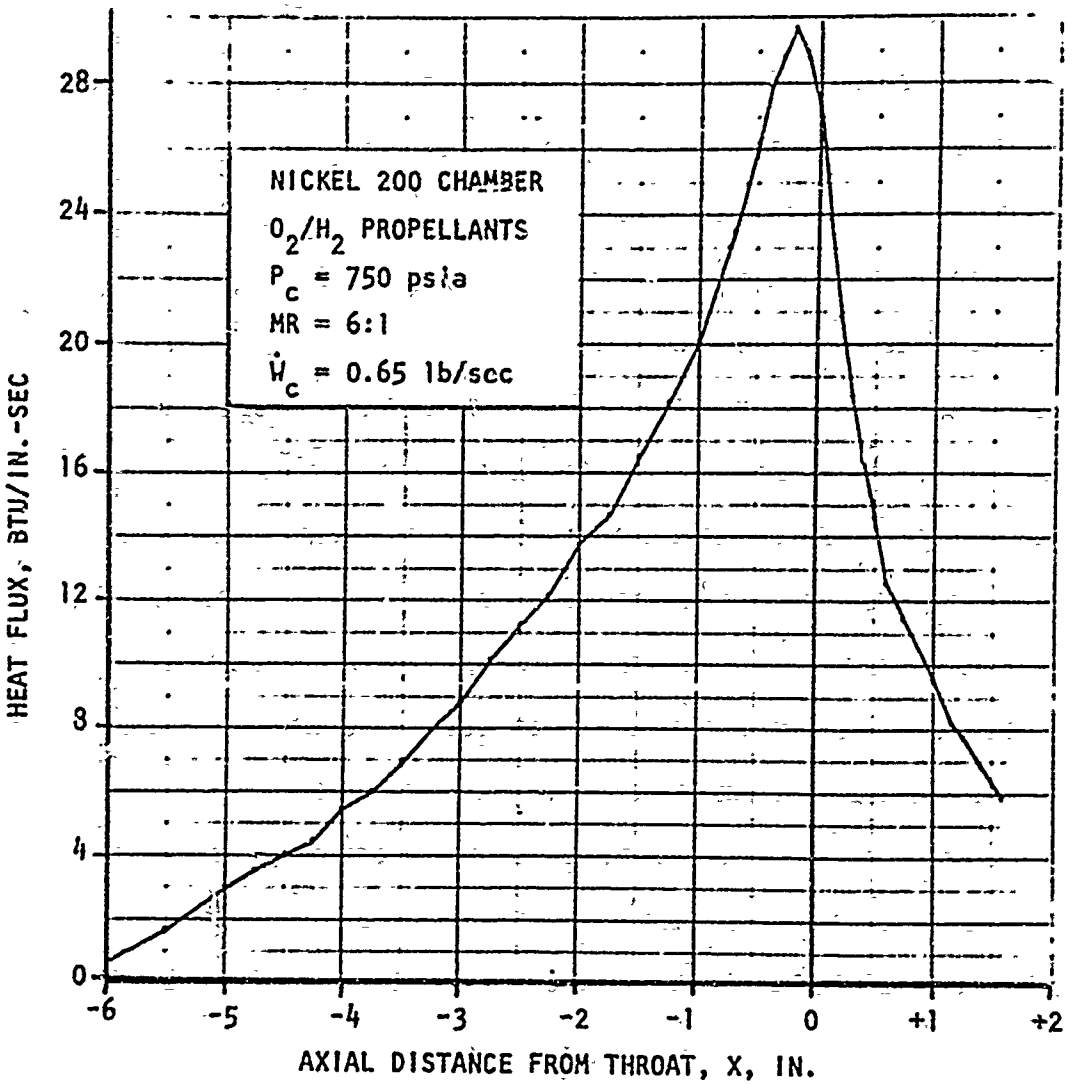

Figure 31. Hydrogen Cooled Chamber Heat Flux Profile for Nickel-200 Chamber

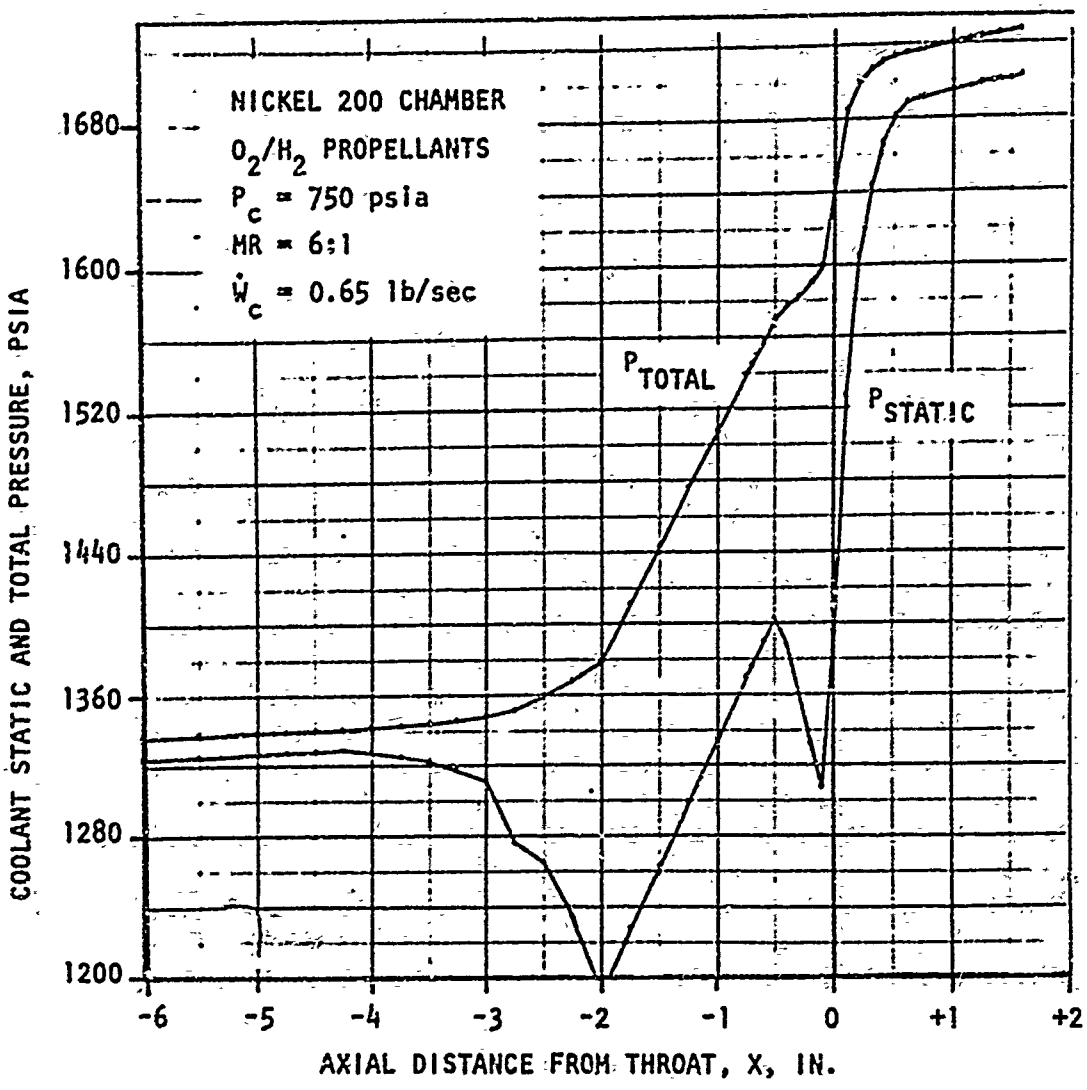

Figure 32. Coolant Pressure Profile

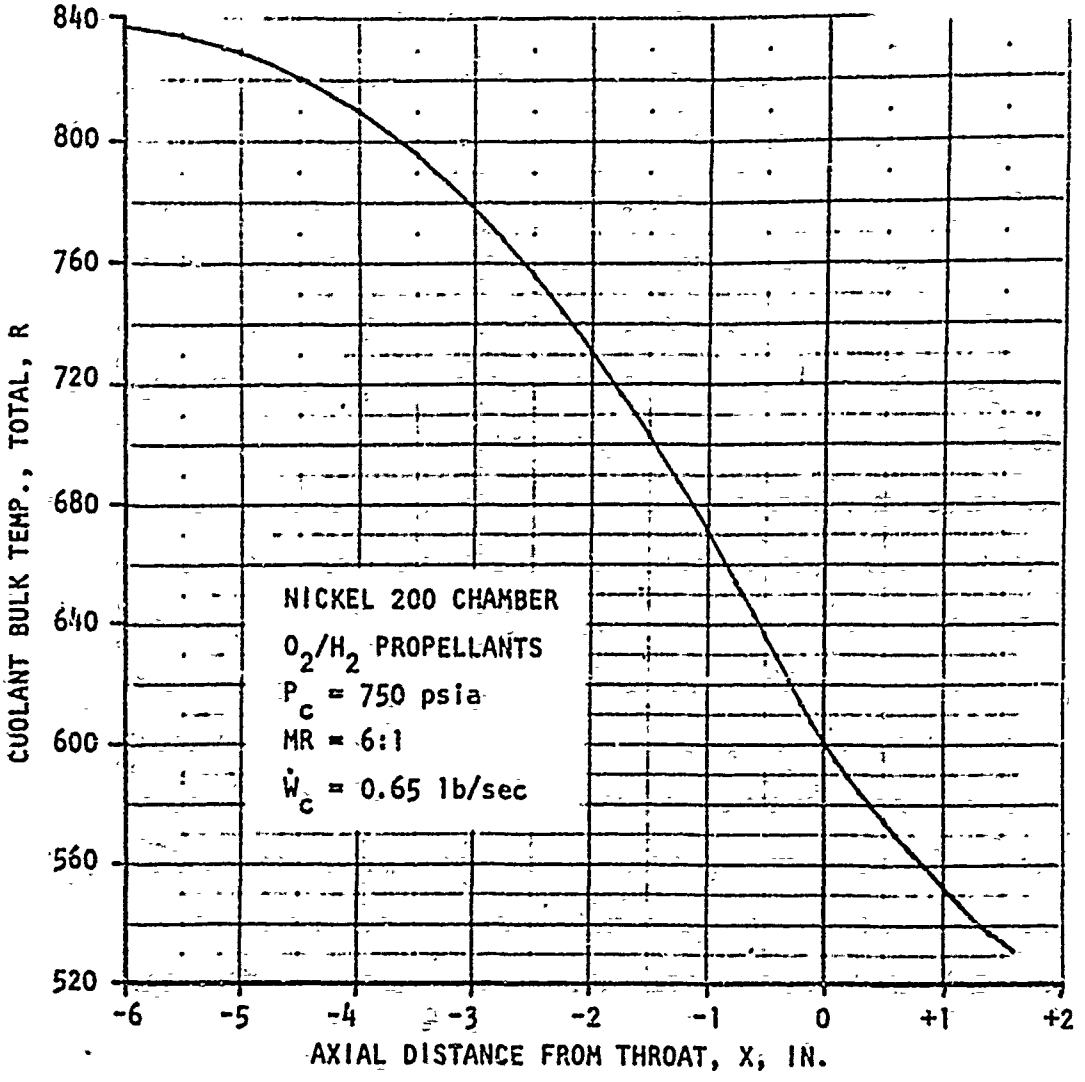

Figure 33. Coolant Bulk Temperature Profile

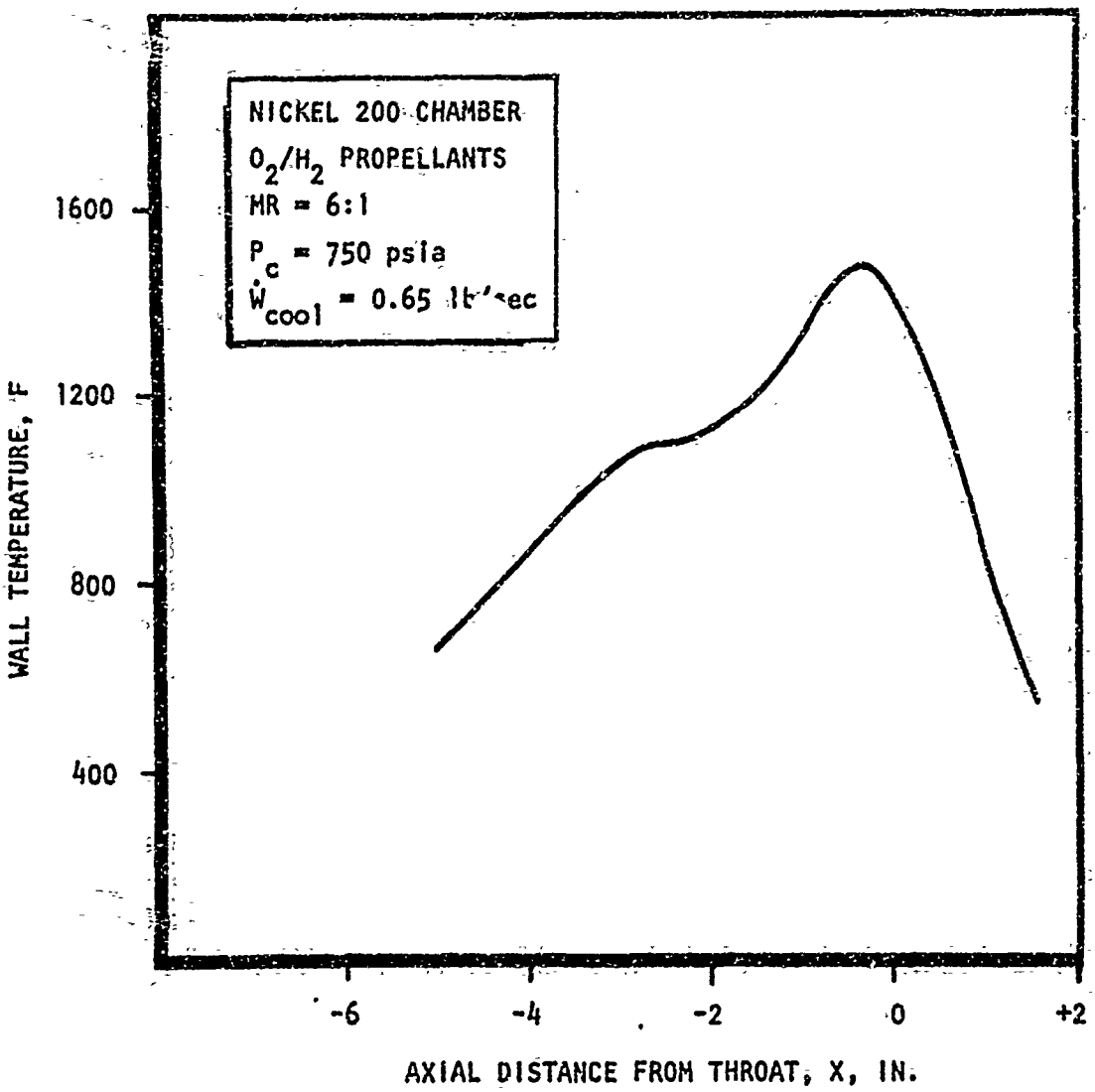

Figure 34. Combustion-Gas-Wide Wall Temperature Profile

testing and providing experimental data to verify predicted operating conditions. Further this allowed for the option of testing with either ambient temperature hydrogen or conditioned hydrogen, providing maximum flexibility and lowest possible test cost.

The results of this study are summarized in Table 1. Coolant pressure and temperatures as well as resultant hot wall and back wall temperatures at selected locations are presented in the Table. The nominal coolant outlet pressure was selected as 1000 psia. This pressure is sufficient to provide a regenerative cooling capability if desired. Lower inlet pressures would result in slightly higher pressure drops due to decreased hydrogen density. The coolant bulk temperature and wall temperatures are relatively insensitive to absolute coolant pressure level.

The coolant pressure profile and bulk temperature profile are presented in Fig. 35 and 36, respectively for nominal chamber operation with ambient hydrogen.

TASK II - THERMAL FATIGUE ANALYSIS

Thermal fatigue life of non-tubular wall regeneratively cooled thrust chambers was evaluated by the individual accumulation of fatigue and creep rupture damage. This is a generally accepted procedure for isothermal conditions (Ref. 1 through 5). Evaluation of the thermal fatigue problem, where temperature varies during the fatigue process, has been given some attention (Ref. 6, 7, and 8) but, due to its complexity, little has been done to formalize a method of damage evaluation. For the creep rupture part of the problem, a generally accepted method of incremental evaluation under variable stress conditions is in use (Ref. 9) and is extended in this report to cover variable temperature conditions. In addition an incremental method is introduced for the evaluation of fatigue damage due to strain cycling under varying temperature conditions.

Methods of evaluating life in a thermal fatigue environment, where strains, stresses and temperature vary, can be separated into three levels for analysis: macroscopic, microscopic and submicroscopic. It was the purpose of this program

TABLE 1. SUMMARY OF COOLING ANALYSIS RESULTS FOR THE COPPER ALLOY THRUST CHAMBERS

Case No.	1	2	3	4	5
P_c (psia)	750	750	750	500	300
H_2 Inlet Temp. (R)	360	530	530	530	530
$\dot{w}_{coolant}$ (lb/sec)	1.07	1.07	1.34*	1.34	1.34
$(T_B)_{out}$ (R)	548	726	691	651	613
ΔT_{Bulk} (R)	188	196	161	121	83
P_{inlet} (psia)	1220	1290	1425	1405	1385
P_{outlet} (psia)	1000	1000	1000	1000	1000
ΔP (psi)	220	290	425	405	385
Location (Inches from Throat)	Wall Temperatures (F) T_{wg}/T_{Back}	T_{wg}/T_{Back}	T_{wg}/T_{Back}	T_{wg}/T_{Back}	T_{wg}/T_{Back}
1.58	218/77	375/241	327/193	251/154	186/122
1.00	420/131	559/284	493/228	371/178	265/136
0.70	515/150	648/301	573/242	429/187	303/142
0.40	598/140	726/293	645/234	482/183	339/139
0.20	688/148	809/298	720/237	537/184	375/140
0	853/185	961/329	855/260	637/200	443/150
-0.10	902/200	1006/343	894/270	665/204	463/154
-0.30	967/226	1067/365	948/285	704/219	486/163
-0.50	987/259	1084/396	960/310	715/237	494/174
-0.75	990/329	1086/460	959/362	713/274	493/198
-1.00	926/352	1028/483	905/383	673/290	466/208
-2.00	768/392	883/525	773/422	579/321	404/231
-3.00	574/329	710/477	619/387	469/298	333/219
-3.50	469/280	615/436	535/356	409/277	294/205
-5.00	238/162	398/327	349/277	274/221	205/169

* 25 percent overcooled at P_c = 750 psia

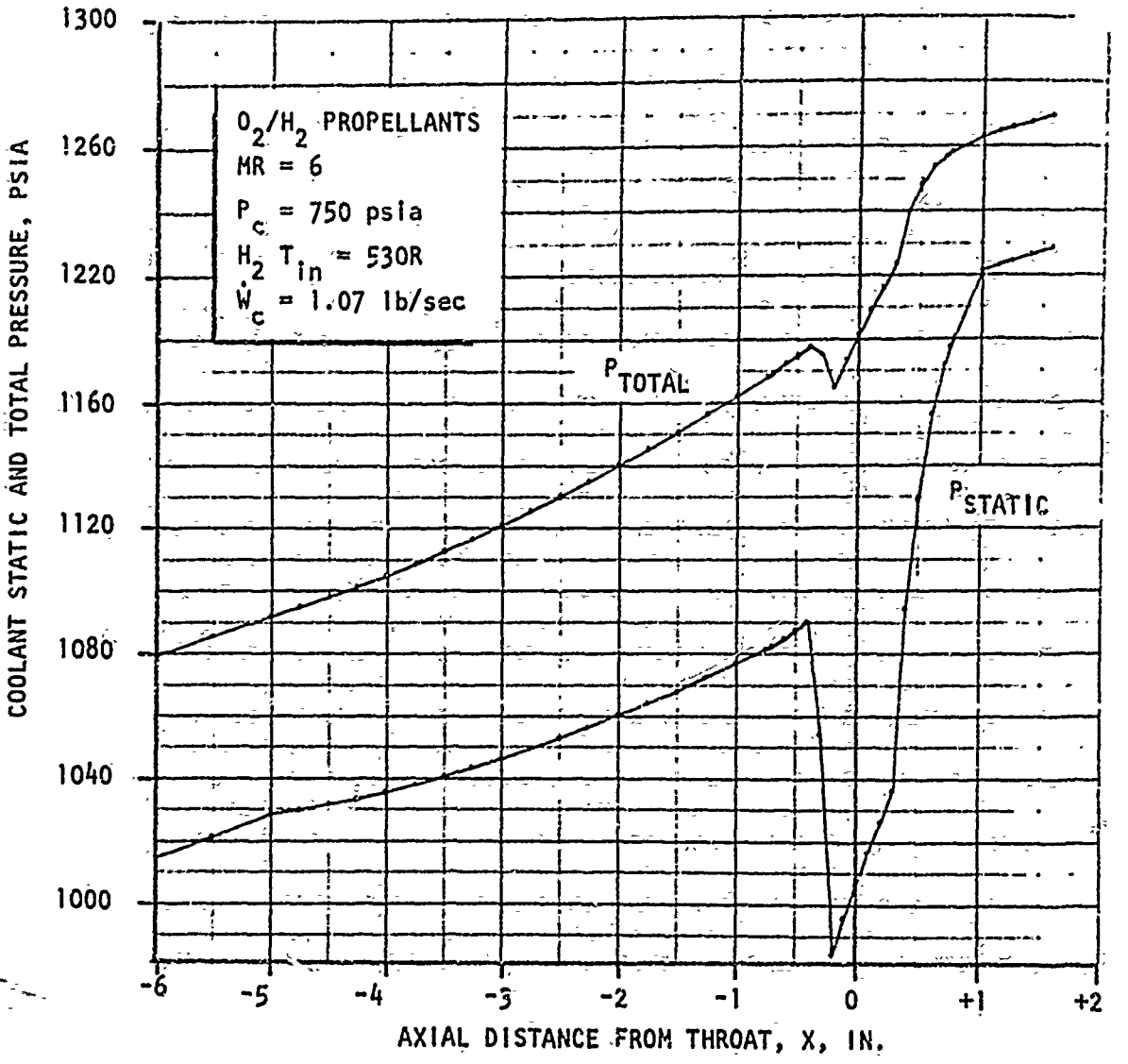

Figure 35. Coolant Pressure Profiles for the Copper Alloy Thrust Chambers

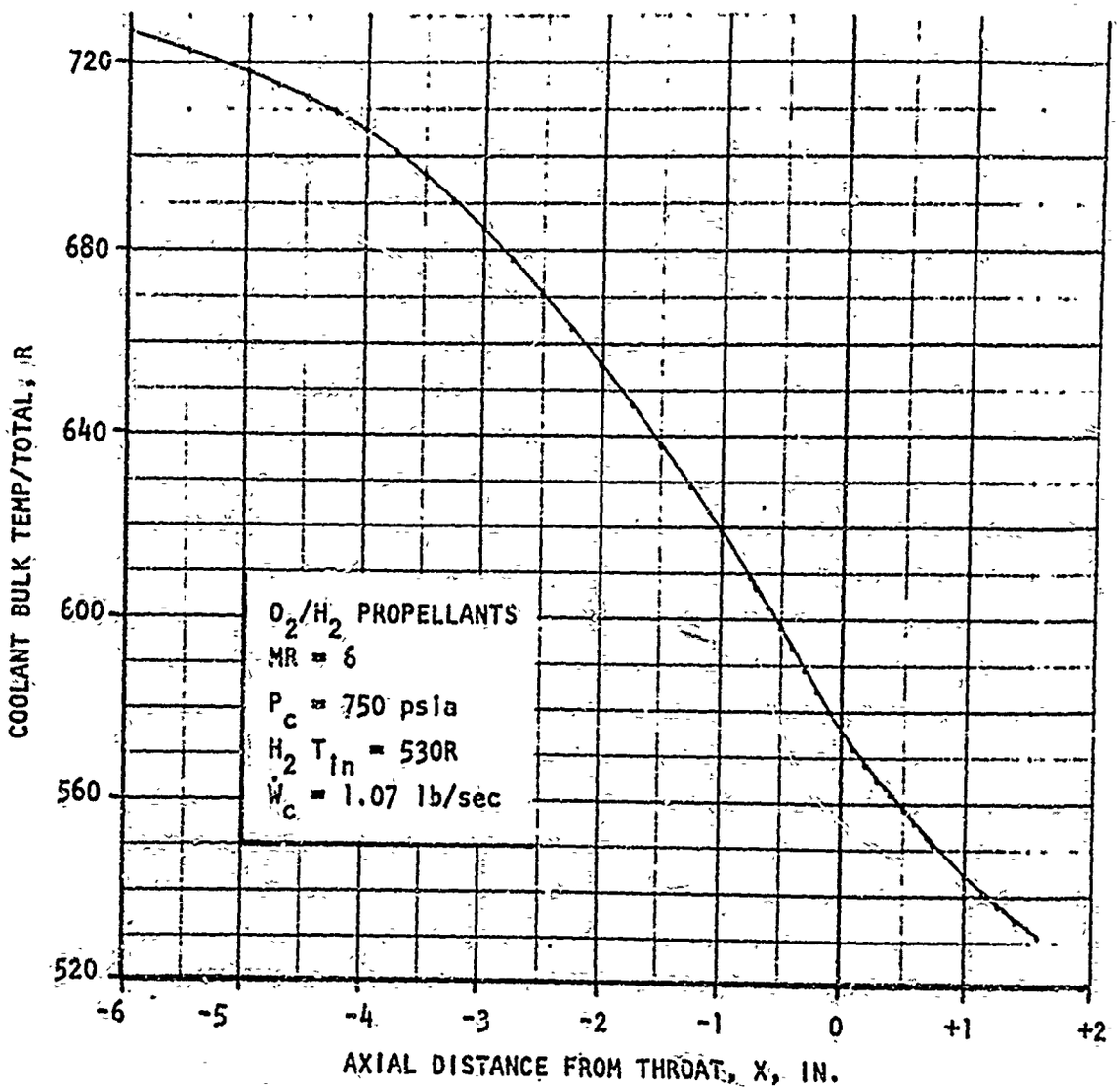

Figure 36. Coolant Bulk Temperature Profile for the Copper Alloy Thrust Chambers

to develop the analyses at the macroscopic level. At this level, the average behavior of relatively large volumes of material is important and the analysis is based on what are believed to be predominant factors in the damage process. These factors include the variation of material mechanical properties with temperature, cyclic elastic and plastic strain and stress ranges, relaxation and creep effects. No attempt is made in this evaluation to include the influence of environment or variation in material metallurgical structure.

Fatigue life was determined by two approaches for a variable temperature-strain cycle. One used a modification of the "method of universal slopes", a correlation equation based on material tensile properties, developed by S. S. Manson at NASA Lewis. The material properties used in the equation were averaged over the temperature range. The other method used the average isothermal fatigue life over the temperature range obtained from specimen test data in an incremental evaluation over the temperature-strain cycle. The latter method was given preference over the correlation equation since it was based on experimental data. After the fatigue life was determined, the fatigue damage was individually assessed following Miner's rule (Ref. 15). This is defined as the incremental damage as determined by the actual number of cycles at the strain range of interest divided by the allowable number of cycles at that strain range.

Creep rupture damage was evaluated using the "life fraction" rule as the time at stress divided by the time to rupture at the same stress and temperature.

A sample problem is presented in the final pages of this section to demonstrate the application of the analysis method to the thrust chamber hot gas wall.

Equation Selection

Analytical methods of predicting fatigue life at room temperature are well known (Ref. 10, 11, and 12) and were investigated at the start of the program for elevated temperature application. At the time, the Coffin equation was selected since it fit ambient data conservatively. This is where

$\Delta\varepsilon_p = 1/2\ \varepsilon_f\ N_f^{-.5}$

ε_f = fracture ductility, as defined as ln (100/(100-RA))

RA = % reduction in area from a standard tensile test

$\Delta\varepsilon_p$ = the completely reversed plastic strain range, in./in.

N_f = cycles to failure

The Coffin equation is based on crack initiation as the failure criteria for data correlation and gives a lower plastic strain range for a given cyclic life. The equation was developed for predicting room temperature cycle life and was to be modified for elevated temperature effects based, in part, on the work done by Taira (Ref. 2). During the program, a more comprehensive correlation equation that considers the influence of creep at elevated temperature on low and intermediate cycle life for a constant temperature test was used. The method, based on the Manson's universal slopes equation (Ref. 1 and 13) correlates elastic, plastic and creep rupture properties at elevated temperature with the fatigue life of laboratory specimens tested at constant elevated temperature at a given total strain range. The universal slopes equation is stated as

$$\varepsilon_t = 3.5\ \left(\frac{F_{tu}}{E}\right)\ N_f^{-.12} + \varepsilon_f^{.6} N_f^{-.6}$$

where

ε_t = total calculated strain range

F_{tu} = total calculated strain range

E = Young's modulus

ε_f = fracture ductility, $\ln \frac{100}{100-RA}$

RA = percent reduction in area

The tensile properties are determined at the elevated temperature of interest at conventional strain rates. The merit of using tensile properties obtained at strain rates comparable to the cyclic strain rates is indicated by Manson and must be kept in mind for more accurate estimates. Complete separation of the specimen is designated as the failure criteria.

Modification of the universal slopes equation was done during this program to account for the varying temperature of the strain cycle. Taira's experiments with several steels demonstrated that it is reasonable to expect that such a modification would be realistic (Ref. 2). Taira's results showed the existence of an equivalent constant temperature strain cycle where fatigue life was equal to that obtained for a variable temperature strain cycle for the same strain range.

Life Prediction Analysis

The basic theory used in the life prediction analysis is that failure depends on the accumulation of creep and fatigue damage. The thermal fatigue analysis method is built on this theory. Data obtained from isothermal fatigue specimens are used to calibrate the method.

The life analysis in general is based on a definition of the stress-strain-time-temperature history of the material during each operating duty cycle. Creep damage is evaluated from the stress-time-temperature cycle and fatigue damage from the strain-time-temperature cycle. The life analysis logic applied to the thrust chamber hot gas wall is given in Fig. 37.

The thrust chamber hot gas wall is structurally modeled to analytically determine the stresses and strains due to thermal and pressure loads. Either manual methods of analysis or finite element computer methods that have been developed are used to obtain the strains and stresses. The analysis is based on a detailed determination of component temperatures and loads at engine start, mainstage (steady state) and cutoff conditions. Once the stress-strain-time-temperature history is known, the cyclic life can be calculated.

Effective Strain. Before the isothermal strain controlled low cycle fatigue data is used in life determination, it is necessary to relate the strains in the test specimen to the strains in the thrust chamber hot gas wall. Effective strain is used for the relationship and defines the uniaxial equivalent of the multiaxial strain state in the specimen and chamber wall. The effective strain, ε_{ff},

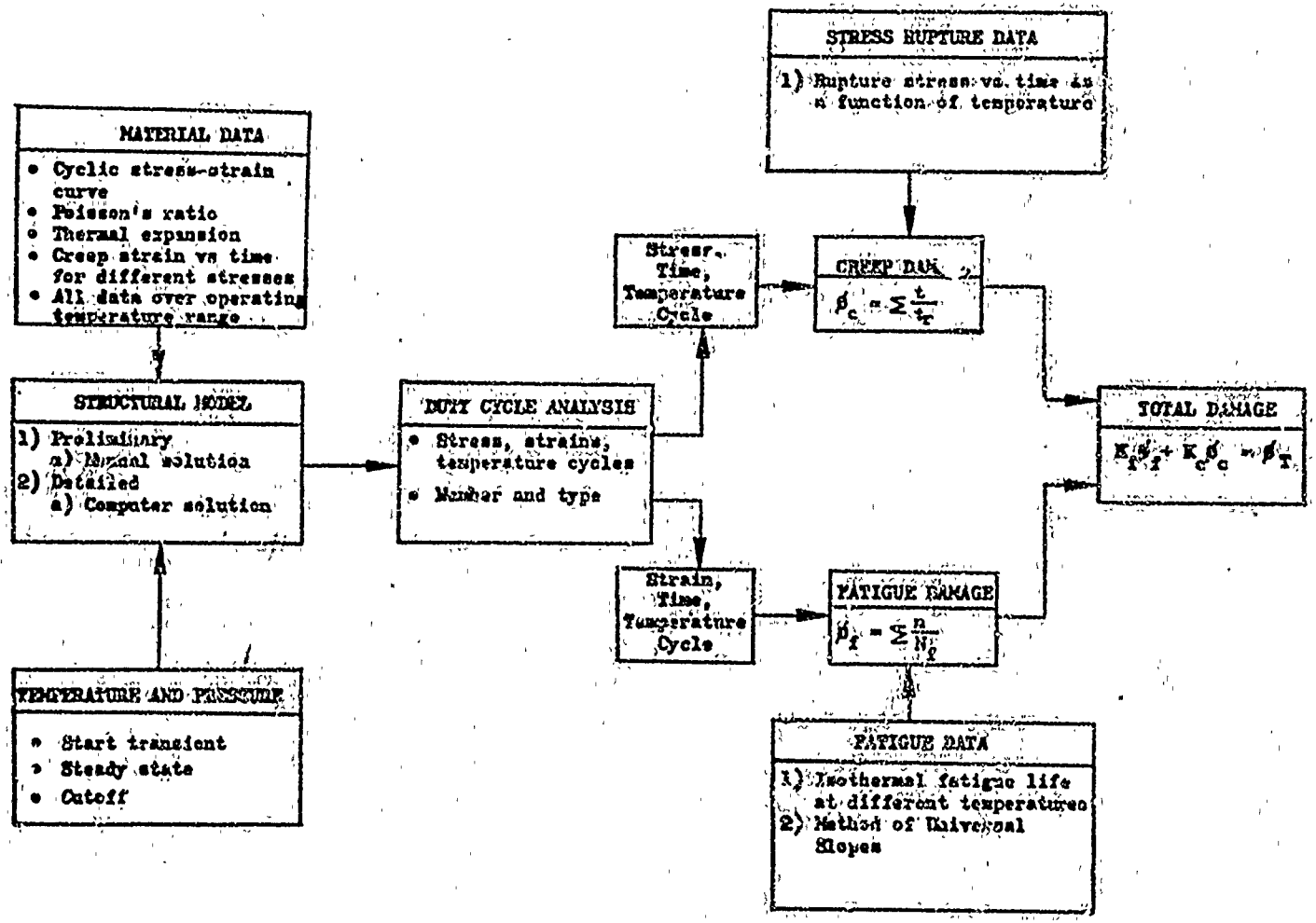

Figure 37. Life Analysis Logic

derived from the Von Mises criteria and the constant volume assumption, is given by

$$\varepsilon_{ff} = \frac{\sqrt{2}}{3}\left[(\varepsilon_1 - \varepsilon_2)^2 + (\varepsilon_2 - \varepsilon_3)^2 + (\varepsilon_3 - \varepsilon_1)^2\right]^{1/2}$$

where ε_1, ε_2, and ε_3 are the three principle strains on an element of material.

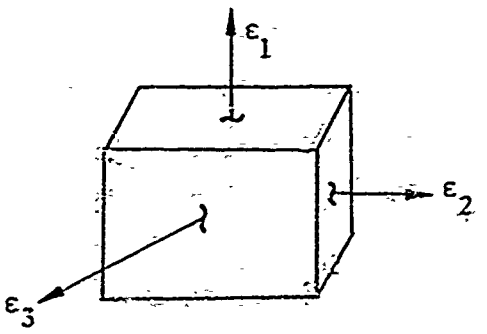

The logic is illustrated in Fig. 38.

Thermal Fatigue Damage Analysis. The thermal fatigue damage analysis makes use of one of two approaches in the individual evaluation of fatigue damage for a variable temperature-strain cycle. One approach utilizes a modification of the "method of universal slopes" which is based on material tensile properties. The other method utilizes isothermal fatigue data in an incremental evaluation of the damage from the strain cycle. The method involving the isothermal fatigue data is given preference since it uses experimental data rather than a correlation equation and would be more accurate.

Thermal Fatigue Damage Analysis Using the Method of Universal Slopes. The thermal fatigue damage analysis which makes use of the method of universal slopes is graphically illustrated in Fig. 39. The method is used when isothermal fatigue data is unavailable. The straining process with temperature varying is considered incrementally. Allowable cyclic life, N_f, for the strain range, ε_t, is based on average values for the F_{tu}/E ratio and RA obtained over the temperature range of the calculated strain cycle. Fatigue damage is then determined by Miner's rule (Ref. 15) which is the linear summation of the required or actual number

ISOTHERMAL FATIGUE SPECIMEN

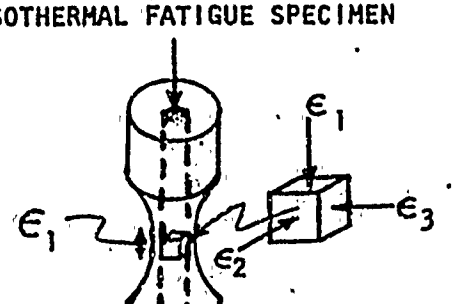

- ISOTHERMAL TEST DATA CONTROLLED ON UNIAXIAL CYCLE STRAIN RANGE, ϵ_1
- CALCULATE TEST SAMPLE EFFECTIVE CYCLIC STRAIN RANGE,

$$\epsilon_{eff} = \sqrt{\frac{2}{3}}\left[(\epsilon_1-\epsilon_2)^2 + (\epsilon_2-\epsilon_3)^2 + (\epsilon_3-\epsilon_1)^2\right]^{1/2}$$

THRUST CHAMBER HOT GAS WALL

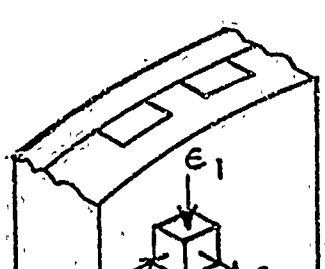

- THRUST CHAMBER ANALYSIS PREDICTS EFFECTIVE CYCLIC STRAIN RANGE,

$$\epsilon_{eff} = \sqrt{\frac{2}{3}}\left[(\epsilon_1-\epsilon_2)^2 + (\epsilon_2-\epsilon_3)^2 + (\epsilon_3-\epsilon_1)^2\right]^{1/2}$$

$\rightarrow N_f \leftarrow$

Figure 38. Thermal Fatigue Life Prediction Based on Effective Strain

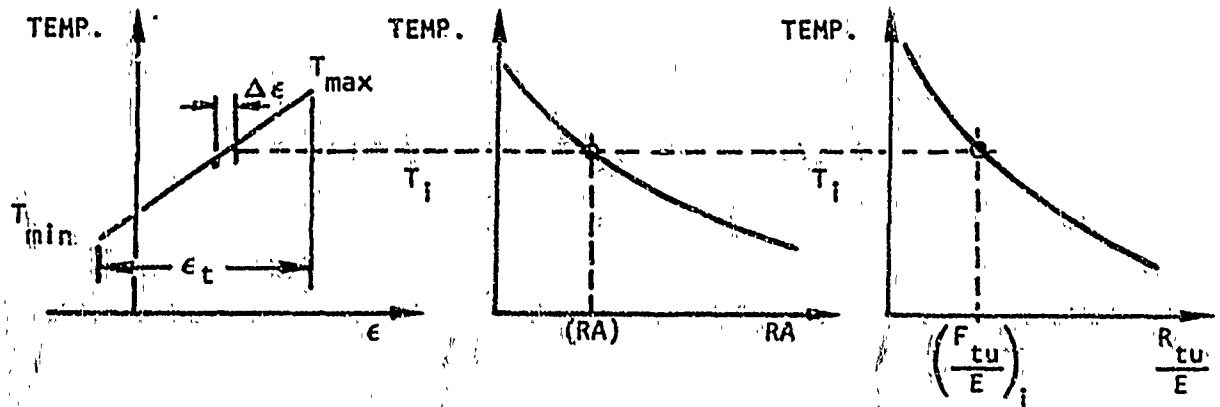

$$\Delta\left(\frac{F_{tu}}{E}\right) = \frac{\Delta\epsilon}{\epsilon_t} \times \left(\frac{F_{tu}}{E}\right)_i \text{ at } T_i$$

$$\left(\frac{F_{tu}}{E}\right)_{avg} = \Sigma\Delta\frac{F_{tu}}{E}$$

$$\epsilon_t = 3.5\left(\frac{F_{tu}}{E}\right)_{avg} N_f^{-.12} + \left[\ln\left(\frac{100}{100-RA_{avg}}\right)\right]^{.6} N_f^{-.6}$$

$$\emptyset_f = \Sigma\left(\frac{n}{N_f}\right)_{\epsilon_t}$$

$$\Delta(RA) = \frac{\Delta\epsilon}{\epsilon_t} \times (RA)_i \text{ at } T_i$$

$$(RA)_{avg} = \Sigma\Delta(RA)$$

Figure 39. Determination of Thermal Fatigue Life from the Method of Universal Slopes

of cycles, n, to be imposed on the material divided by the allowable number of cycles, N_f, predicted for the material at the specific strain range, ε_t, of interest. Plots of F_{tu}, E and RA versus temperature for the materials investigated in this program are given later in Task III.

Thermal Fatigue Damage Analysis Using Isothermal Fatigue Data. A better method of determining fatigue damage using isothermal fatigue data is schematically illustrated in Fig. 40. The straining process with varying temperature is considered incrementally. A plot of fatigue life versus temperature for the specific strain range of interest is the key element in the incremental technique. The cycles to failure for the strain range of interest is obtained for each temperature from the corresponding isothermal strain-cycle curve. The number of allowable cycles, N_f, for the strain range, ε_t, is found by averaging the value of N_f over the operating temperature range. Fatigue damage is assessed by Miner's rule, the summation of the actual number of cycles, n, divided by the number of allowable cycles, N_f, for the specific strain range, ε_t.

Creep Damage Analysis. Total creep damage for the total duration is determined by the summation of the ratios of time spent at a particular stress to the time to rupture at that stress.

$$\phi_c = \sum \left(\frac{\Delta t}{t_r} \right)_\sigma$$

An illustration of the summation process is given in Fig. 41. If the temperature is varying simultaneously with the stress, the time to rupture curve for the specific temperature is used for each stress increment. The time to rupture data that is used in this report is obtained from monotonic load based creep rupture tests. This has been shown to be conservative by Halford (Ref. 16), who obtained the time to rupture from a "cyclic" creep rupture test. "Cyclic" creep rupture data is obtained from an isothermal test that is run at zero net strain. In the test a tensile stress is applied and held constant until a desired amount of tensile creep strain is accumulated, the process is reversed under compressive stress until a similar amount of net compressive creep strain is accumulated.

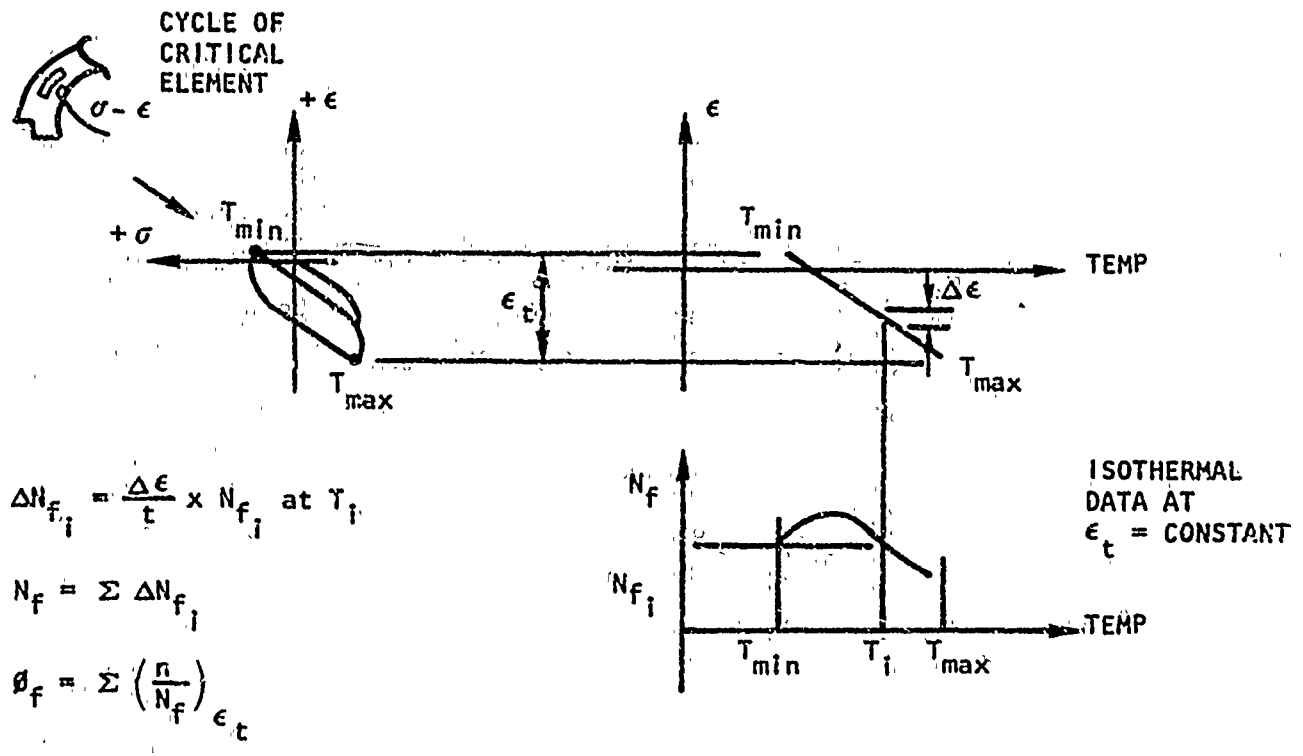

$$\Delta N_{f_i} = \frac{\Delta \epsilon}{t} \times N_{f_i} \text{ at } T_i$$

$$N_f = \Sigma \Delta N_{f_i}$$

$$\phi_f = \Sigma \left(\frac{n}{N_f}\right)_{\epsilon_t}$$

Figure 40. Thermal Fatigue Analysis Based On Isothermal Fatigue Data

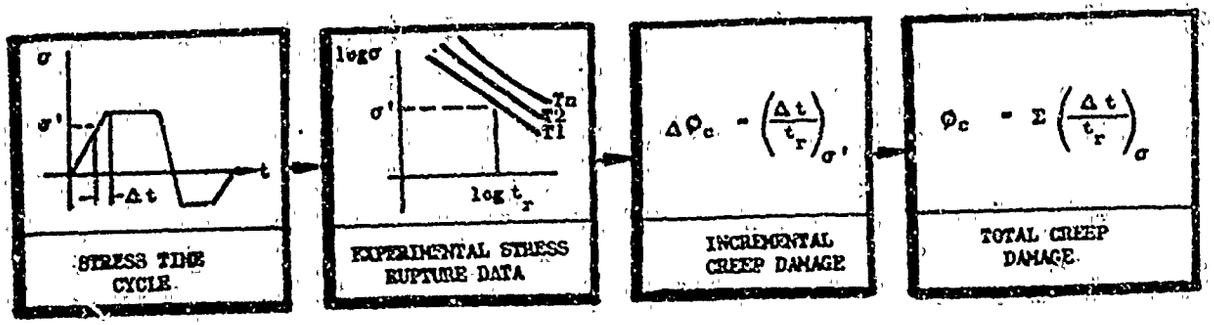

Figure 41. Creep Damage Evaluation

The specimen is cycled in this manner until failure when the time to rupture for the testing is recorded. This is believed to better simulate service conditions since it eliminates the life shortening influence of area reduction, void coalescence and necking instability of the monotonic creep tests which are normally not present in an engineering structure. At the design conditions imposed on the thrust chamber of this program the creep damage component on the thrust chamber wall is small and little inaccuracy is introduced using monotonic creep rupture data. On future designs where operating conditions such as reduced coolant flowrate or available pressure drop or higher heat flux forces the design further into the material creep range, use of cyclic creep rupture data will be of more importance.

Damage During Stress Relaxation. Damage during the stress relazation part of the thrust chamber duty cycle is a special condition that needs to be evaluated. The procedure followed during stress relaxation, when the stress is varying with time, is to evaluate the damage as the accumulation of the incremental creep damage, ϕ_c. The increment of creep rupture damage is set equal to the integral of the time at stress over the time to rupture at that stress (Ref. 17).

$$\Delta\phi_c = \int_0^{t_i} \frac{dt}{t_r} \qquad \text{Equation 1}$$

$\Delta\phi_c$ = creep rupture damage for a stress cycle of duration, t_i

dt = increment of time at the instantaneous stress, σ

t_r = time to rupture at the instantaneous stress, σ

To solve the creep damage integral under the condition of stress decaying at constant strain, two relations are used.

$$\dot{\epsilon} = K\sigma^N$$

and

$$1/E \frac{d\sigma}{dt} + \varepsilon = 0$$

E = Young's Modulus

Creep strain data versus time at constant stress and temperature are used to obtain the creep law constants K and N.

By combining the above equations, the stress at time, t, is

$$\sigma = \left[t\, KE\, (N-1) + S_o^{(1-N)} \right]^{\left(\frac{1}{1-N} \right)} \qquad \text{Equation 2}$$

where S_o = initial stress (at time = 0.0)

A plot of stress versus the Larson-Miller parameter is used to represent rupture time, t_r, as a function of stress and temperature.

$$\log \sigma = AP + C$$

$$P = T\,(20 + \log t_r)$$

T = absolute temperature, F

t_r = rupture time, hours

A and C are material constants so that

$$t_r = \frac{1}{\sigma^{AT}}\, 10^{-\left(\frac{C}{AT} + 20 \right)} \qquad \text{Equation 3}$$

Substitution of Equation 2 in Equation 3 and Equation 3 in Equation 1 and integrating gives the creep rupture damage increment, $\Delta\phi_c$, for the holdtime, t_i.

$$\sigma_c = \frac{AT\ 10^{\frac{C}{AT} + 20}}{KE\ [1+AT(N-1)]} \left[\left[KE(N-1)t + S_o^{(1-N)} \right]^{\frac{1}{(N-1)AT} + 1} \right]_0^{t_i}$$

The total creep damage, ϕ_c, is given by

$$\phi_c = \sum \Delta\phi_c$$

Creep rate law and stress versus Larson-Miller parameter curve constants for NARloy-Z are furnished in Task III.

Total Damage. The equation used to calculate the total damage, ϕ_t, caused by the interaction of fatigue and creep takes the following form:

$$\phi_t = \phi_f + \phi_c$$

where

ϕ_t = total damage
ϕ_f = fatigue damage
ϕ_c = creep damage

} for the variable temperature cycle

Calculation of the individual fatigue and creep damage components have already been discussed. The total damage is found as the sum of the two components with the total equal to one at failure. Thermal fatigue life is calculated as the reciprocal of the total damage per cycle based on the above. Observation presented by other investigators (Ref. 4, 5, 18, and 19) indicate that a more complex interaction equatio between fatigue and creep damage may be more accurate in that a total damage summation of less than one can cause failure, however there was no data available to substantiate this.

Application of Analysis Methods

An example is discussed in this section to demonstrate the method of determining the thermal fatigue life of the thrust chamber hot gas wall. The details of the heat transfer, stress and strain analysis are not included since they do not add to the understanding of the life analysis method.

Description of Problem. The thrust chamber wall is subjected to a duty cycle temperature range of 80 F to 870 F resulting in an effective strain range of 0.0135 in./in. The stress-strain-time-history of the duty cycle is sketched below.

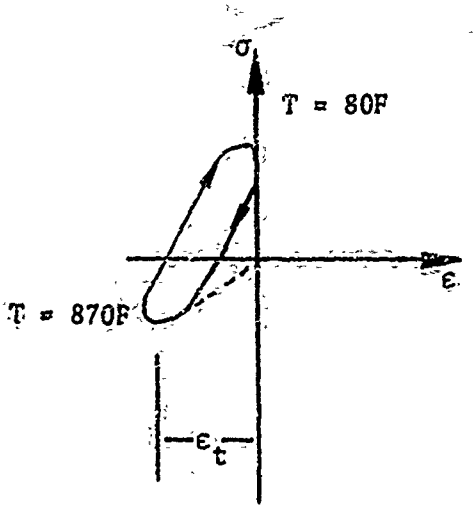

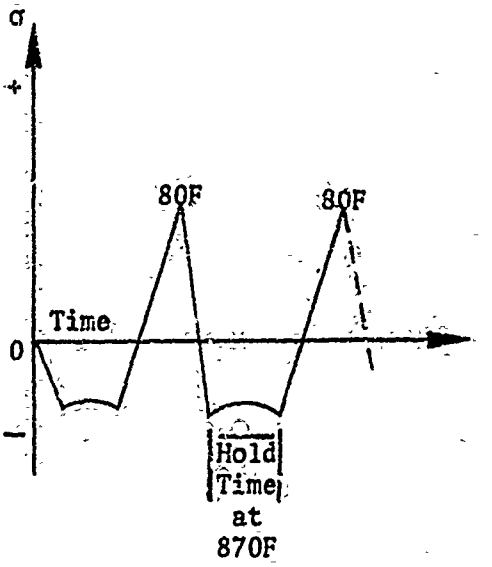

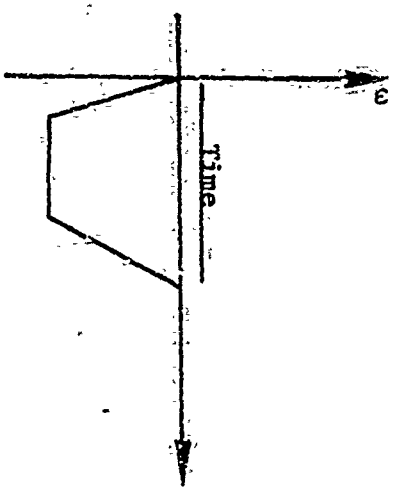

Thrust Chamber Wall Material: NARloy-Z
Hold Time = 2 Seconds

Isothermal Fatigue Damage Analysis. Fatigue life, N_f, is obtained for the duty cycle effective strain range of 0.0135 in./in. from Fig. 42.

N_f = 7200 cycles (best fit)

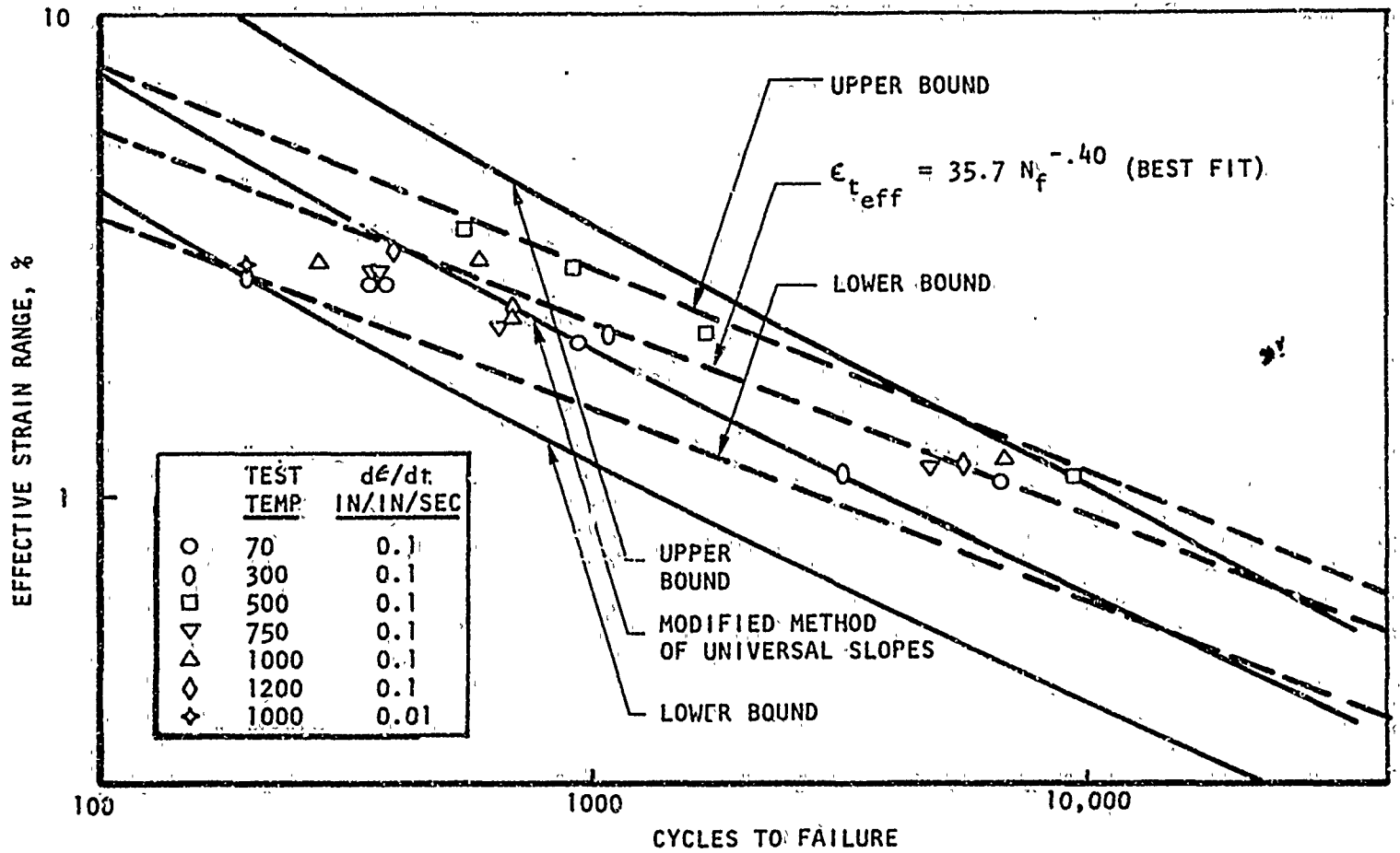

Figure 42. Isothermal Cyclic Test Data - Zirconium Copper Heat 329-6

Fatigue damage, $\Delta\phi_f$, for the duty cycle is determined from:

$$\Delta\phi_f = \frac{n}{N_f}$$

$$\Delta\phi = \frac{1}{7200}$$

$$\Delta\phi = 1.39 \times 10^{-4}$$

Thermal Fatigue Damage Analysis. Using isothermal fatigue data, fatigue damage is calculated for the duty cycle using a life cycle versus temperature curve as an alternative method of analysis, Fig. 43. The curve is constructed from the isothermal fatigue data of Task III for the effective strain range of 0.0135 in./in. The data used for the construction is tabulated below:

Temperature (F)	Cycle to Failure (N_f)
70	4000
300	3200
500	14,500
750	10,000
1000	8,600
1200	3,100

The average number of cycles to failure (N_f) for the 80 F to 870 F temperature range of the thermal cycle as determined from the curve of Fig. 43 is:

$$N_f = 8200 \text{ cycles}$$

Fatigue damage, $\Delta\phi_f$, for the duty cycle is determined from:

$$\Delta\phi_f = \left(\frac{n}{N_f}\right)_{\varepsilon_t}$$

$$\Delta\phi_f = \frac{1}{8200}$$

$$\Delta\phi_f = 1.22 \times 10^{-4}$$

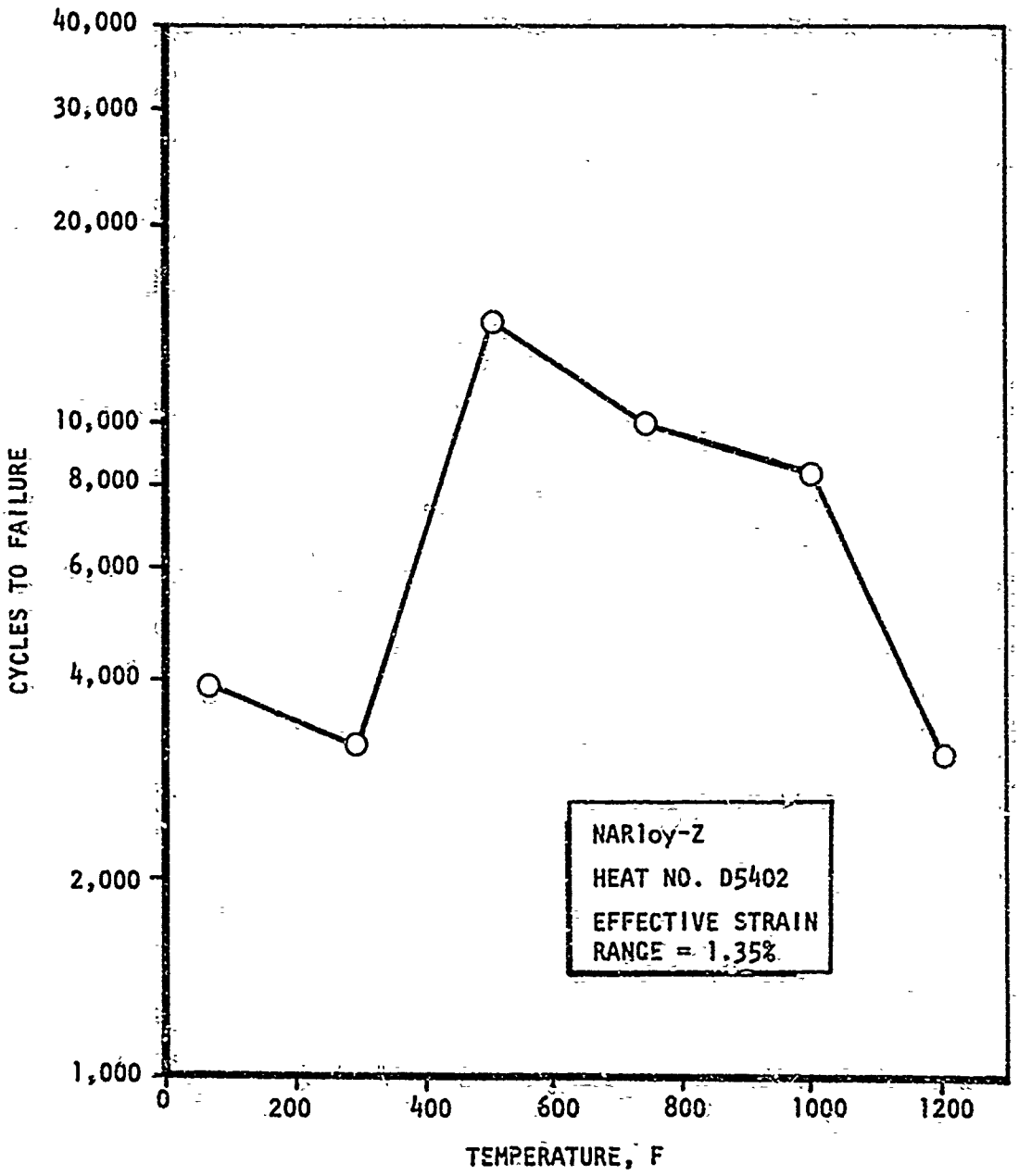

Figure 43. Cycle-Temperature Curve

Procedure for calculating fatigue damage using the method of universal slopes is included for comparison. Average values of F_{tu}/E and RA for the 80 F to 870 F temperature range are determined from curves of these properties versus temperature.

$$\left(\frac{F_{tu}}{E}\right)_{avg} = 2.133 \times 10^{-3} \quad (RA)_{avg} = 63.4$$

Given:

$$\varepsilon_t = 0.0135 \text{ in./in.}$$

N_f is calculated by substituting the above values in:

$$\varepsilon_t = \frac{3.5\left(\frac{F_{tu}}{E}\right)_{avg}}{N_f^{.12}} + \frac{\ln\left[\frac{100}{100-(RA)_{avg}}\right]}{N_f^{.6}}$$

$$N_f = 2000 \text{ cycles}$$

Fatigue damage, $\Delta\phi_f$, for the duty cycle is determined from:

$$\Delta\phi_f = \frac{n}{N_f}$$

$$\Delta\phi_f = \frac{1}{2000}$$

$$\Delta\phi_f = 5.00 \times 10^{-4}$$

The calculation by the universal slopes method indicates a fatigue damage fraction that is conservative (higher) by a 3.5 factor when compared to the calculation of part (a) based on isothermal fatigue data.

Creep Damage Analysis. Creep damage is calculated for the two second hold-time when the material in the hot gas wall is held at a constant level of compressive strain. The creep damage occurring during strain cycling is considered to be

included in the basic zero hold-time fatigue data since the data is obtained at a strain rate similar to that experienced during the transient portion of the duty cycle.

The creep damage for the duty cycle, $\Delta\phi_c$, is calculated from:

$$\Delta\phi_c = \frac{AT\ 10^{\frac{C}{AT}} + 20}{KE\ \ 1 + AT\ (N-1)} \left[\left[KE\ (N-1)\ t + So^{(1-N)} \right]^{\frac{1}{(N-1)\ AT}} + 1 \right] t_i$$

where $t_i = \frac{2}{3000}$ hours

$T = 870\ F + 460\ F = 1330\ F$

$So = 20.2$ KSI (from cyclic $\sigma - \varepsilon$ data at $\varepsilon_t = .0135$ and 870 F)

$E = 12{,}500$ KSI (from same data as So)

$A = -9.0518 \times 10^{-5}$

$C = 3.815$

$K = 10^{-20.2} = 6.31 \times 10^{-21}$

$N = 14.6$

} From Table 2 and 3 and Figure 44

$\Delta\phi_c = 7.23 \times 10^{-5}$

Total Damage and Life Prediction. The total [illegible] for a thermal fatigue duty cycle is given by:

$$\Delta\phi_t = \Delta\phi_f + \Delta\phi_c$$

$$\Delta\phi_t = 10^{-4} + 7.23 \times 10^{-5}$$

$$\Delta\phi_t = 2.133 \times 10^{-4}$$

Table 2. Stress vs Larson-Miller Parameter Constants for NARloy-Z

For $\log \sigma = A\,P + C$

where

$P = T\,(20 + \log t_r)$

$A = -9.0158 \times 10^{-5}$, $C = 3.815$

T = temperature, R

σ = stress, ksi

t_r = time, hr

Table 3. Creep Rate Law Constants

Temperature, F	N	K
700	19.2	2.9×10^{-31}
800	16.1	9.6×10^{-25}
900	13.9	1.0×10^{-19}
1000	12.5	6.2×10^{-16}
1200	8.7	4.5×10^{-9}

σ = stress, ksi

$\dot{\epsilon}$ = strain rate, in./in./hr

Data from Reference 22

The life prediction is given by the reciprocal of the total damage per cycle.

$$\text{Life} = \frac{1}{\Delta\phi_t}$$

Life = 4670 Cycles

TASK III - MATERIALS AND PANEL TESTING

The purpose of Task III was to obtain basic material properties and fatigue properties on the materials of interest. This involved assimilation of available data as well as laboratory testing to obtain (1) basic materials properties, (2) isothermal fatigue data, (3) thermal fatigue data, and (4) thermal cycling tests of panels. Results of each are presented in the following paragraphs.

Material Properties

Basic physical properties of the materials of interest are presented in Fig. 44 through 55. The NARloy-Z and zirconium-copper data were generated on this program, while the Nickel-200 data were taken from the literature and the powder metallurgy nickel data were taken from a previous program.

The material properties were determined using established test parameters and techniques. Thermal conductivity of the two copper alloys was determined on small (0.25 dia by 0.060 to 0.125 long) bars by measuring thermal diffusivity on the apparatus shown in Fig. 56 and converting to thermal conductivity by means of the equation

$$K = \alpha C_p \rho$$

where

K = thermal conductivity
α = thermal diffusivity
C_p = specific heat
ρ = density

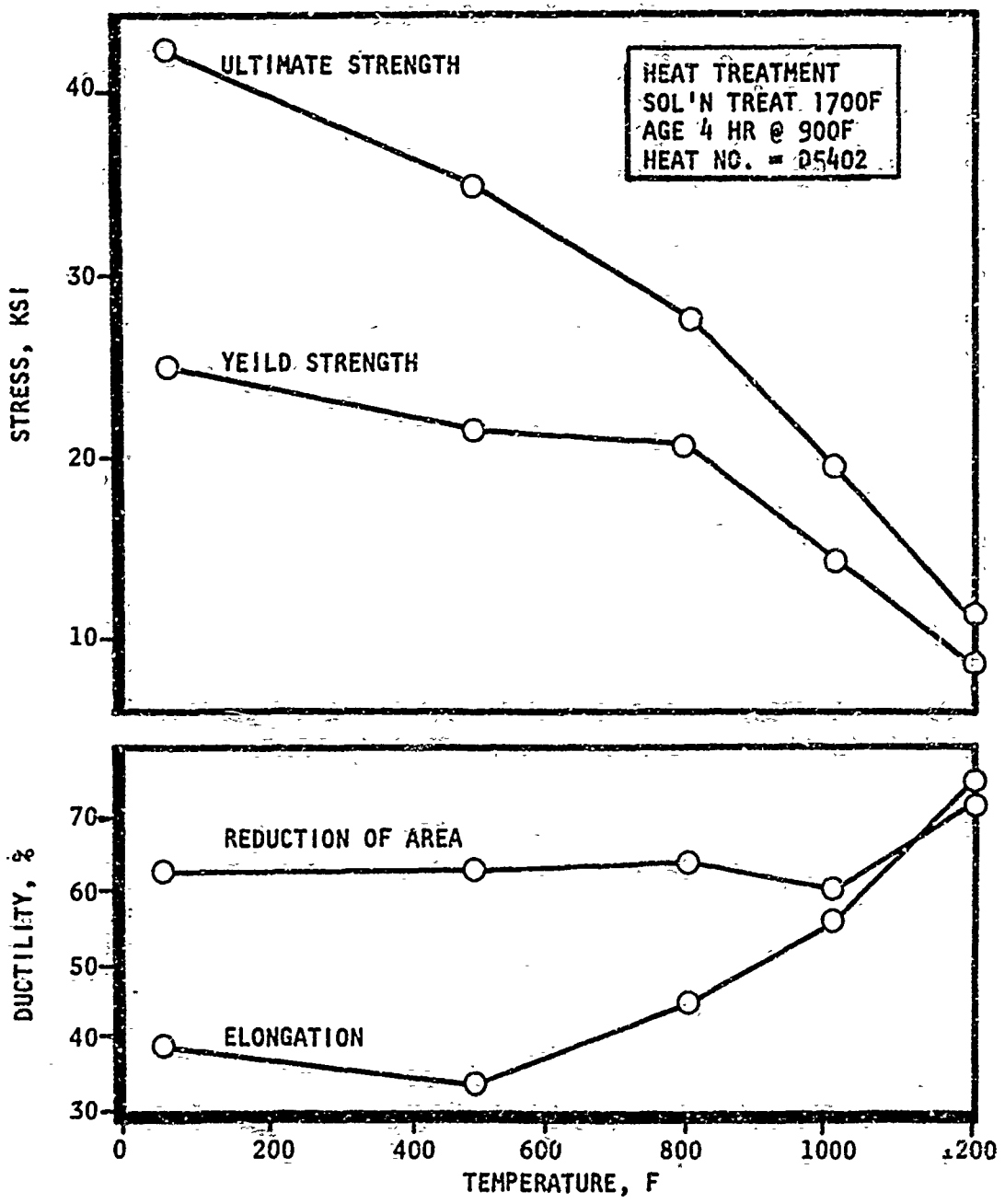

Figure 44. Tensile Properties of NARloy-Z

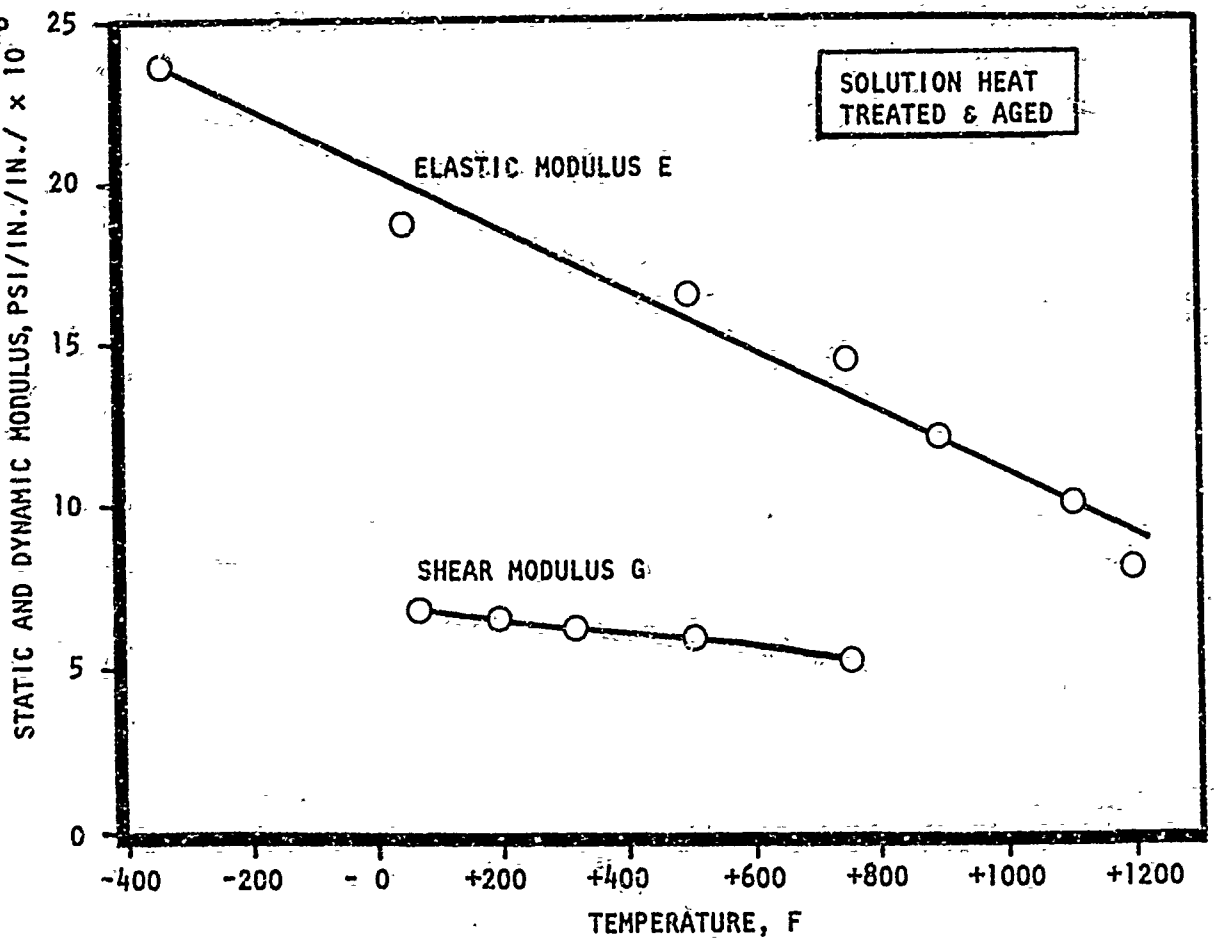

Figure 45. Modulus of Elasticity of NARloy-Z

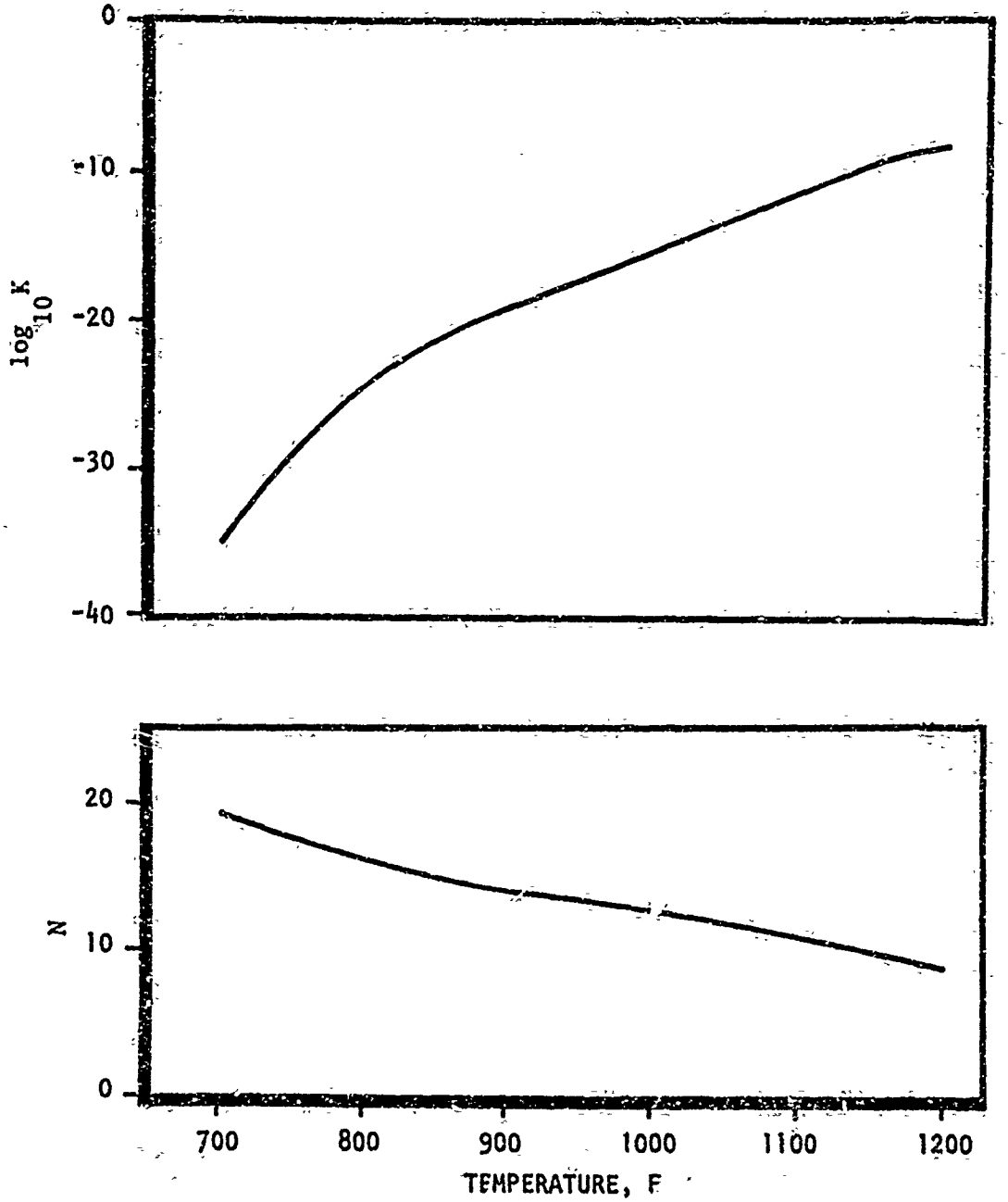

Figure 46. NARloy-Z Creep Rate Data for $\dot{\epsilon} = K\sigma^N$

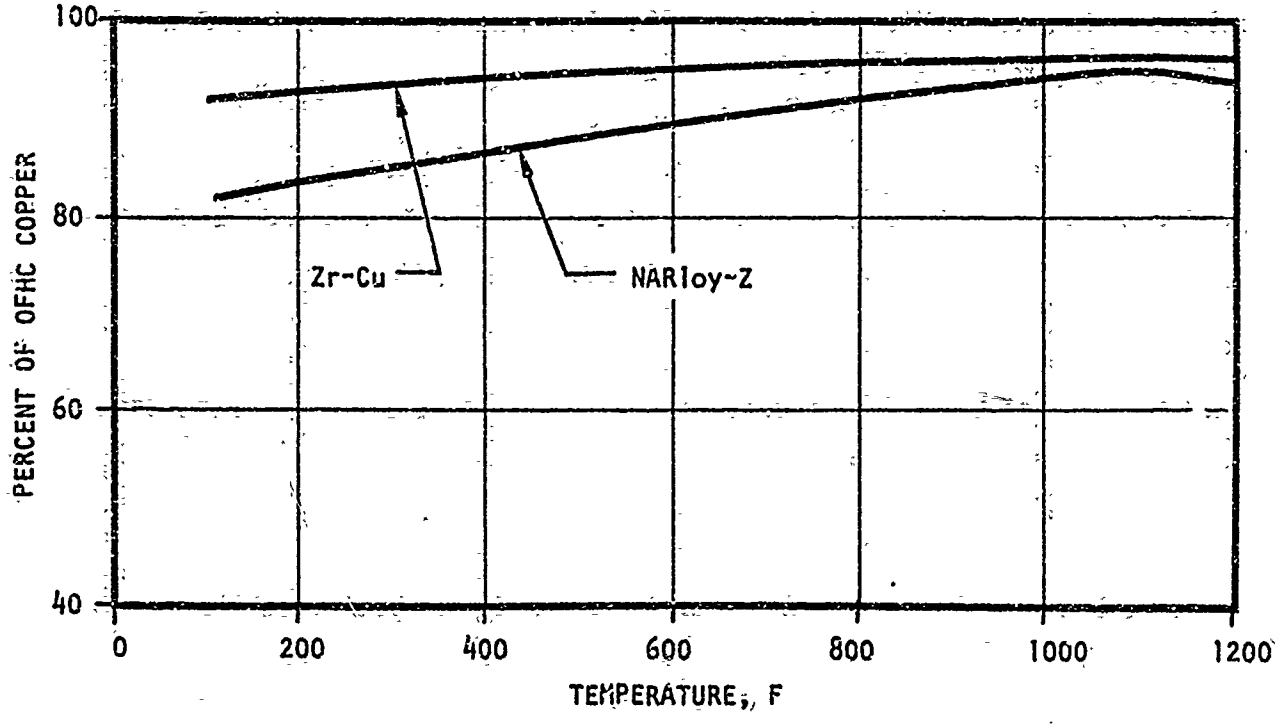

Figure 47. Thermal Conductivity of NARloy-Z and Zirconium-Copper (percent of OFHC Copper)

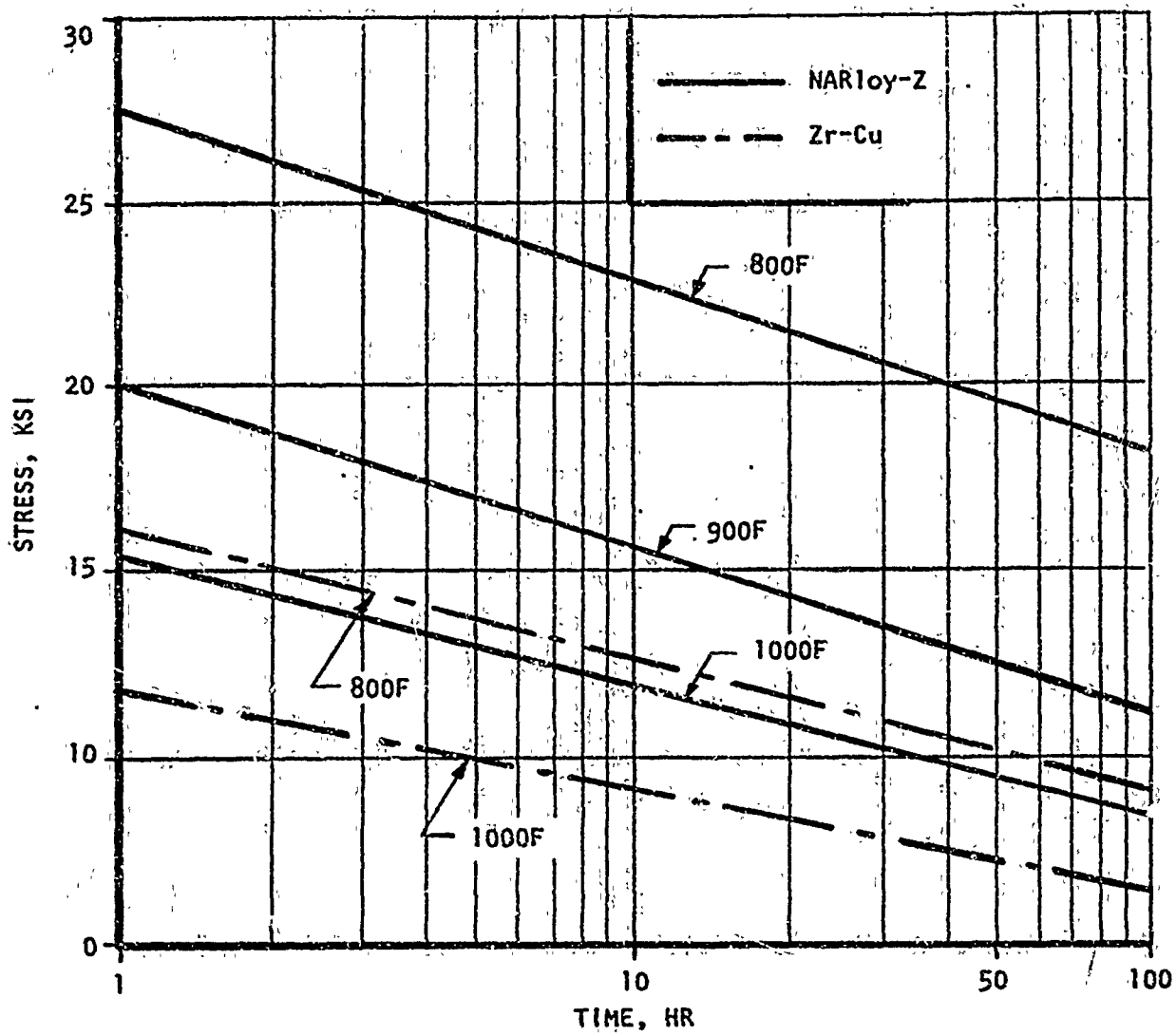

Figure 48. Stress Rupture Properties of NARloy-Z and Zirconium-Copper

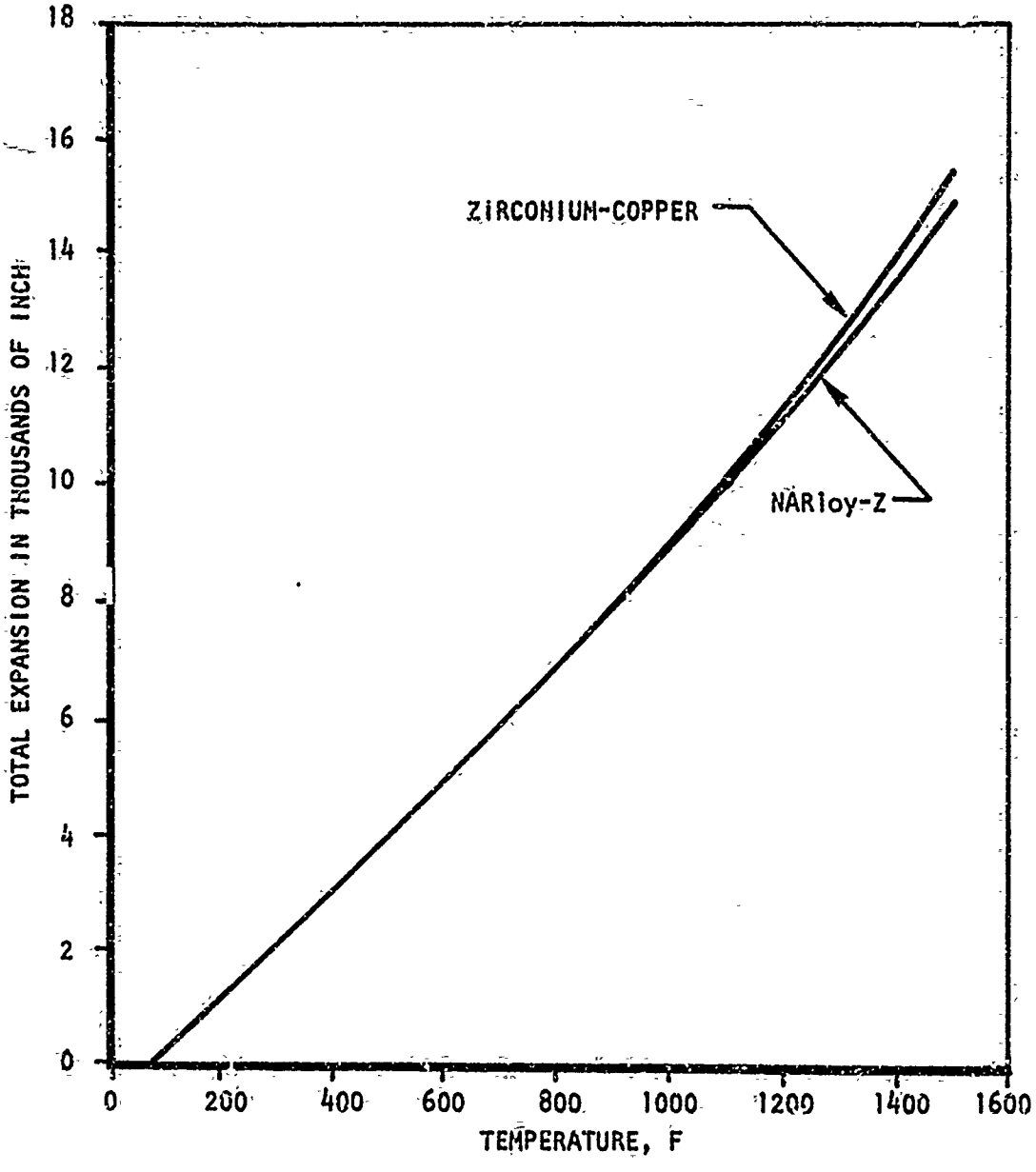

Figure 49. Thermal Expansion of NARloy-Z and Zirconium Copper

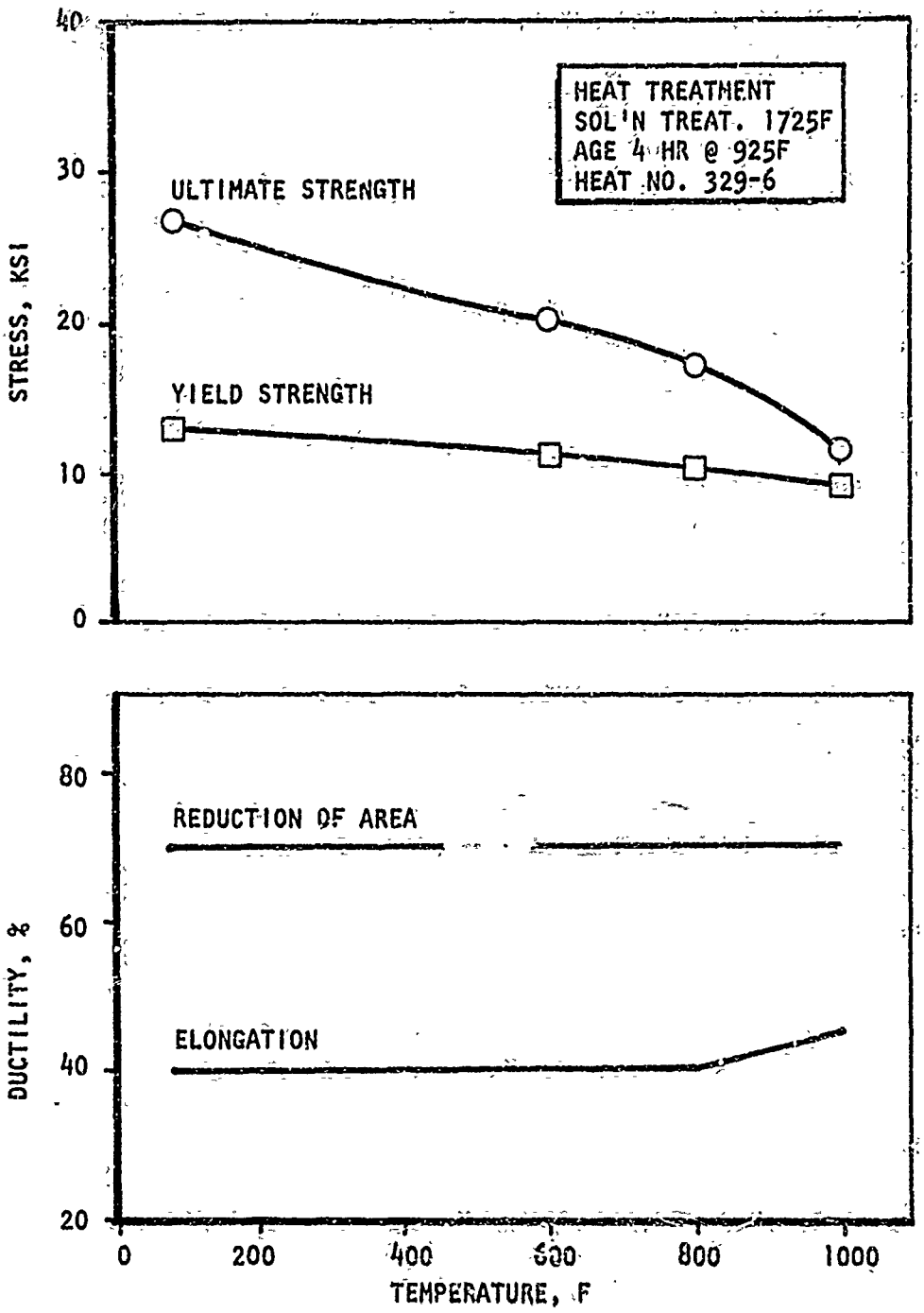

Figure 50. Tensile Properties of Zirconium Copper

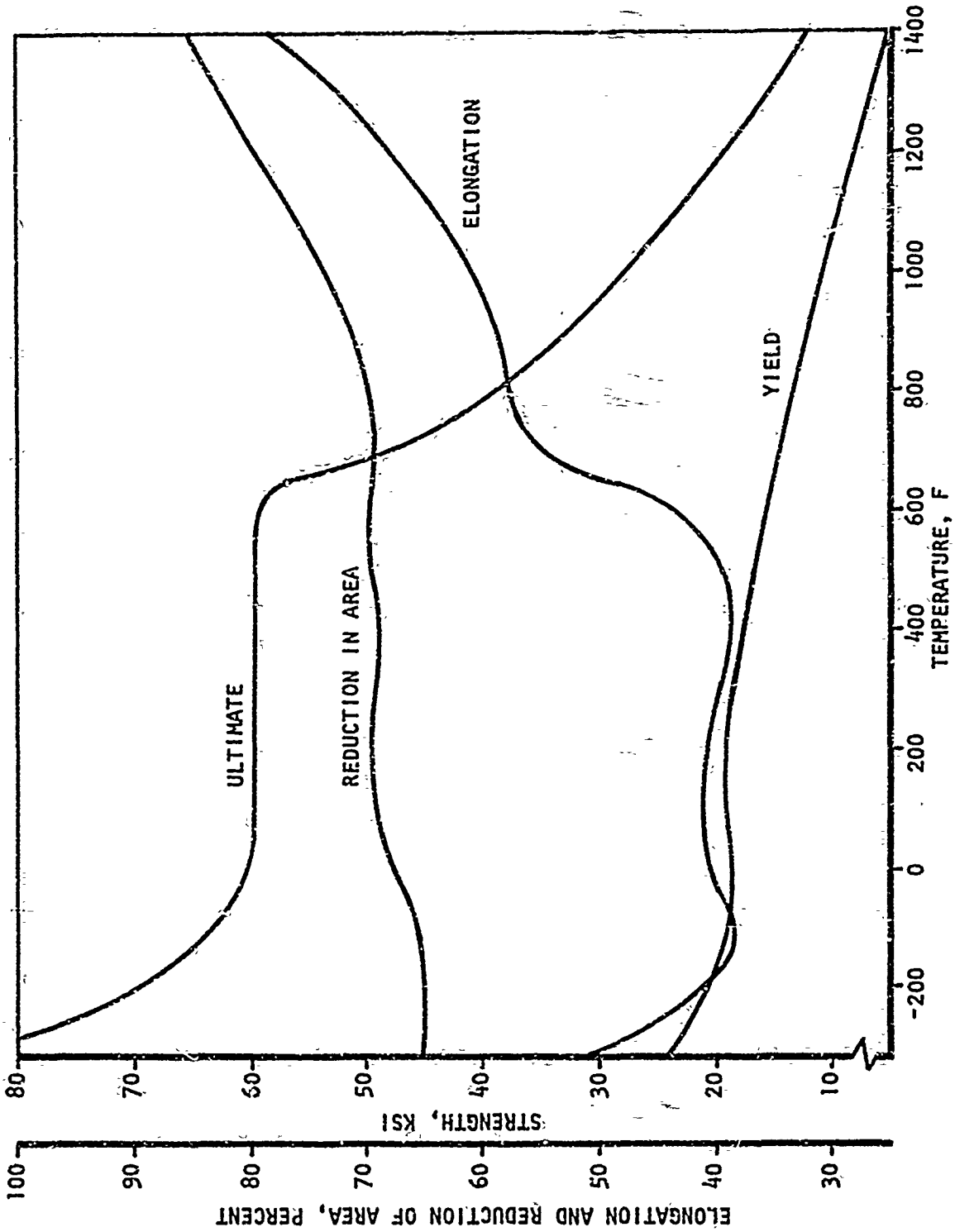

Figure 51. Properties of Annealed Nickel-200

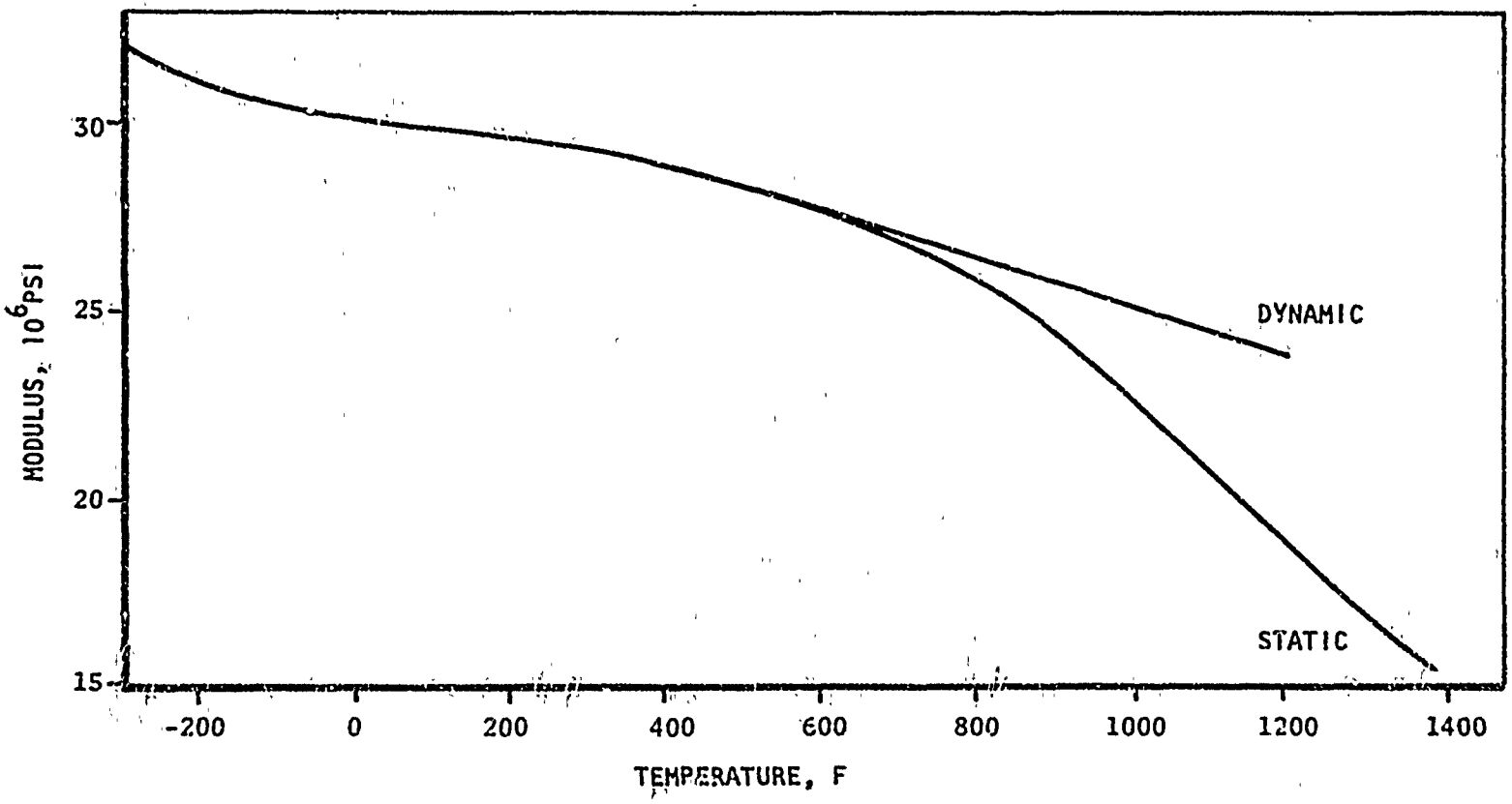

Figure 52. Modulus of Elasticity of Annealed Nickel 200

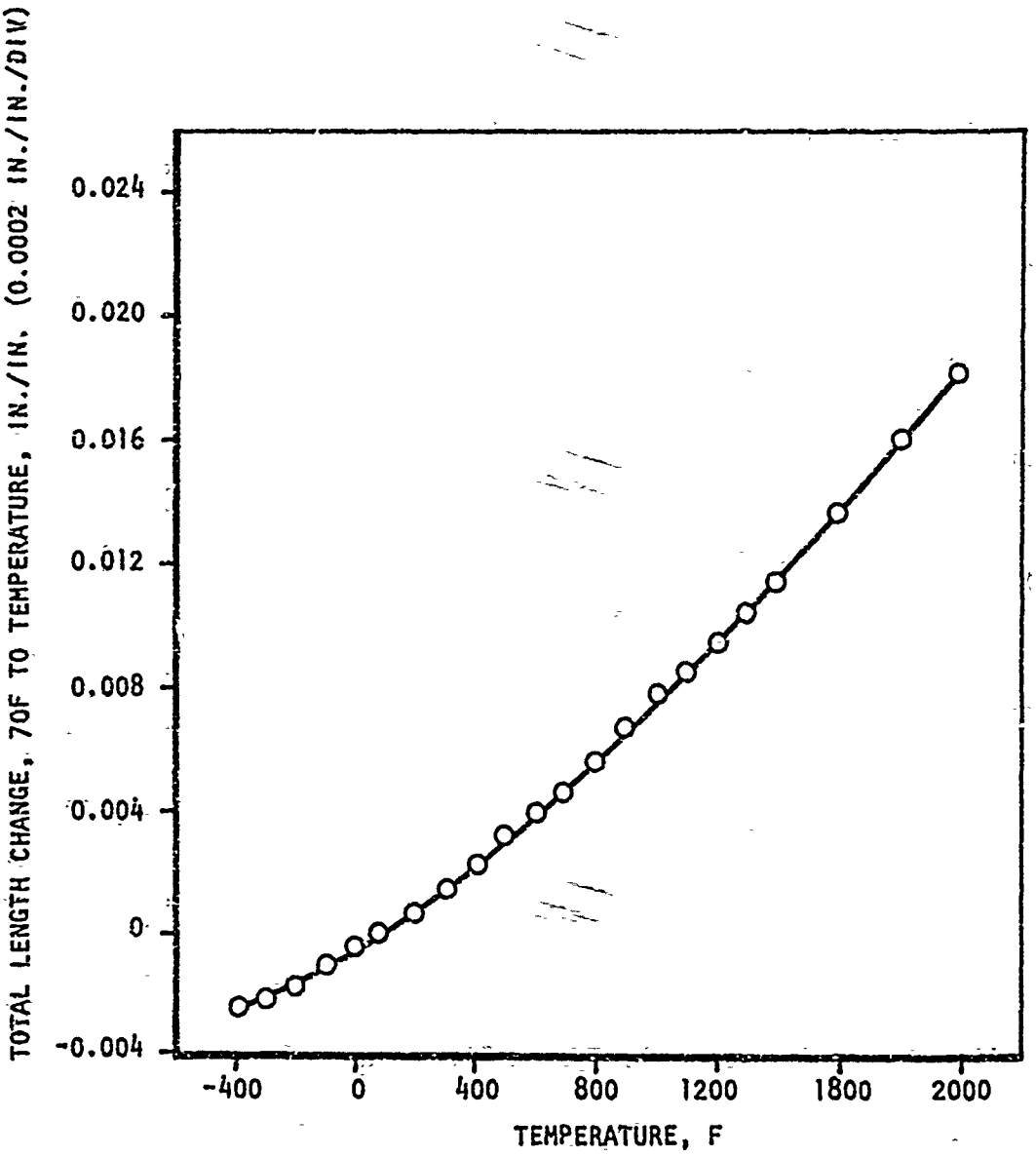

Figure 53. Thermal Expansion Properties of Annealed Nickel-200

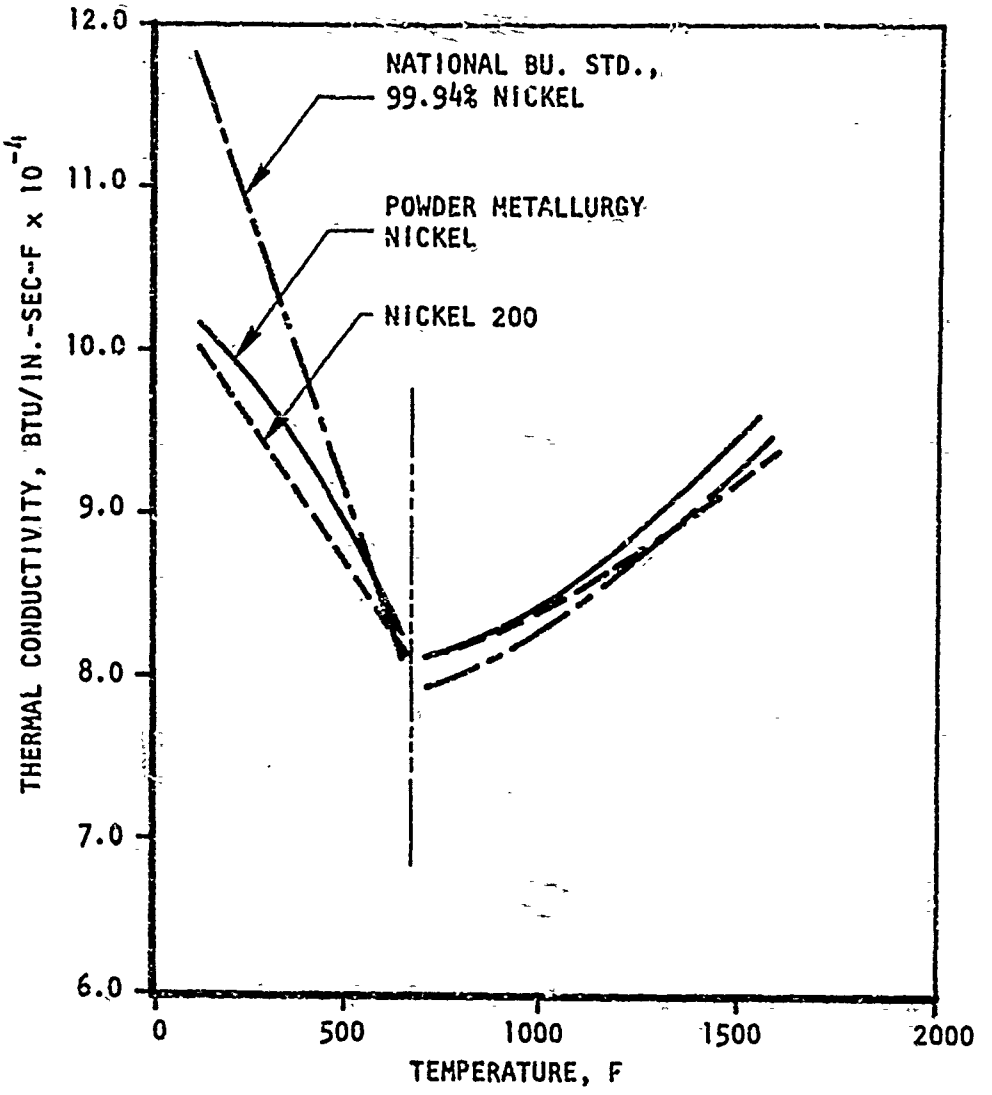

Figure 54. Thermal Conductivity of Pure Nickel

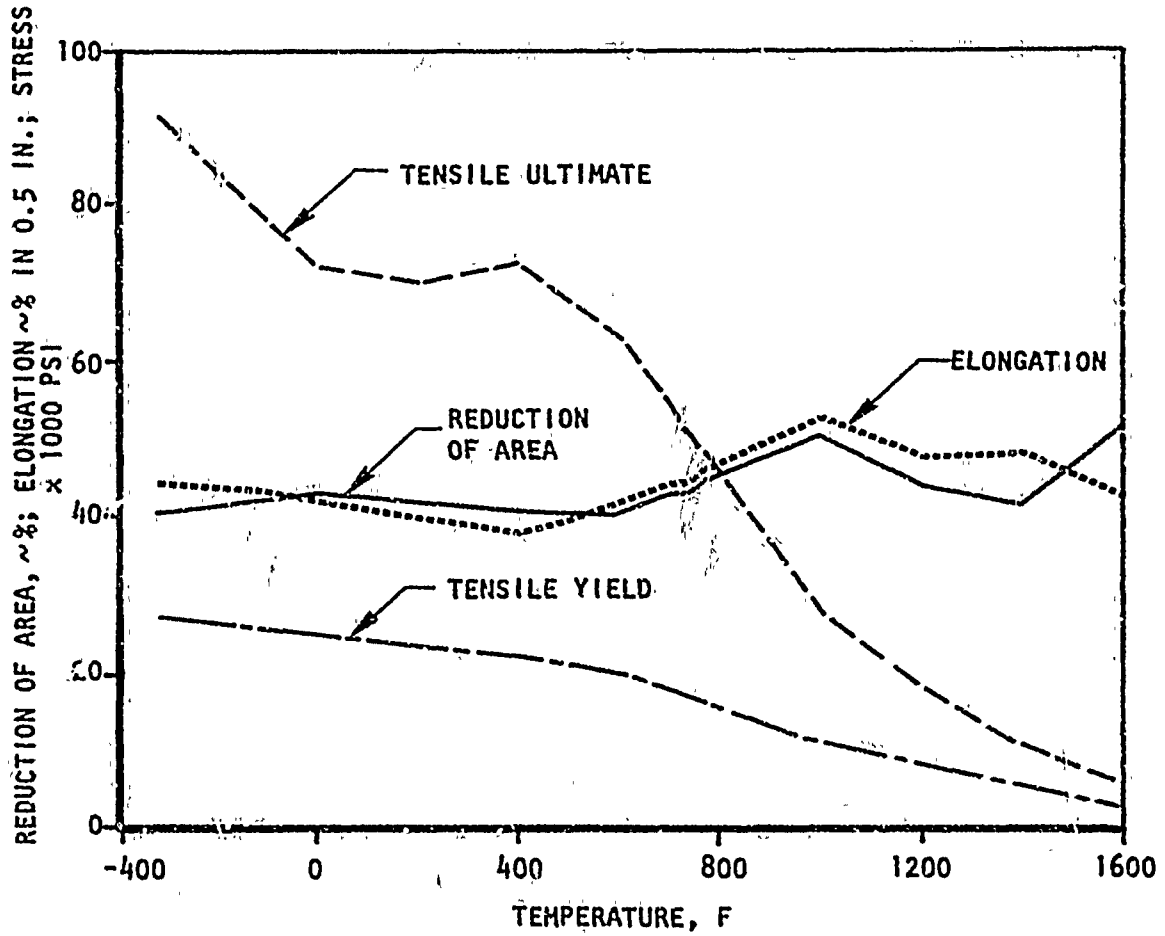

Figure 55. Short Time Tensile Properties of Powder Metallergy Nickel

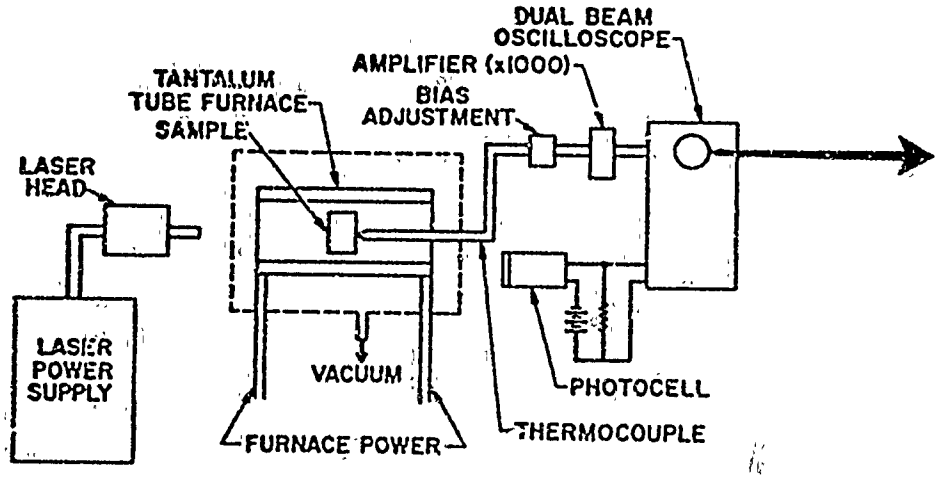

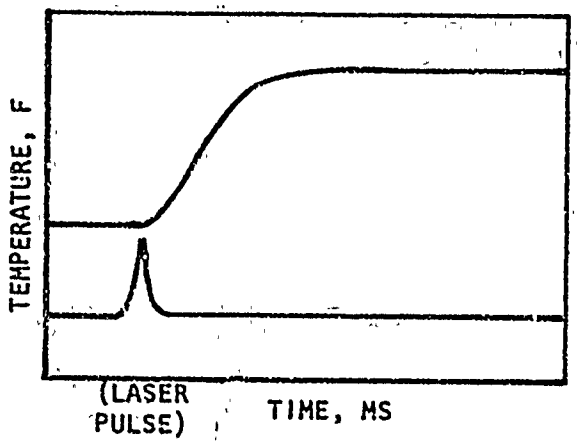

PROCEDURE

- MOUNT SAMPLE (1/4 DIA x 0.080 - 0.160 LENGTH)
- HEAT FURNACE TO DESIRED TEMPERATURE
- SINGLE LASER PULSE TO FRONT FACE OF SAMPLE

TIME-TEMPERATURE RESPONSE THROUGH SAMPLE

↓

DETERMINATION OF THERMAL DIFFUSIVITY

↓

CALCULATION OF THERMAL CONDUCTIVITY AS FUNCTION OF THERMAL DIFFUSIVITY, SPECIFIC HEAT, AND DENSITY

Figure 56. Elevated Temperature Thermal Conductivity Tests

As a reference OFHC copper bars were also tested and results (Fig. 47) presented on a percentage of OFHC copper conductivity.

Isothermal Fatigue Tests

Isothermal fatigue testing was performed on laboratory specimens of NARloy-Z, zirconium-copper, sintered nickel and wrought nickel-200 to determine the effect of strain rate, temperature, strain range and tensile and/or compressive hold time on fatigue life.

The low cycle strain controlled fatigue tests were run on an MTS Universal testing machine. The strain range of the tests was controlled by the output of a linear variable differential transformer (LVDT) that is a component of the extensometer attached to the specimen. The axial surface strains were calibrated as a function of extensometer displacement using strain gages on the specimen gage length. This calibration was done at ambient temperature and 400 F. A quartz lamp furnace was used to radiantly heat the specimen for the elevated temperature testing. The furnace was water cooled, and purged with argon to minimize specimen oxidization.

The NARloy-Z and zirconium copper specimens were tested at various temperatures ranging from 70 F to 1200 F, at axial surface strain ranges of 0.75 to 2.1 percent, and strain rates of 0.1 and 0.01 in./in./sec. Sintered nickel specimens were tested at 70 F, 1000 F and 1400 F at axial surface strain ranges of 1.0 and 2.0 percent and a strain rate of 0.2 in./in./sec. Initial tensile load drop was used as the failure criteria. Some life tests were runs with 15 seconds tensile and/or compressive hold times.

The results can be summarized as follows:

1. The NARloy-Z material exhibited longer life than the zirconium-copper for similar conditions of isothermal low cycle fatigue testing.

2. The zirconium-copper cycle life is reduced by a factor of two by testing at a slower strain rate while the NARloy-Z cycle life was unaffected for tests conducted at 1000 F and the same strain range.

3. Hold time at peak tensile strain lowers specimen life for NARloy-Z and zirconium copper.

4. The onset of rapid tensile load drop was inconclusive as a failure criteria for testing with hold time at peak compressive strain.

5. Nickel-200 material exhibited longer life than the power metallurgy nickel for similar test conditions.

A detailed discussion of test procedures, specimen design, test results, etc. is presented in the following paragraphs.

Test Plan. The isothermal fatigue tests were conducted to investigate the effect of material, temperature, strain rate and hold time at peak strain on elevated temperature fatigue life. The four strain controlled waveforms (illustrated in Fig. 57) investigated were were zero hold time, tensile hold time, compressive hold time and equal tensile and compressive hold time.

Test Description. Low cycle strain controlled fatigue tests were run at constant ambient and elevated temperature on an electro-hydraulic MTS Universal Testing Machine. The main components in the test setup are depicted schematically in Fig. 58 and 59.

The top ram of the MTS loading system introduced axial displacement to the specimen. The ram motion was controlled by the voltage output of a linear variable differential transformer that is part of the extensometer attached to the specimen. Since the extensometer hangs from the specimen, it measures only displacement of the specimen gage length. The extensometer was calibrated using strain gages in the specimen gage length. The specimen axial surface strain was obtained as a known function of extensometer displacement. This is discussed in detail under specimen calibration.

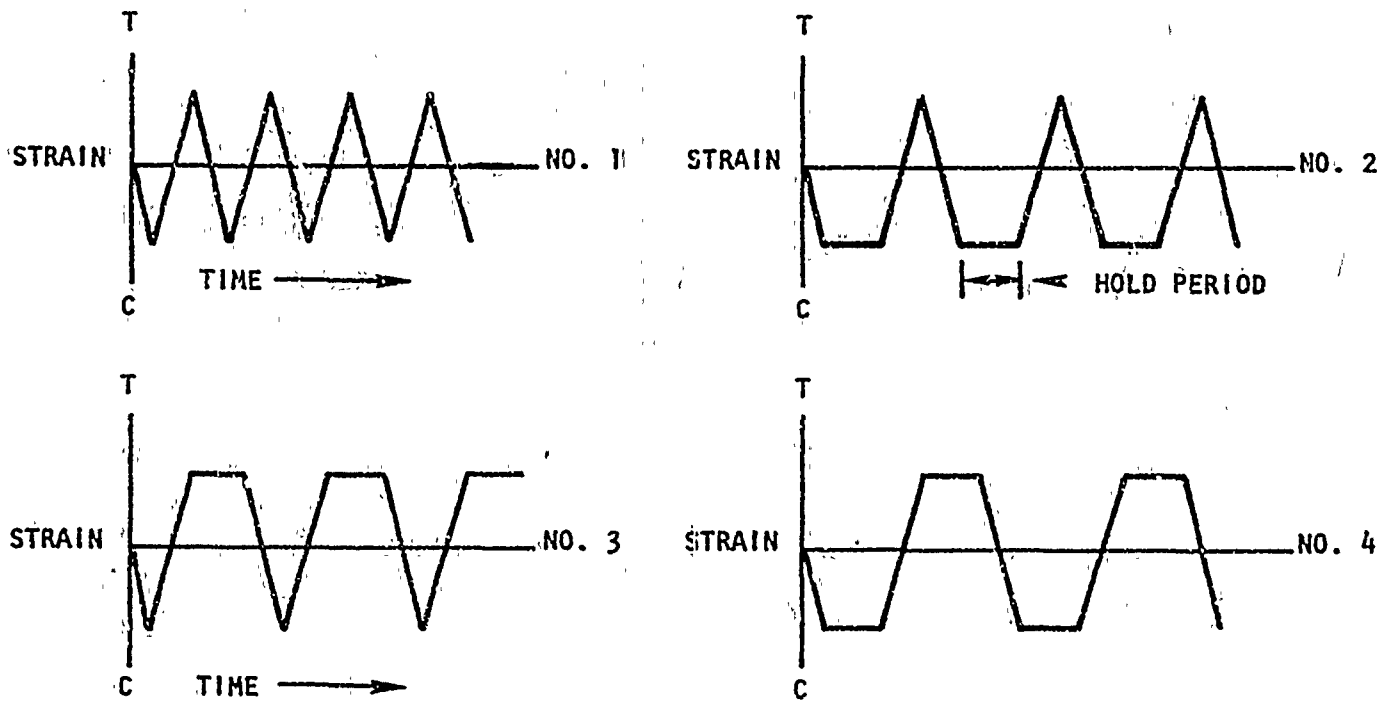

Figure 57. Strain-Wave Forms Used in Evaluating Effects of Low-Cycle Fatigue Resistance

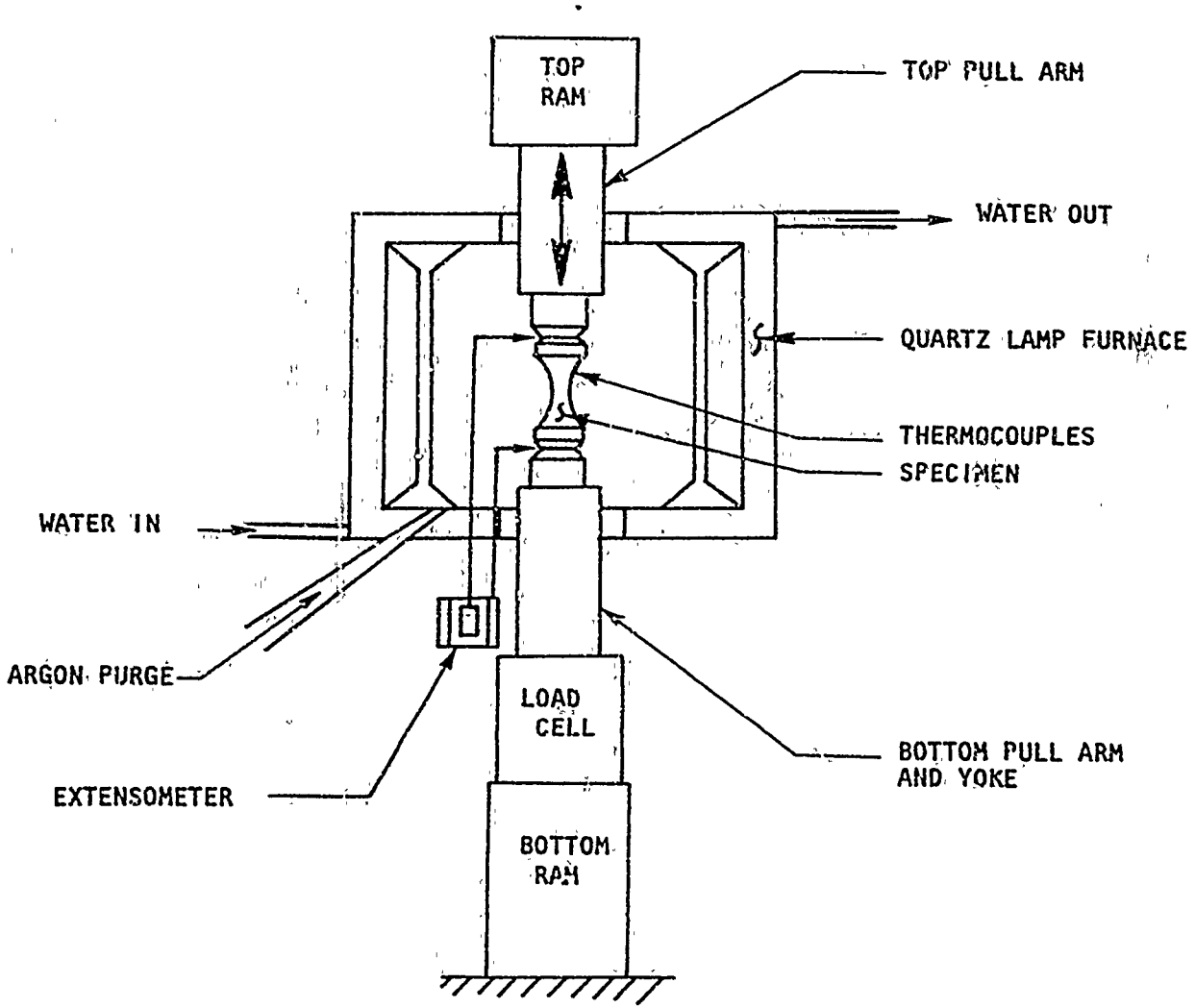

Figure 58. Schematic of Test Assembly

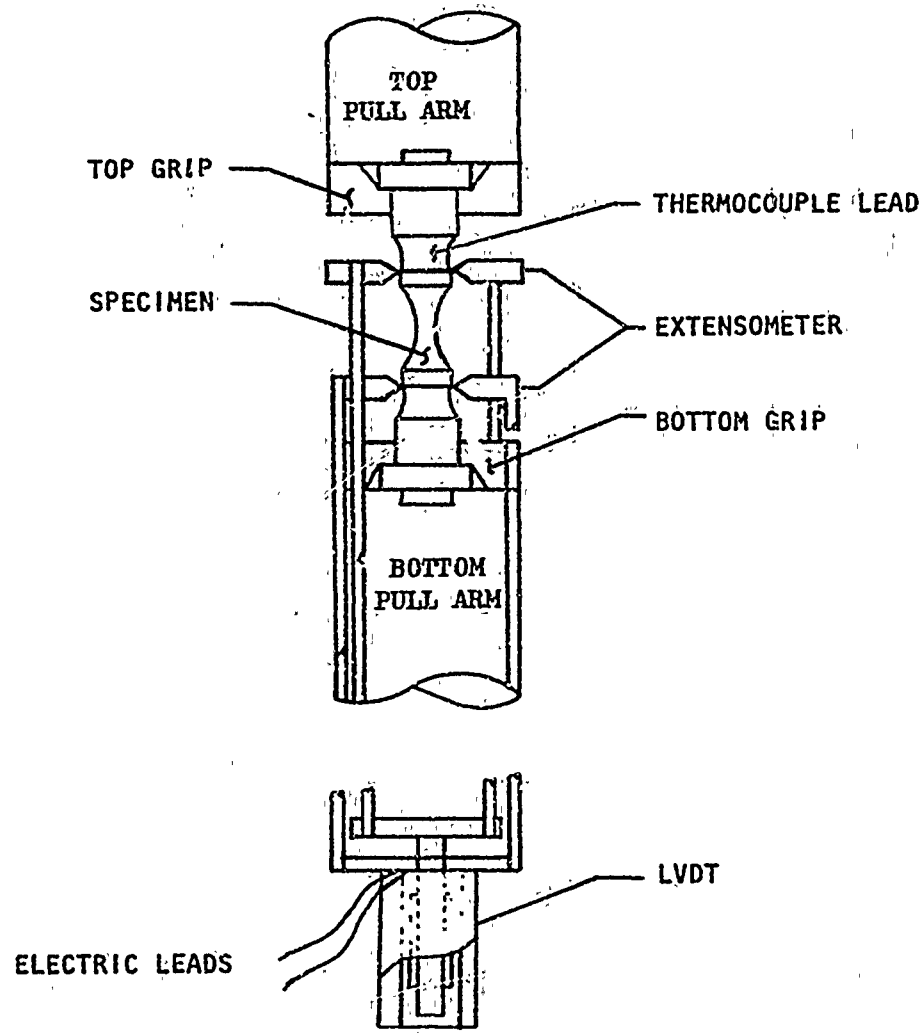

Figure 59. Test Configuration

A quartz lamp furnace was used to radiantly heat the specimen for the elevated temperature testing. The furnace was water cooled and purged with argon to prevent specimen oxidation. The furnace was controlled by thermocouples attached to the specimen as depicted in Fig. 59. Temperature control was maintained within 3 degrees F.

The normal sequence followed during elevated temperature testing is as follows:

1. The specimen was installed in the top pull arm.
2. The top ram was lowered till the specimen rests on the bottom pull arm.
3. The specimen was secured to the bottom pull arm with the load on the specimen kept to a minimum.
4. The extensometer grips were attached to the specimen.
   a. The electronic hookup was made and LVDT core was centered in the coil.
5. The furnace was placed around the specimen (deleted for ambient temperature testing).
   a. Thermocouples were connected.
   b. The cooling water and argon gas attachments were made.
   c. The specimen was heated to the test temperature maintaining zero load on the specimen.
6. The test amplitude, frequency (and hold time) were set on the MTS machine controls.
7. The MTS machine was put in "strain control" (extensometer LVDT) and testing was started. Load, extensometer deflection and ram stroke signals were recorded on an oscillogram.
   a. A polaroid snapshot of the load-extensometer deflection hysteresis loop was taken from the oscilloscope.

The data acquisition network is schematically illustrated in Fig. 60.

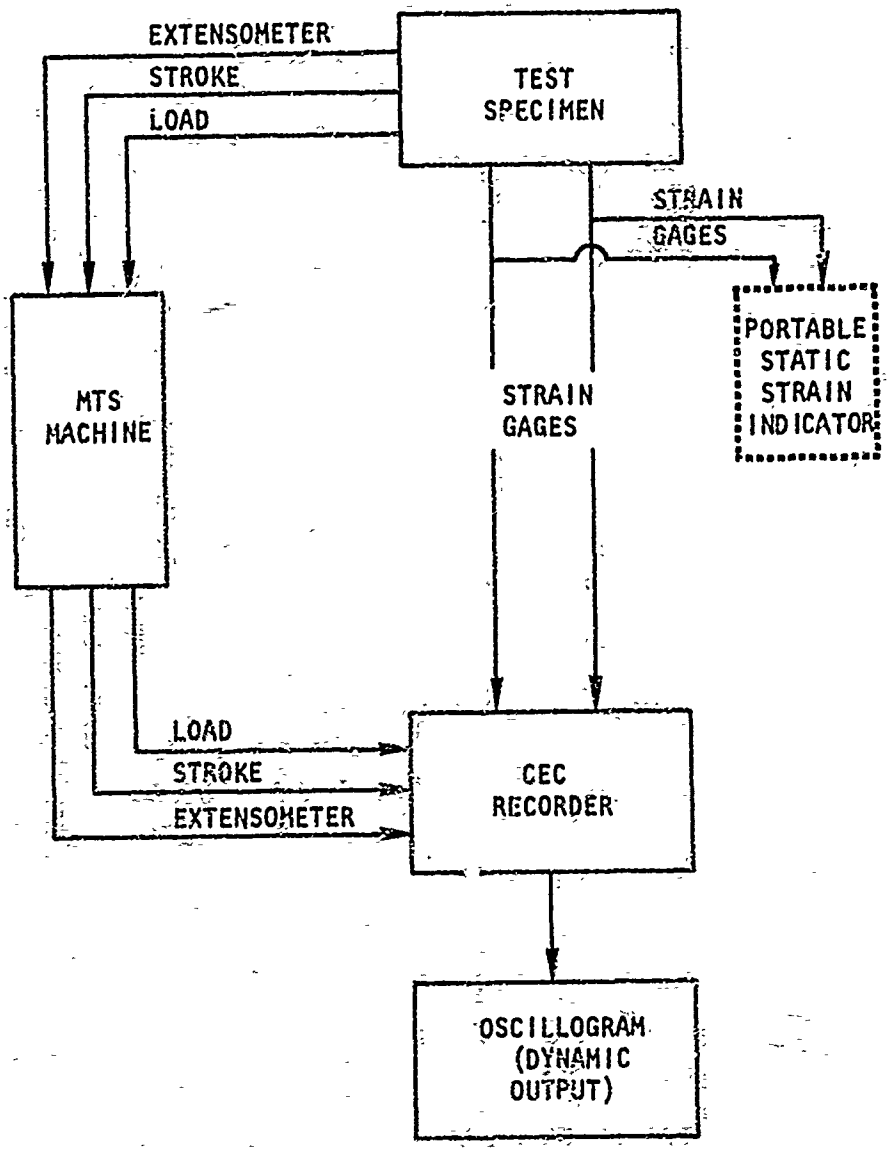

Figure 60. Data Acquisition

Test Fixture Design and Alignment. The fixture assembly (Fig. 61) was designed to be as rigid as possible to minimize deflections during compression loading. The buttonhead specimen grip was designed to minimize high temperature creep which was encountered on earlier threaded specimens. The fixture consists of upper and lower pull bar assemblies and the extensometer assembly. The Quad-Elliptical radiation heating furnace, shown in phantom on Fig. 61, fits around the pull bars and provides a heated zone of approximately 10.0 inches long. Each pull bar has a Rene 41 split flange grip which bolts down on the buttonhead ends of the specimen. The Rene 41 studs and A-286 nuts which hold the split flanges in place are oxidized in air prior to use to provide a high temperature anti-seize coating. The studs are long enough to extend out of the hot zone of the pull bars so that the stud to pull bar threads will not present any galling problems.

The part of the pull bars that is heated by the furnace is made of Inconel 718 and is water cooled just outside of the furnace. Beyond the coolant circuit the top pull bar body is welded to a CRES flange and the bottom pull bar body is welded to a CRES yoke.

The joint between the top pull bar and the ram of the MTS machine consists of a collar threaded onto the ram and a flange on the pull bar which is preloaded against the end of the ram by six bolts through the collar. The pull bar can be adjusted for angularity and concentricity by moving sideways slightly or differentially torqueing the six bolts.

The joint between the bottom pull bar and the load cell on the base of the MTS machine consists of a spherical seat that can be moved sideways and angled for alignment. The joint is preloaded by applying a tension load in excess of the operating loads to the pull bar with the MTS machine and torqueing two spiral washers against each other to take up any slack in the joint. When the load is released the joint is preloaded. After assembly of the fixtures to the MTS load frame, a special strain gaged specimen is installed to obtain system alignment within 200 micro-inches per inch. Adjustment of angle and offset is made at the joint above the load cell (Fig. 62).

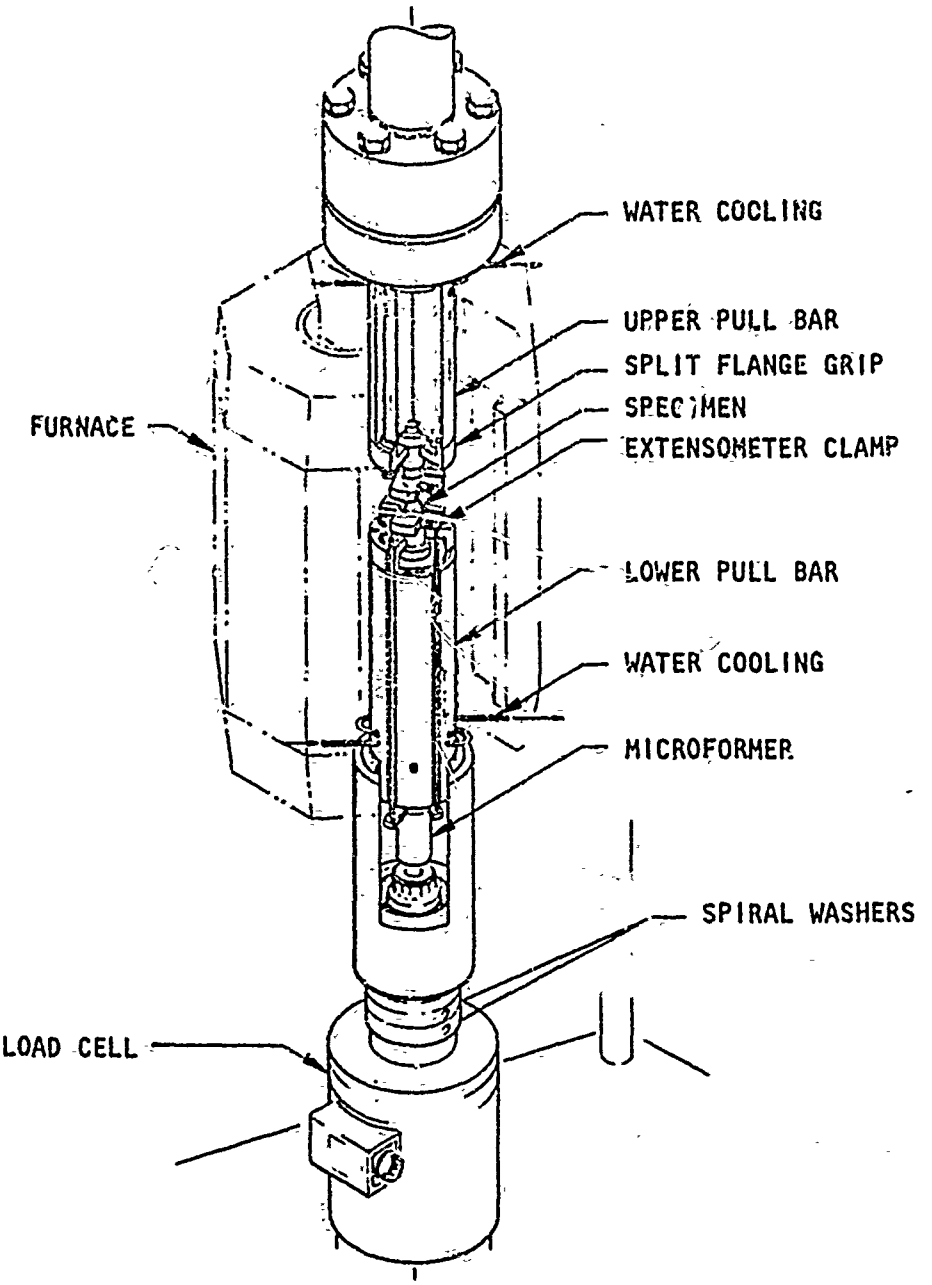

Figure 61. Test Fixture for Isothermal Fatigue Tests

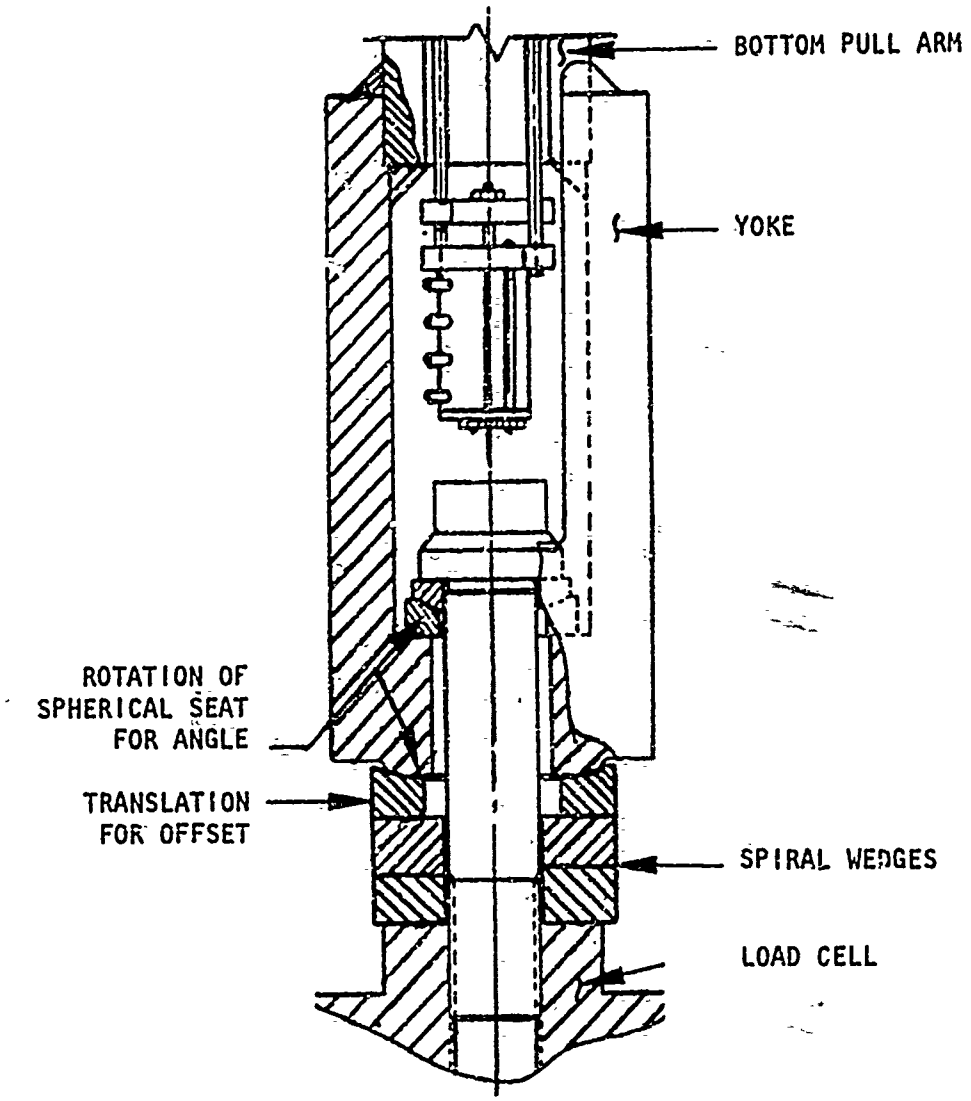

Figure 62. Alignment Joint

The axial extensometer assembly consists of grips which clamp to notches in the body of the specimen, rods which transfer motion to the center of the lower pull bar and a microformer to measure the strain. The core of the microformer is suspended from one notch and the transformer from the other notch so that the relative motion between core and transformer is equal to the motion between notches.

The Quad-Elliptical radiation heating furnace contains four quartz lamps which are focused on the specimen by elliptical water cooled reflectors. The furnace has provisions for purging the heated zone with inert gas. The furnace is supported from the MTS machine frame and is moved into place around the pull bars during tosting.

Specimen Design. The test specimen geometric features that involve special considerations are the tubular shape; the strain gage length and the 3/4-inch transition radius to the gage length. A sketch of the specimen is given in Fig. 63. The tubular shape was chosen to represent a typical thrust chamber wall thickness (~ 0.035 inches). In addition, there is access for cooling if a thermal fatigue test is desired while retaining similarity between isothermal and thermal fatigue specimen. The straight section in the specimen gage length is provided for the location of strain gages used for calibration. The 3/4-inch radius is provided to reduce the strain concentration in the specimen gage length. Early in the program a 1/4-inch radius specimen was used. The strain concentration in the specimen gage length was suspected to be excessive. A computer analysis was made which showed that a 3/4-inch radius specimen would reduce this effect. The large radius makes the strain distribution more uniform. The improvement in the strain distribution effected by the radius was determined for a solid nickel-200 specimen. A comparison of the strain ratio, as shown in Table 4, at the center of the specimen gage length for 1/4-inch and 3/4-inch radii was used as a measure of the improvement. The ratio was checked at 70 F and 1400 F with an average improvement of 28 percent.

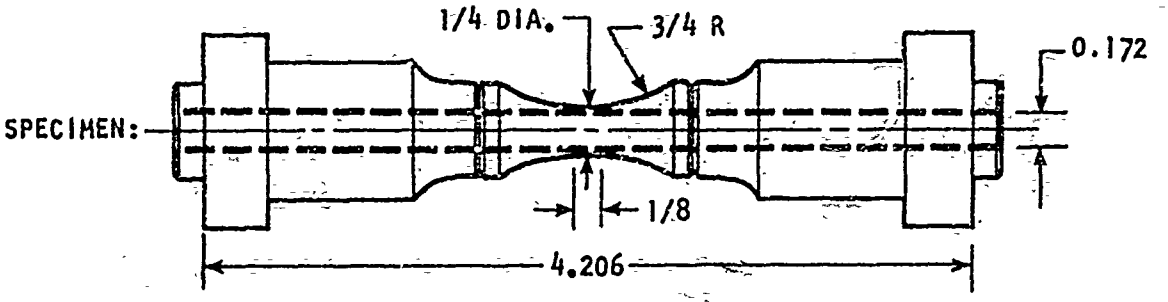

Figure 63. Isothermal Fatigue Specimen

Table 4. Strain Distribution Improvement

	70F			1400F		
	ϵ_{z_1},%	$\epsilon_{z_1}/\epsilon_{z_2}$	PERCENT IMPROVED*	ϵ_{z_1},%	$\epsilon_{z_1}/\epsilon_{z_2}$	PERCENT IMPROVED*
1/4 IN. RADIUS	1.61	1.47	27.5	2.71	1.63	29.0
3/4 IN. RADIUS	1.95	1.15		3.44	1.26	

$$* \% \text{ IMPROVED} = \frac{\left(\epsilon_{z_2}/\epsilon_{z_1}\right)_{1/4\ R} - \left(\epsilon_{z_2}/\epsilon_{z_1}\right)_{3/4\ R}}{\left(\epsilon_{z_2}/\epsilon_{z_1}\right)_{1/4\ R}} \times 100$$

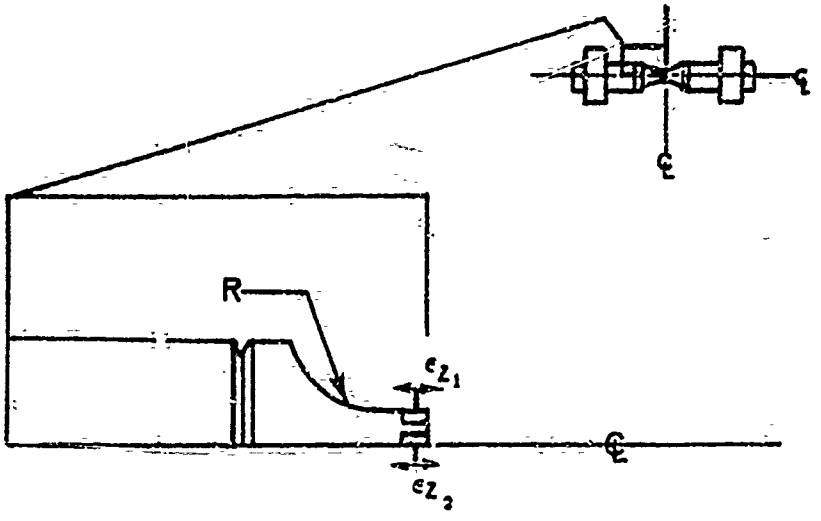

Specimen Fabrication

The NARloy-Z, zirconium-copper and nickel-200 specimens were machined from forged plates using the same parameters and procedures established for thrust chamber fabrication. The powder metallurgy nickel specimens were fabricated using specially blended nickel powders and a two-step pressing and sintering procedure previously established at Rocketdyne.

The nickel powder blend was processed by blending and pressing into bars a mixture of 80 percent medium mesh (7-9 microns) powder with 20 percent fine mesh (2-3 microns) powder. These bars were then crushed, pulverized and screened to a 50-150 micron mesh and blended (in an 80-20 percent ratio) with additional fine powders to form the powder blend to be used in making the hardware. The resulting powder blend has very high purity, good compaction, ductility and flowing parameters (required for high fill densities), excellent sinterability, and good grain strength allowing for precision machining of as-pressed hardware.

The nickel powder was initially packed and pressed at 55,000 psig while at ambient temperature. This was followed by sintering of the free standing part at 2300 F for three hours. Following this the specimens were machined to final configuration for laboratory testing.

Specimen Calibration. Specimen calibration was performed under both static and dynamic conditions using strain gages mounted on the specimen. Calibration was made at 70 F and 400 F for each of three strain ranges for the NARloy-Z and zirconium-copper materials and each of two strain ranges for the Nickel-2000 and sintered nickel. The upper bound calibration temperature was 400 F since it was the limiting temperature of the strain gages. Typical curves of strain versus extensometer displacement obtained from calibration are plotted in Fig. 64 through 67. The average strain of two strain gages located 180 degrees apart on the specimen gage is plotted. The gages measured surface strain in the axial direction. During calibration the MTS machine displacement was imposed manually.

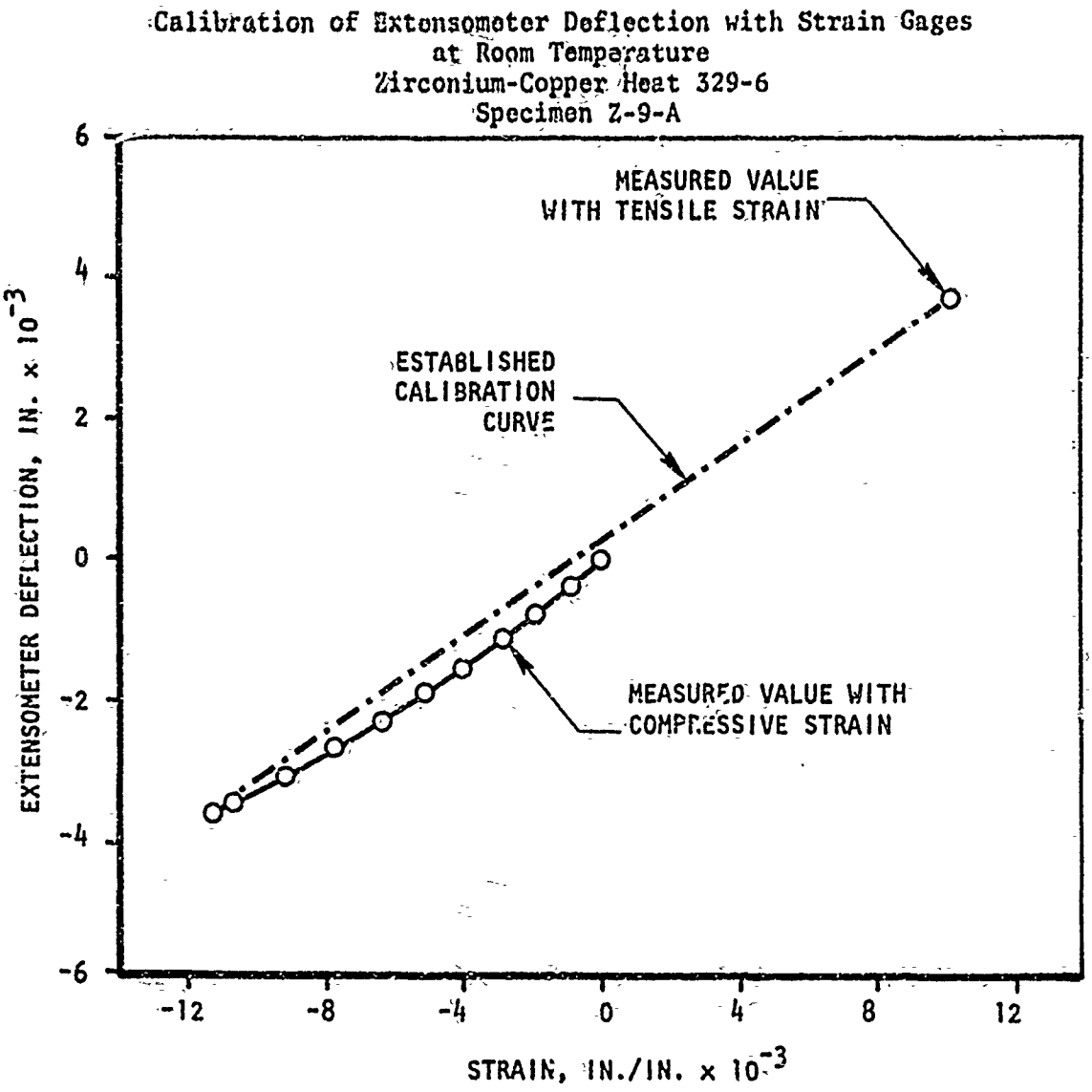

Figure 64. Isothermal Fatigue Test Extensometer Deflection vs Strain

Calibration of Extensometer Deflection with Strain Gages
at Room Temperature
NARloy-Z Heat 5402
Specimen 17-C-27-A

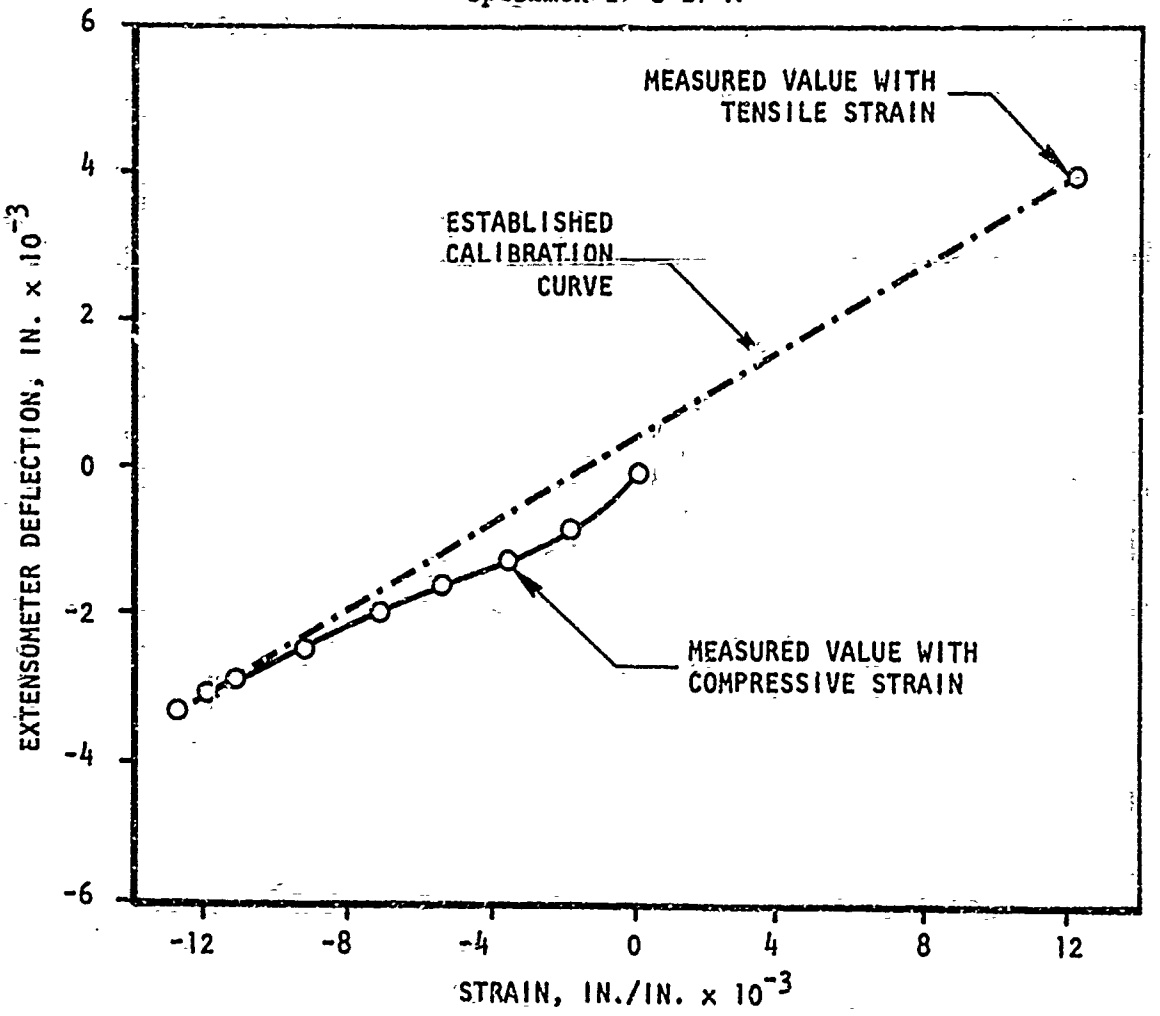

Figure 65. Isothermal Fatigue Test Extensometer Deflection vs Strain

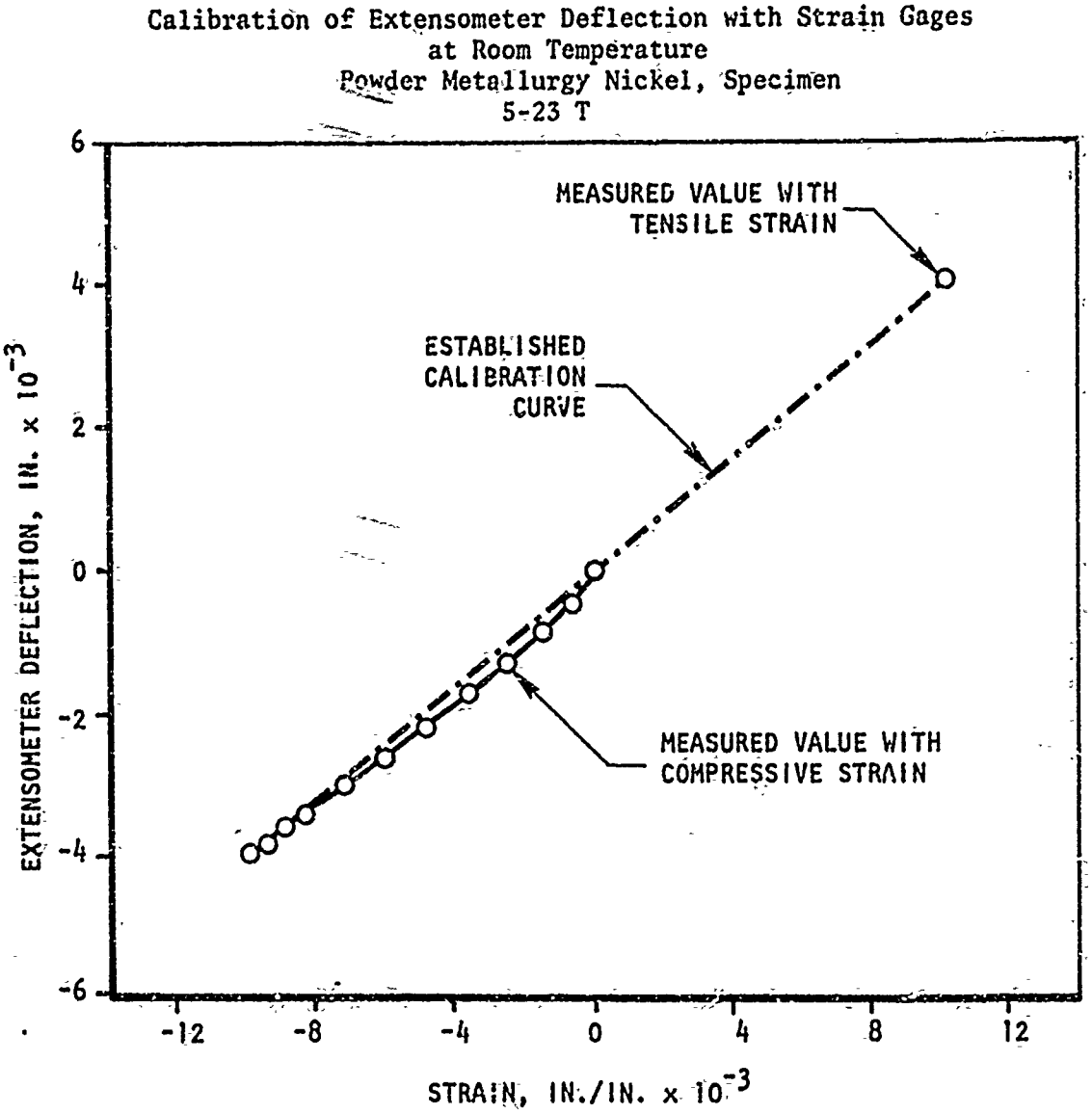

Figure 66. Isothermal Fatigue Test Extensometer Deflection vs Strain

Calibration of Extensometer Deflection with Strain Gages
at Room Temperature
Nickel-200
Specimen N-13-C

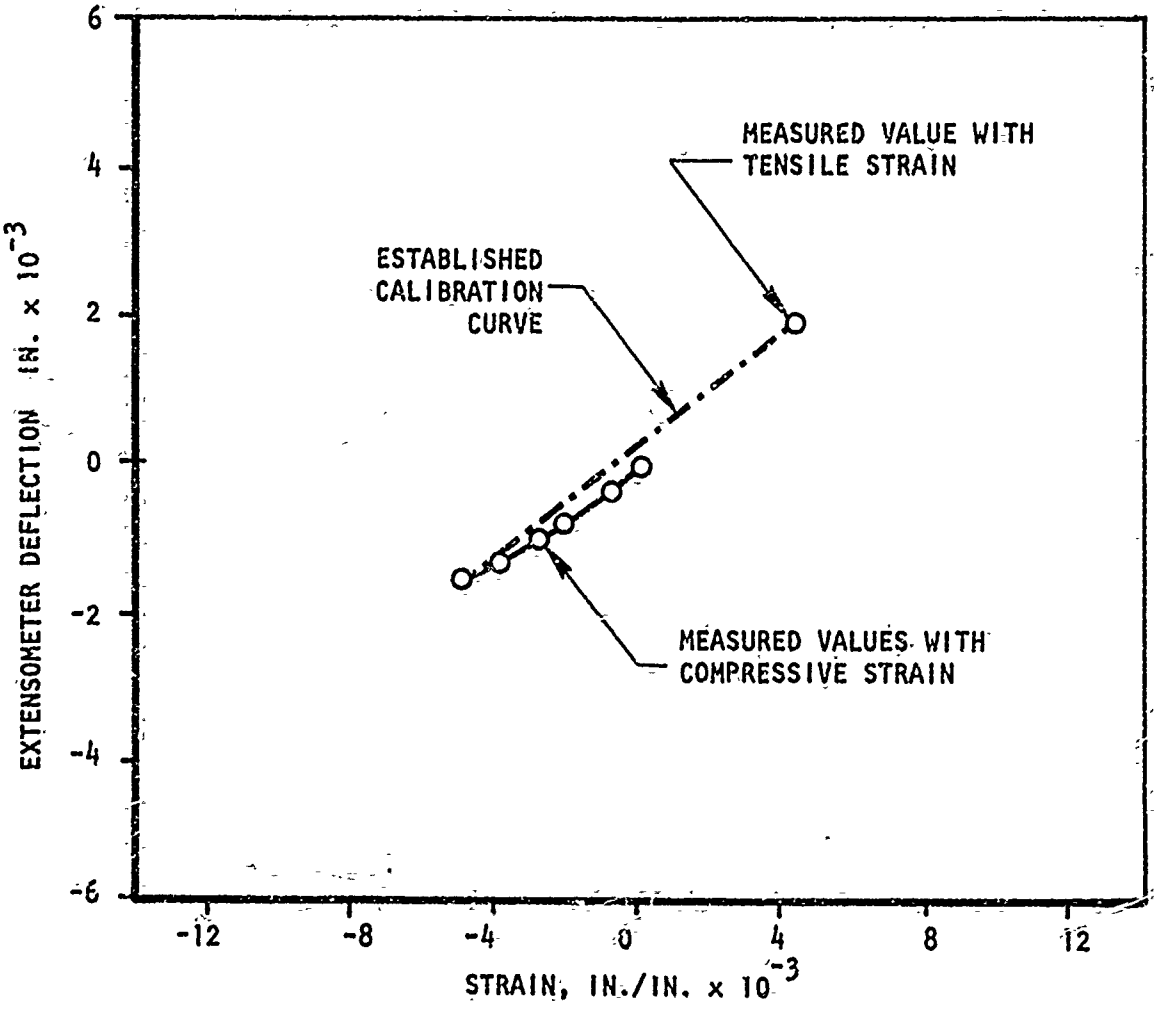

Figure 67. Isothermal Fatigue Test Extensometer Deflection vs Strai

The calibration was made in compression corresponding to the first direction the material is strained during its use. The strain-displacement relationship from the first quarter cycle was used to set the extensometer displacement amplitude for each test as illustrated below.

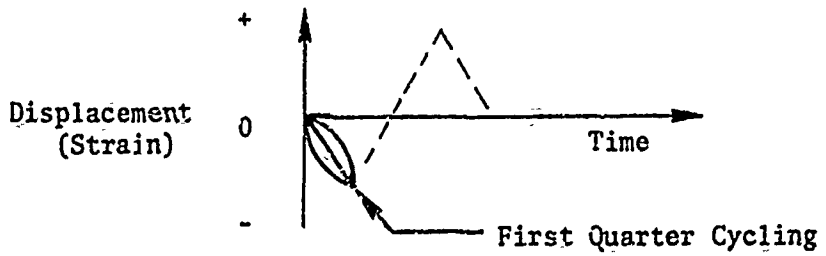

This was done to eliminate the effect of cycling on the strain-displacement relationship so the data could be applied directly to the life analysis of the engine hot gas wall. After the initial calibration the specimen was manually and dynamically cycled at the test displacement to verify that the static output equaled the dynamic output. The strain gage output for the manual cycles was read on a portable strain recorder. The dynamic output was read from the record of an oscillograph as the specimen was cycled. The manual and dynamic verification was repeated at 400 F. In all cases, the readings were the same.

A computer analysis of a test specimen was performed early in the program to determine the influence on experimental accuracy of testing beyond the calibration temperature range. The specimen geometry used in this analysis was the solid 1/4-inch diameter gage length with a 1/4-inch radius transition section, Fig. 68. Nickel-200 was used for the specimen material. Using the room temperature calibration data to predict the strain for a given displacement at 1400 F, the error introduced was calculated. The results are summarized in Fig. 69. Based on the results for maximum test strain amplitude, ε_t, of .011 in./in. an error of 10 percent would be estimated. The error would be on the conservative side since the results would indicate the strain to be lower than it actually is, giving a lower life for the strain amplitude than would be the case for the real value.

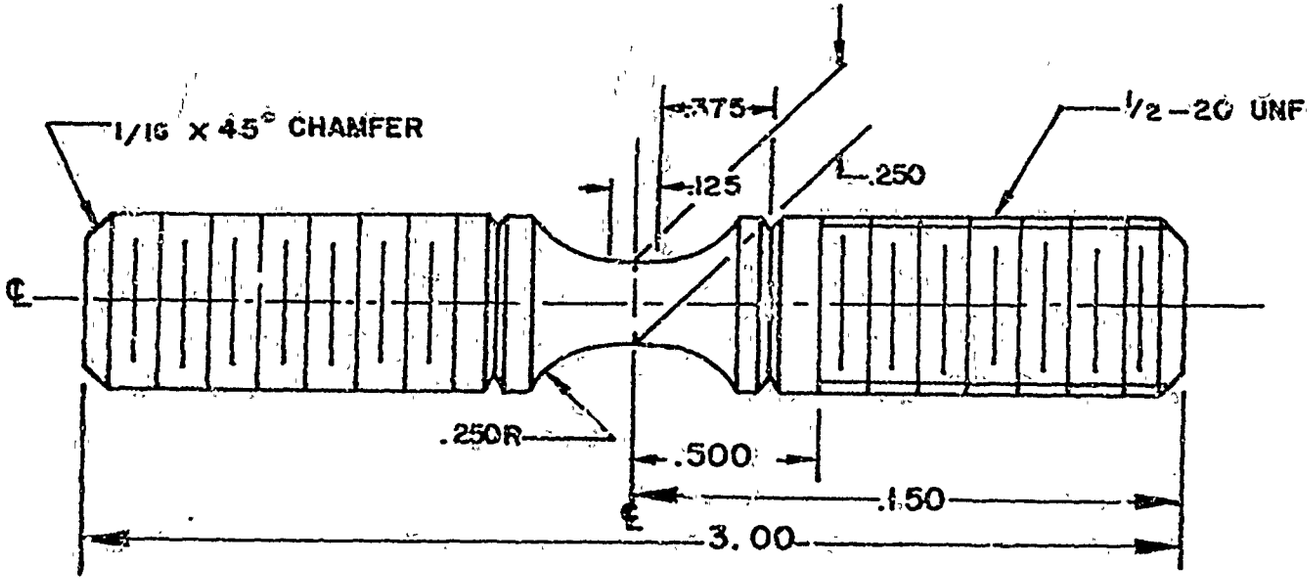

Figure 68. Isothermal Fatigue Specimen

EXTENSOMETER DISPLACEMENT δ, IN.	CALCULATED STRAIN AMPLITUDE ϵ_z, IN./IN.	CALCULATED STRAIN AMPLITUDE ϵ_z, IN./IN.	PERCENT* DIFFERENCE %Δ
	1400F	70F	
0.00216	0.0076	0.0075	-7.6
0.00390	0.0147	0.0132	-11.3
0.00585	0.0227	0.0200	-13.5

$$* \quad \%\Delta = \frac{\epsilon_{z_{1400F}} - \epsilon_{z_{70F}}}{\epsilon_{z_{70F}}} \times 100$$

The negative sign indicates the imposed strain at 1400F is underestimated based on the room temperature calibration.

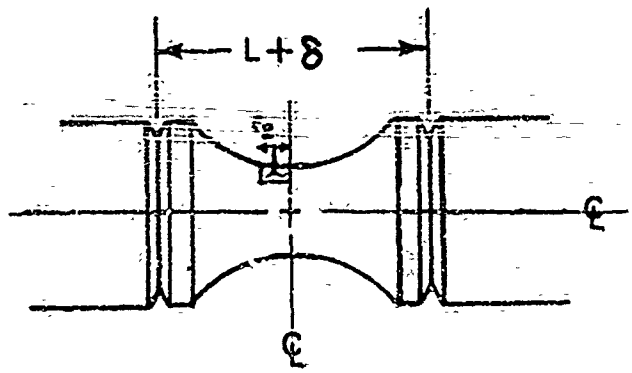

Figure 69. Specimen and Computer Model

Test Results. Isothermal strain controlled low cycle fatigue data obtained on the materials of interest (NARloy-Z, zirconium-copper, sintered nickel and wrought nickel-200) are presented in this section.

It is noted that before the isothermal low cycle fatigue data was plotted, the axial surface strain range for each test was changed to the effective strain range using the results of a finite element eleastic-plastic computer analysis of the specimen as discussed previously in Task II. This is done to provide the method of relating the strains in the test specimen to those in any general application.

The onset of rapid tensile load drop detected from tensile load-cycle plots was used to determine the number of cycles to failure for each test. Plots of typical tensile load-cycle data are given for zirconium-copper in Fig. 70 to illustrate the method.

The basic cycle life data (zero hold time) for the NARloy-Z and zirconium copper are presented in two ways for each material (Fig. 71 through 83): a composite plot is given for all data points at all test temperatures and a second set of plots is given for the data at each test temperature. Data on the composite plots, Fig. 41 and 42, are fitted either by a curve obtained using a modified form of the Universal Slopes Manson equation discussed previously (Ref. 24), based on average material properties for the temperature range, or by a curve obtained for the "best fit" to the data. The "best fit" was found using a numerical procedure that permits the choice of curve constants that minimize the standard deviation of the data. For zirconium-copper, the modified Universal Slopes and "best fit" curves are translated up or down to define the corresponding upper or lower bound of the data. It is worth noting that the slope of the zirconium-copper and the NARloy-Z "best fit" curves differ markedly from the slope of the respective modified Universal Slopes curves. For NARloy-Z, the modified Universal Slopes curve plots below the data and is translated up to define both the lower and upper bounds. The "best fit" curve is translated

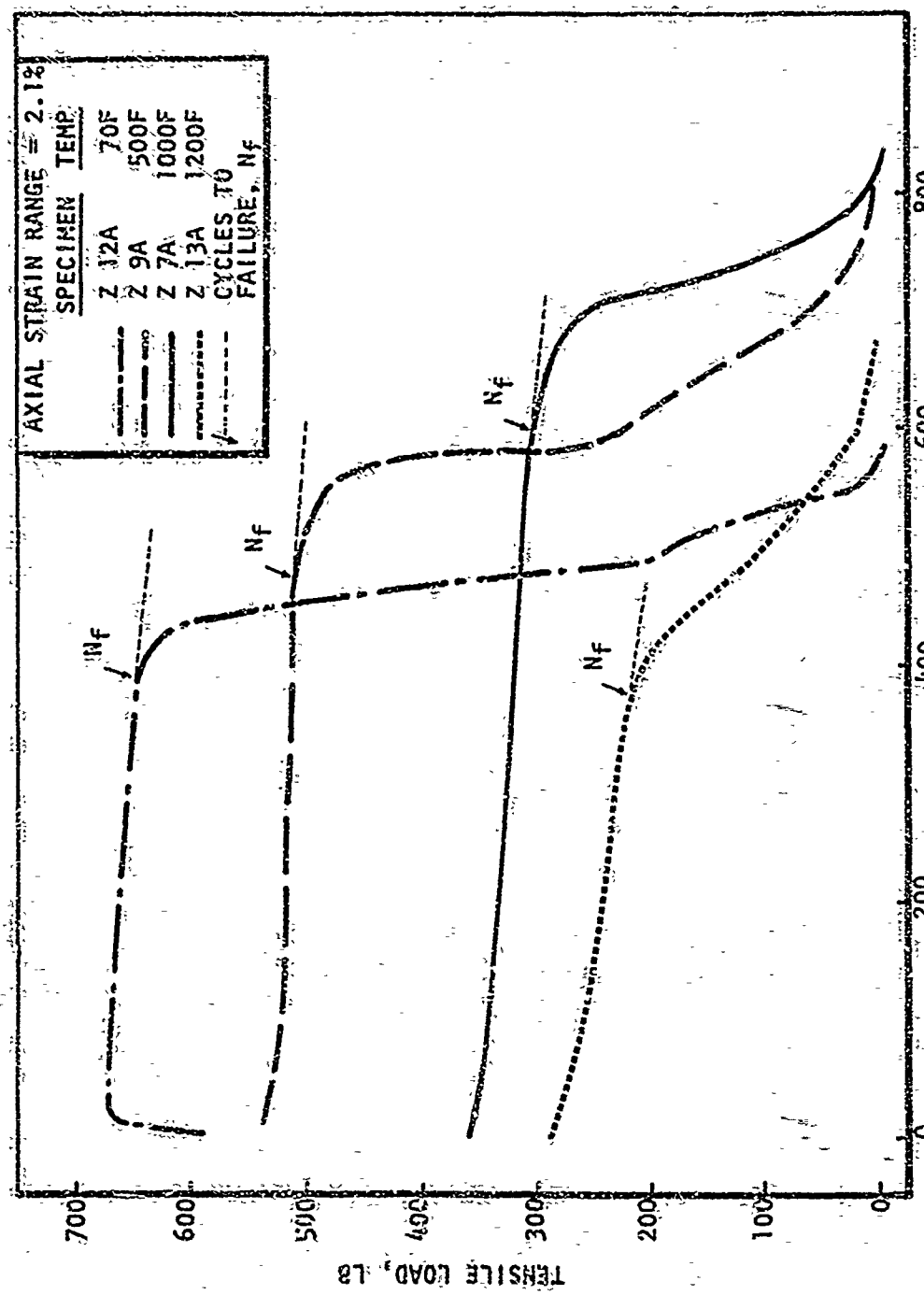

Figure 70. Tensile Load vs Cycles - Zirconium-Copper

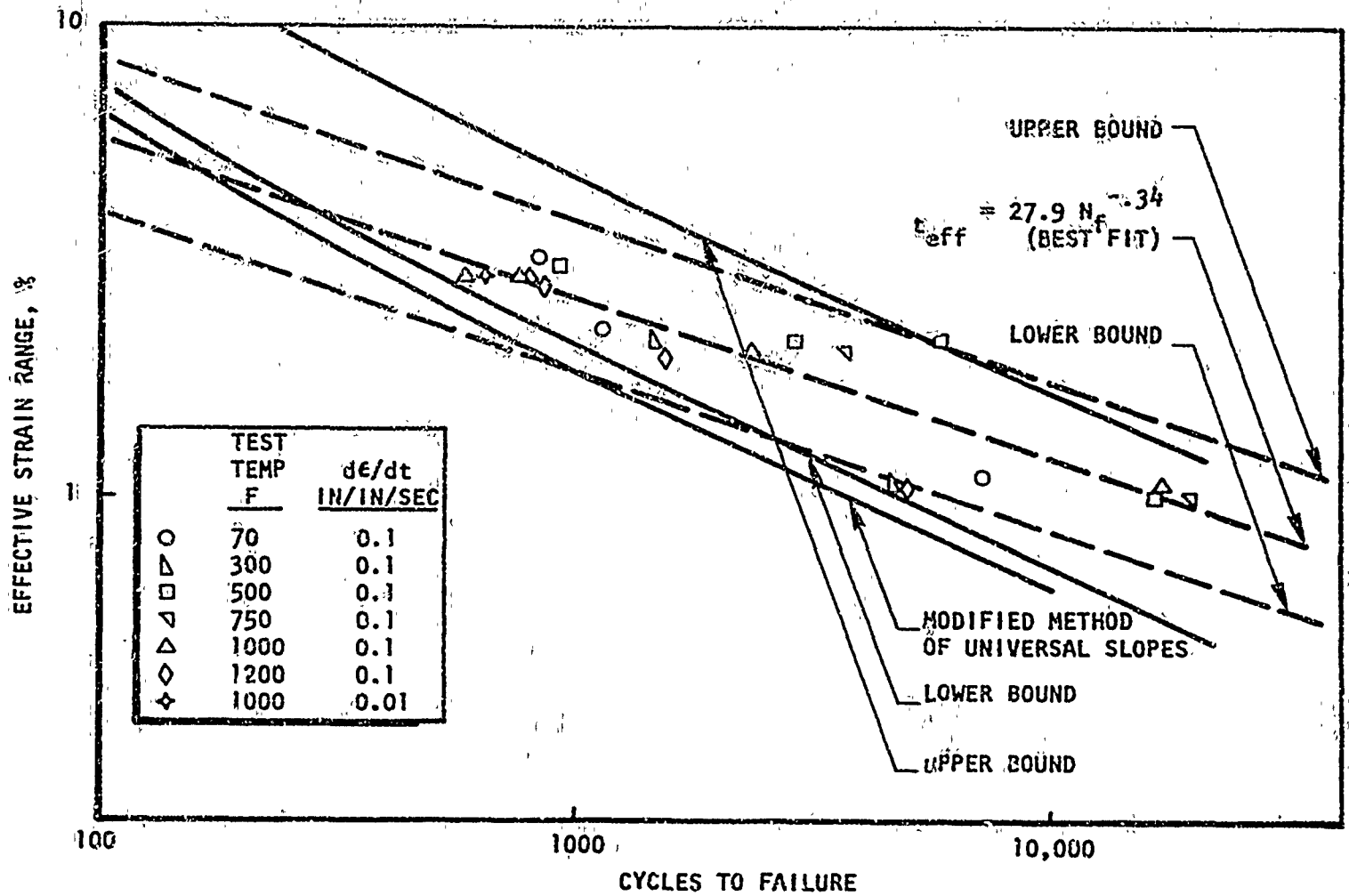

Figure 71. Isothermal Cyclic Test Data - NARloy-Z Heat 5402

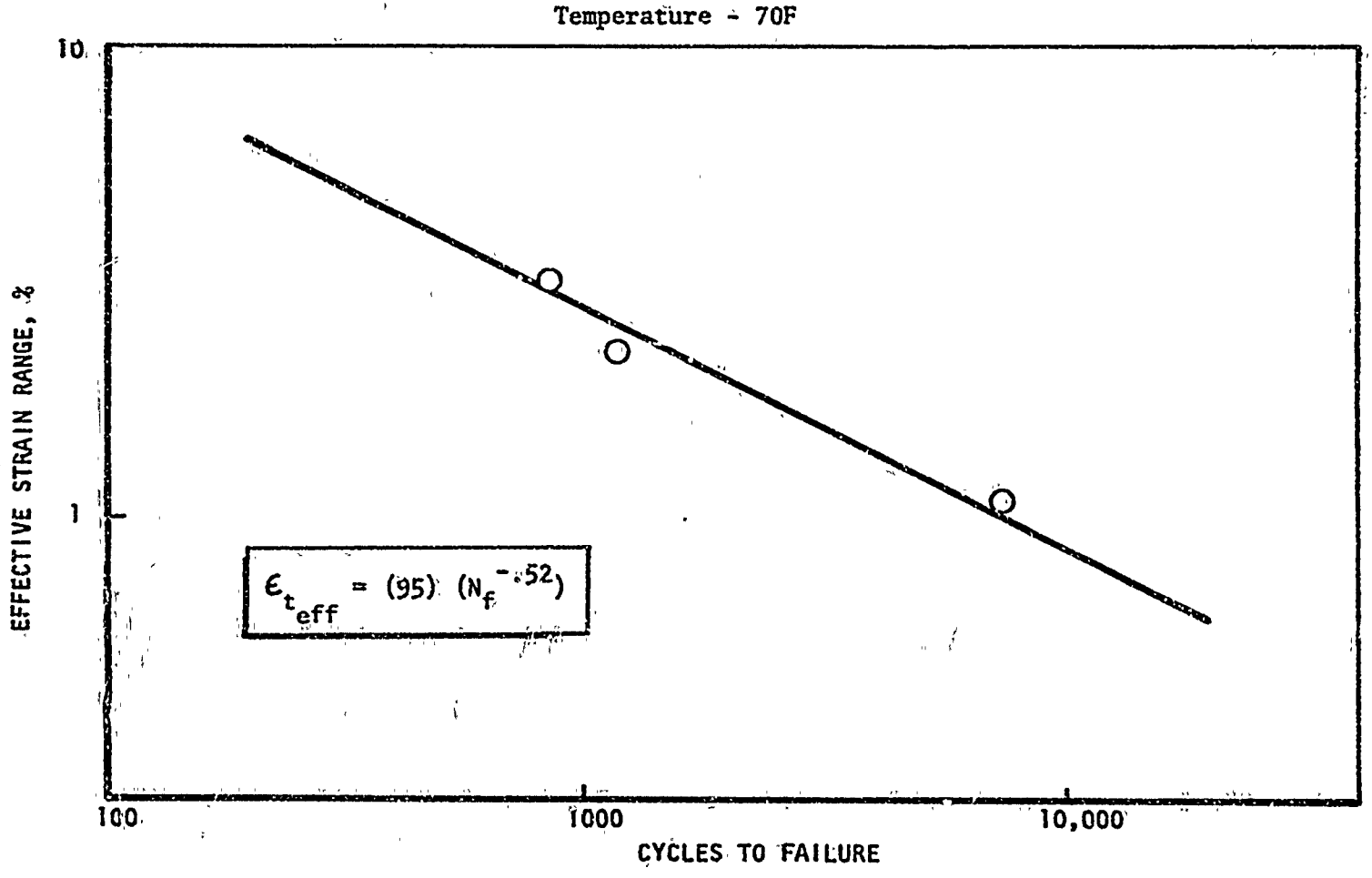

Figure 72. Isothermal Cyclic Test Data Effective Strain Range vs Cycles to Failure - NARloy-Z Heat D-5402

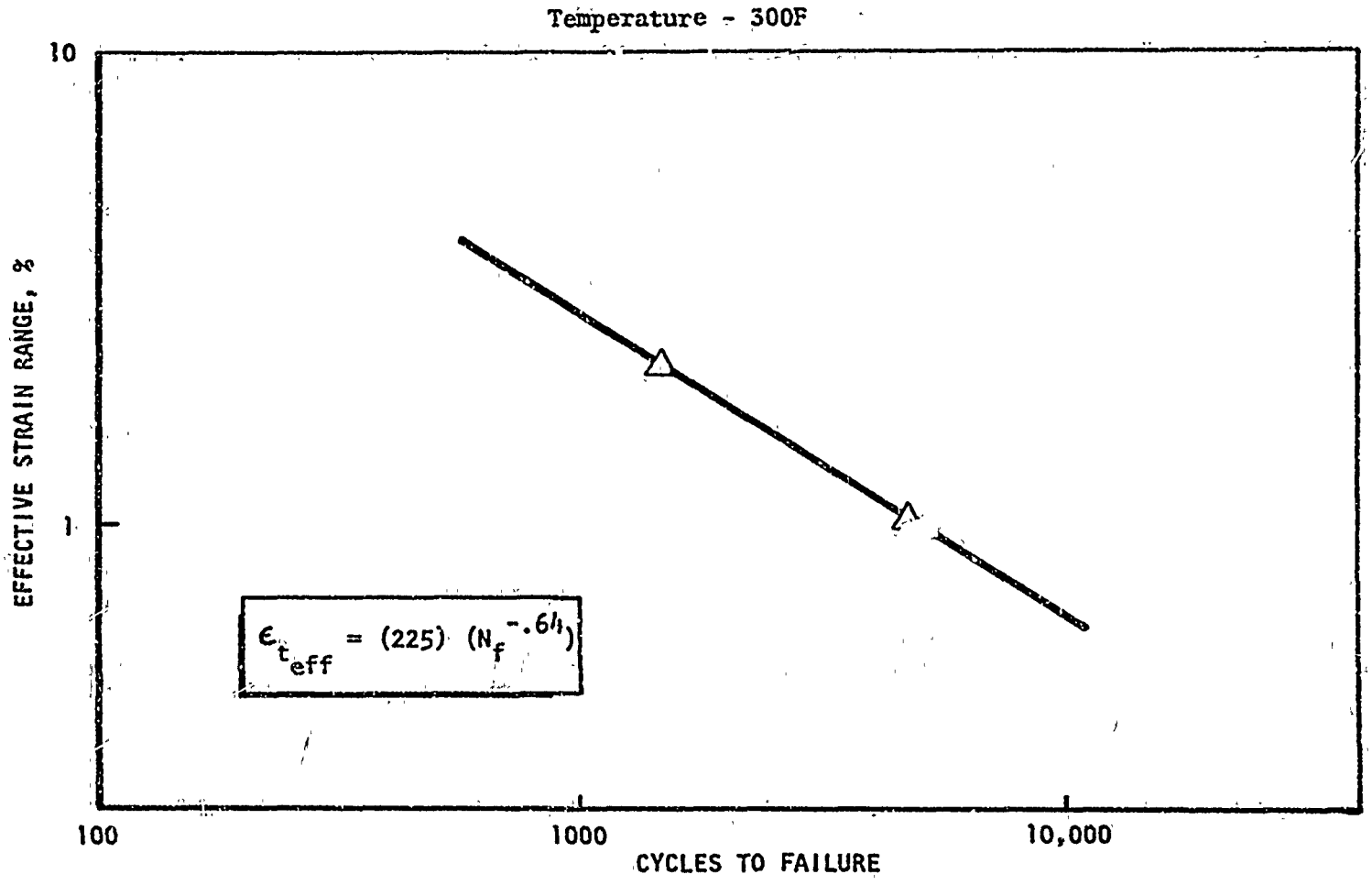

Figure 73. Isothermal Cyclic Test Data Effective Strain Range vs Cycles to Failure - NARloy-Z Heat D-5402

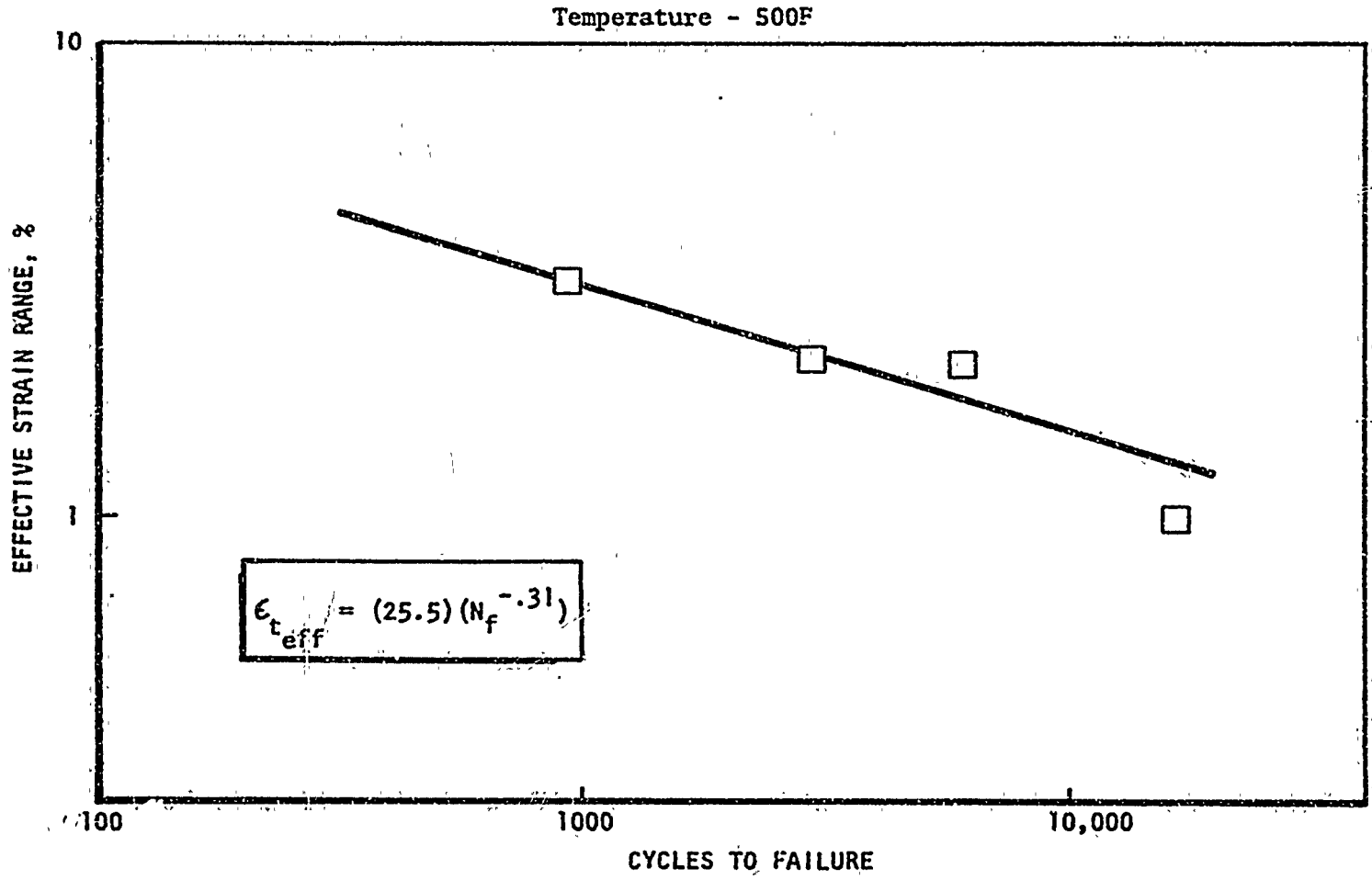

Figure 74. Isothermal Cyclic Test Data - Effective Strain Range vs Cycles to Failure - NARloy-Z Heat D-5402

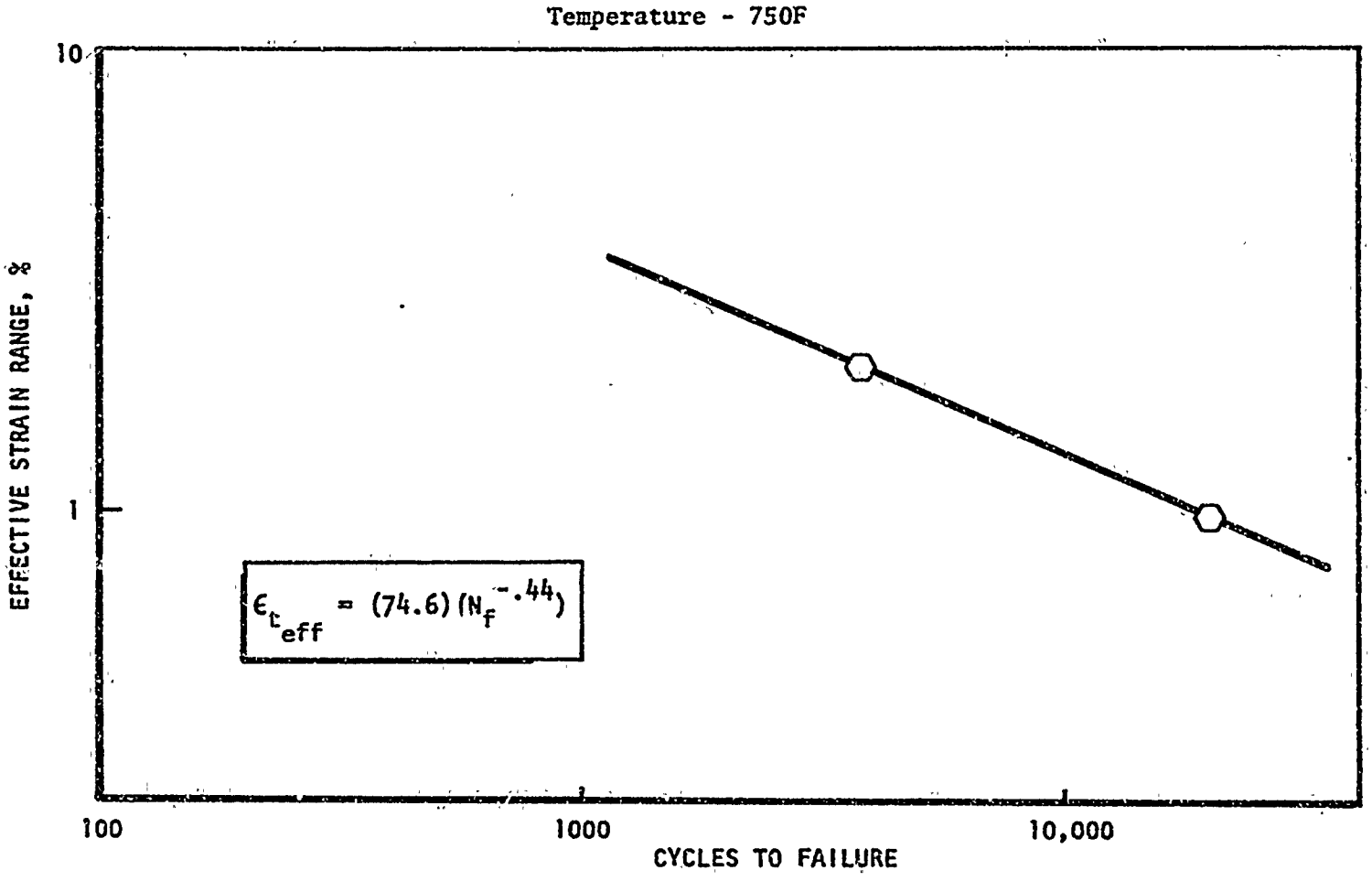

Figure 75. Isothermal Cyclic Test Data Effective Strain Range vs Cycles to Failure - NARloy-Z Heat D-5402

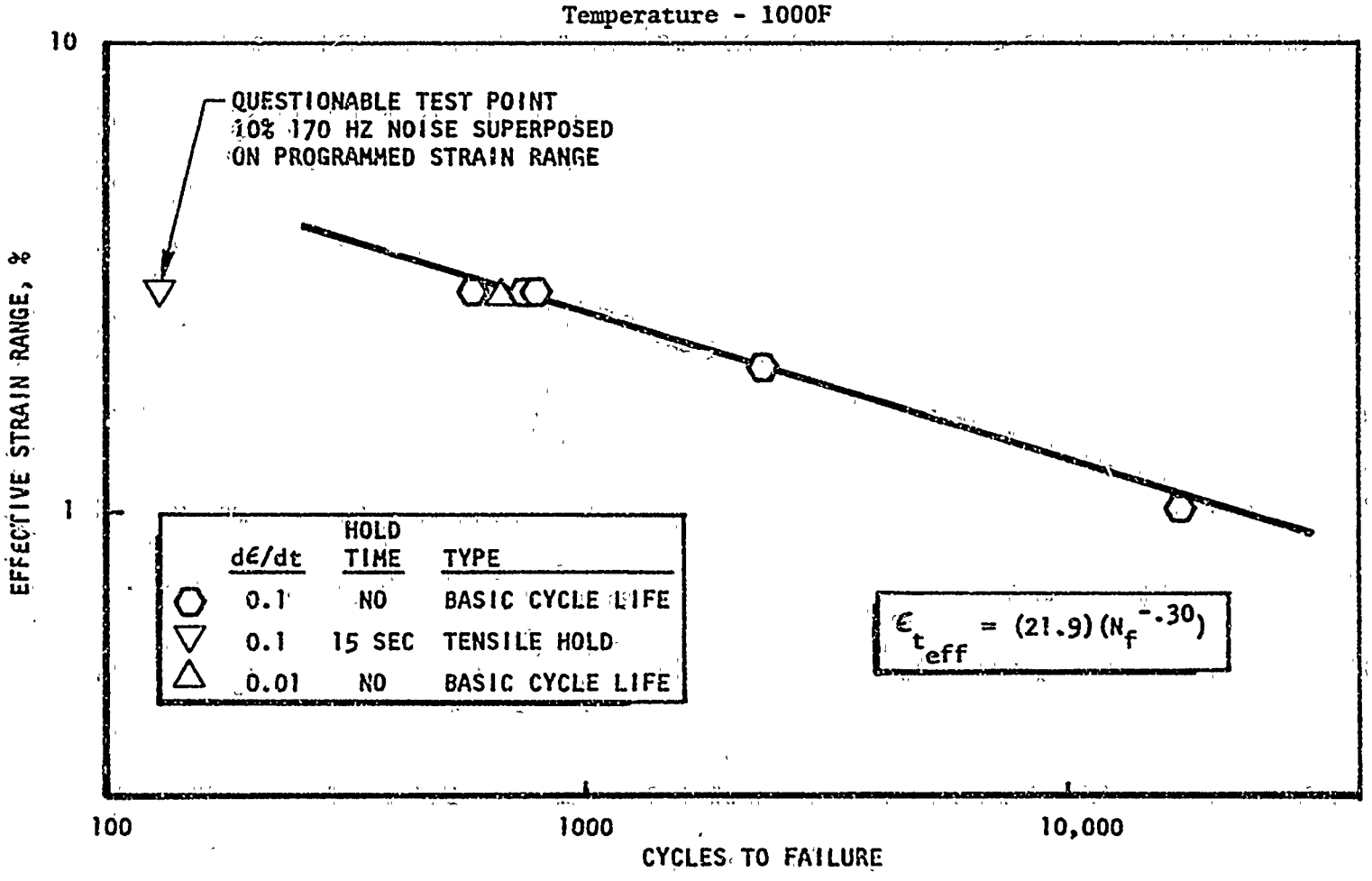

Figure 76. Isothermal Cyclic Test Data Effective Strain Range vs Cycles to Failure - NARloy-Z Heat D-5402

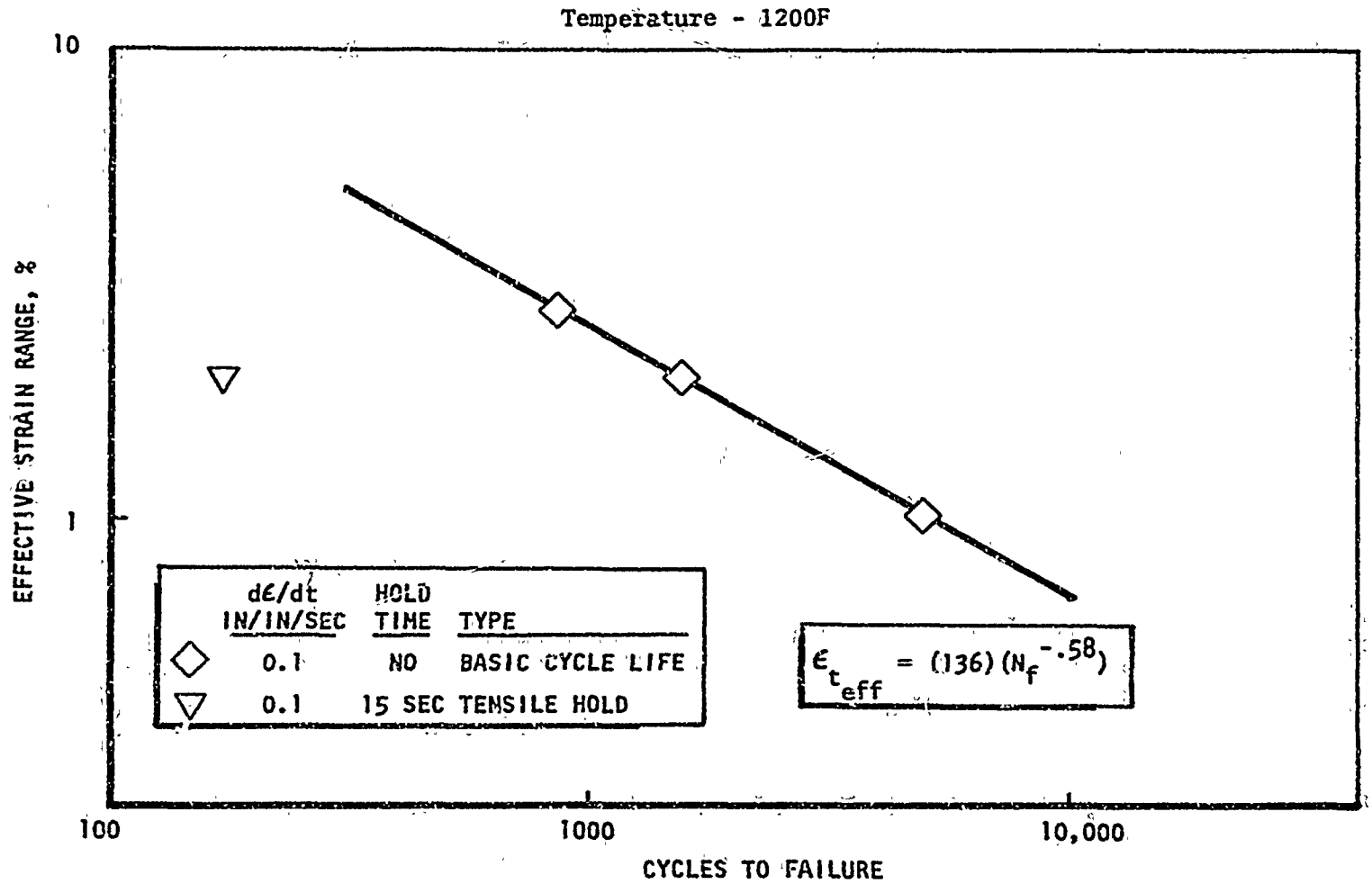

Figure 77. Isothermal Cyclic Test Data Effective Sbrain Range vs Cycles to Failure - NARloy-Z Heat D-5402

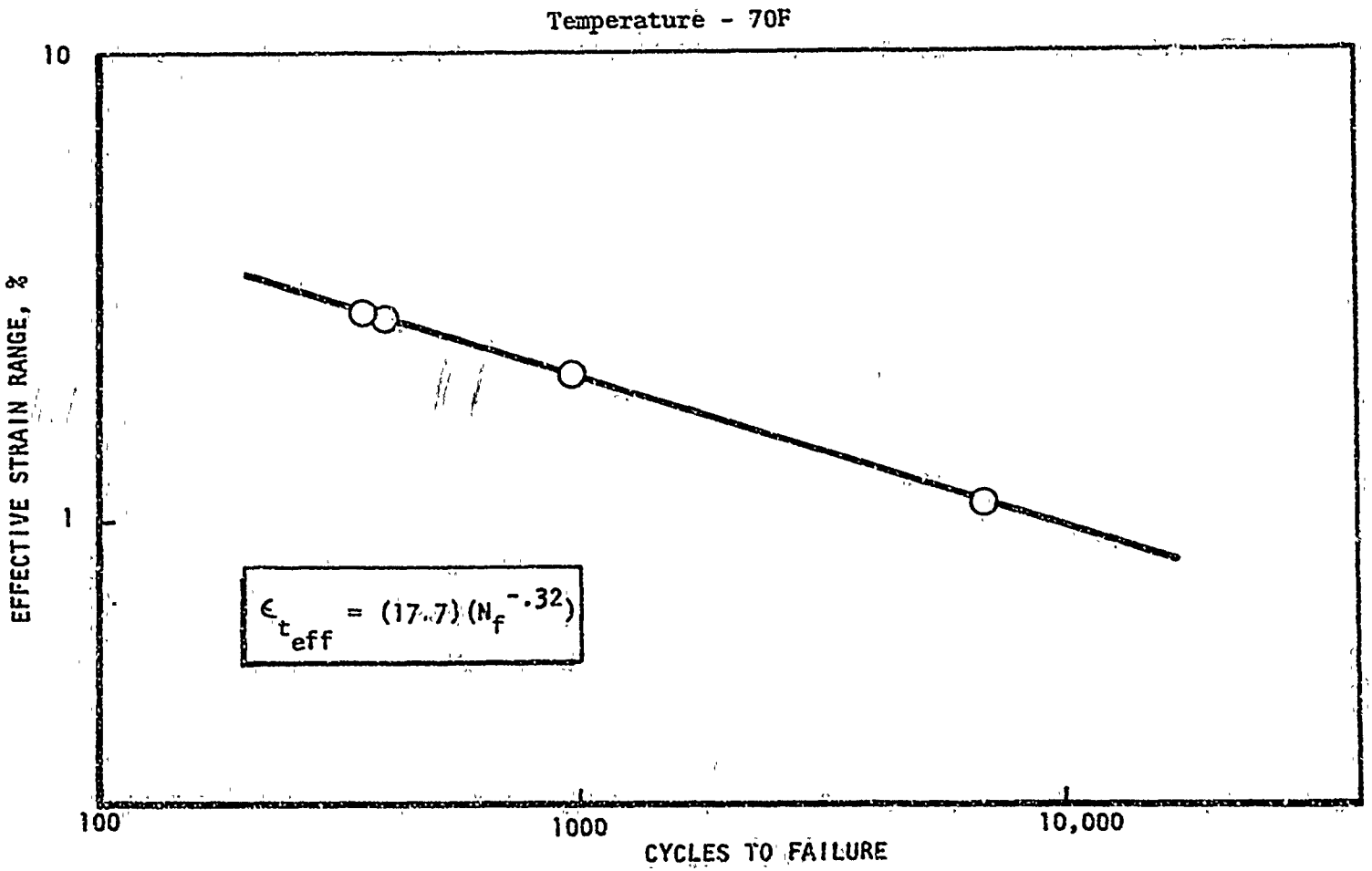

Figure 78. Isothermal Cyclic Test Data Effective Strain Range vs Cycles to Failure - Zirconium Copper Heat 329-6

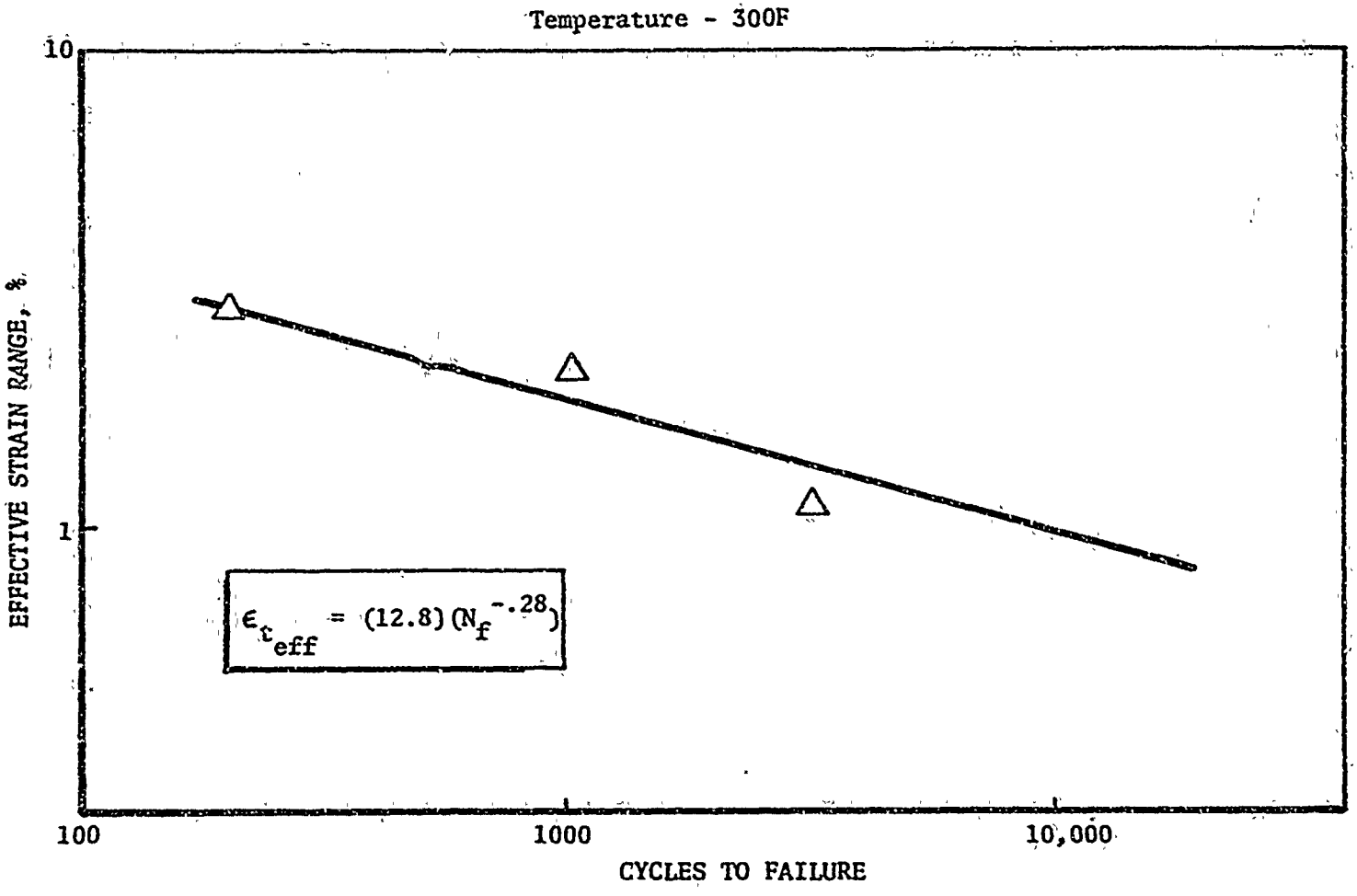

Figure 79. Isothermal Cyclic Test Data Effective Strain Range vs Cycles to Failure - Zirconium Copper Heat 329-6

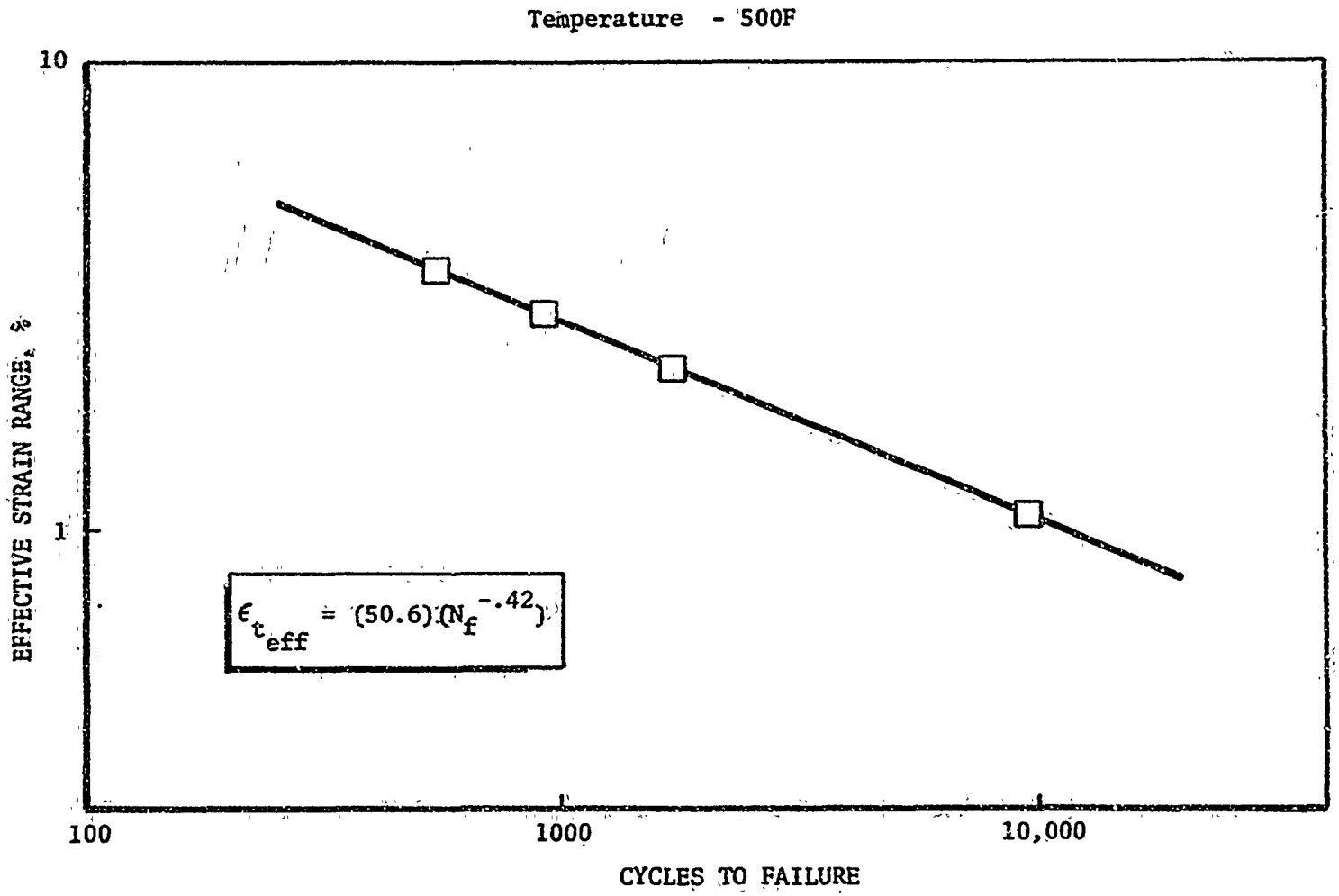

Figure 80. Isothermal Cyclic Test Data Effective Strain Range vs Cycles to Failure - Zirconium Copper Heat 329-6

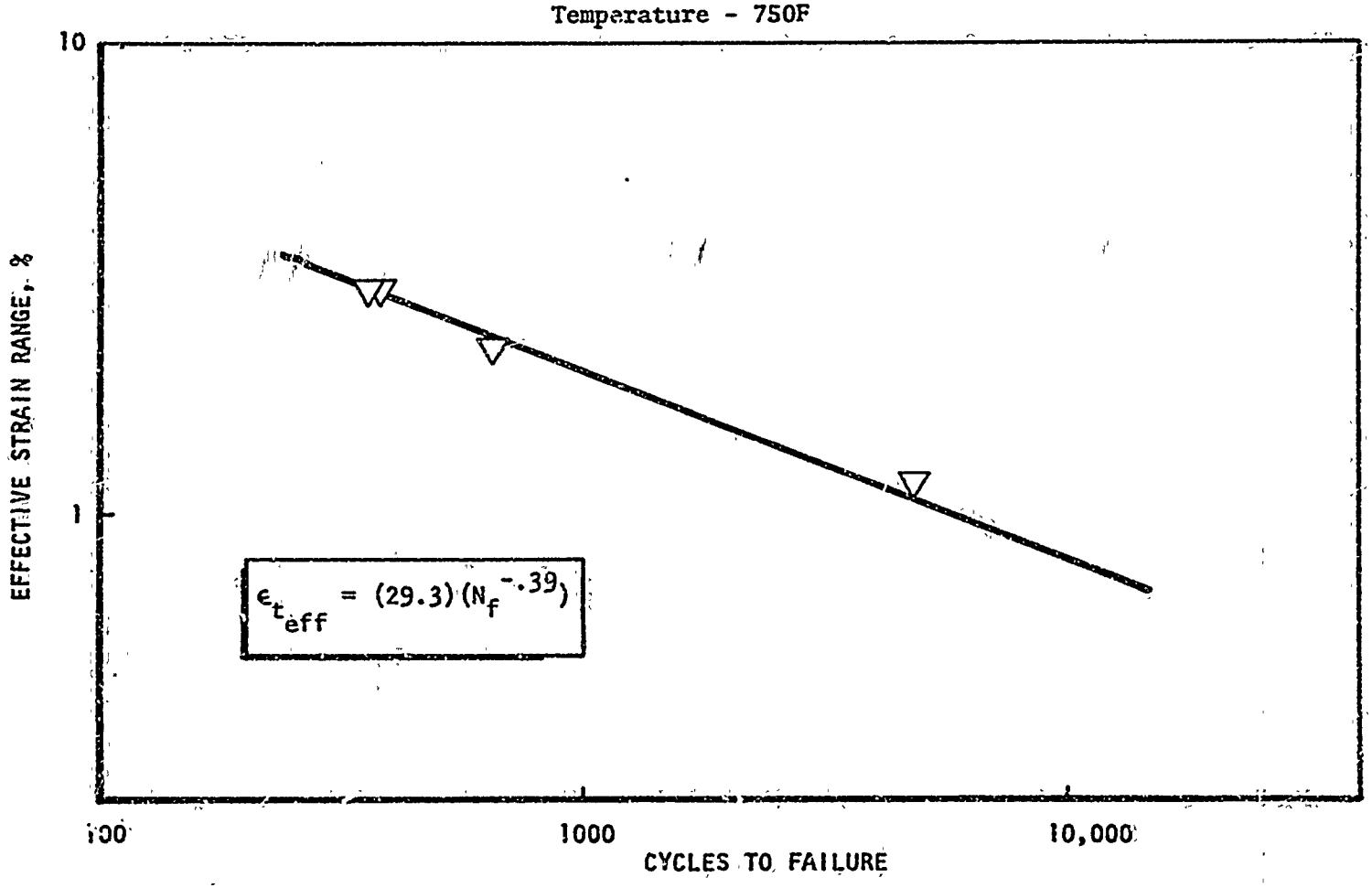

Figure 81. Isothermal Cyclic Test Data Effective Strain Range vs Cycles to Failure - Zirconium Copper Heat 329-6

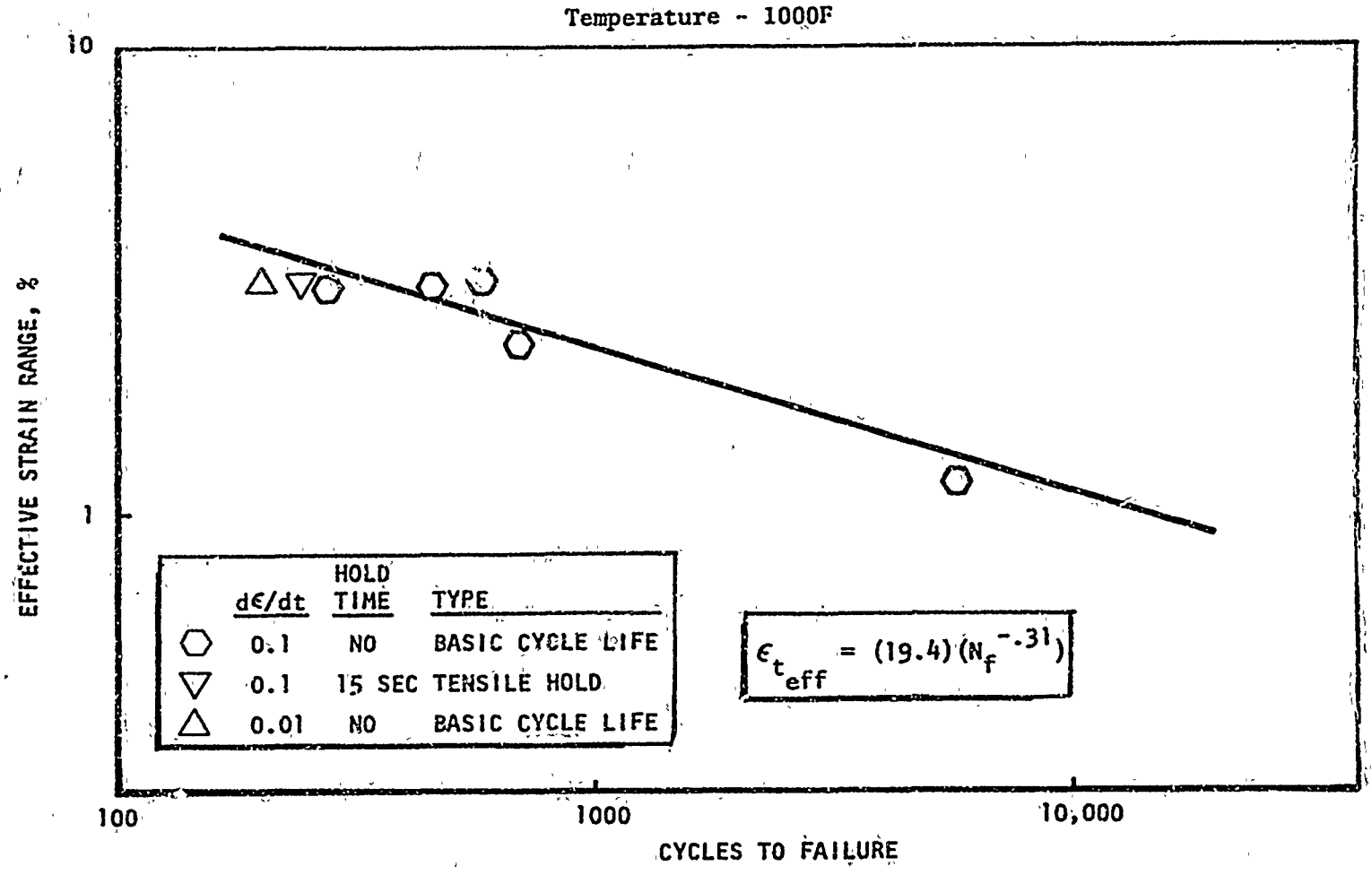

Figure 82. Isothermal Cyclic Test Data Effective Strain Range vs Cycles to Failure - Zirconium Copper Heat 329-6

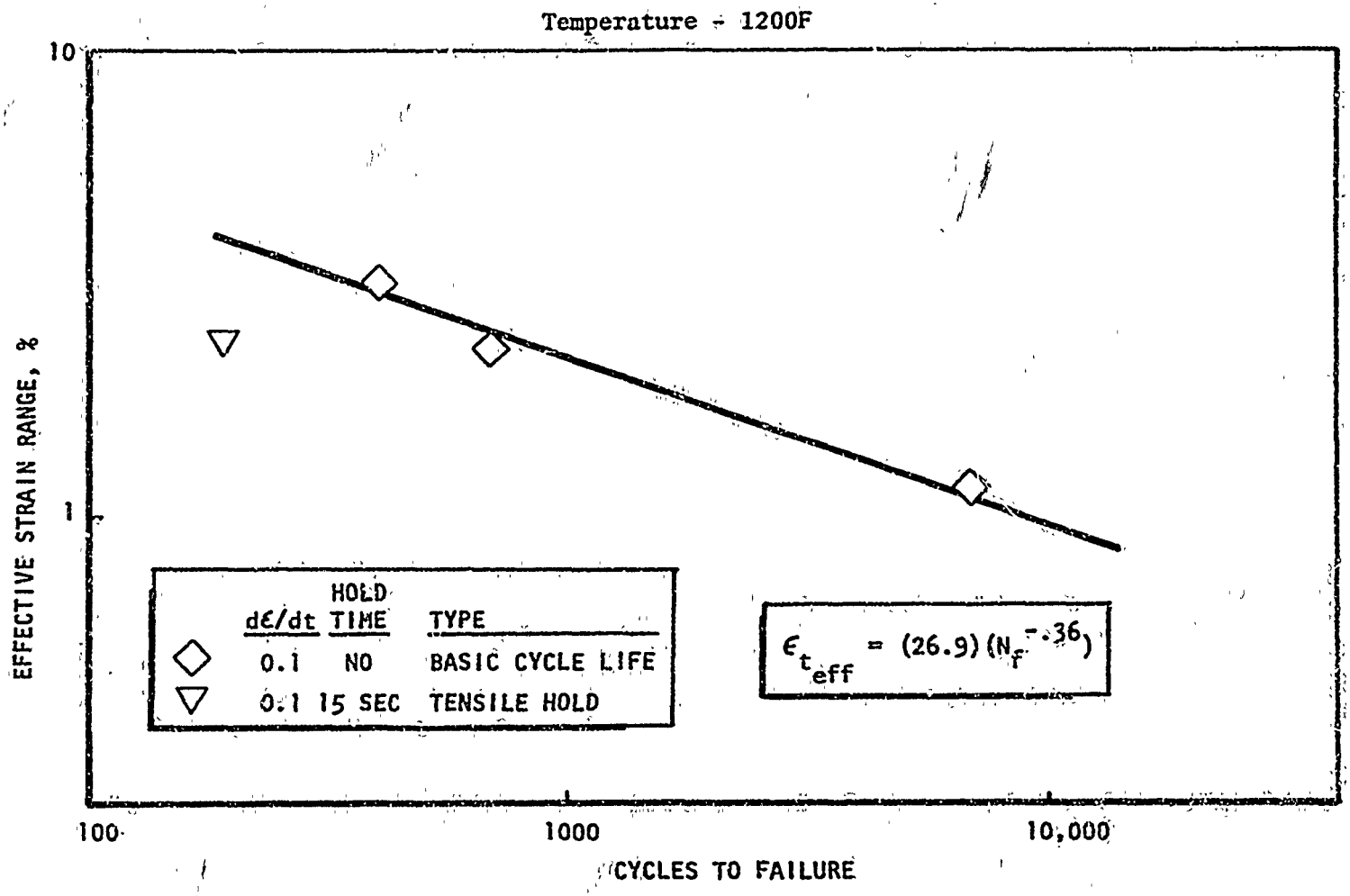

Figure 83. Isothermal Cyclic Test Data Effective Strain Range vs Cycles to Failure - Zirconium Copper Heat 329-6

up or down to define the upper and lower bounds. A comparison of the "best fit" curves for NARloy-Z and zirconium-copper is shown in Fig. 84 . It indicates that cyclic life of NARloy-Z is considerably greater than that of zirconium-copper over the full strain range of interest.

The second set of plots given for the NARloy-Z and zirconium-copper data at each test temperature are also furnished with "best fit" curves. These individual temperature plots give a better definition of the data than the composite plots but more data is needed to verify the accuracy of the curve constants.

All of the NARloy-Z and zirconium-copper tests except two were run at a strain rate of 0.1 in./in./sec. These two, one per material, were run at 0.01 in./in./sec, 1000 F and an axial surface strain range of 2.1 percent. The results are included in the cycle life plots of Fig. 42 and 71.

Several tests with 15 second hold times at peak strain were run on both NARloy-Z and zirconium-copper specimens. Data where cyclic life could be determined are plotted in Fig. 76, 77, 82, and 83. These included two tests of NARloy-Z and two on zirconium-copper all with 15 second hold times at peak tensile strain. The NARloy-Z tests were run at 1200 F and 1.5 percent axial surface strain range and 1000 F and 2.1 percent axial surface strain range. The accuracy of the latter test point is questionable because a 170 Hz noise at 10 percent of the test strain range was present on the 2.1 percent strain range. This noise was associated with the hydraulic pump used on the MTS machine. This could reduce the recorded cyclic life. The zirconium-copper tests were run at 1200 F and 2.1 percent axial surface strain range. All hold times at peak tensile strain lowered life. Cycles to failure could not be determined for the tests containing compressive hold time because the onset of rapid tensile load drop could not be detected from the load-cycle plots. Examples of this are seen in Fig. 85, 86, and 87 . In one case, specimen cracking was observed without any discernible load drop. The materials were apparently too weak at the 1000 F and 1200 F test temperature to respond with other than a gradual load decay.

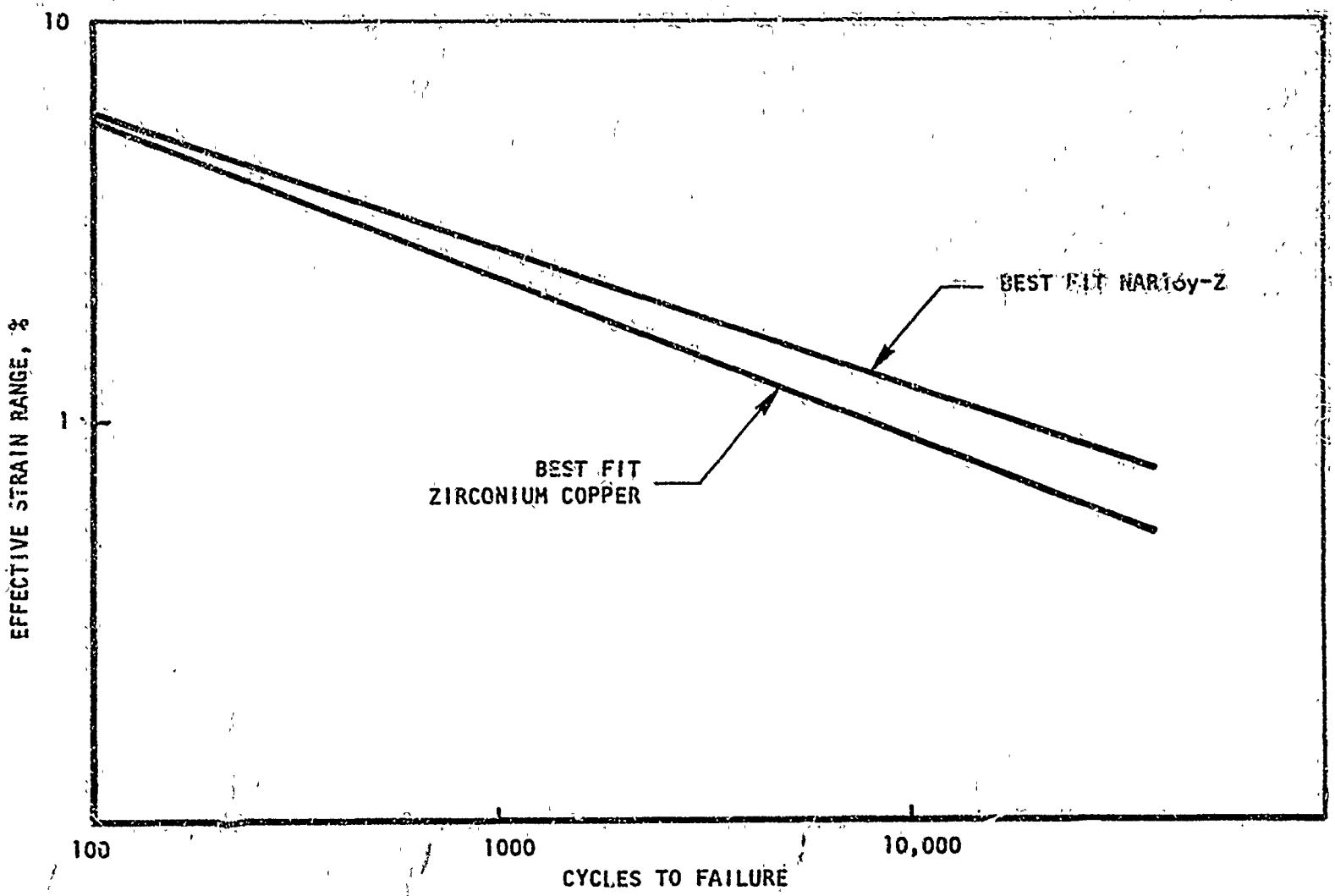

Figure 84. Comparison of the "Best Fit" Curves for NARloy-Z and Zirconium Copper, Effective Strain Range vs Cycles to Failure

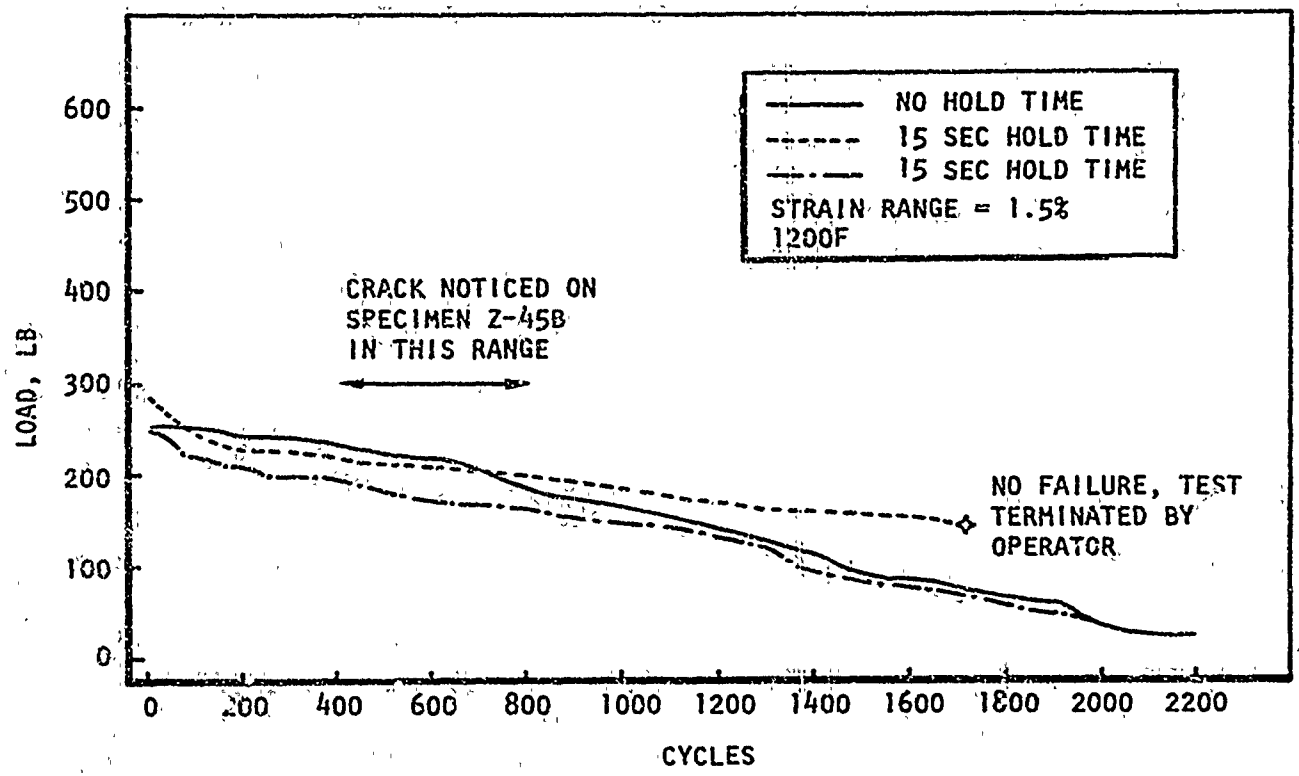

Figure 85. Load Trace for Zirconium Copper Hold Time Test

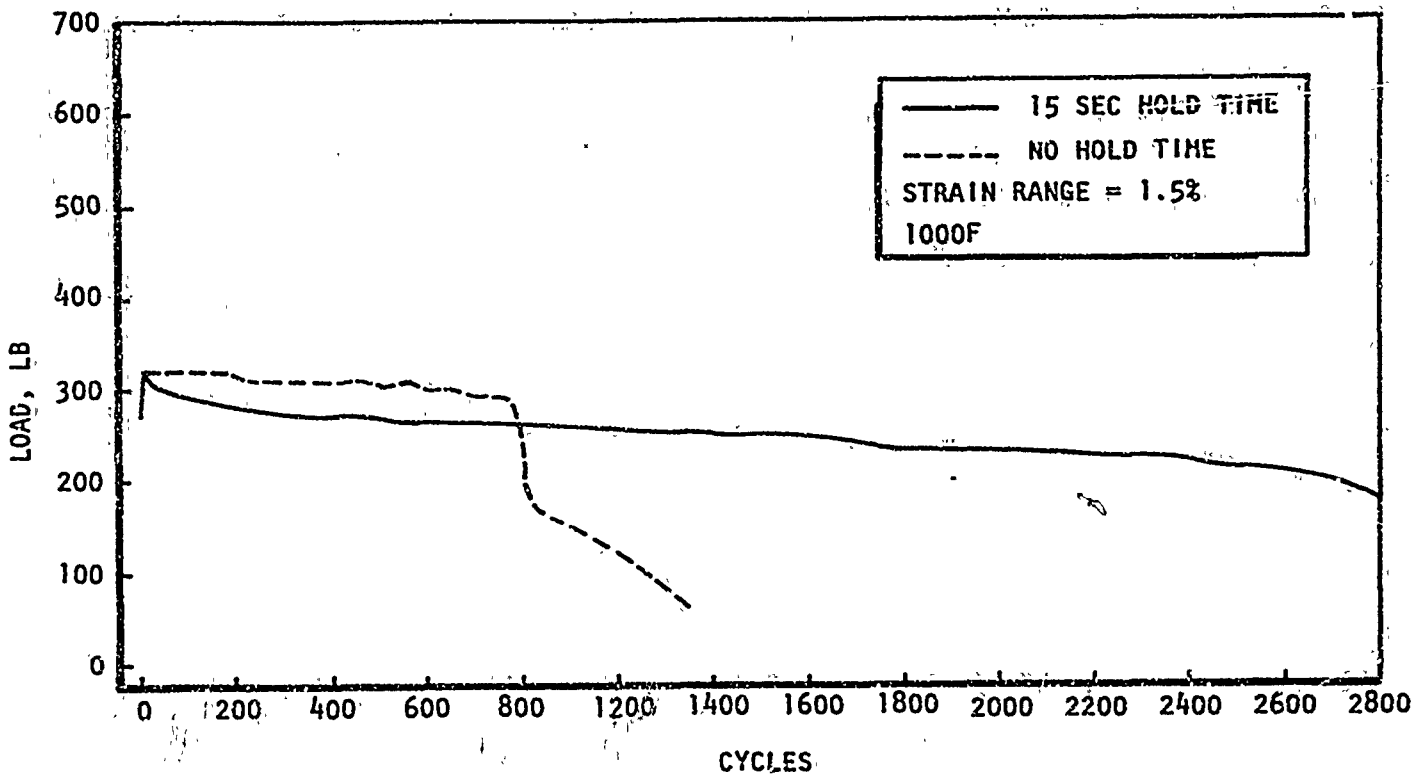

Figure 86. Load Trace for Zirconium Copper Hold Time Test

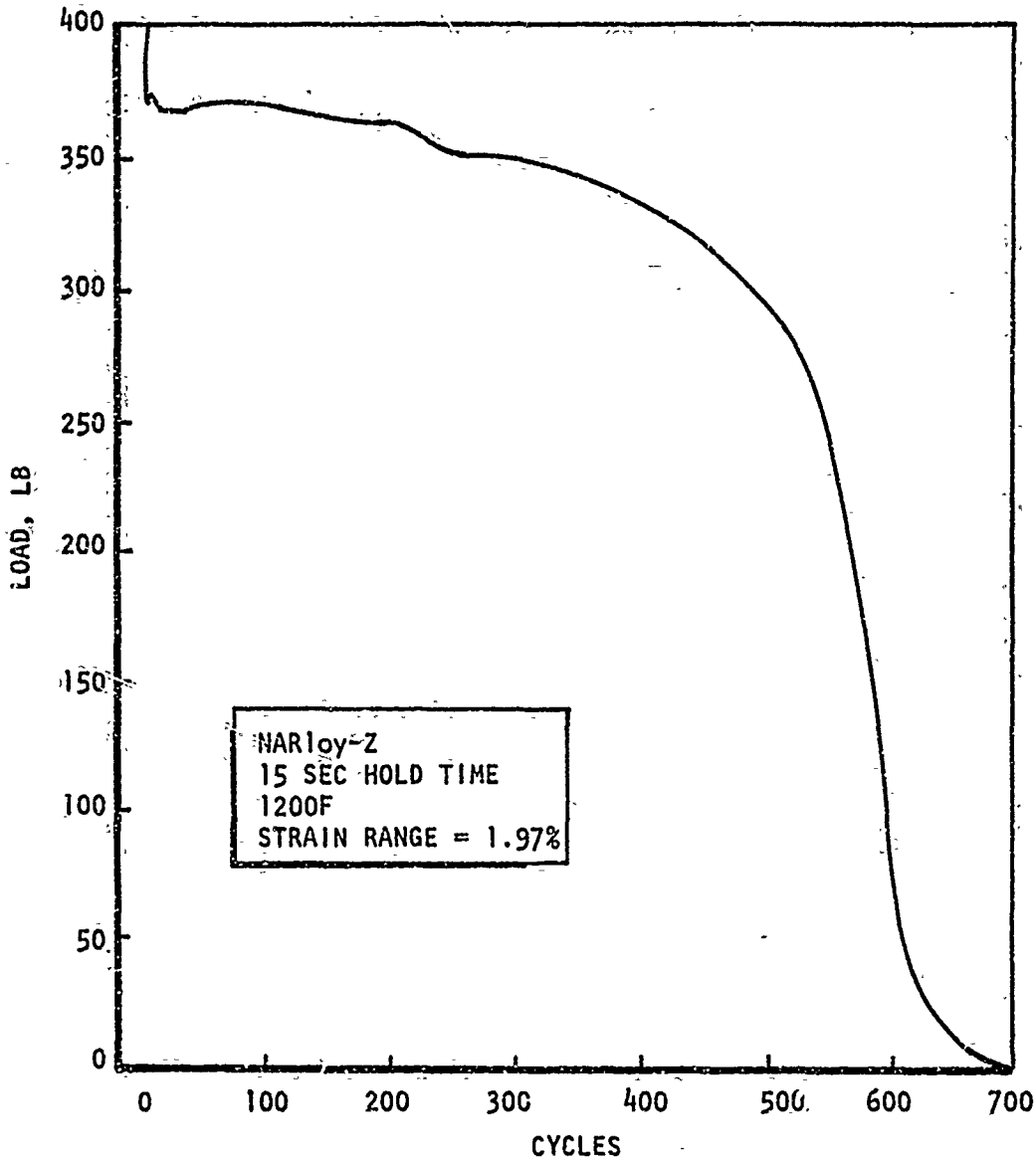

Figure 87. Load Trace for NARloy-Z Compressive Hold Time Test

Cycle life was obtained for wrought nickel-200 for two axial surface ranges: 1 percent and 2 percent and three temperatures 70 F, 1000 F and 1400 F, Fig. 88. Two tests of the powder metallurgy nickel were completed at 1400 F, one at 1 percent and the other at 2 percent axial surface strain range. The nickel 200 material had more cyclic life than the powder metallurgy nickel at the 1400 F test condition. The one hold time test at peak compressive strain run on nickel 200 material at 2 percent axial surface strain gave inconclusive results.

Differential Temperature Fatigue Tests

In addition to the isothermal fatigue test effort discussed previously, consideration was also given to conducting differential temperature fatigue tests on appropriate specimens. In this type of testing the specimen is totally restrained while being heated from ambient to some predetermined elevated temperature level and then cooled to ambient. This imposes an $\alpha\Delta T$ type of strain on the specimen more closely duplicating the environment of a thrust chamber than the isothermal fatigue testing.

Specimen Design. Two types of specimens (Fig. 89), tubular and beam-type, were designed. The tubular specimen consists of a tube restrained at both ends while being cyclically resistance heated and air cooled. The temperature gradient is established in the beam-type specimen by electron beam heating the upper tip of the beam while cooling the remainder by flowing water through a cylindrical coolant passage. A comparison of the advantages and disadvantages of the two types of specimens is made in Table 5.

Test Results. Feasibility testing was conducted on both types of specimens. Tests on the tubular specimens showed a large, axial temperature gradient (~ 100 F) over the 1/2 inch gage length. As a result it became virtually impossible to quantitatively determine the magnitude of the strain imposed on the specimen.

Beam type specimens of both NARloy-Z and nickel-200 were tested to determine the temperature distribution. A 30 KW Sciaky electron beam welder was used for heating. The beam was defocused to cover the 3/16-inch specimen width and

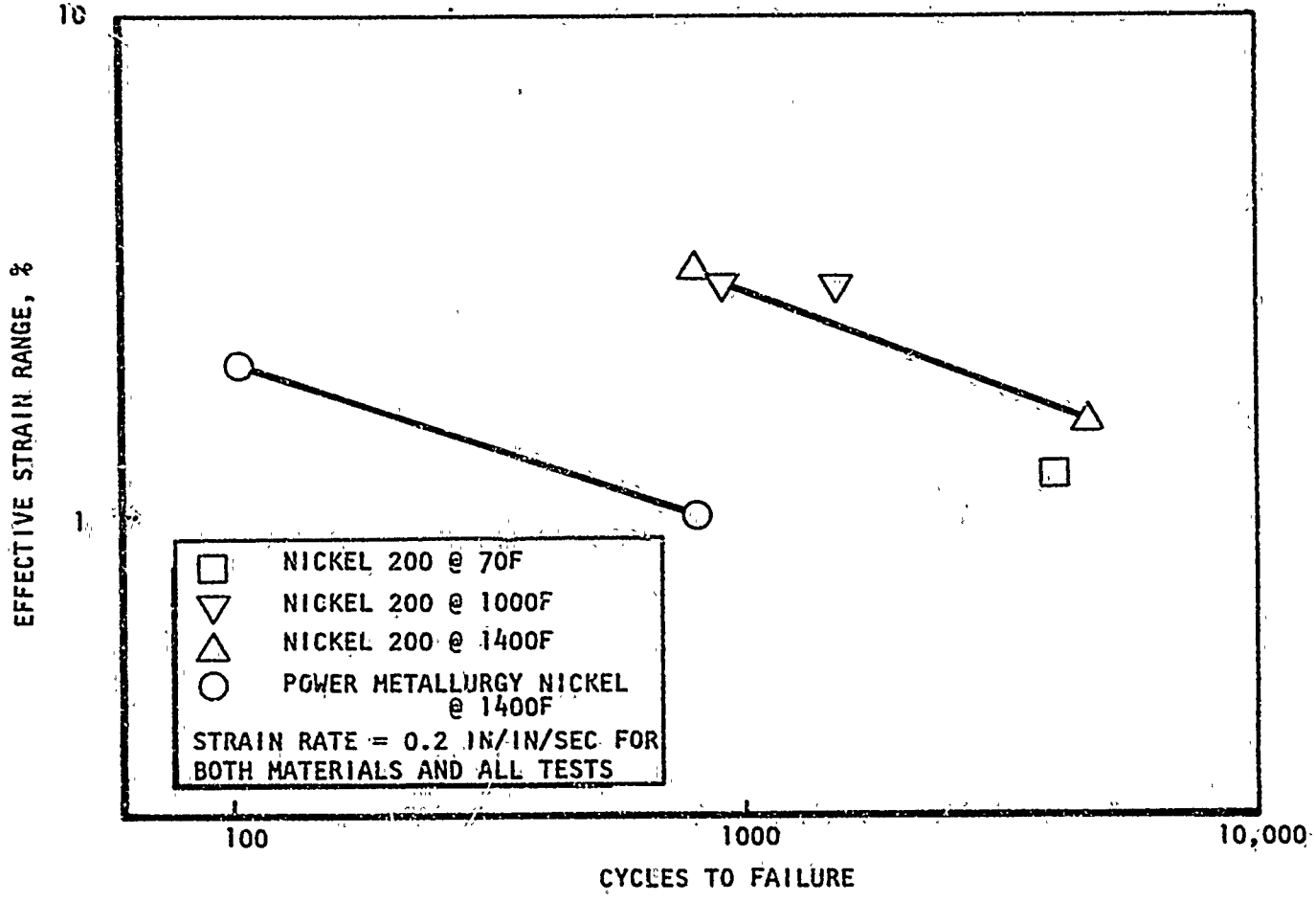

Figure 88. Isothermal Cyclic Test Data Effective Strain Range vs Cycles to Failure - Powder Metallurgy Nickel and Nickel 200

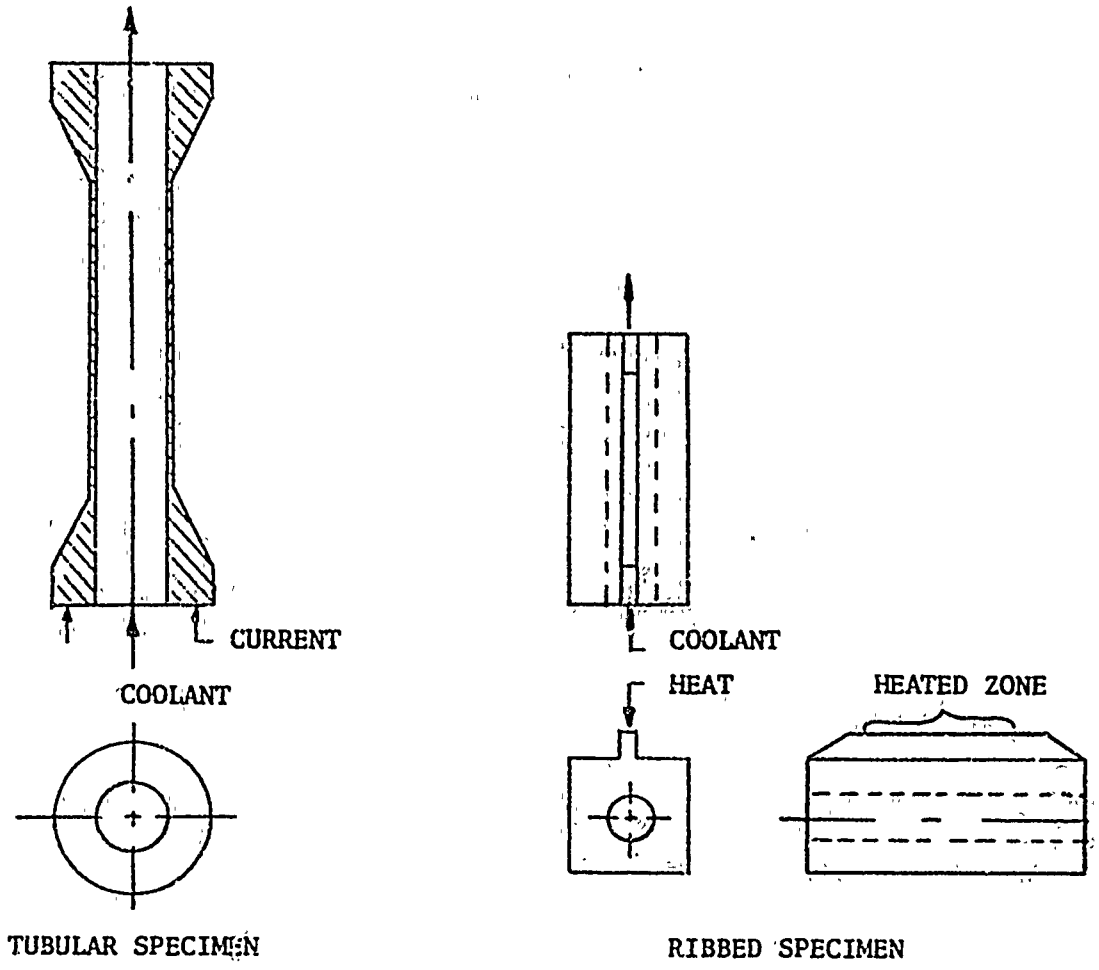

Figure 89. Differential Temperature Fatigue Specimen

Table 5. Critique of Differential Temperature Fatigue Specimens

SPECIMEN TYPE	ADVANTAGES	DISADVANTAGES
Tubular	1. Load can be measured during the thermal cycle 2. Analysis is straightforward if constant temperature and constant strain can be maintained over the gage length 3. Temperature measurement is simplified by the absence of temperature gradient perpendicular to the surface 4. Criterion for failure can be established as the number of cycles for the crack to penetrate tube wall	1. For high conductivity copper alloys it has not been possible to reduce the temperature spread to less than 50F over the 1/2 inch gage length 2. Dimensional instability has been prevalent for nickel and copper in the softest conditions
Beam Type	1. Surface heating and internal cooling is analogous to thrust chamber 2. Plastic instability is prevented by the resistance to distortion provided by the water cooled portion of the specimen	1. Load cannot be monitored 2. Temperature gradient increases difficulty of temperature measurement 3. Criterion of failure is not obvious

oscillated over the length of the specimen at a frequency of 60 cps. In the initial tests the EB welder sine wave generator was used resulting in hot spots at either end of the swept length and some erratic non-uniformity in temperature. Intergranular cracking was observed in the hotter area of the nickel specimen after 136 cycles under these rather severe conditions. The NARloy-Z specimen showed fairly good temperature uniformity in the middle third of the specimen.

Subsequent to the above tests an oscilloscope was used to generate a triangular wave at temperatures high enough to visually monitor temperature uniformity. This modification resulted in greatly improved temperature uniformity. Problems noted with this test effort were (1) slow heating cycle and (2) extreme surface roughening along the rib where the electron beam was concentrated.

It was felt at the conclusion of these tests that the beam type specimen could be modified and developed to the point that meaningful quantitative differential temperature fatigue data could be obtained if the surface roughness problem could be resolved and adequate heating and cooling rates could be established. However, it was felt that development of this technique was outside the scope of this program and all further effort was terminated in favor of more effort on the isothermal fatigue testing.

Panel Testing

Consideration was also given to the possibility of laboratory testing panels representative of non-tubular thrust chambers. The objective was to establish a low-cost laboratory test technique which would produce thermal and structural environment comparable to that experienced by the thrust chamber during hot firing. To accomplish this the panels required a heat input of sufficient magnitude to simulate the hot gas wall temperature of typical thrust chambers and sufficient coolant to establish a thermal gradient through the panel comparable to that experienced by a thrust chamber.

Candidate Heating Techniques. Candidate heating techniques that were evaluated to accomplish this goal included:

(1) electrical (resistance)
(2) laser
(3) induction heating
(4) electron beam heating

A brief discussion of each follows.

Electrical Heating. Electrical (resistance) heating of test panels was considered possible using the electrically heated tube tester located in the Propulsion Research Area at Santa Susana. Briefly, this fixture would consist of a panel brazed between two copper bus bars. Heating is accomplished by passing an electrical current through the specimen by way of the bus bars. Cooling is accomplished by passing hydrogen through the panel and the surrounding environment is oxygen. This test fixture has the advantage of testing panels in an environment similar to that of an actual thrust chamber; however, only the hot gas wall is simulated. In addition, the temperature gradient through a resistance heated, surface cooled panel is approximately half that through an equivalent panel which is surface heated and surface cooled.

Laser Heating. Cursory evaluation resulted in the conclusion that there was no available laser which had sufficient power to heat a panel to any significant heat flux level.

Induction Heating. High frequency induction heating was also evaluated as a possible panel heating technique. Results indicated that induction heating was capable of surface heating a nickel panel of 1 to 1-1/2 square inches to a heat flux level equivalent to that of the point design thrust chamber. However, due to its higher thermal conductivity, the ability to successfully heat the copper alloy panels such that a large thermal gradient could be established through the panel was questionable. Panels in this test fixture could be tested in either an air or argon environment or a vacuum and be cooled with water or nitrogen.

Electron Beam Heating. The use of an electron beam welder to heat the panels was also considered (and ultimately selected for experimental evaluation). In this set up the panel would be mounted inside a vacuum chamber and internally cooled with water or nitrogen. Surface heating is accomplished when the electron beam is scanned over the panel surface. The power of the electron beam gun is such that a surface area of 0.5 in.^{2} can be heated to approximately 20-21 Btu/in.^{2}-sec; approaching the peak heat flux values of the point design and establishing a significant thermal gradient on the panel. Since the panel is surface heated and surface cooled, the thermal gradients are quite similar to those in a thrust chamber.

Selection of Heating Techniques. Evaluation of these heating techniques with respect to the established criteria discussed previously led to the selection of the electron beam heating technique for experimental evaluation.

The equipment for this effort was an existing 30 kilowatt electron beam welder located in the Experimental Manufacturing Department at Rocketdyne. The panels were to be water cooled using an existing water pump capable of delivering 5 gpm at pressures greater than 1500 psig.

The power of this machine would theoretically allow fatigue testing of panels up to 1-inch square; with final size dependent on material, beam efficiency and channel geometry.

Feasibility Evaluation. Experimental evaluations of the electron beam heating technique was undertaken using instrumented nickel-200 panels as shown in Fig. 90 and 91. Tests on the first panel were encouraging in that an area approximately 0.37 x 0.50 inches was apparently being uniformly heated. Temperature measurements taken by the surface thermocouples agreed fairly well with the optical pyrometer measurements of the hot surface. Also back wall temperature measurements which remained quite close to ambient indicated that a reasonable thermal gradient was being imposed on the panel. There was indication of hot spots on

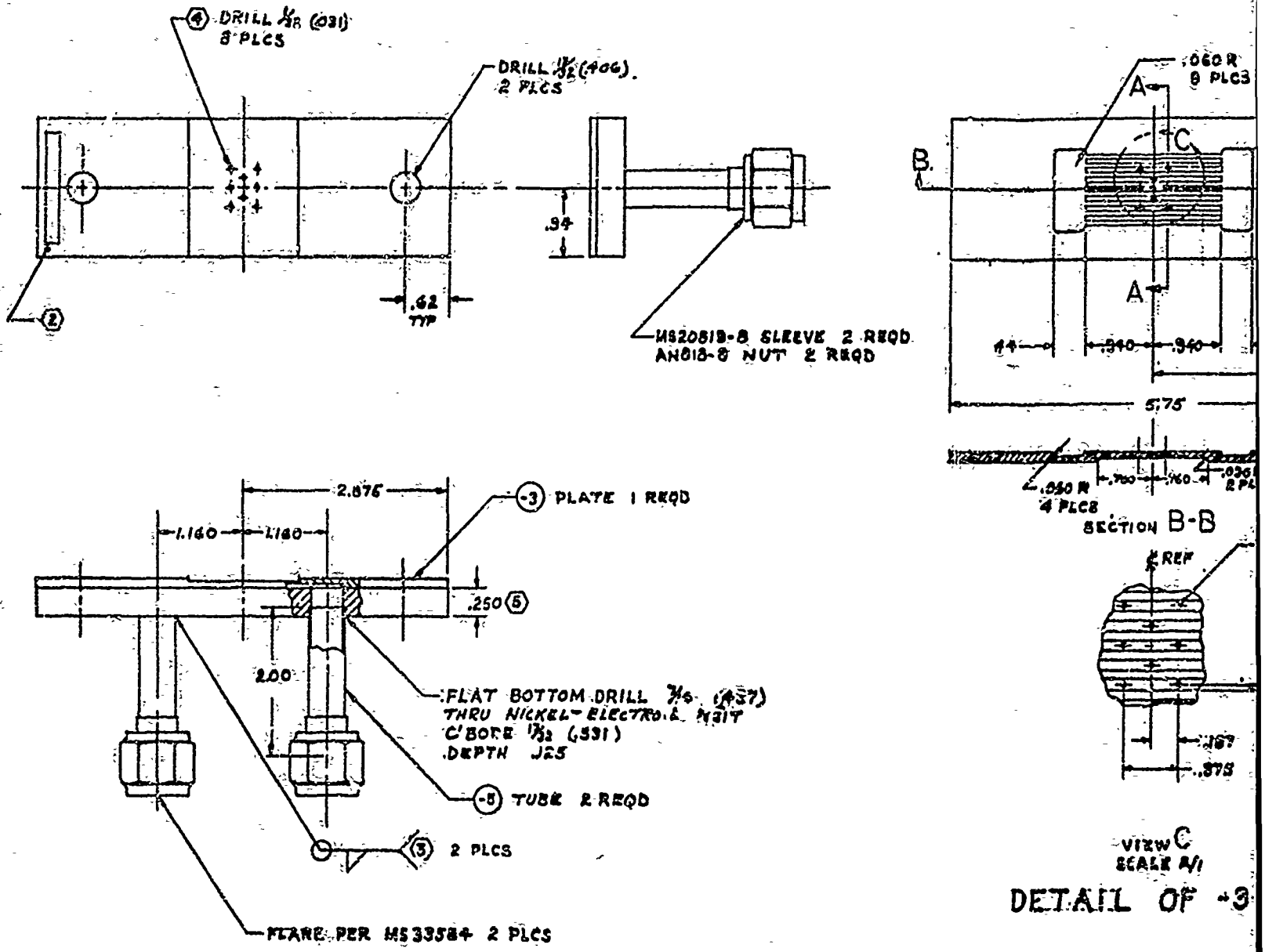

DETAIL OF -3

③ NICKEL-ELECTRO DEPOSIT, ULT TENSILE STRENGTH 80,000 LB/IN² MIN. YIELD 48,000 MIN. ELONGATION 20% MIN.
④ AFTER NICKEL-ELECTRO DEPOSITING USE THE HOLES IN THE -3 PLATE AS PILOT TO DRILL THRU THE NICKEL DEPOSIT.
③ TIG BRAZE WITH NIORC PER RA0107-027 CL II
② IDENTIFY PER RA0104-003.
MACHINE PER RA0103-002.

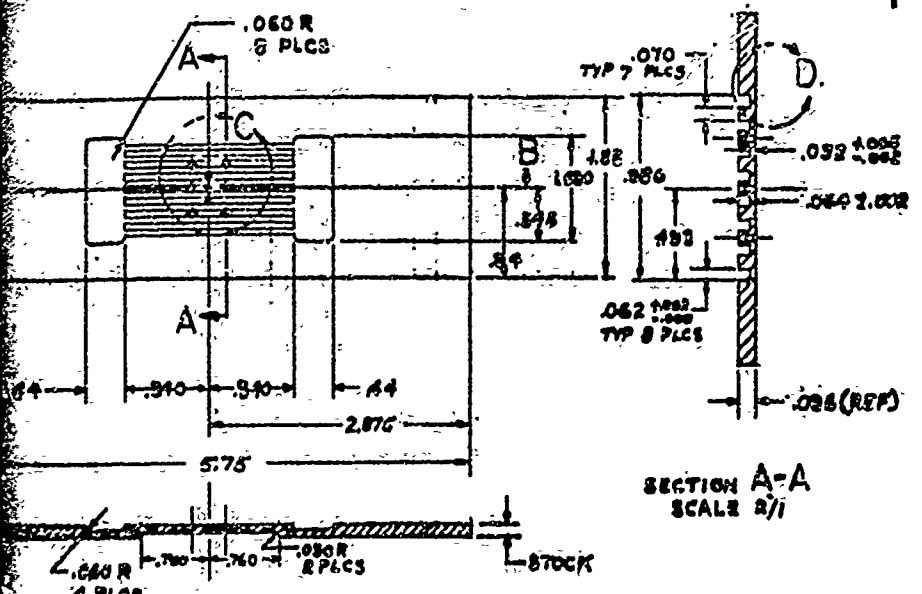

DETAIL OF -3 PLATE

Figure 90. Test Panel Assembly

DASH NO	MATERIAL	SIZE	SPECIFICATION
-5	347 CRES TUBE	.5040 D x .035 W x 2.00	MIL-T-6808 TYPE I
-3	VI 200 SHEET	.125 x 1.68 x 5.75	ASTM-B162-61

TEST PANEL ASSY

D 02602 EWR 165561

TENSILE STRENGTH
ELONGATION 20%
OVER THE HOLES IN THE -3
NICKEL DEPOSIT
MIL-C-26074 CL E

NOTED

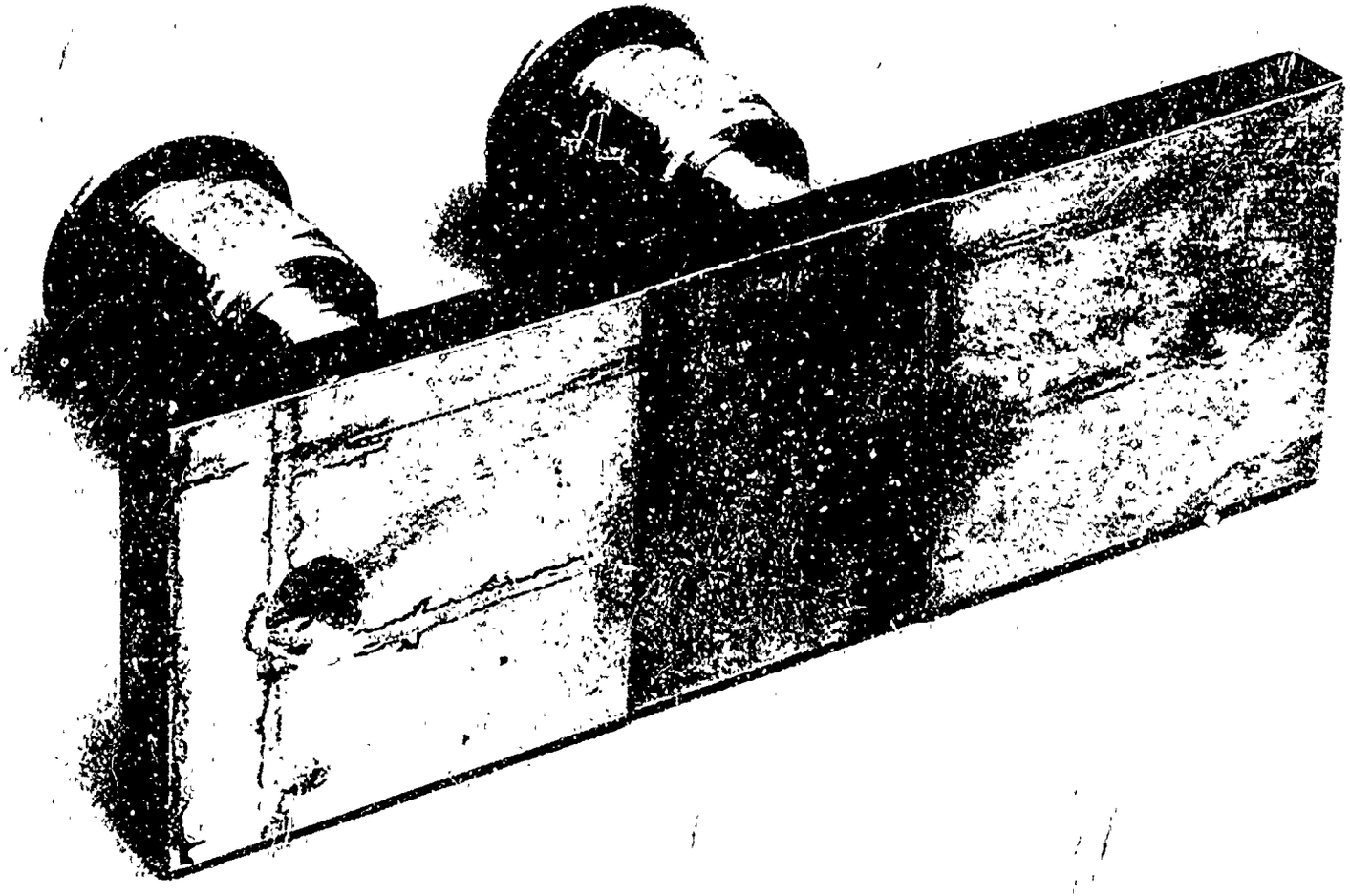

IEC32-8/3/70-C1A

Figure 91. Nickel Fatigue Test Panel

the surface of each thermocouple and the surfaces showed considerable roughening. This roughening appeared to be cathodic etching, apparently due to the electron bombardment of the surface. Subsequent sectioning showed surface roughness and cracks to a depth of ~0.004 inches.

A second panel was subsequently tested with the thermocouple holes plugged with braze alloy to eliminate the hot spots. However, tests on this panel also exhibited hot spots and considerable surface roughness.

It was apparent at this time that two problems existed with this type of testing and resolution of both was necessary before meaningful fatigue data could be obtained. These were (1) accurate determination and repeatability of surface temperature and (2) elimination of surface roughening.

It was decided to forego any additional effort in this area in favor of more isothermal fatigue testing. It is noted, however, that this is an area that should be explored in more depth since the successful development of a panel test technique would greatly enhance the capability to accurately predict thrust chamber life.

PHASE I - TASK IV - FINAL DESIGN REGENERATIVELY COOLED THRUST CHAMBER

Presented in this section is a detailed design description of the non-tubular regeneratively cooled thrust chambers which were fabricated and tested in Phase II. These chambers were fabricated with spun and machined liners and electroformed nickel closures using procedures developed on a previous program (Ref. 23). Liner materials were nickel-200 for the F_2/H_2 design and copper alloy (zirconium copper and NARloy-Z) for the O_2/H_2 designs. As discussed previously the internal contour of the chambers was specified by the AFRPL (Fig. 2). The nozzles were truncated to a lesser area ratio to facilitate manufacturing and testing at site ambient pressure. Design criteria are listed in Table 6.

Table 6. Thrust Chamber Design Criteria

Thrust, lb	3300	3300
Propellant	O_2/H_2	O_2/H_2
Mixture Ratio (o/f)	6:1	6:1
Chamber Pressure, psia	750	750
Coolant	H_2	H_2
Expansion Area Ratio	4	4
Contraction ratio	4	4
Chamber Length (injector face to throat centerline), in.	6.0	5.0
Hot Gas Wall Material	Zirconium-Copper NARloy-Z	Nickel-200

These chambers were designed to interface with AFRPL designed injectors (discussed later in Task V). A description of each follows.

Nickel-200 Thrust Chamber

The nickel-200 liner for this chamber contains 72 step width, variable depth channels as shown in Fig. 92. The coolant passage width is 0.040 inches from $\epsilon = 4$ to a point 2.88 inches upstream of the throat. From here forward the passage width is 0.080; accomplished as a step change in width thus allowing manufacture by conventional cutters. The hot gas wall thickness was a constant 0.025 inches throughout.

Coolant circuit closeout and chamber structure was provided by the use of annealed electroformed nickel. Experimental evaluation on another program at Rocketdyne had shown as-deposited electroformed nickel to be susceptible to hydrogen embrittlement when stressed into the plastic region while exposed to hydrogen. This evaluation had also shown the resistance of electroformed nickel to hydrogen could be markedly improved by the use of a thin copper barrier between the hydrogen and electroformed nickel or by subjecting the electroformed nickel to a moderate temperature (600 to 900 F) "annealing" cycle prior to exposure to hydrogen. Experimental testing of both was underway at Rocketdyne, however, the finalization of processing parameters for the copper barrier had not proceeded to the same point for annealing of the electroformed nickel. Consequently it was decided to use the annealed electroformed nickel approach for the closure. It is noted that subsequent metallurgical evaluation of the two copper alloy chambers after the cyclic test series showed no signs of hydrogen embrittlement of the electroformed nickel closure. The manifolds and closure were designed to assure that gross yielding of the annealed electroformed nickel closure does not occur while exposed to hydrogen.

The forward flange and coolant outlet manifold was designed to interface with the AFRPL supplied injector. Injector to chamber sealing was accomplished by using redundant metal O-rings with the O-ring grooves machined into the injector flange. The aft flange and coolant inlet manifold incorporated provisions for bolting on

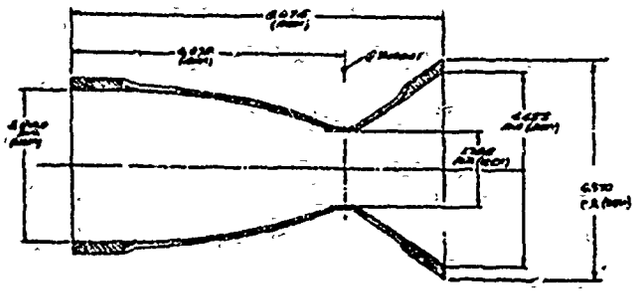

SECTION J-J

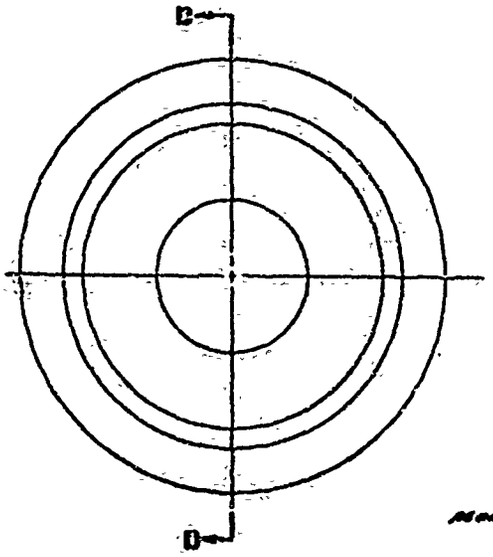

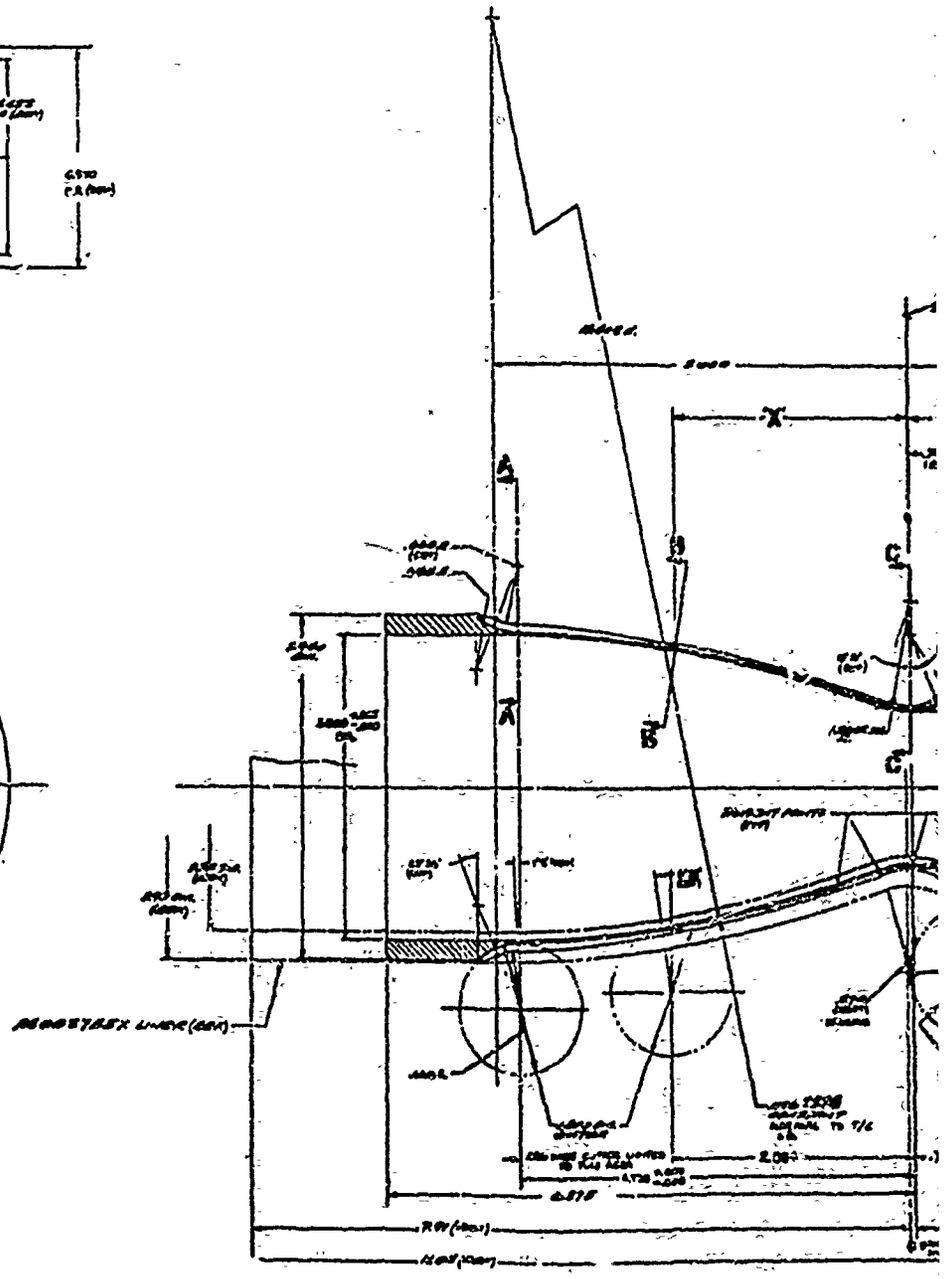

SECTION H-H

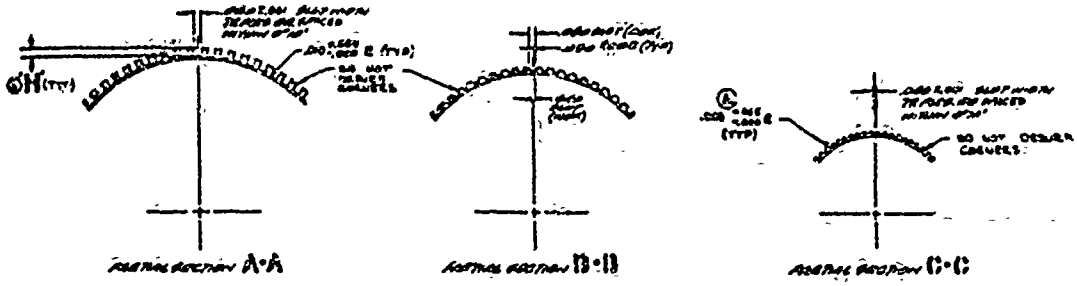

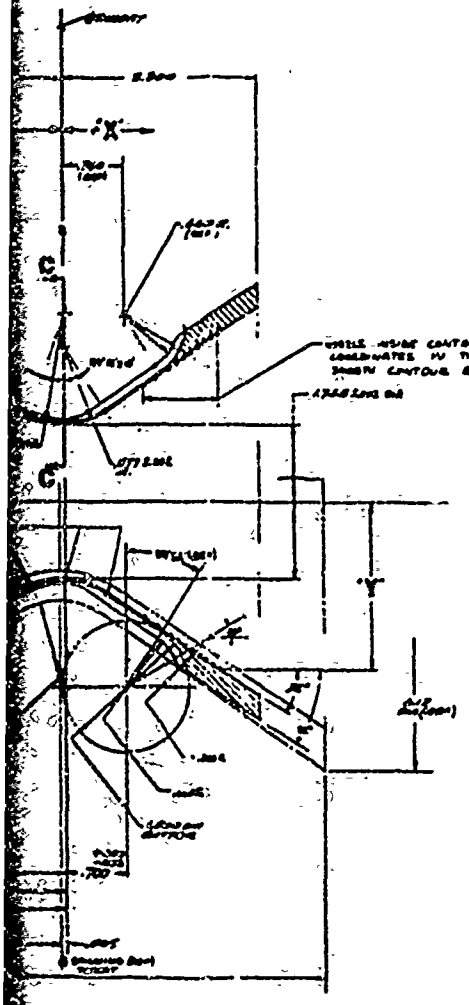

STA "X" (SEE NOTE 1) DIM A MOLD LINE	ⓒH ±.002 NORMAL TO "A" MOLD LINE	"B" MOLD LINE "X" REF	"B" MOLD LINE "Y" REF	"C" MOLD LINE "X" REF	"C" MOLD LINE "Y" REF
4.3462	.0970			-4.3440	1.8429
4.3000	.0990			-4.2987	1.8156
4.2800	.0990			-4.2836	1.8033
4.0000	.0820			-3.9720	1.6198
3.9800	.0740			-3.9409	1.6020
3.9000	.0660			-3.8815	1.5763
3.8800	.0580			-3.8342	1.5579
3.4000	.0500			-3.3685	1.4741
3.3800	.0500			-3.3541	1.4734
3.2000	.0419			-3.2859	1.4339
3.1800	.0327			-3.2361	1.4108
3.0000	.0440			-1.9665	1.4772
1.7800	.0418			-1.7394	1.4162
1.5000	.0427			-1.4823	1.3502
1.3800	.0420			-1.3712	1.3190
1.0000	.0419			-.9802	1.2024
.7731	.0408			-.7774	1.1331
.8000	.0400			-.6338	1.0374
.9937	.0374			-.5751	1.0206
.6000	.0390			-.5357	.9720
.4000	.0325			-.1309	.8502
.1000	.0300			-.0934	.8383
0.0000	.0350			0.0000	.8345
.1000	.0230			-.0927	.8448
.1400	.0482			-.1831	.8728
.2000	.0534			-.3711	1.0097
.4000	.0436			-.5369	1.0582
.5947	.0732			-.6339	1.1165
.6002	.0800			-.7372	1.1771
.8204	.0330	.5443	1.5438	-.8557	1.4472
1.0449	.0300	1.0929	1.4426	-1.0026	1.5124
1.1340	.0300	1.1181	1.4845	-1.0679	1.5353

STA "X" (SEE NOTE 1) "X" MOLD LINE	STA "Y" (SEE NOTE 1) "X" MOLD LINE
.9604	1.3228
1.0665	1.4201
1.1387	1.5190
1.1899	1.549
1.4081	1.6476
1.4989	1.7033
1.5780	1.7539
1.6603	1.8104
1.7419	1.8621
1.8227	1.9168

1. CONSTRAINT INSPECT "A" MOLD LINE FOR BLOCKS 110 TYPE II & "B" MOLD LINE = .2 CONTOUR, "B" MOLD LINE = BOTTOM OF BLOCKS, "C" MOLD LINE = TOP OF LANDS.
2. AIR CONTOUR TO BE 32 RMS FINISH
3. TOLERANCE IN GENERAL HEIGHT "H" TO BE WITHIN VAL "X" BETWEEN POINTS INDICATED.
4. IDENTIFY SEE MIL-STD-24-008 (TAG ONLY)
5. MACHINED FINISH OF FOLLOWING PARTS TO BE AS FOLLOWS:-
   BOTTOMS 20-40 RMS FINISH
   SIDES 20-40 RMS FINISH
6. BOTTOM OF PLATE TO BE MACHINED TO BLOCK FINISH, SEE
7. EDGES OF BLOCK "A" TO BE PARALLEL TO "A" SIDE
8. LANDING AREA AND 21-008

Figure 32.

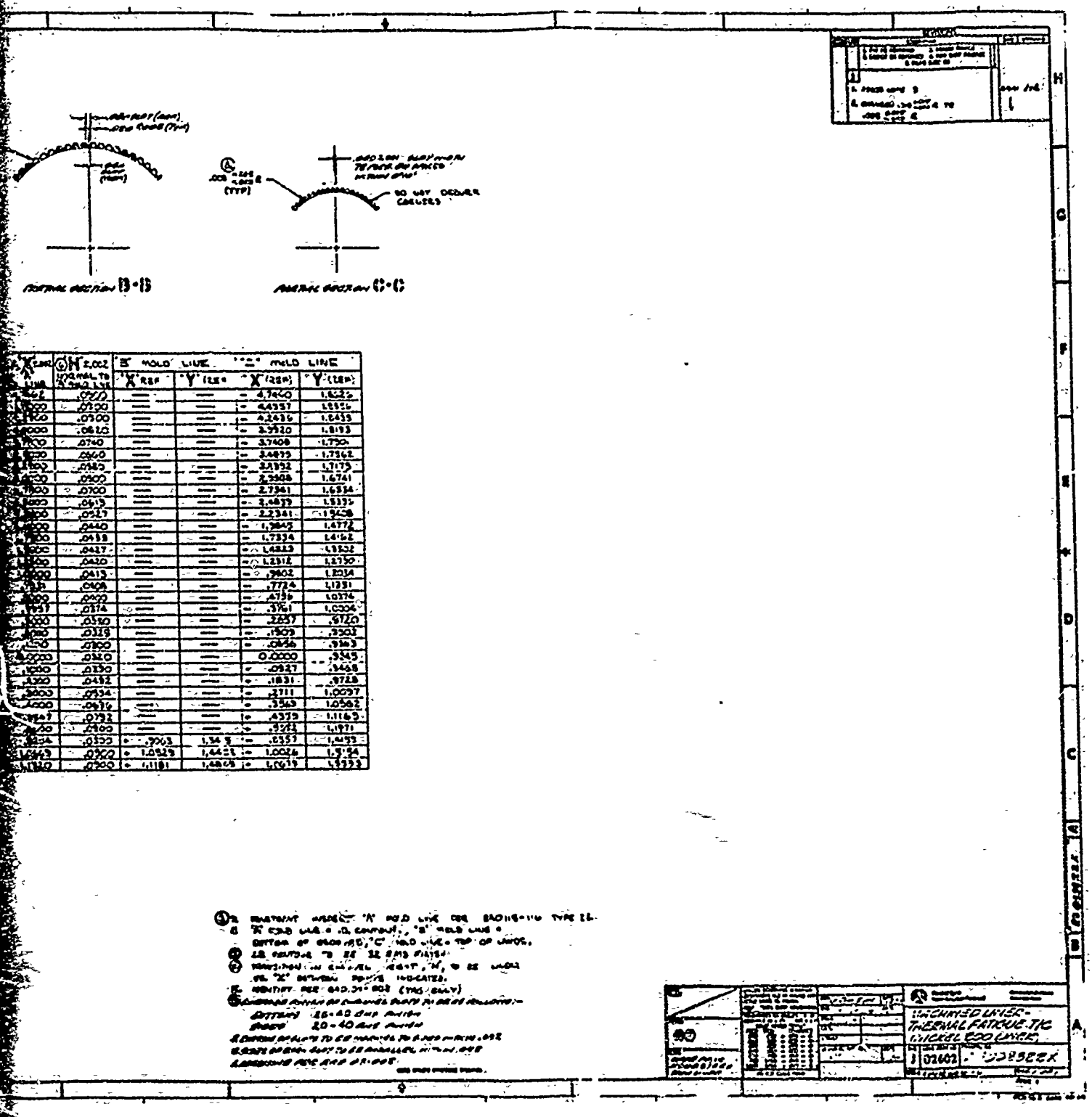

Figure 92. Thermal Fatigue Thrust Chamber Machined Liner (Nickel-200 Liner)

a pressure test plate. The flanges were TIG brazed to the thrust chamber liner and electroformed nickel closeout. The axial loads were taken through the end joints to the thrust chamber liner and the relatively thin manifold closeout is attached to the electroformed nickel. The flanges were made of 304l stainless steel and all fittings were of 300 series stainless steel.

The coolant manifolding was designed with a single inlet and a single outlet. Quarter inch diameter Swagelok fittings were provided on the inlet and outlet manifolds for coolant bulk temperature measurements. Quarter inch diameter AN fittings were provided on each manifold for coolant inlet and outlet pressure measurements. The complete chamber is shown in Fig. 93.

Copper Alloy Thrust Chambers

The copper alloy thrust chambers are identical in design except for liner material. The liners, shown in Fig. 94, are of spun and machined NARloy-Z and zirconium-copper and incorporate 40 constant width, variable depth coolant passages 0.080 inches wide. The hot gas wall thickness was 0.080 inches. As discussed previously, the internal contour was identical to that of the nickel chamber except the combustion zone length was increased by 1-inch to assure adequate combustion performance with O_2/H_2 propellant.

The coolant circuit closure and chamber structure is provided by annealed electroformed nickel as discussed for the nickel chamber.

The coolant manifolding and flange design are identical to the Nickel-200 thrust chamber. Since the manifolds were conservatively sized for the nickel thrust chamber flowrates, no size increase was found necessary for the increased flowrate used by the copper alloy thrust chambers.

Minor dimensional changes were made in the flange and electroform nickel contours to accommodate the different channel heights used with the copper alloy chamber designs. The complete chamber is shown in Fig. 95.

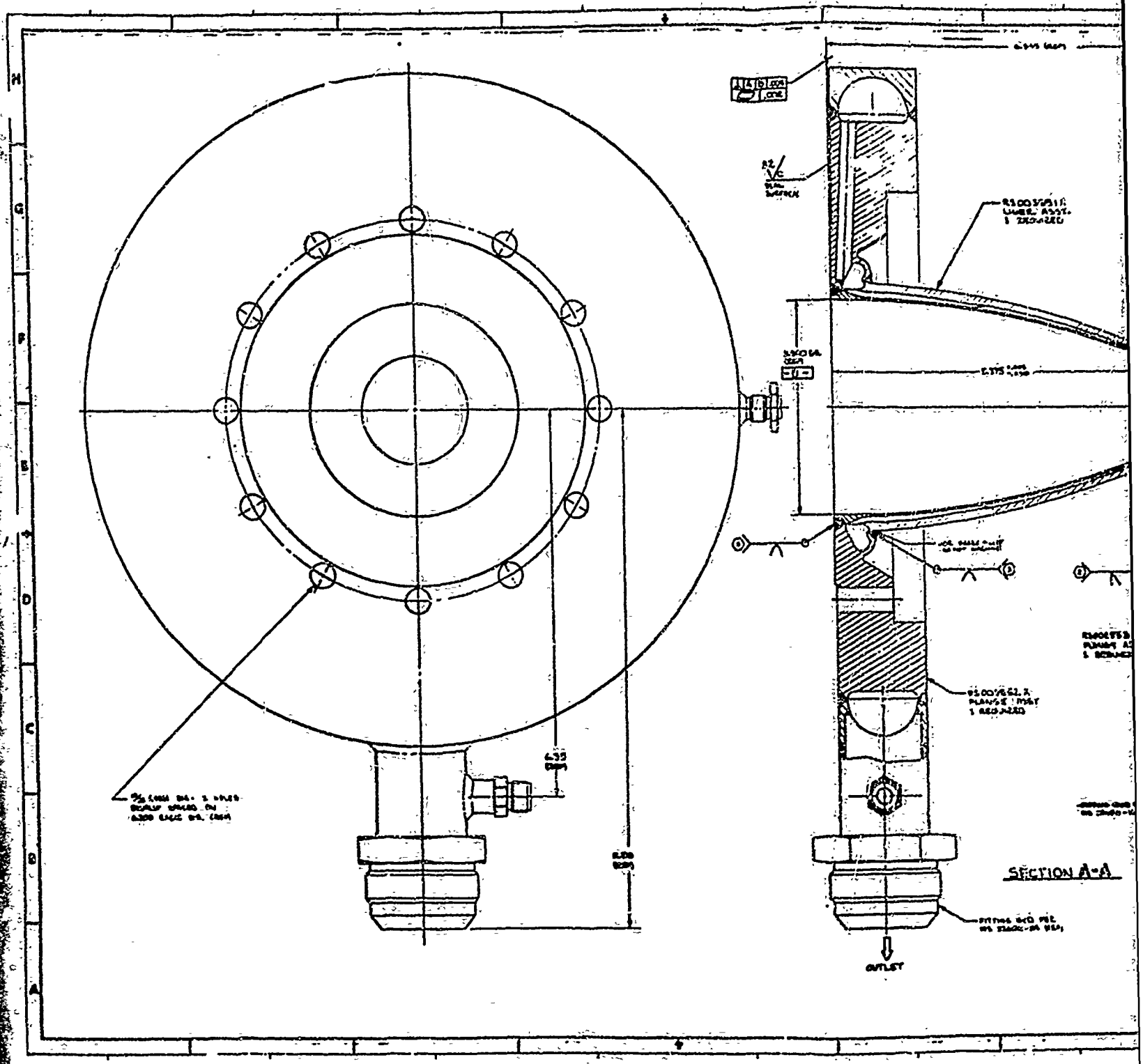

SECTION A-A

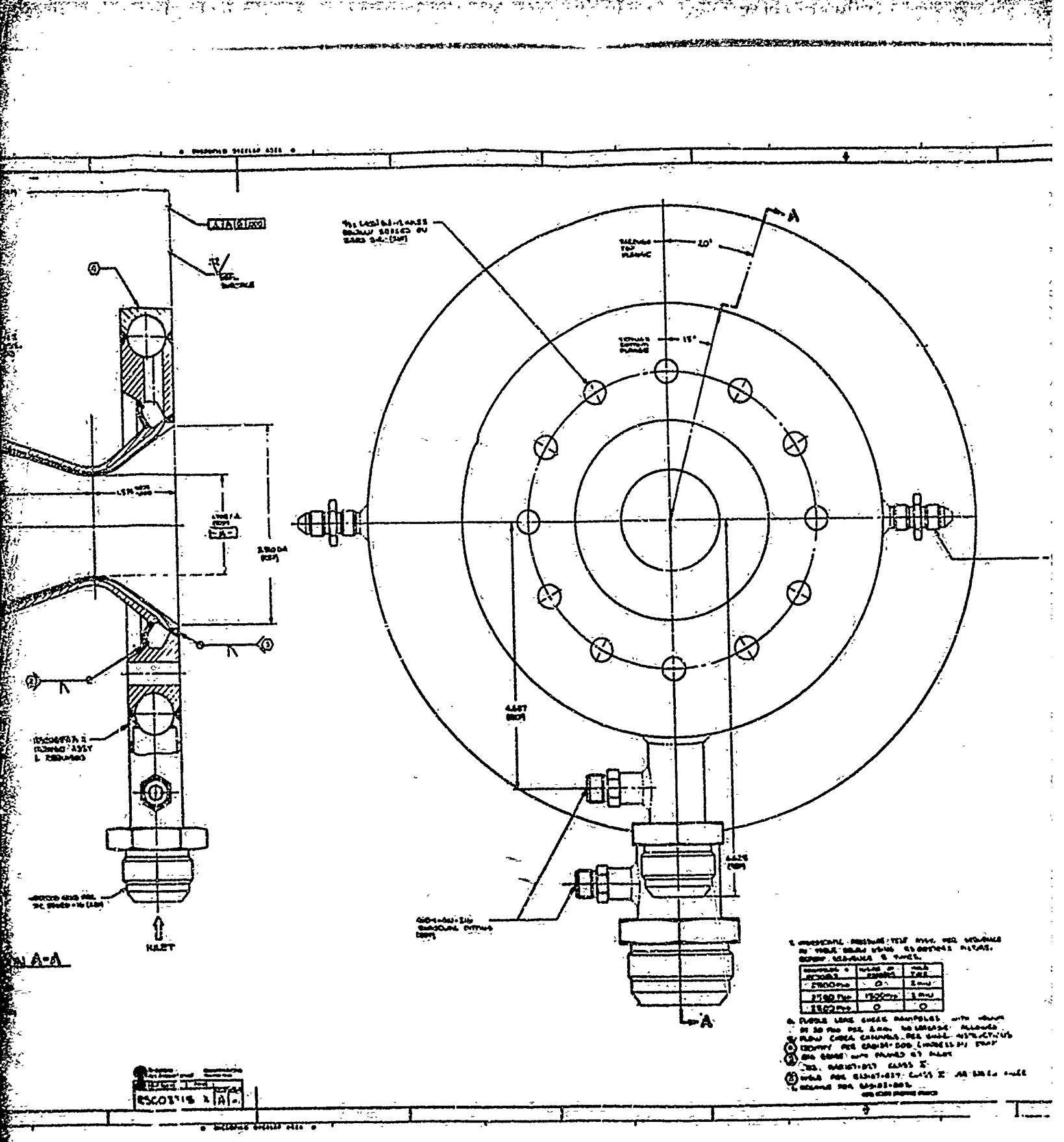

Figure 93.

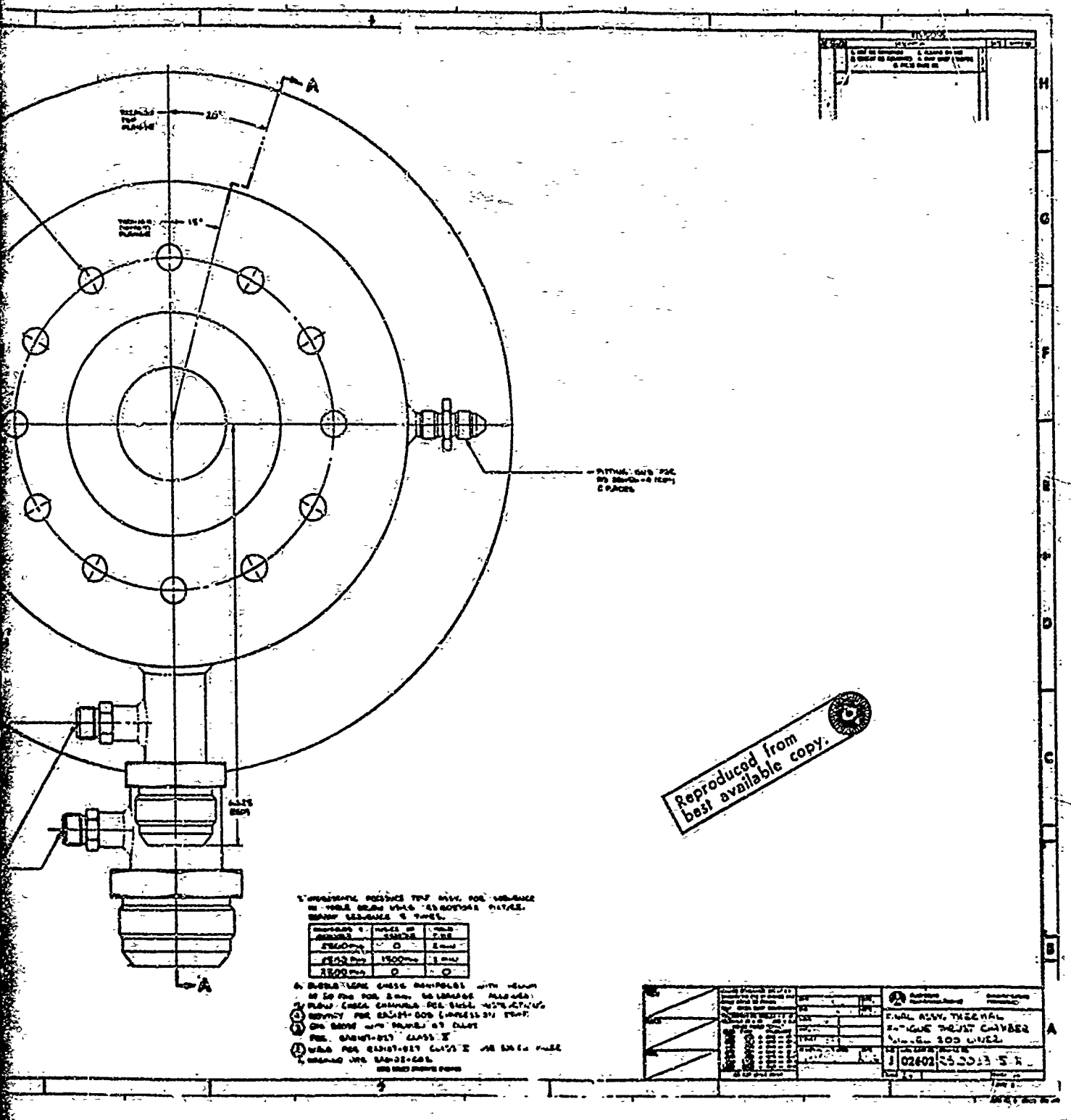

Figure 93. Final Assembly Thermal Fatigue Thrust Chamber (Nickel-200 Liner)

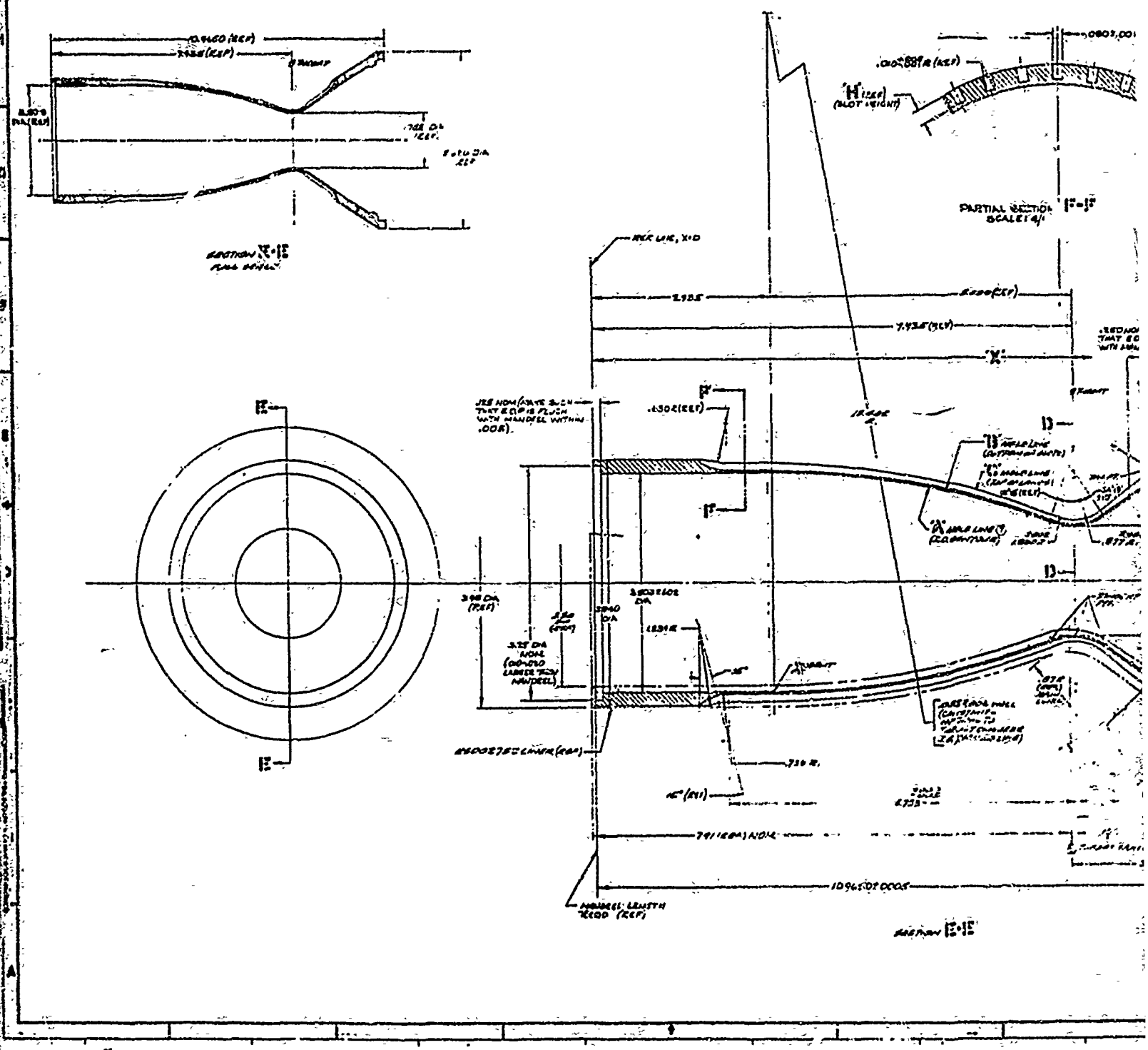

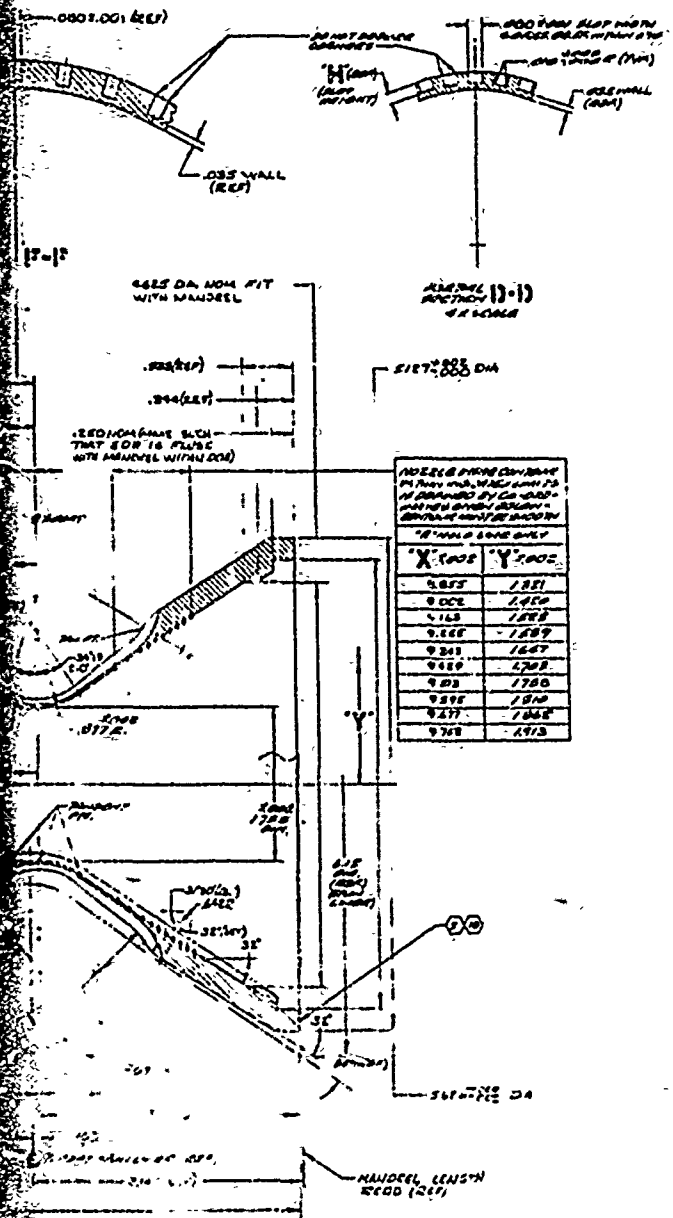

"X" (mm)	"Y" (mm)
9.855	1.851
9.002	1.850
9.148	1.848
9.295	1.839
9.341	1.847
9.389	1.798
9.103	1.786
9.295	1.810
9.477	1.868
9.768	1.913

"X" (mm)	"H" (mm)	"X" (mm)	"Y" (mm)	"X" (mm)	"Y" (mm)
1.962	.020	1.962	1.786	1.962	1.904
2.988	.020	2.932	1.786	2.933	1.906
3.188	.110	3.100	1.784	3.191	1.902
3.679	.015	3.681	1.746	3.687	1.880
3.975	.113	3.978	1.750	3.936	1.852
4.448	.110	4.447	1.701	4.459	1.810
4.936	.107	4.939	1.634	4.935	1.742
5.180	.105	5.186	1.594	5.204	1.700
5.480	.102	5.467	1.501	5.748	1.601
5.936	.100	5.942	1.446	5.964	1.543
6.186	.099	6.183	1.385	6.217	1.482
6.436	.097	6.446	1.319	6.470	1.414
6.685	.095	6.695	1.250	6.721	1.341
6.937	.094	6.945	1.174	6.971	1.260
7.187	.092	7.198	1.092	7.227	1.179
7.235	.092	7.246	1.076	7.175	1.163
7.336	.094	7.347	1.042	7.336	1.129
7.435	.094	7.446	1.009	7.475	1.096
7.535	.090	7.545	.976	7.575	1.064
7.636	.077	7.643	.948	7.662	1.038
7.735	.064	7.741	.918	7.751	.991
7.835	.054	7.839	.896	7.843	.980
7.935	.054	7.935	.893	7.935	.977
8.035	.054	8.031	.918	8.035	.972
8.086	.054	8.127	.938	8.112	.997
8.235	.044	8.223	.965	8.214	1.023
8.335	.033	8.319	1.005	8.296	1.078
8.435	.021	8.415	1.048	8.370	1.130
8.504	.000	8.514	1.130	8.464	1.206
8.635	.018	8.618	1.199	8.560	1.280
8.681	.101	8.666	1.233	8.697	1.316
8.885	—	8.836	1.350	8.772	1.419
8.935	.120	8.918	1.406	8.850	1.501
9.002	.120	8.992	1.445	8.915	1.569
9.068	—	9.064	1.504	8.597	1.603
9.163	—	9.163	1.551	9.027	1.657
9.255	—	9.255	1.618	9.109	1.719

Figure 94. M
F

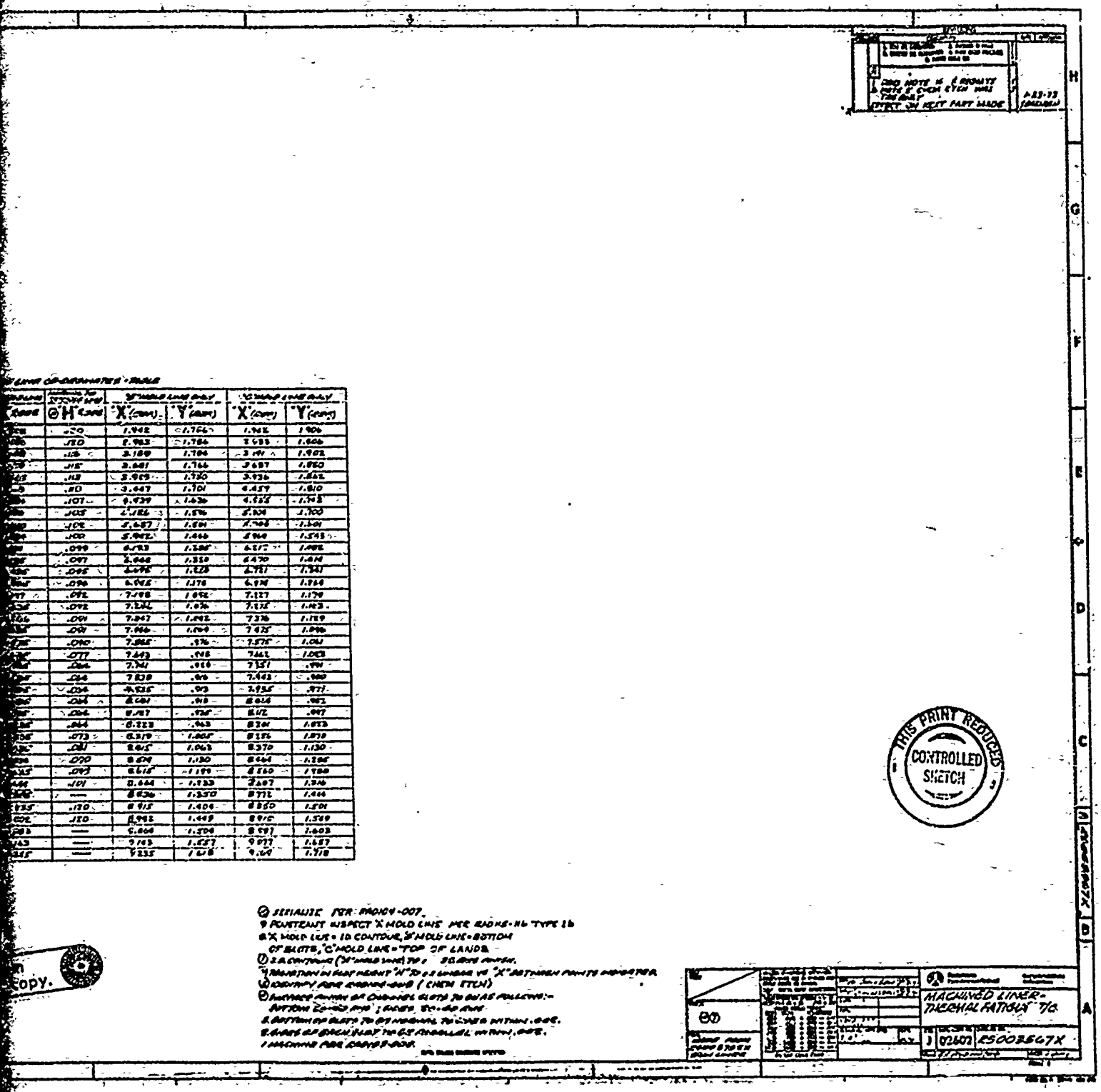

Figure 94. Machined Liner - Thermal Fatigue Thrust Chamber

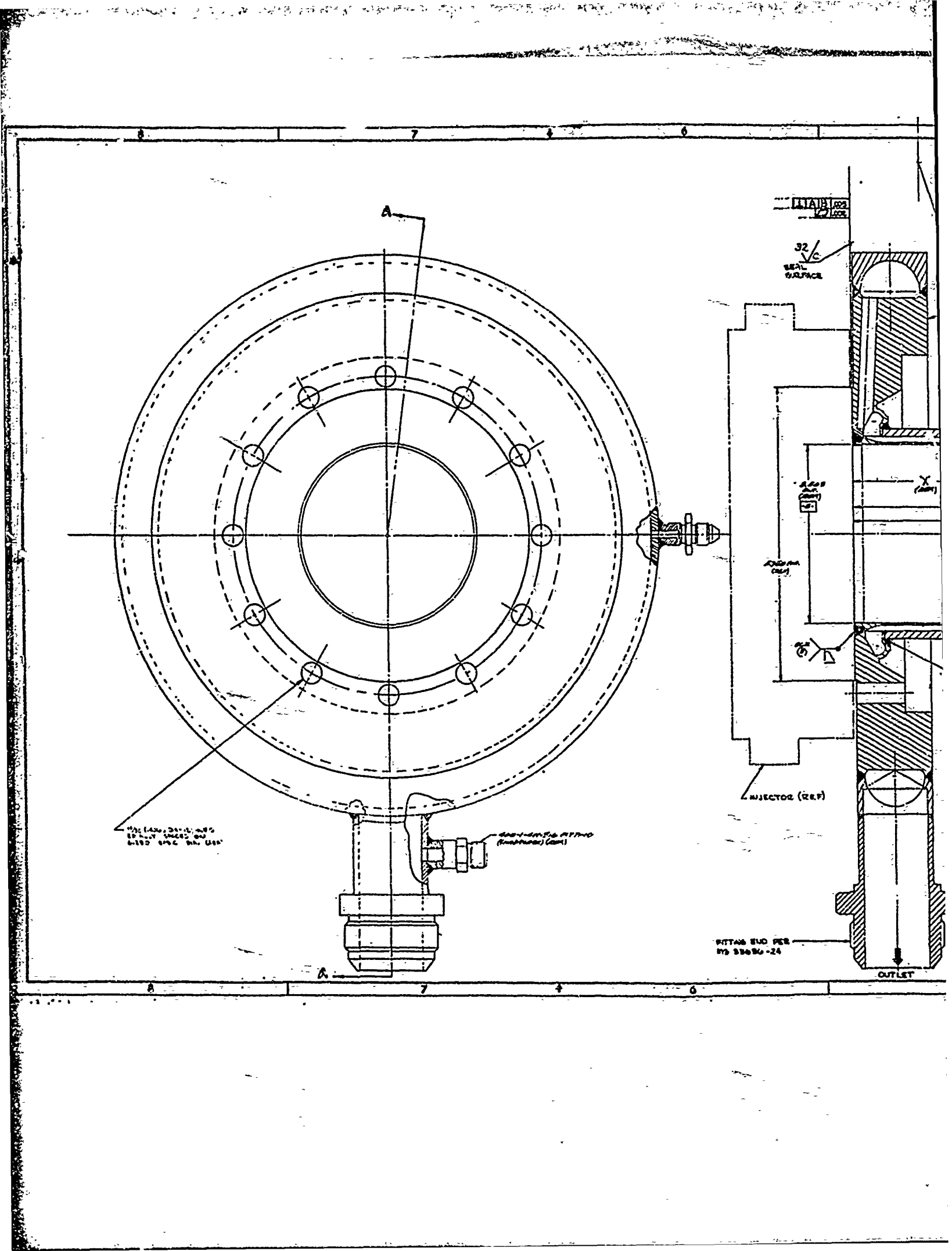
A
A
32
SEAL SURFACE
X
INJECTOR (REF)
OUTLET

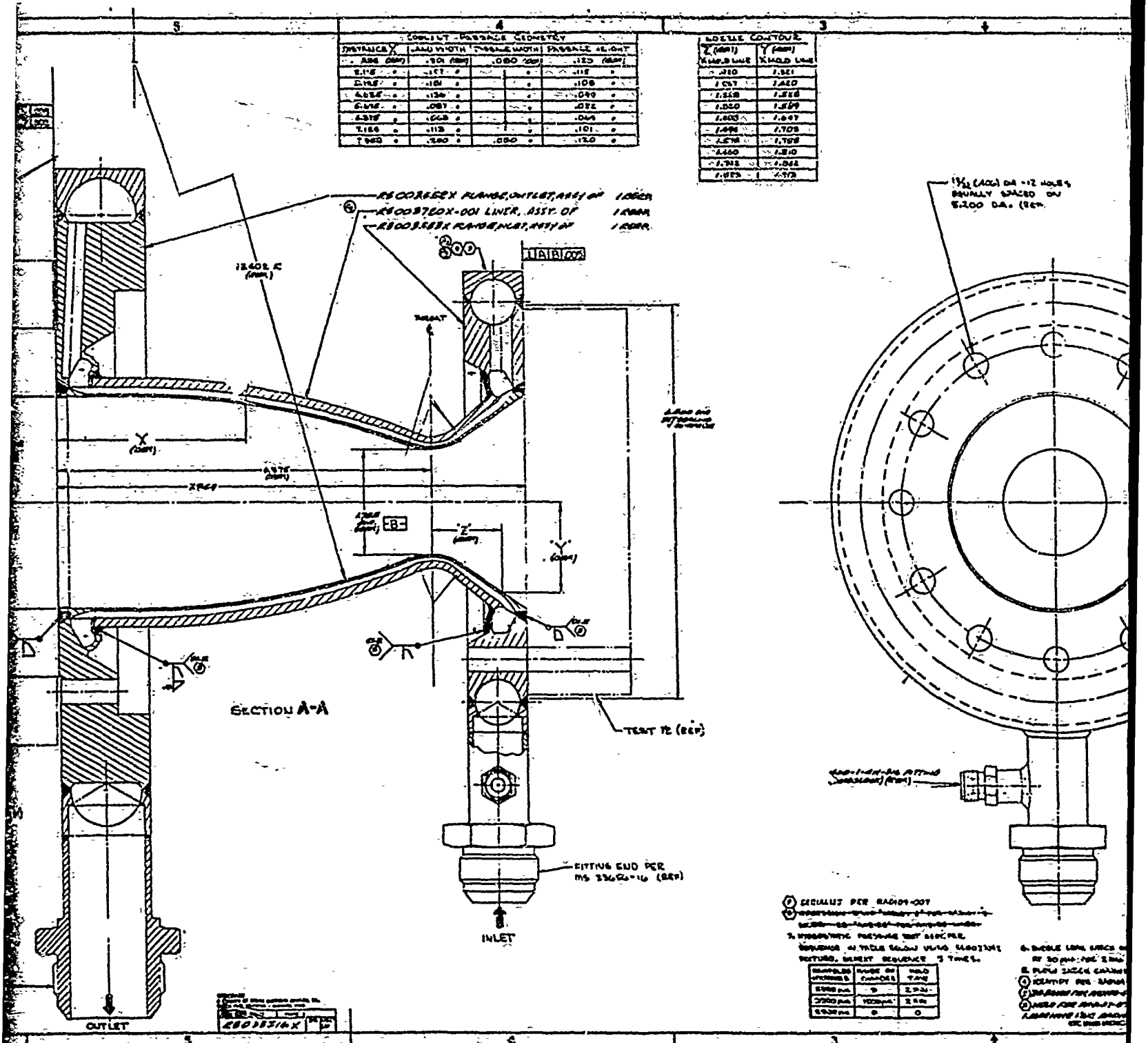
COOLANT PASSAGE GEOMETRY
LOCUS CONTOUR
SECTION A-A
INLET
OUTLET
TEST PT (REF)
FITTING END PER MS 33656-16 (REF)
EQUALLY SPACED ON 8.200 DIA. (REF)

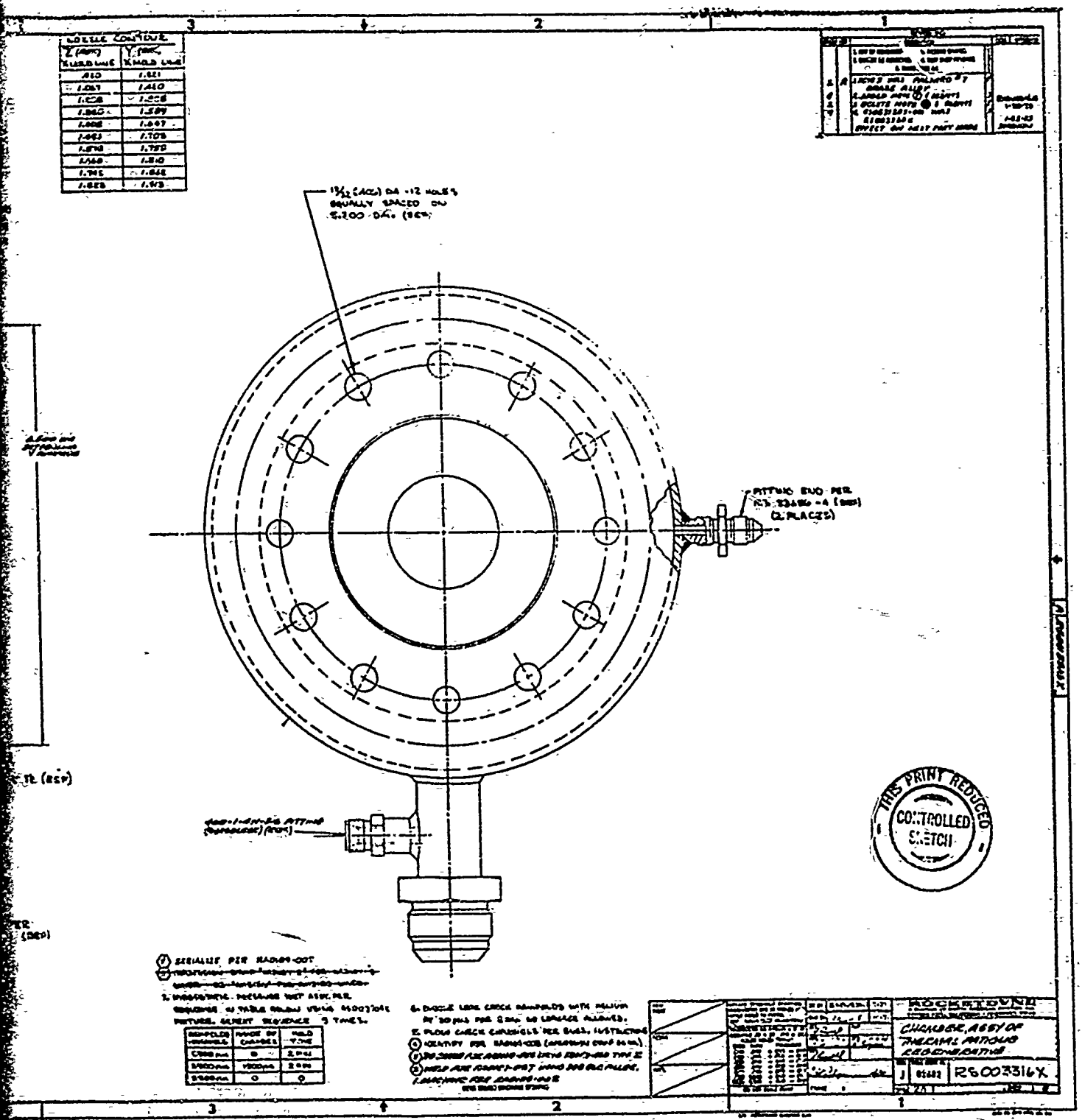

Figure 95. Chamber Assembly of Thermal Fatigue Regenerative

PHASE I - TASK V - CALORIMETER THRUST CHAMBER ASSEMBLY DESIGN

In order to obtain a heat flux profile for the injector to be used in the Phase II test effort, a calorimeter thrust chamber assembly was designed. This assembly consists of an OFHC copper hot gas wall thrust chamber with circumferential water coolant passages and a coaxial element injector of AFRPL design. A design description of each follows.

Calorimeter Thrust Chamber

The original AFRPL calorimeter thrust chamber design, X69F16199, was modified to incorporate the same internal contour as the copper alloy regeneratively cooled thrust chambers, the 6-inch injector to throat length, and to facilitate fabrication by Rocketdyne. The injector and exit end flange designs were also changed to the same interface specifications as the regeneratively cooled thrust chambers. The revised thrust chamber design is shown in Fig. 96 and operating parameters are shown below:

Chamber Pressure, psia	750
Mixture Ratio	6:1
Propellants	LO_2/GH_2
Coolant	Water
Coolant Inlet Pressure, psia	1000
Coolant Total Flowrate, gpm	100
Coolant Inlet Temperature	Ambient

The thrust chamber liner is machined from an OFHC copper billet. The liner contains 16 circumferential coolant grooves. All grooves are 0.250 inches wide and have a hot gas wall thickness of 0.125 inches. The passage depth is constant for each passage and varies from 0.125 inches at the injector end to 0.060 at the throat.

The coolant circuit closeout and structural shell is annealed electroformed nickel. The shell is annealed to improve brazeability to tubes and flanges.

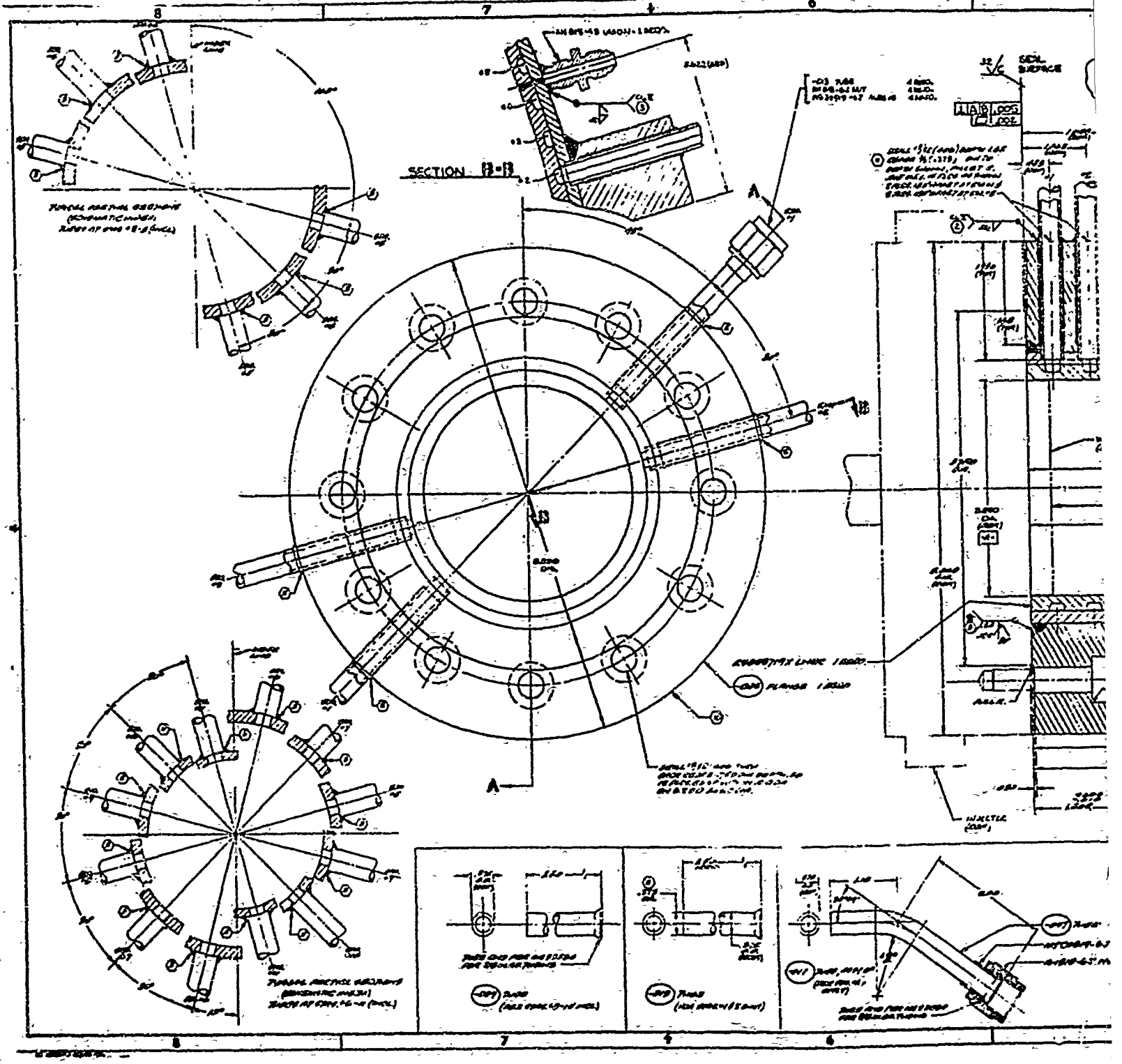
SECTION
SEAL SURFACE

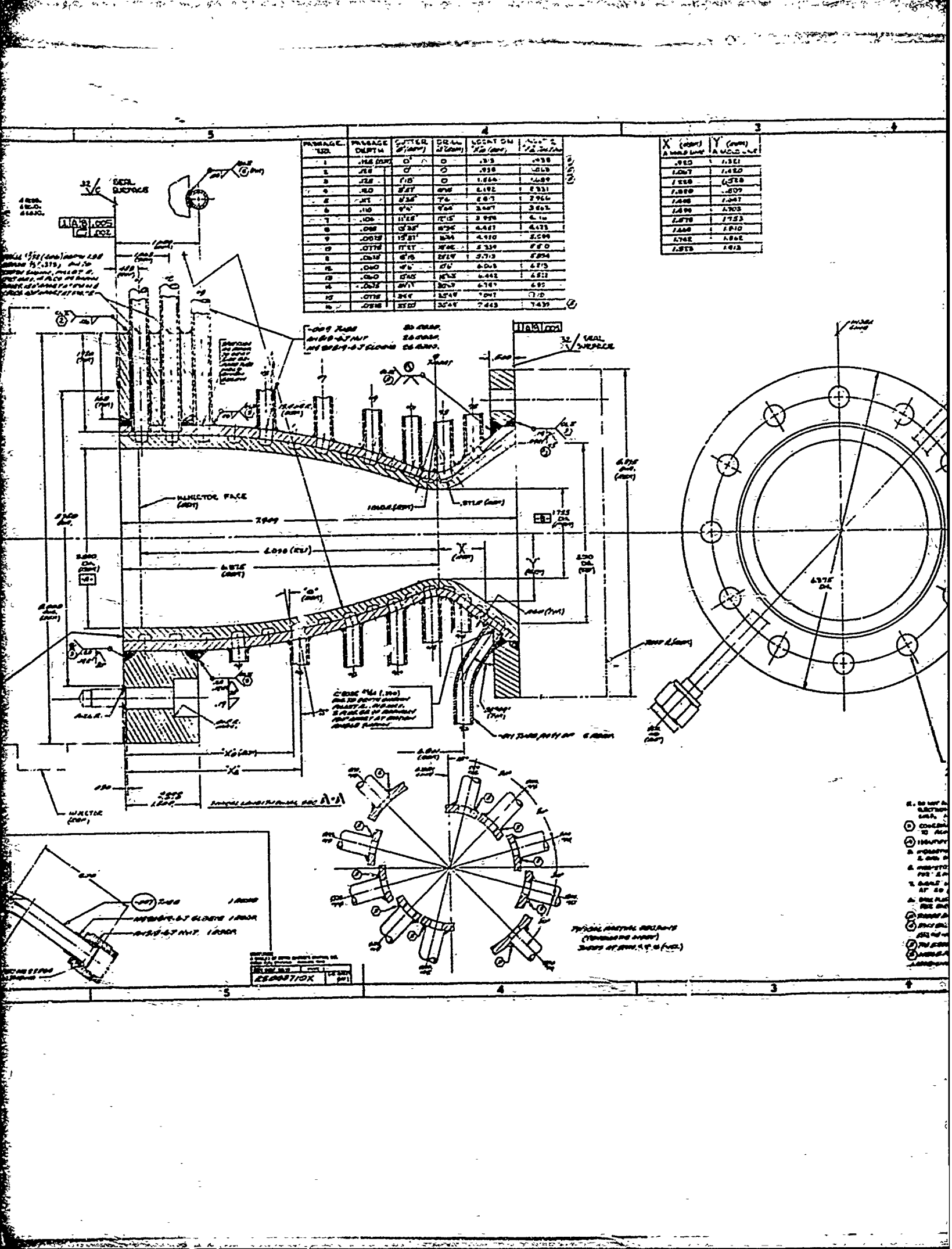

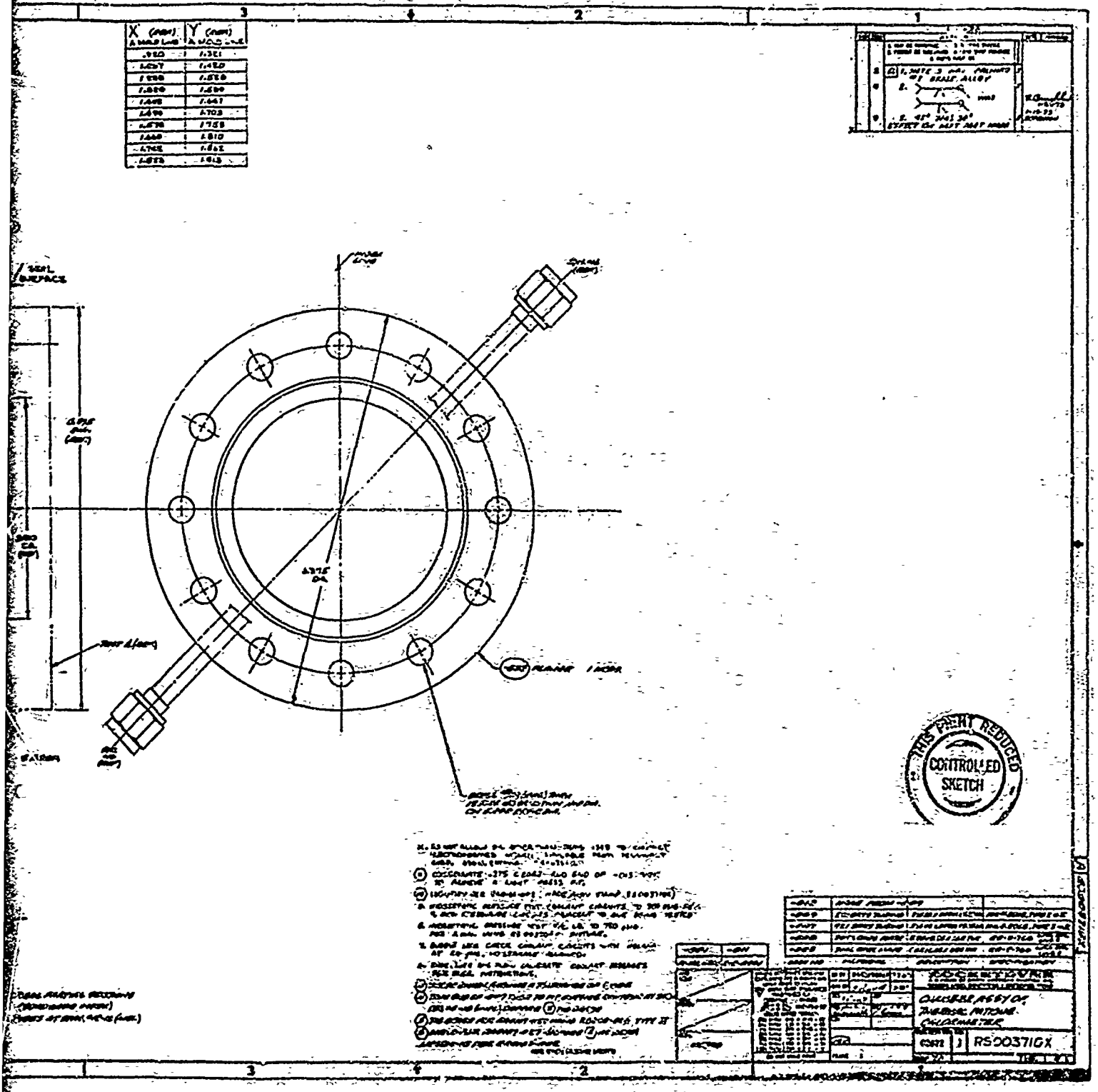

Figure 96. Chamber Assembly of Thermal Fatigue Calorimeter

The coolant manifolding consists of an individual inlet and outlet tube, 180 degrees opposed, for each coolant channel. There are, therefore, 16 inlet tubes and 16 outlet tubes. The tubes are TIG brazed over holes drilled through the electroformed structural shell.

The tubes that go through the top flange into the two top grooves are press fit into the electroformed nickel and TIG welded to the outside diameter of the flange. The press fit seal into the electroformed nickel prevents excessive leakage between the top two grooves and the weld joint to the flange seals against external leakage. The manifold tubes are made of 321 CRES. The thrust chamber flanges are made of 304L CRES and are TIG brazed to the electroformed nickel structural shell. A chamber pressure tap is located between grooves No. 4 and 5 at a distance of 2.25 inches from the injector face.

Coaxial Injector

The injector assembly, Fig. 97 and 98, is identical to the AFRPL design with the exception of changes to add structural support to the rigimesh face. Seventeen nickel posts are threaded through the nickel face into the intermediate manifold plate. The manifold was also made thicker which necessitated moving and increasing the number of distribution holes to the oxidizer cavity. The flow area of the distribution holes was held constant and the number of holes was increased to 12 so that they could be positioned half way between the entrances of each of the 12 elements in the outer row of the injector.

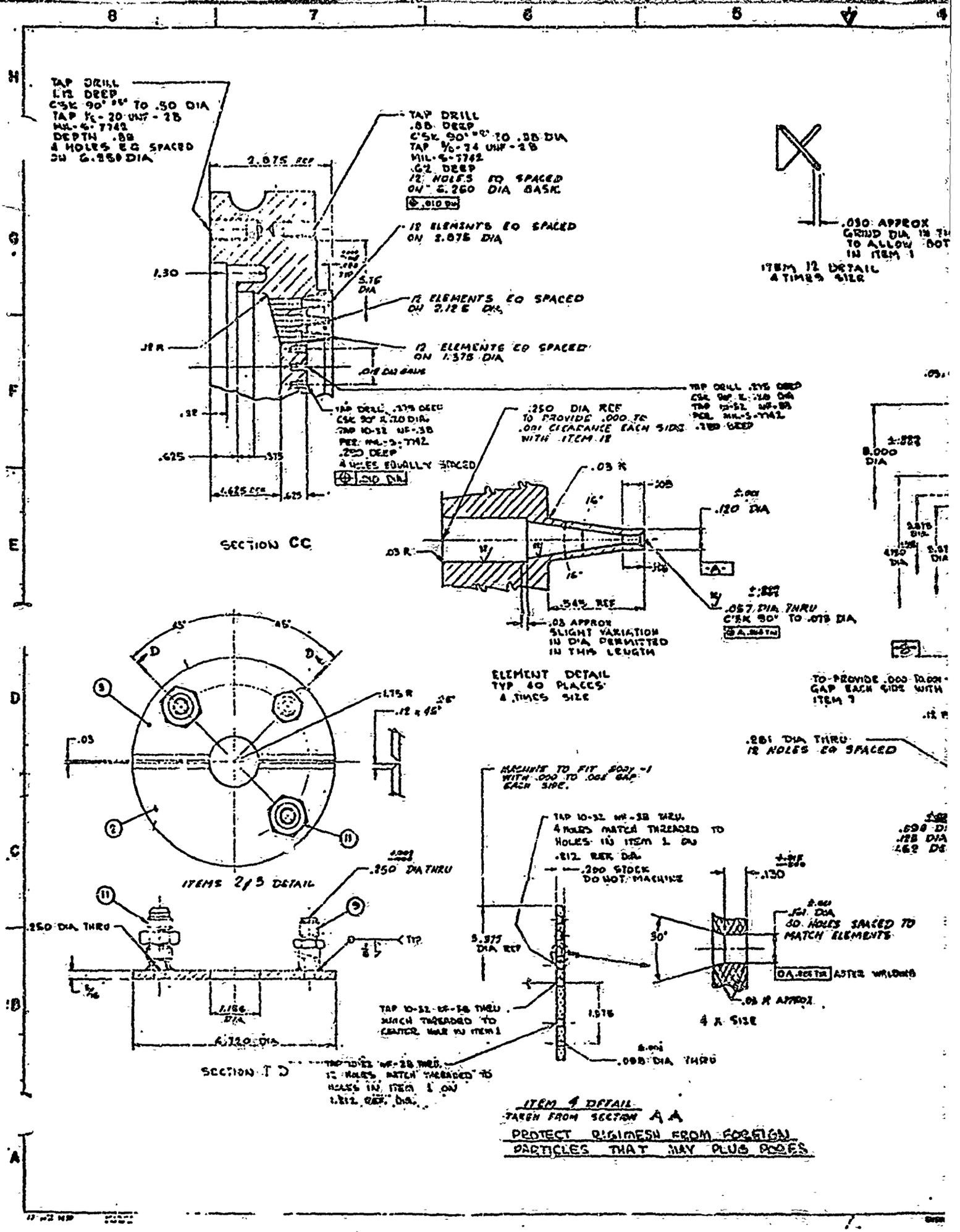
TAP DRILL
1.12 DEEP
C'SK 90° TO .50 DIA
TAP 5/8-20 UNF-2B
MIL-S-7742
DEPTH .88
4 HOLES EQ SPACED
ON 6.250 DIA
2.875 REF
TAP DRILL
.88 DEEP
C'SK 90° TO .38 DIA
TAP 5/16-24 UNF-2B
MIL-S-7742
.62 DEEP
12 HOLES EQ SPACED
ON 5.250 DIA BASIC
.010 M
12 ELEMENTS EQ SPACED
ON 2.875 DIA
1.30
5.76 DIA
12 ELEMENTS EQ SPACED
ON 2.12 5 DIA
12 ELEMENTS EQ SPACED
ON 1.375 DIA
.625
.375
1.625 REF
.625
TAP DRILL .375 DEEP
C'SK 90° X .70 DIA
TAP 10-32 UNF-2B
PER MIL-S-7742
.250 DEEP
4 HOLES EQUALLY SPACED
.010 M
SECTION CC
.030 APPROX
GRIND DIA, TO
TO ALLOW
IN ITEM 1
ITEM 12 DETAIL
4 TIMES SIZE
.250 DIA REF
TO PROVIDE .000 TO
.001 CLEARANCE EACH SIDE
WITH ITEM 12
TAP DRILL .375 DEEP
C'SK 90° X .70 DIA
TAP 10-32 UNF-2B
PER MIL-S-7742
.250 DEEP
.03 R
.208
16°
.120 DIA
.03 R
.344 REF
.057 DIA THRU
C'SK 90° TO .078 DIA
.03 APPROX
SLIGHT VARIATION
IN DIA PERMITTED
IN THIS LENGTH
ELEMENT DETAIL
TYP 40 PLACES
4 TIMES SIZE
8.000
DIA
TO PROVIDE .000 TO.001
GAP EACH SIDE WITH
ITEM 9
.281 DIA THRU
12 HOLES EQ SPACED
45°
45°
D
D
.175 R
.12 x 45°
.03
2
9
11
ITEMS 2 & 5 DETAIL
MACHINE TO FIT BODY -1
WITH .000 TO .002 GAP
EACH SIDE.
TAP 10-32 UNF-2B THRU
4 HOLES MATCH THREADED TO
HOLES IN ITEM 1 ON
.812 REF DIA
.200 STOCK
DO NOT MACHINE
.130
.350 DIA THRU
.250 DIA THRU
TYP
3.375
DIA REF
2.60
.561 DIA
30 HOLES SPACED TO
MATCH ELEMENTS
30°
DIA AFTER WELDING
.03 R APPROX
TAP 10-32 UNF-2B THRU
MATCH THREADED TO
CENTER HOLE IN ITEM 1
1.375
.098 DIA THRU
4 A SIZE
1.186
DIA
6.720 DIA
SECTION D D
TAP 10-32 UNF-2B THRU
12 HOLES MATCH THREADED TO
HOLES IN ITEM 1 ON
1.812 REF DIA.
ITEM 4 DETAIL
TAKEN FROM SECTION A A
PROTECT DISIMESH FROM FOREIGN
PARTICLES THAT MAY PLUG PORES

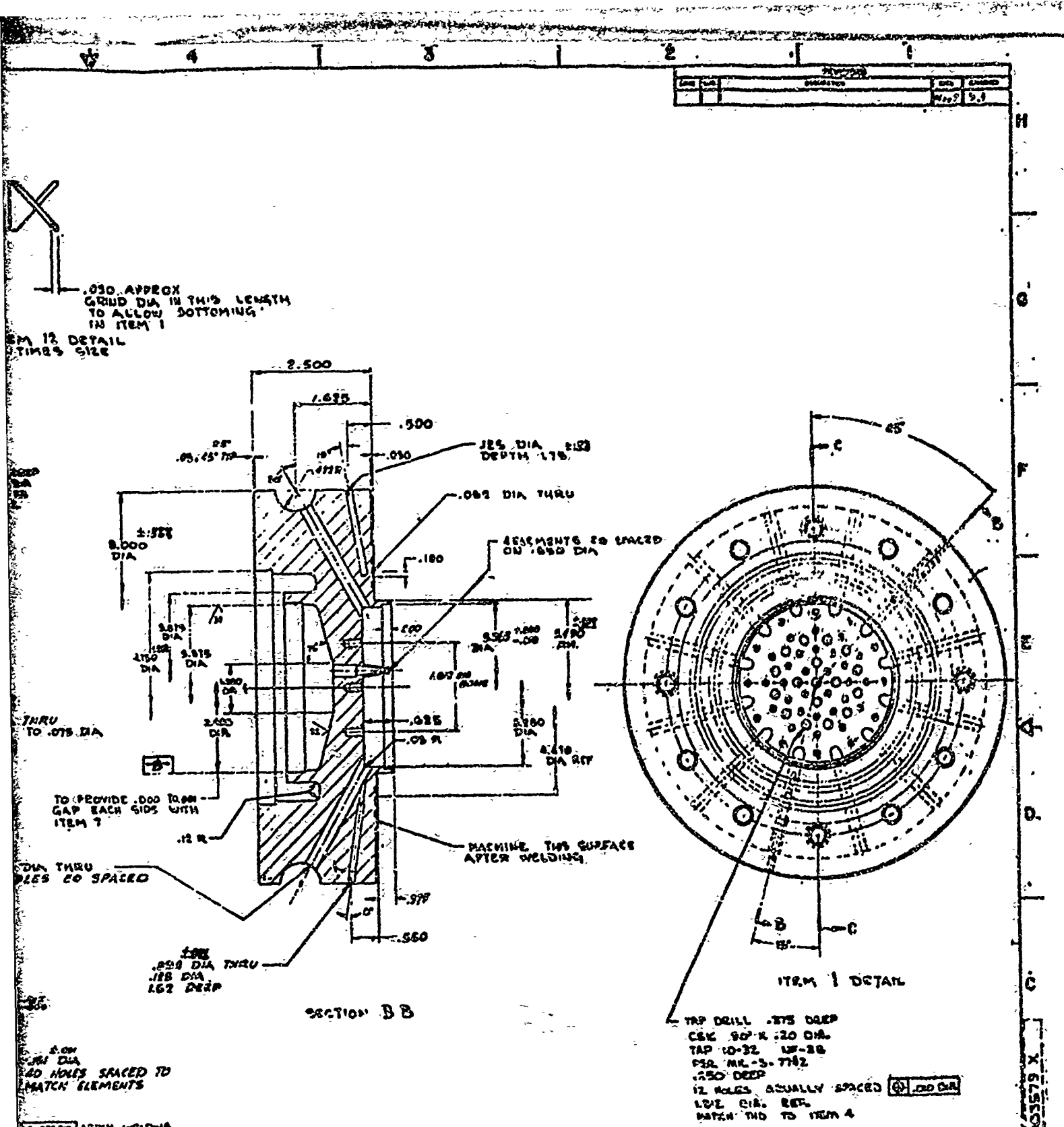

Figure 97. Injector Assembly Thermal Fatigue

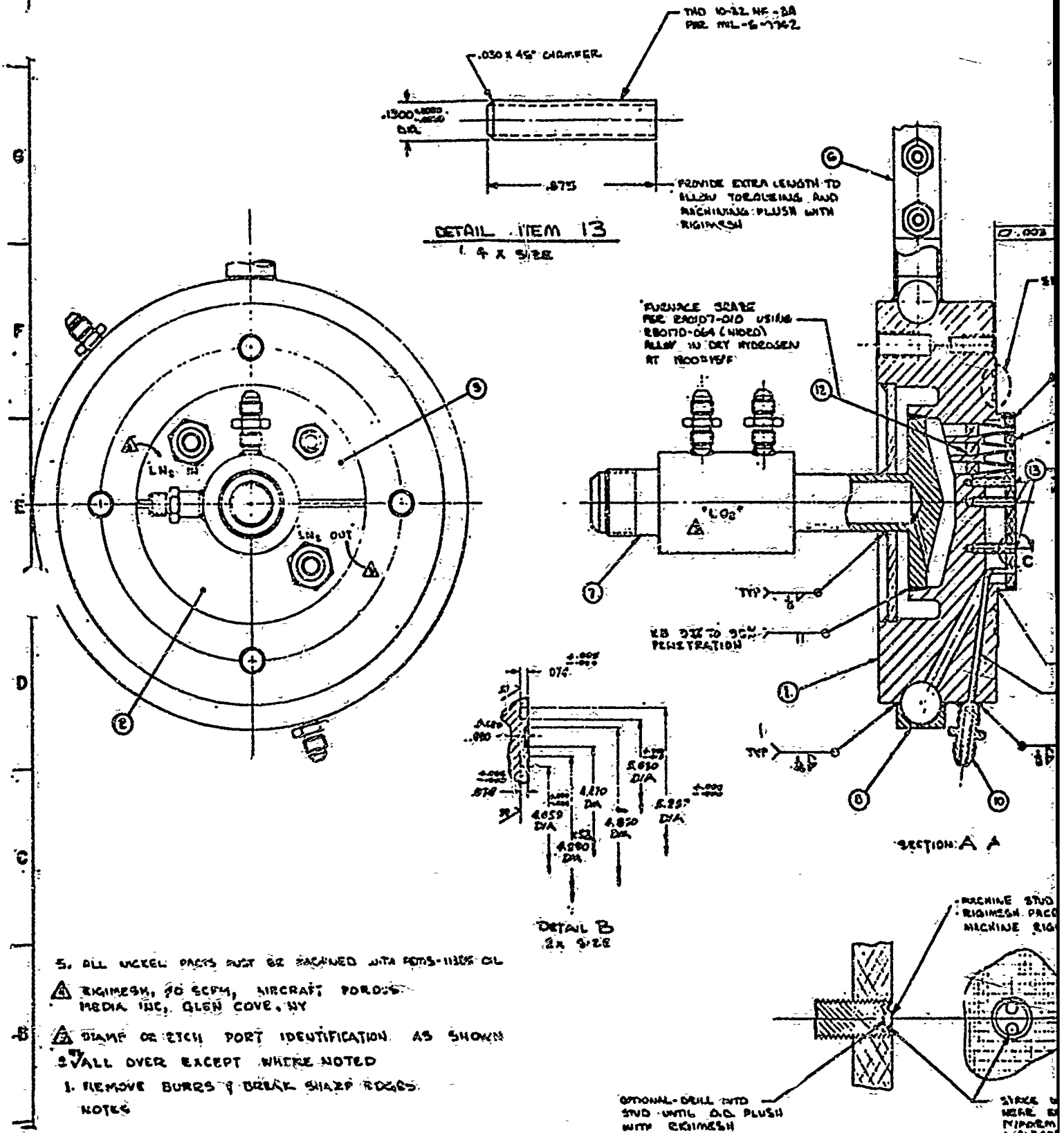

5. ALL NICKEL PARTS MUST BE MACHINED WITH PETRO-LUBE OIL

4 RIGIMESH, 90 SCFM, AIRCRAFT POROUS MEDIA INC., GLEN COVE, NY

3 STAMP OR ETCH PORT IDENTIFICATION AS SHOWN

2 ALL OVER EXCEPT WHERE NOTED

1. REMOVE BURRS & BREAK SHARP EDGES

NOTES

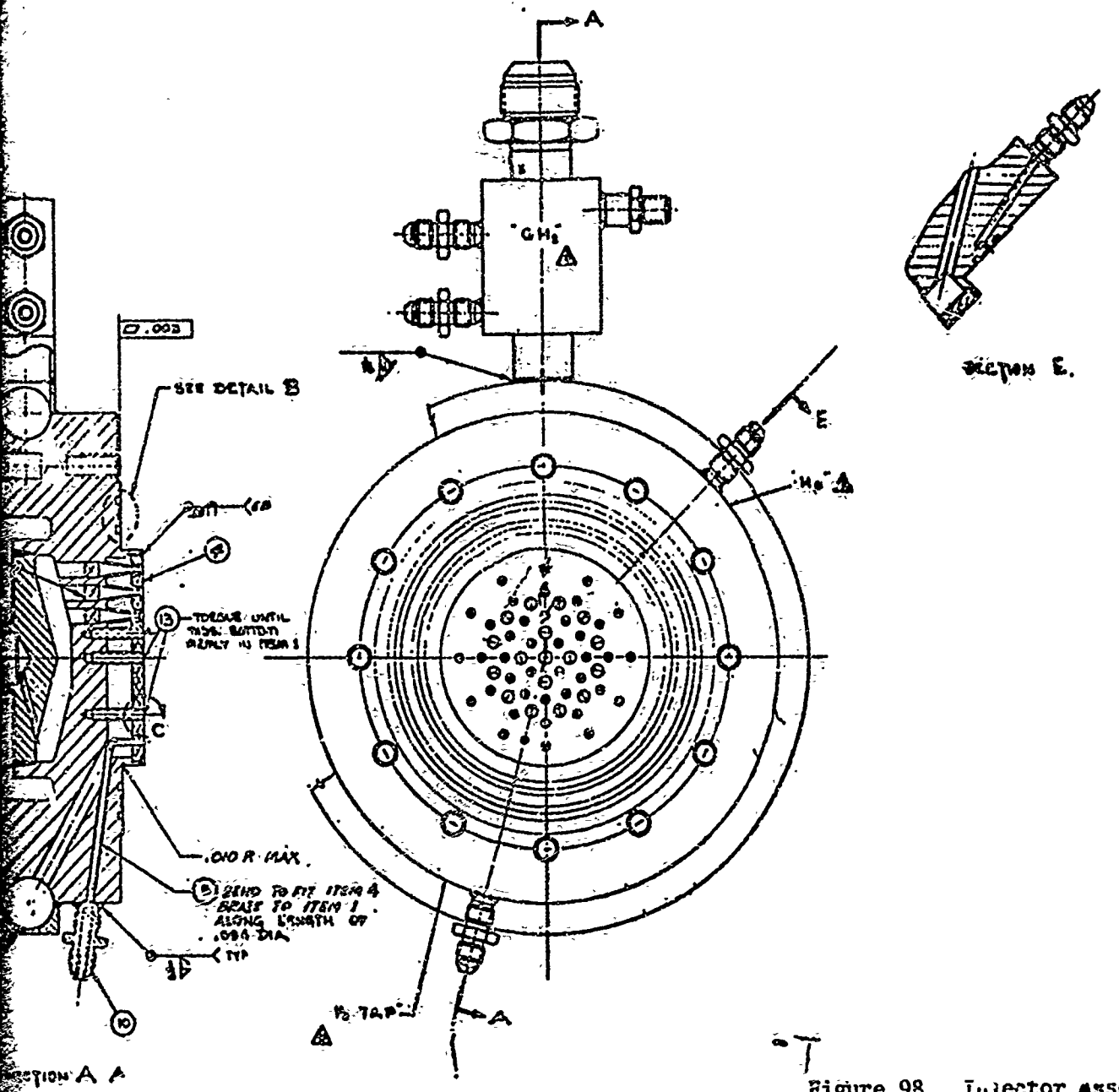

SECTION E.

SECTION A A

Figure 98, Injector Assembly Thermal Fatigue

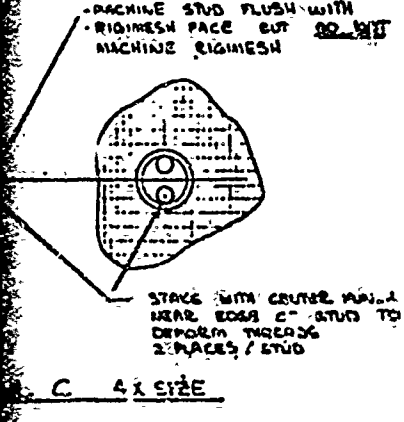

17		STUD		-13	CORR STD	INCONEL 718		13
60		SCREEN GFE				304 MONEL		12
2		UNION ½ TUBE		AN815-4J				11
2		UNION ¼ TUBE		AN815-4J				10
1		CONNECTOR S-SPACER		600-1-4N-316				9
1		MANIFOLD		RS 003578 X				8
1		LOX INLET		RS 003576 X				7
1		FUEL INLET		RS 003577				6
1		TUBE .098 OD .065 ID .078		-	CORR STD	ANNEALED		5
1		FACE PLATE		-4	SEE NOTE	INCONEL 718		4
1		COVER HALF		-3	00-S-765	SST 304		3
1		½ VEE HALF		-2	00-S-765	SST 304		2
1		BODY		-1	CORR STD			1
NO REQD	DWG	NOMENCLATURE		CHANGE NO	ORIGINAL	MATERIAL	WT	ITEM

UNLESS OTHERWISE SPECIFIED DIMENSIONS ARE IN INCHES

			INJECTOR ASSY THERMAL FATIGUE
		F 07870	RS 003579 X

CONCLUSIONS AND RECOMMENDATIONS

The results of the Phase I effort were highly encouraging in the area of analysis and laboratory fatigue testing. Considerable progress was made in developing the analytical tools for predicting the thermal cycle life capability of non-tubular regeneratively cooled thrust chambers. Also the thermal analysis effort laid the initial groundwork in exploring design and/or operational innovations which could be incorporated on an engine to increase life capability. The isothermal fatigue test procedures and specimen design represent great strides in producing the data more directly applicable to the thrust chambers and in establishing the life capability of the candidate materials. The differential fatigue and panel test efforts showed promise; however, it was apparent that successful development of the laboratory test techniques to the point where they would yield meaningful quantitative data was beyond the scope of this program.

Based on these results several recommendations for future effort can be made. These are:

1. Conduct additional isothermal fatigue testing to establish a failure criteria for cyclic testing with hold times at peak compressive strain and to repeat questionable test data.
2. Conduct more isothermal fatigue testing, data reduction and analysis to determine creep rate law material constants for the relaxation process at peak tensile and compressive strain.
3. Conduct additional isothermal fatigue testing to more accurately define the fatigue curve constants as a function of temperature.
4. Conduct isothermal fatigue tests on various heats of material and on specimens machined directly from spun liners to determine effect of chemical composition variances and processing on the material fatigue capability.

5. Deepen the analytical and experimental evaluation of candidate panel test techniques to determine if an economically feasible technique can be developed which more closely resembles the thermal and strain environment of a regeneratively cooled thrust chamber.

6. The life analysis methods should be verified by comparison with the results from additional rocket engine duty cycle testing.

7. Cyclic creep rupture data should be obtained and used in place of monotonic creep rupture data to reduce the conservatism in evaluating creep rupture damage. Part of the effort would include the development of a test procedure to obtain the data. The test procedure requires the introduction of a load reversal after the desired creep strain has accumulated on each side of the hysteresis loop.

8. Thermal fatigue and duty cycle simulation test data should be obtained to more accurately refine life analysis. The thermal fatigue test run in strain control involves developing the test technique to independently vary temperature and strain. The accuracy of the incremental approach adopted in the analysis can, therefore, be evaluated. The duty cycle simulation requires the development of a test procedure to switch from deflection to load control and back within the cycle.

9. The latest fatigue life prediction theories should be evaluated for inclusion into thermal fatigue life prediction methods. These include Coffin's approach involving a frequency modified life (Ref. 20) and Manson's partitioning of the total strain range into plastic and creep components (Ref. 21).

REFERENCES

1. Manson, S. S., Halford, G. R., "A Method of Estimating High-Temperature Low-Cycle Fatigue Behavior of Materials," International Conference on Thermal and High-Strain Fatigue, Institute of Metals, London, June 1967.

2. Taira, S., "Thermal Fatigue and Its Relation to Creep Rupture and Mechanical Fatigue," Office of Naval Research Structural Mechanics Series, High-Temperature Structures and Materials, Proceedings of the Third Symposium on Naval Structural Mechanics, Edited by Freudenthal, Boley, and Liebowitz, pp. 187-213, published by Pergamon Press, 1964.

3. Danforth, C. E., "Designing to Avoid Fatigue in Long Life Engines," SAE Paper No. 660311, National Aeronautic Meeting, New York, New York, April 25-28, 1966.

4. Venter, A., Wilbers, L. G., "Advancing the Engineering Properties of a Ni-Fe Base Superalloy through Conventional Control Procedures," Journal of Metals, May 1970, pp. 46-54.

5. Wood, D. S., "The Effect of Creep on the High Strain Fatigue Behavior of a Pressure Vessel Steel," Welding Research Supplement, February 1966, pp. 90s-96s.

6. Coffin, L. F., and J. F. Tavernelli, "The Cyclic Straining and Fatigue of Metals," Trans. AIME, Vol. 215, 1959, pp. 794-806.

7. Carden, A. E., "Thermal Fatigue Evaluation," Manual on Low Cycle Fatigue Testing, ASTM STP 465, pp. 163-188.

8. Swindeman, R. W., Douglas, D. A., "The Failure of Structural Metals Subjected to Strain-Cycling Conditions," Journal of Basic Engineering, June 1959, pp. 203-212.

9. Spera, D. A., The Calculation of Elevated-Temperature Cyclic Life Considering Low-Cycle Fatigue and Creep, NASA TND-5317.

10. Coffin, L. F., Tavernelli, J. F., "Experimental Support for Generalized Equation Predicting Low-Cycle Fatigue," Journal of Basic Engineering, December 1962, pp. 533-541.

11. Manson, S. S., "Fatigue: A Complex Subject . . . . Some Simple Approximations," The William M. Murray Lecture, 1964, Experimental Mechanics, July 1965, pp. 193-226.

12. Morrow, Jo Dean, "Cyclic Plastic Strain Energy and Fatigue of Metals," ASTM STP 378, 1965, pp. 45-87.

13. Halford, G. R., Manson, S. S., "Application of a Method of Estimating High-Temperature Low-Cycle Fatigue Behavior of Materials," Transactions of the ASM, Vol. 61, March 1968, pp. 94-102.

14. Manson, S. S., Thermal Stress and Low-Cycle Fatigue, McGraw-Hill Book Company, 1966, pp. 89.

15. Miner, M. A., "Cumulative Damage in Fatigue," Trans. ASME, Vol. 67, Sept. 1945, pp. A159.

16. Halford, G. R., Cyclic Creep-Rupture Behavior of Three High-Temperature Alloys, NASA TN D-6304.

17. Cooper, R. A., "Creep Effects on Elevated Temperature Fatigue," Paper presented at WESTEC 1971, Los Angeles.

18. Campbell, R. D., "Creep/Fatigue Interaction Correlation for 304 Stainless Steel Subjected to Strain Controlled Cycling with Hold-Times at Peak Strain," Paper presented at First National Pressure Vessel and Piping Conference, ASME, May 10-12, 1971, San Francisco.

19. Lagneborg, R. and Attermo, R., "The Effect of Combined Low-Cycle Fatigue and Creep on the Life of Austenitic Stainless Steels," Metallurgical Transactions, Vol. 2, July 1971, pp. 1821-1827.

20. Coffin, L. R., The Effect of Frequency on High-Temperature Low-Cycle Fatigue, AFFDL TR-70-144, 1970, pp. 301-311.

21. Manson, S. S., Halford, G. R., Hirschberg, Creep-Fatigue Analysis by Strain Range Partitioning, NASA TMX-67838, May 1971.

22. Lewis, J. R., Creep Behavior of NARloy-Z, MPTR 70-902, July 1971.

23. Manson, S. S., "Thermal Stress and Loy Cycle Fatigue," McGraw Hill Book Co., dated 1966, pp. 89.